

MOLDOVA STATE UNIVERSITY

manuscript
C.Z.U. 530.145+535.14

MÎRZAC ALEXANDRA

QUANTUM DYNAMICS IN MOLECULAR DIPOLAR SYSTEMS

131.01 - MATHEMATICAL PHYSICS

Thesis in physics

PhD Supervisor: M. Macovei Macovei Mihai, dr. hab. in phys. and math., prof.

Guidance commission: Bouroş Pavlina Bouroş, dr. in chemistry, assoc. prof.

Bardetchi Profirie Bardetchi, dr. in phys. and math., assoc. prof.

Cojocaru Ion Cojocaru, dr. in phys. and math., assoc. prof.

Author: Alexandra Mîrzac Alexandra Mîrzac

CHIŞINĂU, 2022

UNIVERSITATEA DE STAT DIN MOLDOVA

Cu titlu de manuscris
C.Z.U. 530.145+535.14

MÎRZAC ALEXANDRA


STUDIUL DINAMICII CUANTICE ÎN SISTEMELE MOLECULARE
DIPOLARE

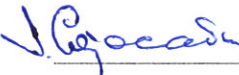
131.01 - FIZICĂ MATEMATICĂ


Teză de doctor în științe fizice

Conducător de doctorat:  Macovei Mihai, dr. hab. în șt. fiz.-mat.

Comisia de îndrumare:  Pavlina Bouroș, dr. în chimie, conf. univ.

 Profirie Bardețchi, dr. în șt. fiz.-mat, conf. univ.

 Ion Cojocaru, dr. în șt. fiz.-mat., conf. univ.

Autor:  Alexandra Mirzac

CHIȘINĂU, 2022

© Mîrzac Alexandra, 2022

OUTLINE

ACKNOWLEDGEMENTS	6
SUMMARY (Engl., Rom., Rus.)	7
SHORTCUTS	10
INTRODUCTION	11
1. MOLECULAR DIPOLAR SYSTEMS IN QUANTUM OPTICS	19
1.1. Two-level systems possessing a permanent dipole moment	20
1.2. Resonance fluorescence and squeezing in molecular dipolar systems	25
1.3. Cooling phenomena in dipolar systems	33
1.4. Terahertz lasing in quantum dipolar systems	40
1.5. Multiphoton dynamics of quantum dipolar systems	47
1.6. Conclusions to the Chapter 1	54
2. PROPERTIES OF NON-CLASSICAL LIGHT SCATTERED BY LASER-PUMPED MOLECULES POSSESSING PERMANENT DIPOLES	55
2.1. The theoretical framework	57
2.2. Resonance fluorescence spectrum of a two-level system	65
2.3. Squeezing spectra and quantum fluctuations	75
2.6. Conclusions to the Chapter 2	83
3. DYNAMICS OF A QUANTUM OSCILLATOR COUPLED WITH A THREE-LEVEL Λ-TYPE EMITTER	84
3.1. The theoretical framework	86
3.2. The dressed-state master equation of the three-level Λ -type system	92
3.3. Lasing and cooling effects in the three-level Λ -type system	99
3.3.1. Lasing and cooling in the resonant case (I)	104
3.3.2. Lasing and cooling in the resonant case (II)	106
3.4. Conclusions to the Chapter 3	110

4. MICROWAVE MULTIPHOTON CONVERSION VIA COHERENTLY DRIVEN PERMANENT DIPOLE SYSTEMS	111
4.1. The theoretical framework	115
4.2. Results and discussions	122
4.3. Conclusions to the Chapter 4	129
CONCLUSIONS AND RECOMMENDATIONS	131
REFERENCES	135
RESPONSIBILITY DECLARATION	148
ANNEXES	149
CURRICULUM VITAE	155

ACKNOWLEDGEMENTS

I would like to cordially thank my supervisor Mihai Macovei for his inspiring guidance through all my work presented here. I'm very honoured to be his fellow and thankful for his tremendous guidance effort in my formation.

I'm very thankful to all my colleagues, Profirie Bardeţchi, Corneliu Gherman, Viorel Ciornea, Sergiu Cârlig, Elena Cecoi, Victor Ceban and Ion Cojocaru, for their fruitful conversations and debates and the teamwork and support they have provided me since my first day at the Institute of Applied Physics.

I cordially thank my beloved parents for their constant support, help and advises and unique spirit of team work.

SUMMARY

**to the thesis "Quantum dynamics in molecular dipolar systems",
presented by Alexandra Mîrzac
for conferring the scientific degree of Ph.D. in Physics, Speciality 131.01 "Mathematical
Physics", Chişinău, 2021.**

The thesis has been written in English language and consists of the introduction, 4 chapters, general conclusions and recommendations, and the list of 205 references. The thesis contains 134 pages of basic text, 19 figures and 141 formulae. The results presented in the thesis are published in 16 scientific papers.

Key words: two-level system, three-level Λ -system, permanent dipole moment, resonance, fluorescence, squeezing, terahertz lasing, multi-quanta processes, quantum interference, multiphoton conversion, quantum emitter, super-Poissonian statistics.

The goal: The detection of new quantum dynamical properties in two and three-level Λ -type systems possessing a non-zero permanent dipole moment strongly coupled with quantum optical cavity or opto-mechanical resonators.

Research objectives: The calculation of squeezing effects in the resonance fluorescence processes of laser-pumped two-level system possessing a permanent dipole moment; The determination of the total quantum fluctuation spectra of laser-pumped dipolar two-level systems; The investigation of a laser-pumped three-level Λ -type system having the upper state coupled with a quantum oscillator described by a single quantized leaking mode; The identification of three-level model particularities leading to lasing and cooling effects; The demonstration of quantum interference effects induced by emitter's dressed states responsible for flexible lasing and deeper cooling effects; The investigation of frequency conversion from optical to microwave region, via the resonant pumping of an asymmetrical two-level system incorporated in a quantized single-mode resonator; The demonstration of multiphoton features of cavity quantum dynamics containing an asymmetric two-level system using certain multiphoton superposition of generated states.

Scientific novelty and originality of the results: the new features of resonance fluorescence spectrum of spontaneously emitted photons by dipolar two-level system were demonstrated; two distinct mechanisms of lasing and cooling based on single- or two-quanta processes were detected in the three-level Λ -type system; conversion of photons from optical to microwave domains, via resonantly pumped asymmetrical two-level quantum emitter embedded in a quantized single-mode resonator.

The main scientific problem solved consists in computing and analyzing the quantum dynamical properties of few level atomic systems possessing a permanent dipole moment interacting with external coherent laser field.

Theoretical significance and applicative value: in the thesis, one has investigated the steady state-quantum dynamics of a laser pumped two-level system possessing a non-zero permanent dipole moment. New features of the dipolar two-level system have been found in the resonance fluorescence spectrum, squeezing spectrum and total quantum fluctuations.

The model of a laser-pumped three-level Λ -type system with highest energetic level coupled with a quantum oscillator described by a single quantized leaking mode has been investigated. Two distinct regimes leading to cooling and lasing effects of the model have been identified. In the first regime, the model functions as a two-level system. Whereas in the second regime, the model evolves into a three-level equidistant system.

The quantum multiphoton dynamics of a two-level system possessing unequal permanent dipoles, placed in a leaking single-mode quantized cavity field and coupled to it has been investigated. The photons conversion from optical to microwave frequency domains was proved.

The implementation of the scientific results: the research presented in this thesis have been successfully implemented in the framework of the national project (15.817.02.09F) also with support of Moldavian National Agency for Research and Development, grant No. 20.80009.5007.07 and National Scholarship of World Federation of Scientists in Moldova.

ADNOTARE

la teza "Studiul dinamicii cuantice în sistemele moleculare dipolare", elaborată de Alexandra Mîrzac pentru conferirea gradului științific de doctor în științe fizice la specialitatea 131.01 "Fizică matematică", Chișinău, 2021.

Teza este scrisă în limba engleză și constă din introducere, 4 capitole, concluzii generale și recomandări, și lista a 205 referințe bibliografice. Teza conține 134 pagini de text de bază, 19 figuri și 141 formule. Rezultatele prezentate în teză sunt publicate în 16 lucrări științifice.

Cuvinte cheie: sistem cu două nivele, Λ -sistem cu trei niveluri, dipol permanent, fluorescența la rezonanță, comprimare, laser terahertz, procese cuantice multiple, interferență cuantică, conversia multifotonică, emițător cuantic, statistică super-Poissoniană.

Scopul tezei: Detectarea proprietăților noi în dinamica cuantică a sistemelor cu două niveluri și trei niveluri energetice de tip Λ care posedă dipol permanent nenul și sunt cuplate cu cavitatea optică cuantică sau rezonator opto-mecanic.

Obiectivele tezei: Demonstrarea efectelor de comprimare în spectrul fluorescenței de rezonanță a sistemelor cu două niveluri pompate laser; Determinarea spectrului fluctuațiilor cuantice totale a sistemelor dipolare cu două niveluri; Identificarea mecanismelor de emisie laser și răcire în domeniul THz în sistem cu trei nivele energetice de tip Λ cuplat prin dipol permanent nenul cu un oscilator cuantic; Demonstrarea efectelor de interferență cuantică care induc emisie laser și răcire cuantică într-un domeniu extins de frecvențe; Cercetarea metodei de conversie optică de la domeniul optic spre domeniul microundelor, prin pomparea rezonanță a sistemelor asimetriche cu două nivele încorporat de un rezonator cuantic unimod; Demonstrarea proprietăților multifotonice ale cavității cuantice care conține un sistem asimetric cu două niveluri, prin suprapunerea multifotonică a stărilor generate.

Noutatea științifică și originalitatea rezultatelor: au fost demonstrate proprietățile noi ale spectrului fluorescenței de rezonanță al fotonilor emiși spontan de către un sistem dipolar cu două niveluri; au fost determinate două mecanisme distincte ale emisiei laser și răcirii cuantice într-un sistem de tip Λ cu trei niveluri cu dipol permanent nenul, implicând procese cuantice unitare și binare; a fost demonstrată conversia frecvenței fotonilor din domeniul optic în domeniul microundelor prin pomparea rezonanță a unui emițător asimetric cu două niveluri încorporat într-un rezonator cuantic unimodal.

Problema științifică soluționată constă în calculul și analiza proprietăților dinamicii cuantice a sistemelor cu două și trei niveluri energetice, care posedă dipol permanent nenul și interacționează cu câmpuri externe coerente laser.

Semnificația teoretică și valoarea aplicativă: în această teză, este investigată dinamica complexă cuantică a unui sistem cu două niveluri, cu dipol permanent nenul, interacționând cu câmp laser. Au fost determinate noi proprietăți ale sistemului dipolar cu două niveluri prin observarea unor aspecte distincte în spectrele fluorescenței la rezonanță ale fotonilor emiși spontan, comprimării fluorescenței de rezonanță și fluctuațiilor cuantice totale, față de cazul neglijării dipolului permanent. A fost cercetat modelul unui sistem de tip Λ cu trei niveluri energetice cu nivel superior cuplat cu un oscilator cuantic unimodal. În cadrul acestui model au fost identificate două cazuri distincte de emisie laser și de răcire laser în domeniul THz. În primul caz, modelul este redus la un sistem cu două nivele. În al doilea caz, modelul este extins la un sistem echidistant de trei niveluri, în care frecvența qubitului este apropiată de frecvența generalizată Rabi. A fost modelată dinamica multifotonică a sistemului dipolar cu două niveluri plasat într-o cavitate optică cuantică și cuplată cu aceasta prin dipol permanent. A fost demonstrată modularea frecvenței fotonilor din domeniul optic în domeniul microundelor prin pomparea rezonanță a emițătorului optic asimetric cu două niveluri plasat într-un rezonator cuantic unimodal.

Implementarea rezultatelor științifice: studiile prezentate în această teză au fost implementate cu succes în cadrul proiectului național (15.817.02.09F), cu suportul financiar al Agenției Naționale pentru Cercetare și Dezvoltare, grant Nr.20.80009.5007.07 și cu suportul Bursei Naționale oferită de Federația Mondială a Savanților în Moldova.

АННОТАЦИЯ

к диссертации «Исследования квантовой динамики молекулярных дипольных систем», представленной Александрой Мырзак на соискание ученой степени доктора физических наук по специальности 131.01 «Математическая физика», Кишинэу, 2021

Диссертация написана на английском языке и состоит из введения, четырёх глав, общих заключений и рекомендаций, и списка цитируемой литературы из 205 источников. Диссертация содержит 134 страниц основного текста, 19 графиков и 141 формул. Результаты диссертационной работы опубликованы в 16 научных публикациях.

Ключевые слова: двухуровневая система, трёхуровневая система Λ -типа, постоянный диполь, резонантная флуоресценция, сжатие, терагерцовое лазерное излучение, многоквантовые процессы, квантовая интерференция, генерация фотонов, генерация фононов, многофотонное преобразование, квантовый излучатель, одномодовый резонатор, многофононная генерация, супер-Пуассоновская статистика, квази-Пуассоновская статистика.

Цель диссертации: Обнаружение новых квантовых динамических свойств в двух- и трехуровневых системах Λ -типа, обладающих ненулевым постоянным дипольным моментом, сильно связанным с квантовым оптическим резонатором или оптико-механическими резонаторами.

Задачи диссертации: Расчет и моделирование эффектов сжатия в процессах резонансной флуоресценции двухуровневой системы с лазерной накачкой, обладающей постоянным дипольным моментом; Моделирование спектров полной квантовой флуктуации в дипольных двухуровневых системах с лазерной накачкой; Исследование новых свойств трехуровневой системы Λ -типа с лазерной накачкой приводящих к гибкому лазерному излучению и охлаждению; Доказательство квантово-интерференционных эффектов ведущих к гибкому лазерному излучению и более глубокому лазерному охлаждению; Исследование преобразования частоты из оптической области в микроволновую с помощью резонансной накачки несимметричной двухуровневой системы; Доказательство многофотонных особенностей квантовой динамики резонатора, содержащего несимметричную двухуровневую систему, с использованием некоторой многофотонной суперпозиции генерируемых состояний.

Научная новизна и оригинальность результатов: доказаны новые особенности спектра резонансной флуоресценции спонтанно испускаемых фотонов дипольной двухуровневой системой; в трехуровневой системе Λ -типа обнаружены два различных механизма лазерного излучения и охлаждения, включающие одно- или двухквантовые процессы; доказано преобразование фотонов из оптической в микроволновую область с помощью асимметричного двухуровневого квантового излучателя с резонансной накачкой, встроенного в квантованный одномодовый резонатор.

Основная научная задача, решаемая диссертацией, состоит в вычислении и анализе квантовых динамических свойств малоуровневых атомных систем, обладающих постоянным дипольным моментом, взаимодействующими с внешним когерентным лазерным полем.

Теоретическая значимость и прикладная ценность: в диссертации исследовались новые особенности спектров резонансной флуоресценции спонтанно испускаемых фотонов, сжатия и полных квантовых флуктуаций в двухуровневой системе с лазерной накачкой, обладающей ненулевым постоянным дипольным моментом

Исследованы два различных механизма лазерного излучения и охлаждения в трехуровневой системе Λ -типа с лазерной накачкой. Согласно им, модель обладает одновременно свойствами двухуровневой и трёхуровневой эквидистантной системы.

Исследована квантовая многофотонная динамика двухуровневой системы с неодинаковыми постоянными диполями и преобразование фотонов из оптической в микроволновую частотную область с помощью асимметричного двухуровневого квантово-оптического излучателя с резонансной накачкой, помещенного в квантованный одномодовый резонатор.

Внедрение научных результатов: исследования, представленные в этой диссертации, были успешно внедрены в рамках национального проекта (15.817.02.09F), а также при поддержке Нац. Агентства по Исследованиям и Развитию Молдовы, грант (20.80009.5007.07) и Нац. Стипендии Всемирной Федерации Ученых (Швейцария) в Молдове.

SHORTCUTS

BWO - Backward Wave Oscillators

CW - Continuous Wave

DFG - Difference Frequency Generation

EO - Electro-Optic

EIT - Electromagnetic Induced Transparency

EHF - Extremely High Frequency

FEL - Free-Electron Laser

JCM - Jaynes-Cummings model

PDM - Permanent Dipole Moment

QCL - Quantum Cascade Laser

QD - Quantum dot

QED - Quantum Electrodynamics

QW - Quantum Well

RWA - Rotating Wave Approximation

SPDC - Spontaneous parametric down conversion

TLS - Two - Level System

THz - Terahertz

$\{a, a^\dagger\}$ - the photonic operators

$\{b, b^\dagger\}$ - the phononic operators

$\{S^+, S^-\}$ - the molecular bare-state operators

$\{R^+, R^-\}$ - the molecular dressed-state operators

$\{\tilde{R}^+, \tilde{R}^-\}$ - the molecular double dressed-state operators

γ - the spontaneous emission rate

κ - the damping rate of a reservoir

\bar{n} - the mean phonon number of a thermal reservoir

$\langle n \rangle$ - the mean phonon (or photon) number of a resonator

$g^{(2)}(0)$ - the second-order phonon-phonon (or photon-photon) correlation function

ρ - the density operator

H - the Hamiltonian

Ω - the Rabi frequency

INTRODUCTION

Actual research status:

The quantum properties of light are the object of studies in quantum optical dynamics. During last decades, experimental and theoretical progress emerged together in explaining light-matter interaction and provided a test-bed of various fundamental aspects of quantum mechanics such as coherence, resonance fluorescence, squeezing, laser cooling and quantum entanglement. Quantum optics has a direct and indirect impact on the development of quantum technologies, whose purpose is to integrate non-classical quantum effects in industrial manufacturing and real feasible quantum computational setups. Quantum properties of light are the foundation of the most promising and potentially challenging quantum technologies.

The study of photon dynamics is the core of quantum optics as the concept of *particles of light* has evolved through various stages of theoretical and technological development. The definition of coherent state of photons as eigenstate of the annihilation operator and the description of photon number statistics and the coherence properties of a laser field was proposed by [1]. One of the main advantages of photons is the implementation of quantum technology operating at temperatures that don't require cryogenic level and they are hardly affected by the environment. In order to maintain the feasibility and optical setup portability, photonic circuits are manufactured as *photonic chips*, where all the basic elements embedded into a small chip to fulfill the operational stable requirements. The effort in building photonic chips has been improved to integrate photon sources made of nonlinear materials deposited in the chip for on-chip spontaneous parametric down conversion (SPDC). Using the photonic chips, various problems of photonics quantum information processing have been proved experimentally including boson sampling [2].

The key concept of quantum optics is the exploration of light matter interaction employing the concept of coherent states and used further to explore high-order coherence of light. Squeezed light a non-classical sample of light-matter interaction has played a major role in quantum optics development [3]. Quantum optics manages to combine both theoretical and applied technology studies. Thus, squeezed light enables a new type of precision measurement, with application in gravitational wave detection [4] and for noiseless communication [5]. In particular, a squeezed vacuum is generated by spontaneous parametric down conversion (SPDC) and is the most frequently used process to generate squeezed states, but also, for example, to generate single and entangled photons. Though isolated two-level systems such as an atom, an ion, a quantum dot or a defect in a

diamond are also proper candidates to generate single photons [6].

The Jaynes-Cummings model (**JCM**) provides the description of interaction between a two-level system, for example an atom, and the modes of the electromagnetic field, gives the best theoretical tools for studying the non classical features of atom-light interaction [7, 8]. The major consequence of the field quantization was the collapse and revivals of Rabi oscillation, which was checked experimentally in quantum electrodynamics (**QED**) setups. Beside this Jaynes-Cummings model (**JCM**) offers an information theoretic approach for the study of cavity field dynamics, which was initially prepared in a large amplitude coherent state and well turn into a coherent superposition state at a certain interaction time. While quantum optics studies the physics of light-atom interaction, quantum information focuses on the properties and applications of the qubit, which is a quantum bit and the quantum-mechanical extension of a conventional bit $\{0, 1\}$. The quantum-mechanical superposition of the qubit is the counter part of the coherence in quantum optics. The superposition of multiple qubits leads to entanglement and the information procession in a non-classical way. Thus a quantum computer is able to compute complex factoring algorithms in a more effective way than standard computers. A scheme of creating one-time pad between distant partners using non-classical light fields prepared in superposition states was proposed by [9]. The further development of quantum technology and quantum information processing is based on the ability to control and manipulate the coherence of a quantum system as one of the main challenge is the system's interaction with the environment. Consequently, there have been done extensive studies of decoherence in the framework of Markovian and non-Markovian open quantum systems [10].

The quantum optical properties of two-level systems interacting with electromagnetic field constitutes the basis for a wide spectrum of applied problems, including laser science [11], fluorescent spectroscopy [12], nano-imaging [13], design of single photon and multiphoton sources [14, 15] and efficient light emitting devices [16]. It has a certain impact in the development of quantum information theory in the context of coherent qubits control. In particular, single photons are the main tool for quantum key distribution using the quantum informational protocol and for more advanced schemes, required for long-distance quantum communication. The information is usually encoded in the polarization of the photon, and in sources emitting single photons on-demand with high entanglement are of major importance for the implementation of quantum information protocols. In this context, semiconductor quantum dots (**QDs**) are two-level systems perfectly functioning as triggered sources of single photons. Also, quantum dots (**QDs**) are highly advantageous because at resonant excitation they emit single photons with outstanding quantum properties of multiphoton

suppression and photon indistinguishability [17].

Indeed, one can say that the advances of modern quantum optics are based on the concept of a few-level system. Beside Jaynes-Cummings model used to describe a laser single mode driven two-level system, the projection into the Fock states is used to derive the complex quantum dynamical statistics of the emitted field. Additionally, some other relevant approximations are employed to picture coherent light-matter interaction. First, the dipole approximation presumes that the wavelength of the radiation field is much greater than the atomic dimensions and rotating wave approximation (**RWA**) considers only near resonant terms are effective and essential in studying light-matter interaction. Not enough to describe the radiation-matter interaction, the concept of *dressed states* was introduced by [18] for two-level systems to complete the rotating wave approximation (**RWA**) explaining experiments in the regime of microwaves [19].

The theoretical aspects of light-matter interaction often describe the quantum optical system dynamics using the non-diagonal matrix element of the dipole moment operator. However, many systems possess non-zero permanent dipole moment such as polar molecules, an atom polarized by static electric field or an asymmetric quantum dot [20], magnetic dipole atomic transitions detected in rare-earth ions [21, 22] possess a non-zero magnetic dipole different from the case of electric dipole transitions, which are considered zero for atomic eigenstates.

In the majority of studies, two-level systems (**TLS**) are considered to possess a certain spatial parity, or their diagonal dipole matrix has a zero value. However, two-level system with permanent dipole moment or two-level systems (**TLS**) with broken inversion symmetry exhibit appealing properties. Some of the following features have been proved in two-level systems (**TLS**) with broken inversion symmetry: high harmonic generation [23], two-color multiphoton resonances [24], additional resonances in nondegenerate four-wave mixing [25], high reflectivity two-photon phase conjugation [26], new set of peaks detected in the emission spectra [27], revivals and collapse of Rabi oscillations [28, 29], population inversion [30], and enhanced features in the one- and two-photon nonlinear absorption and dispersion [31]. Quantum systems possessing permanent dipole moment are widely explored in the context of multiphoton processes. It was proved that the presence of permanent dipole moment enforces certain changes in multiphoton absorption rates. Dipolar quantum systems can radiate at Rabi frequency and can serve as emitters in the THz frequency region. Also, two-level systems with permanent dipole manifest population inversion in the steady state if they are pumped by two monochromatic laser fields.

Two-level systems exhibit an important non-classical property, namely, the squeezing of the field quadratures in the resonance fluorescence spectrum. In connection with development of

highly precision measurement devices and quantum computation, the squeezing of the fluorescent field is an endeavouring research subject of laser driven two and three-level systems. Therefore, the issue of generation non-classical light with enhanced squeezing in dipolar few-level atomic systems is still an interesting area of study. More over the presence of permanent dipole moment (**PDM**) changes straightforward the optical feedback of the system, for example, modification in multiphoton resonant excitation [32, 33]. Regarding the three-level quantum systems possessing a permanent dipole moment (**PDM**), one notes their novel feature to embedded simultaneously the properties the two- and three-level systems as function of the tunable Rabi frequency due to the laser driving due to the presence of permanent dipole moment [34, 35]. Also quantum systems containing a supplementary quantum state reveal a large class of coherent interference effects, as well as the application of three-level qubits in composing and testing quantum protocols and information storage. One of the best experimental examples of three-level systems possessing a permanent dipole moment are semiconductor quantum wells (**QW**), which exhibit quantum interference due to interband transitions and intersubband absorption due to asymmetric structure of the system [37]. The permanent dipole moment within three-level systems influences the levels shifting due to charge redistribution, as well the permanent moments interact with optical fields-an aspect rather less studied.

Consequently, few level atomic systems possessing a non-zero permanent dipole moment can be used for tunable generation of electromagnetic waves. This is especially laborious for frequency ranges where known methods are inefficient, such as terahertz (**THz**) domain [38]. This domain is especially challenging because it lies between radio and optical frequency ranges, thus neither optical nor microwave techniques are not suitable for generating **THz** waves. Therefore, a search of novel and effective **THz** radiation sources is an emerging task for applied and theoretical quantum optics. Also, multiple quanta processes are considered feasible quantum technologies within few level atomic systems. Thus, the non-resonant multiphoton conversion from optical to microwave and vice versa region is an emerging task.

The purpose of the thesis:

The computation and analysis of quantum dynamical properties of few level atomic systems possessing a permanent dipole moment interacting with external coherent laser fields.

The objectives of the thesis:

- The demonstration of impact of permanent dipole moment (**PDM**) in the resonance fluorescence, squeezing and total quantum fluctuations spectra of a two-level system.
- The investigation of a laser-pumped three-level Λ -type system the upper energy level coupled with a quantum oscillator described by a single quantized leaking mode.
- The demonstration of quantum interference effects induced by emitter's dressed states responsible for flexible lasing and deeper cooling effects.
- The investigation of the possibility of frequency conversion from optical to microwave region, via the resonant pumping of an asymmetrical two-level system incorporated in a quantized single-mode resonator.
- The demonstration of multiphoton features of cavity quantum dynamics containing an asymmetric two-level system using certain multiphoton superposition of generated states.

Research hypothesis:

Two- and three-level systems possessing a non-zero permanent dipole moment interacting with external coherent laser fields exhibit important nonclassical features. Consequently, the permanent non-zero dipole moment becomes an advantageous tool to engineer the properties of novel quantum systems exhibiting novel properties in comparison to the similar systems yet in the absence of permanent dipoles will be demonstrated below.

Analytical methods:

- The rotating wave approximation has been applied in order to neglect the quickly oscillating terms in the Hamiltonian and keep only terms expressing detunings or frequency differences. As well, the Born-Markov approximation has been adopted in order to eliminate the vacuum modes of the electromagnetic field reservoir.
- The method of transformation into the interaction picture was applied in order to remove the time depending terms in the system Hamiltonian using a time dependent unitary operator. Rewriting the Schrödinger equation in the interaction picture using the unitary transformation operator, one has modified properly the system Hamiltonian.
- The method of projecting the Bloch equations has been applied in order to describe the evolution of atomic operators, due to the driving and spontaneous emission of the system. An equivalent procedure involved the derivation equations of motion for single or more average operators, which is possible in the Heisenberg picture.
- The method of projecting the master equation into Fock states basis has been applied in order to detect the quantum dynamics of the system, described by a solvable system of coupled equations projected in the system state basis. This methods permits one to derive from the equation of motion the investigated parameters describing the system dynamics.

Obtained scientific results to be defended:

- Detection of new spectral lines in the resonance fluorescence emission in the two-level systems with permanent dipole moment.
- Demonstration of extra squeezed frequency domains in the two-level systems with permanent dipole moment.
- Identification of two disting lasing and cooling regimes in a laser-pumped three-level Λ -type system.
- Possibility to identify sources of coherent terahertz photons generation in a laser-pumped three-level Λ -type system.
- Investigation of quantum multiphoton dynamics of a two-level system possessing unequal permanent dipoles, placed in a leaking single-mode quantized cavity field.

Thesis's structure:

In the **first Chapter** is presented a review giving a certain insight in the quantum dynamical phenomena detected in few level atomic systems possessing a permanent dipole moment. This chapter highlights that these systems are the proper models suitable for the description of and forecasting new light-matter interactions and propose feasible quantum-optical devices with a wide range of emerging applications. One has over-viewed the two-level system framework altogether with phenomena and applications embedding them. Another specially interesting discussion in this chapter regards the lasing and cooling phenomena in quantum optical systems. The topic of THz waves and multiphoton states generation in quantum optical systems is also considered. Nevertheless, the impact of permanent dipole moment on the quantum dynamical properties of various setups is still neglected and presumed to be zero. Thus, one has contoured the missing block of last decade researches in the field of quantum optics and helped one to define the problem considered in the thesis.

In the **second Chapter** is considered a two-level system possessing a permanent dipole moment interacting with two external coherent field. One of them has a near resonant frequency with the transition in the two-level system, while the second one has a resonant frequency with the transition between the dresses-state levels generated by the first laser pumping. The purpose of the chapter is to model the influence of the non-zero dipole moment on the resonance fluorescence and total quantum fluctuations processes in the two-level system. The system has been described using the semi-classical laser-molecule dressed-state picture due to the first laser pumping. The dressed-state transformation was applied to the system in order to project the system Hamiltonian at the frequency of the second laser. The Hamiltonian describing all types of interactions detected in the system is presented. Unlike, earlier published similar problems yet in the absence of the permanent dipole moment, one will present the fluorescence spectrum, which will exhibit supplementary spectral lines and additional squeezing regions will be shown, within the corresponding chapter.

In the **third Chapter** is investigated the quantum dynamical properties of a quantum oscillator coupled with the most upper state of a three- level Λ -type system, which possess orthogonal dipole moments and is coherently pumped with a single or two electromagnetic field sources. These systems are particularly compelling for engineering of novel quantum systems exhibiting lasing in a wider range of parameters, lasing and cooling in adjustable microscale and nanoscale devices. The chapter discusses the determination of flexible ranges of lasing and cooling phenomena determined

by the quantum oscillator's degrees of freedom and describes the mechanism behind them. Also, in this chapter is proved the interplay between single- or two-quanta processes appearing with quantum interference effects among the induced emitter's dressed states are in charge of flexible lasing or deeper cooling effects. Consequently, this conducts to reciprocal influence between the quantum oscillator's dynamics and the three-level emitter's quantum dynamics. Additionally, one has determined that the quantum setup presented in this chapter is suitable for terahertz photon generation.

In the **fourth Chapter** is investigated the multiphoton dynamics of a two-level system possessing non-zero permanent dipole moment, which is placed in a leaking single-mode quantized cavity field and coupled to it. The frequencies of the cavity and the two-level system are presumed to belong to different range frequencies: microwave and optical. Thus the presented setup consists of two interacting subsystems, which are coupled through the permanent dipole moments. Thus, the created highly dispersive regime in the system results in multiphoton quantum dynamical behavior and causes photon conversion from optical to the microwave range. The chapter gives the description of the system Hamiltonian required to derive the master equation adopted for the characterization of the multiphoton emission processes. The calculations were completed by considering the accompanying damping effects due to qubit's spontaneous emission and cavity's photon leakage. The main result presented in the chapter is the demonstration of photon frequency conversion from optical to microwave, via resonantly pumped asymmetrical two-level quantum optical emitter placed in a quantized single-mode resonator. The chapter contains the demonstration of multiphoton states generation feasibility. The corresponding photon statistics changes from super-Poissonian to quasi-Poissonian is assigned particularly in the chapter and the physical mechanism behind it is explained.

1 MOLECULAR DIPOLAR SYSTEMS IN QUANTUM OPTICS

In this thesis we consider the quantum dynamics of few level atomic systems possessing a permanent non-zero dipole moment and coupled to an optical or mechanical cavity. Few level atomic systems are considered a proper theoretical model to explore and forecast the non-classical features of real materials as atoms, artificial atoms, quantum dots, which are attractive candidates for many optoelectronic devices as single-photon sources, multiphoton sources, frequency down-converting devices, phonon lasers, lasing or cooling in a wide range of parameters, and computational building blocks of a quantum computer.

Thus in this chapter, one gives a review of quantum dynamical phenomena observed in few level atomic systems, alongside with approximations and assumptions considered while research. This review helped one to contour the missing building block in revealing non-classical features of few level atomic systems possessing non-zero permanent dipole moment and consequently formulated the problem considered in this thesis.

The introductory chapter consists of five paragraphs considering different aspects of few level dipolar atomic systems interacting with coherent light. In the first paragraph 1.1, one presents the two-level system framework overview and the experimental setups described within this framework and the phenomena occurring within them. In paragraph 1.2, one reviews the resonance fluorescence and squeezing detected in two-level systems possessing a permanent dipole moment, which describes the non-classical aspects of light-matter interaction and is presented graphically by the Mollow spectrum. The physics underlying the Mollow spectrum is presented as well with the framework of dressed-state picture.

Another particularly interesting discussion about cooling phenomena in quantum optical systems is presented in 1.3, where are reviewed the existing cooling techniques, setups and the practical usefulness of laser cooling. In paragraph 1.4 one presents the terahertz lasing methods and the motivation to propose devices functioning in the THz-gap. In paragraph 1.5 one discusses the multiphoton behave of quantum dipolar systems, which can generate multiple photon states required for the practical building of the quantum communication channels based on photons, so-called flying bits. An overall conclusion is given in paragraph 1.6.

1.1 Two-level systems possessing a permanent dipole moment

Two-level systems have attracted much attention since the early years of development of quantum mechanics. A two-level system may be considered a spin-1/2 systems or two level atoms pumped by a classical electromagnetic field, exhibit a wide range of phenomena as self-induced transparency, photon echoes, Autler-Townes splitting, dynamic Stark splitting, Rabi oscillations [39, 40, 41]. Simple two-level model exhibits rich physics and is advancing constantly the understanding of the light matter interaction. Here it is important to remind that in the early 1937 Rabi [42], foresaw that in the presence of a classical single-mode field, a two-level systems exhibits periodical flips between its states. This paragraph reviews varies classes of quantum optical and quantum mechanical devices, which are treated theoretically as two-level systems. Further one will contour the requirement to consider the permanent dipole moment (**PDM**) and its impact on the properties of these devices.

In the current period, a renewed interest is directed to two-level systems, as they are considered as an essential source of quantum fluctuations or and decoherence in various quantum devices. This enlists superconducting quantum bits or briefly named qubits. Quantum bits or qubits are resonant microwave frequency circuits, built from micro-structured inductors, capacitors and Josephson junctions. For the proper functioning of such devices, it is required to have two states or eigenstates, which are considered as logical states, $|1\rangle$ and $|2\rangle$ and transitions between these states can be driven to realize logical quantum gates. The main issue in this circuits is the existence of several excited states, they are required to be anaharmonic so that all transition frequencies are separable. This is achieved by embedding the Josephson junctions [43, 44, 45], which can be modeled as nonlinear inductors tuned through a bias current or a magnetic flux. From the first experiment detection of coherent quantum dynamical behave in Cooper pair box in 1999 [46], qubits developed into of the leading tools for the implementation of large-scale quantum computing. Nevertheless, fluctuations and losses occurring due to coupling with two-level system present a significant source of decoherence and a parameter measuring the fluctuations for superconducting qubits.

Thus the physics of two-level systems makes up the basis for quantum optics and quantum cavity electrodynamics. It is also a widely employed model in the field of photonic quantum technologies, because it allows a secure exchange channel of information through the single photons and it is a proper tool for efficient quantum computation using linear optics. This means that two-level systems and the single photon transitions within them are the basic source for quantum key distribution in certain approved quantum computing protocols and for more advanced schemes, which could comprise a quantum repeater for remote quantum communication. In such quantum

computing protocols requires secure direct communication. This is achieved through encoding of information in the polarization of the photon, also employing the sources emitting single photons with high indistinguishability or entanglement. In this circumstances, the technological implementation of quantum computing protocols is realized in the quantum dots, which are almost ideal two-level systems, acting as sources of single photons, where material properties can be used for generation of linearly polarized photons [17].

Currently, quantum circuits are manufactured from superconducting aluminium as it allows to fabricate high-performance Josephson junctions using evaporation techniques. An amorphous oxide layer is growing on the sample once exposed to air. This layer is described by large dielectric loss, which corresponds to high density two-level system in the amorphous material. If the two states of a two-level system are used to describe the displacement of a charge, then the system possesses an electric permanent dipole which coupled it to the oscillating electric field present in capacitive resonant circuits. In two-level systems build in the few nm-thin Josephson junction, where the electric field strength is up to 100 V/m, the coupling is strong. Strong coupled two-level systems are not efficient for qubit operation as their coherent interaction with the circuit dynamic properties provides a tool towards direct control of the state of microscopic defects using macroscopic host device. Considering two-level systems built in a quantum device, it is necessary to know the classification of two-level systems as function of incoherent and coherent processes within it. Each particular two-level system is coupled to an ambient environment consisting of phonon modes at a certain temperature T or other quasiparticles formed from residual charge carriers in the superconducting device. The type of coupling leads to incoherent or coherent transitions between two-level systems eigenstates such as dissipation, excitation, random fluctuations and energy dephasing.

Another class of two-level systems are name fluctuators. This devices are in strong coupling with their own environment and incoherently flip between states the system. The incoherent transitions between the two states are due to quantum tunneling through the barrier and decoherent transitions take place due to the coupling to the environment.

On the other hand, coherent two-level systems are the ones in which the coupling between the two-level system and their environment is weak enough, so it can remain in one of their eigenstates, or in a coherent superposition of states, during a short time. A feature specific for coherent two-level systems is the energy splittings, which are larger than the thermal energy of the environment, $E > k_B T$ [47]. Strong coupling regime with the host environment of coherent two-level systems is described by a coupling strength that exceeds the decoherence rate of both two-level systems and

the host environment. The change of coupling regime modifies the energy level structure and the quantum dynamical behavior of the two-level system and the host environment, for example anticrossings in qubit spectroscopy. Both quantum fluctuators and coherent two-level systems may be formed in the same physical entities or devices. However, the difference between fluctuators and coherent two-level systems are useful to be considering while distinguishing the dynamical effects arising from the individual system and the host environment [48, 49].

The development of semiconductor nanotechnology boosted the considerable research and construction of photonic devices in the quantum limit. In this context, structures embedding quantum dots (**QDs**), which are acting as two-level quantum emitters of single photons or might be considered as sources of entangled photons for the upcoming quantum communication networks. For example, microlasers embedding quantum dots (**QDs**) exhibit a certain advantage due to the spontaneous emission coupling into the lasing mode, which makes possible to construct microlasers with ultra-low thresholds and having several **QD** or single **QD** as gain medium [50]. Lasing devices containing quantum dots (**QDs**) have an improved sensitivity and properties allowing to study the nonlinear effects in quantum systems like dynamical antibunching in the photon statistics of the emitted light or thermal bunching [51]. Supplementary, semiconductor quantum dots (**QDs**) incorporated in an optical cavity placed in a magnetic field serves as an alternative setup for linear optical quantum computing schemes, which use photons as qubits suffering of slight decoherence. Resonant scattering generates photons emitted from the quantum dot, while the magnetic field detects the encoding of the photons. Thus multiphoton states can be step by step built up [52]. In this way, nonlinear-optics and nanophotonics are paving the way for engineering of physical elements assuring advanced secure communication networks.

In majority of studies, the ground and the excited states of a two-level system possess a certain spatial parity or the diagonal dipole matrix elements are zero. Appealing properties and phenomena exhibit two-level systems with broken inversion symmetry like: high harmonic generation [23], two-color multiphoton resonances [24], additional resonances in non-degenerate four wave mixing [25], two-photon optical bistability [53], new set of peaks in the emission spectra [27], collapse and revival of Rabi oscillations [29], population inversion [30] and enhanced features in the one- and two-photon nonlinear absorption and dispersion [31].

All these theoretical and experimental researches have been performed in the framework of symmetry inversion approximation. Formally, in systems with broken inversion symmetry the transversal and but also longitudinal coupling with electromagnetic field becomes possible. This circumstance opens a radiative channel between the neighboring dressed levels at Rabi frequency.

Nevertheless, the violation of the inversion symmetry is emergent in many quantum setups and arises from nonzero permanent dipole moment (**PDM**) matrix elements of the ground and excited states. For instance, in polar molecules [54, 55] permanent dipole moments arise from parity mixing of the molecular states, but in quantum dot-artificial molecular systems it is generated due to the asymmetry of the confining potential of the dot. The existence of permanent dipole moment is not just a theoretical assumption, it is an experimentally proved fact determined in several experimental systems [56, 57, 58, 59, 60]. The presence of nonzero permanent dipole moment changes considerably the optical features of the system, leading, for instance to modification of multiphoton resonant excitation, creation of the second harmonic-generation, correlated photon pairs, additionally, the generation of new optical transitions within the system possessing a permanent dipole moment.

The coherent excitation of quantum systems with permanent dipole moment is an area of active research in last decades. Most theoretical researches regarding nonlinear features of atoms and artificial molecules, namely quantum dots, drop off the presence of permanent dipole moment. Dipole systems include polar molecules [61, 62] and some solid materials [57, 63]. The features of coherent nonlinear optical processes within polar systems can be greatly change, due to the permanent dipole moment itself. For example, the extension of harmonic spectrum was detected in a dipolar gas, both the odd and even harmonics parts of the spectrum was extended [64].

Nevertheless, the effects of permanent dipole moments, themselves can be manipulated by the electric field applied to the quantum system. It has been found that the improved ionization of the asymmetric molecule (HeH^{2+}) is much more deep if the electric field is applied antiparallel to the permanent dipole moment in comparison the parallel application of the field to the permanent dipole moment [65]. This effect is proved by a stronger emission when the electric field pulse is antiparallel to the permanent dipole moment. The corresponding physical picture of this phenomena involving two-level systems with permanent dipole moments can be illustrated in the dressed state picture or interpretation [66].

These advances in laser physics, nanotechnology have established the proper base for researching the strong light-matter interaction in various quantum systems. In comparison to weak electromagnetic field, the interaction between electrons and a strong field is impossible to be considered as fluctuation or perturbation. Thus, the system consisting of electron interacting with the strong field is generically considered as electron-field composite system, which is named *electron dressed by field* or *dressed states* [67].

The concept of dressed states appears also in systems placed in a strong external laser field.

The generation of dressed states was foreseen in a wide range of experimental systems: solid-state setups, bulk-semiconductors, mesoscopic structures. The energy separating dressed states is named Rabi splitting, which can be easily tuned by the intensity of the dressing field. The radiative transitions between the states of the electromagnetically dressed systems was predicted theoretically and proved experimentally in various setups, such as systems with broken inversion symmetry, atomic media, condensed-matter structures and superconducting circuits.

The field-induced changes of the physical features of the dressed electrons was explored in atomic systems, various condensed-matter structures, graphene, quantum wells, quantum rings, quantum dots, which are named in sources *artificial atoms*, being the most perspective materials for applications in nanophotonics, as in contrast with natural atoms, quantum dots due to strong built-in electric field acquire anisotropy or inversion symmetry. This makes quantum dots specially attractive for the theoretical and experimental of quantum optical effects [68].

1.2 Resonance fluorescence and squeezing in molecular dipolar systems

Light-matter interaction is specially interesting for several reasons because light scattered from matter contains a lot of information about the matter itself and generating quantum light sources is crucial for new applications in quantum technology. A generic example is the interaction of a coherent laser beam, with a quantum optical cavity or quantum optical resonator, which as the output generate non-classical light or photons exhibiting non-classical features such as fluctuations, squeezing, and or resonance fluorescence.

Resonance fluorescence is a simple and most fruitful phenomenon describing the light-matter interaction, playing a major role in understanding the particularities of the quantum dynamical interaction of light and matter. Basically, it describes the photon emission of a two-level system that is coherently pumped and it further emits photons and the same coherent drive frequency. Also, resonance fluorescence offers a straightforward graphic demonstration of quantization of the coherent light field [69, 70].

For the first times, resonance fluorescence in the high excitation regime was observed and theoretically described in 1969 by Benjamin Mollow [71]. Also, he has been the first to observe the crossing at resonance of a low-density gas of sodium atoms with a dye laser beam with a two-level Na atom transition, namely the $F = 2 \rightarrow 3$ hyperfinetransitions of the D_2 line. Thus, the obtained spectra of resonance fluorescence from highly-driven two-level dipolar system had a peculiar line shape, namely a triplet. The general solution of the problem in the case of the arbitrary strong driving field has been derived by Mollow. It is necessary to mention in this context that Mollow's approach is based on optical Bloch equations (**OBE**), resonance fluorescence is explained as emission of photons by an atom pumped by laser field. Additionally, the quantum features of the vacuum field is dropped off from the consideration, and all physical features of the emitted radiation are expressed through the terms of operators for the atomic variables. Also in this approach, the atomic system, treated in the framework of the dipole and rotating wave approximation, interacting with an isotropic radiation reservoir is mathematically solved employing an effective one-dimensional model. This type of mathematical approach is used in several theoretical problems: in condensed matter this is specific for the theory of magnetic alloys and in quantum optics this approach is used in the theory of Dicke superradiance in which a bosonic field interacts with an impurity, which in quantum optical problems usually is considered an atom.

The interpretation of the resonance fluorescence Mollow triplet of the two-level system is interpreted within dressed-state base formalism. The laser pumped dressed-state base gives rise to new eigenstates $|\pm\rangle$, which consist of a combination of bare states: ground and excited, noted with

corresponding letters g and e , namely $|g, n + 1\rangle$ and $|e, n\rangle$ and n is an integer number counting the number of photons from the laser. Eigenstates of the two-level system due to dynamic Stark splitting form a family of such states whose total energy is equal with each other, form a *manifold of excitation*. Each *manifold* consists of eigenstates, which are split by the Rabi frequency, while the energy difference between two neighboring manifolds is that of the bare states, or their average if it is non resonant. The transitions between neighboring manifolds hold several features: the spectra consisting of three peaks, named *triplet*, in which the total spectral intensities of its peaks shape correspond to 1 : 2 : 1 proportions, in case of resonant laser pumping of a two-level system. The Mollow triplet spectrum has become a universal signature of quantum system exhibiting resonance fluorescence and cannot be interpreted within optical optics. The basic features of the Mollow triplet are the following: the central peak occurs at the driving laser frequency and the sidebands are displaced from the central peak by the Rabi frequency. At resonance, the resonance fluorescence spectrum is dominated by incoherent emission, also a radiative cascade emission generates photon antibunching and blinking. These features were proved experimentally in artificial atomic systems as quantum dots, and nitrogen vacancy defects.

The physics and properties of the underlying states $|\pm\rangle$ are quantitatively described in the dressed state picture. The usual quantum optics approach allows to make the following assumptions: the two-level system is driven by the incident field and relaxes as the radiation field, namely a reservoir of un-occupied photon modes, gains population by fluorescence. The solutions of the quantum optical Bloch equations are derived in the rotating wave approximation (**RWA**), which allows to obtain analytical expressions. The solutions with rotating wave approximation (**RWA**) account for quantum dynamics describing the resonant photon emission transition. The theoretical efforts regarding the explanation of photon correlations in the Mollow triplet spectrum have been limited to photon computation from the peaks. At the same time, the theories of frequency-resolved photon correlations generate complex models, involving laborious computations to adjust all the time-orderings of the radiated photons. Particularly, if we expand the correlations to a greater number of photons then we tackle this problem through approximations based on the dressed-state picture. Below, one is reviewing some basic theoretical frameworks developed to explain the physics of resonance fluorescence in certain particular quantum optical systems.

Apanasevich and Kilin [72] have been among the first to derive the theoretical framework of dressed-state picture and used it to compute the photon correlations between the peaks and predicted the qualitative cross-correlations between the peaks, such as photon antibunching for the side peaks, corresponding to emission and bunching between them. Independently from them, Co-

hen Tannoudji and Reynaud [18] have explored the photon correlations between the side peaks of Mollow triplet. Their research confirms the radiative cascade occurring in the two-level system using the dressed-state picture formalism. Scharma et al.[73] have improved the theory regarding the resonance fluorescence in the two-level system. They have taken into account the interference between the emitted photons, which outcomes for example in antibunching between a side peak and a central peak contesting the assumption of uncorrelated emission proposed in earlier theories. Ulhaq et al.[74] has revised the photon correlations of peaks in resonance fluorescence spectra of an quantum dot In(Ga)As.

Carreno et al. [70] in their paper proposed an exact description of high-order photon correlations from the Mollow triplet spectrum and proposed setups which extend the field of possible experimental configurations and applications, which have been already intensively explored, replacing real-state transitions by strongly correlated leapfrog transitions. The resonance fluorescence line spectrum explored by them reveal rich physics standing behind it. The two-photon correlation spectrum describes the direct transitions from one manifold to the following two manifolds situated below, jumping over intermediate manifold in the bottom of the ladder. The photon transitions involved here result in strong correlations of the emitted pair of photons. The two-photon correlation spectrum proved that the interpretation of the Mollow triplet peaks are particular cases of a more complicated process.

Further, Kryuchkyan et al.[68] have elaborated the quantum theory of resonance fluorescence for bichromatically dressed quantum systems. Their aim was to fill the gap between quantum optics and physics of nanostructures. The problem was solved within strong light-matter interaction regime. The interaction of an asymmetric quantum dot with a bichromatic laser is greater than the spontaneous emission and spontaneous decay of quantum dot excitation. The obtained spectral lines of resonance fluorescence spectrum for an asymmetric quantum dot driven by a bichromatic lasing field were analyzed using the concept of quasienergetic or dressed electronic states. The asymmetry of the quantum dot is described by a non-zero difference of diagonal dipole matrix elements. As a result, the obtained resonance fluorescence spectrum has the following features: an infinite set of Mollow triplets, the quench of fluorescence peaks generated by dressing field, and the oscillating aspect of the fluorescence intensity as a function of the dressing field amplitude.

On the other side, Florescu et al.[75] developed an exact multiphoton scattering theory of the resonance fluorescence in a frequency-dependent photonic reservoir. In their approach, the resonance fluorescence is generated by scattered laser photons on the atomic systems. This approximation is applicable for any arbitrary laser's field intensity. Additionally, the proposed approach has

no coupling restrictions between atom and reservoir, required for the perturbational methods and can be applied for any non-Markovian system. The resonance fluorescence spectrum was derived using optical Bloch equations without Born-Markov approximation. Also, the spectrum for a certain quantum state of the incident field, one has to compute the average of the Mollow spectrum over this quantum state, only if the incident light is in a coherent state. They have proved Mollow spectrum dependence of quantum-statistical properties of incident light.

Additionally, Anton et al.[32] presented the optical quantum dynamical properties of the scattered field by a quantum emitter with broken inversion symmetry. The polar system interacts with an optical fields, which generates the electronic transitions and at the same time is irradiated with a second low-frequency field that coupled to the non-zero permanent dipole moment. The effective Hamiltonian is derived in the double-dressed state basis, used for the computation of resonance fluorescence and squeezing spectra. The shown resonance fluorescence spectrum exhibits nine spectral lines or three triplets. This achievement is contrasting to the Mollow triplet well-known for systems without permanent dipole moment. The peak value of each triplet depends on the Rabi resonance condition of the two driving fields also the second low frequency driving fields tunes the spectral features. Additionally, the squeezing spectrum of the resonance fluorescence, where some reduced fluctuations were detected at certain sidebands. These research is of high interest due to its potential application in quantum information technologies, quantum amplifiers and attenuators. Resonance fluorescence spectrum exhibits a number of interesting features such as asymmetries and suppression of the spectral lines. Asymmetries of the spectral lines occur when the fluorescence field of the two-level system is damped by the thermal field. Unusual features are detected only at the central line of the incoherent component part of the spectrum and is assisted with a decay of the spontaneous emission from the system.

Zhou et al.[76] have shown some anomalous features arising in the spectrum in the bichromatic case, for a weak squeezed vacuum and high intensities of the bichromatic field. Under bichromatic irradiation of the two-level system, the resonance fluorescence spectrum consists of a series of symmetric sidebands situated by half of the frequency difference between the two frequencies of the driving field. The manifolds of the dressed states make up a quantum ladder of populations. The dipole coupling allows transitions from one manifold to another, with no spontaneous transitions within each sublevel. In the spectrum presented by them, the sidebands are separated independently of the Rabi frequency of the driving field. However, the number of the sidebands increases as function of the Rabi frequency. Also, it was observed the spectrum is changing getting an asymmetric aspect and the central peak and even sidebands split into doublets when the components of

the bichromatic field have unequal amplitudes. Thus the resonance spectrum contains more peaks because of the symmetric distribution of populations is broken and dressed state levels are strongly displaced as function of amplitudes ratio.

In the above, we have shown that the Mollow triplet reveals a lot of information about light-matter interactions proven by quantum correlations and dressed-state transitions. We have shown the Mollow spectrum for resonance fluorescence is derived straightforward from the dipole-approximation Hamiltonian, using Born-Markov approximation. Also, the occurrence of the spectral features for various experimental setups and theoretical approaches. This review explains the possibilities residing in the Mollow triplet. It means that resonance fluorescence phenomenon portrayed by Mollow triplet is still of great interest for endeavoring for quantum computing using photonic sources as programmable quantum input.

Despite the conceptual simplicity of resonance fluorescence, as Mollow triplet emission spectrum, it possesses a fundamental feature-squeezing in the form of reduced quantum fluctuations in the single photon stream emitted by an atom in free space, was predicted by Walls and Zoller [77, 78, 79]. In 1981, Walls and Zoller have foreseen that the quadratic squeezing can be generated through different methods: the interaction of a two-level system with a coherent light field, described Jaynes-Cummings Hamiltonian [77]. They have proved that fluctuations in one quadrature, expressed by their variance, can be minimized theoretically up to 12,5 percent lower than vacuum fluctuations, keeping the intensity statistics antibunched. In comparison with nonlinear optics, the specific form of squeezed light comes from atomic coherence, which, once projected onto the emitted field, outcomes in the creation of coherent states in the weak excitation regime. Higher number states are dropped off by photon antibunching or by the fermionic features of the atomic operators. Namely, Walls and Zoller have investigated an unusual source of non-Gaussian quadrature squeezing obtained in the multimode resonance fluorescence field of a driven two-level emitter, where the emitted photons are antibunched. Photon antibunching was experimentally proved using a semiconductor quantum dot platform, which exhibits the necessary high photon collection efficiency which is impossible to observe in most atomic setups. The two-level system emitter setup relies on the steady-state coherence between the ground and the excited state, i. e. a state expressed in the following form $|g\rangle + c|e\rangle$ with some appreciable c . In the ordinary regime of atomic resonance fluorescence only a reduced set of atomic coherence expressed through the values of c can be explored, and squeezing is possible to achieve in the weak-driving limit, with squeezing values rather smaller than the fundamental bound for a two-level system [77].

Squeezed light has become a naturally extended source of continuous variable quantum infor-

mation applications. Squeezed states can be generated by reducing the fluctuations of the variance of the electric field below the vacuum with respect to some phase [80]. These states are employed to improve the accuracy in interferometric measurements metrology applications, as well the interferometric power of Gaussian systems in a squeezed thermal bath [81] and for quantum key distribution. The Markovian dynamics of the Gaussian interferometric power of two-mode Gaussian states, for a system composed of two bosonic modes, each of them interacting with its squeezed thermal bath was investigated by [81]. The dynamics was modelled within the approach of the theory of open systems based on completely positive quantum dynamical semigroups. Additionally this dynamics was described in terms of the covariance matrix for Gaussian input states. According covariance matrix, the behaviour of the Gaussian interferometric power depends on the initial state of the subsystem (squeezing parameter and thermal photon numbers) and on the parameters describing the squeezed thermal reservoirs (temperatures, dissipation coefficient, squeezed parameter of the baths and squeezing angle). Regardless of the initial state, in the limit of large times the Gaussian interferometric power decays asymptotically to a zero value.

Experimentally, squeezed states can be generated by various methods, and a various classes of squeezed states have been simulated theoretically. In this context, we can mention the canonical Gaussian squeezed coherent states, also various non-Gaussian squeezed states are generated by photon addition or subtraction, or by building superpositions of Gaussian coherent states [82, 83]. Currently, the highest level of squeezing has been obtained in a squeezed vacuum environment employing an optical parametric amplifier.

Various phase-dependent nonlinear optical processes are used to accomplish the experimental realization of the squeezed states of light [84]. Some of them include parametric amplifier [84, 85], four-wave mixing [86], second harmonic generation [84, 87], involving additionally also nonresonant interaction between the light field and the atomic system. Other experimental setups comprise interactions closer to resonance, comprehending two-photon correlated emission lasers also Rydberg atom lasers. All these examples of experimental setups include atomic systems exposed to phase-dependent excitation mechanisms leading to the generation of light squeezing. Also, various studies of such systems have been performed for single- or two-mode field cases, namely Jaynes-Cummings models, where the squeezing is related to the phase dependence of the initial state of the atomic system and the field [88]. However, squeezing can be achieved in a large variety of other situations comprising:

- (a) an excited two-level atom coupled with a single- mode cavity in a coherent state [89],
- (b) a two-level atom coherently driven and coupled with a single- mode cavity in a vacuum

state [90],

(c) a pair of two-level atoms in a squeezed state coupled with a single- mode cavity in a vacuum state [91],

(d) several two-level atoms coupled with a single mode cavity in the following configurations, as follows: atoms in a coherent state coupled with the cavity in the vacuum state or all atoms are in the excited state coupled with the cavity in the coherent state, and all atoms are in the ground state coupled with the cavity in a coherent state [92, 93].

It is important to highlight the concept of squeezing of states is based on the concept of quantum fluctuations. The minimum fluctuations in any quantum measurement of the corresponding canonically conjugate variables are bound to the Heisenberg uncertainty principle, which cannot be violated. Although this principle cannot be trespassed, the fluctuations of one variable, such as position or momentum, can be reduced below a minimum value, enhancing the fluctuations of the conjugate variable. The most evident accomplishment of this non-classical phenomenon is the squeezed light, where the quadrature operators of the electric field are canonically conjugate operators. Assuming the quadratic dependence of the bosonic creation and annihilation operators in the Hamiltonian, squeezed light is generated applying intense lasers and nonlinear optical media. This type of squeezed light has various practical appliance in the field of quantum optics, the most endeavoring example being interferometry with reduced quantum noise.

Experiments with superconducting-circuit qubit and squeezed microwave photons [80] allowed researches to extend the limits of observations of resonance fluorescence from two-level system placed in a bath possessing ordinary vacuum fluctuations to the one placed in a reengineered squeezed bath, which allowed to narrow the spectroscopic lines of the resonance fluorescence spectrum. Here, it might be better to remind once again that the spectrum of resonance fluorescence revealing new properties of light in the quantum theory versus semiclassical theory. This picture emerges the following features: a two-level system driven resonantly by a laser scatters elastic photons which have the same frequency as the drive and quasielastic photons. With increase of the intensity of the driving field, inelastic scattering dominates and creates, as mentioned before, the typical Mollow triplet spectrum of resonance fluorescence consisting of a central peak at the frequency of the drive and symmetrical sidebands arising from Rabi flopping. The central peak linewidth is inverse proportional to the spontaneous decay rate of the system's excited state, while the sidebands are wider by a factor of $3/2$. Basically, the Mollow spectrum describes the photon emission into a bath, which doesn't contain photons. Unlike in a thermal bath, photons in a squeezed thermal bath are emitted as correlated pairs, with frequencies of each pair symmetrically situated around the reference reso-

nance frequency of the two-level system. In the case of the squeezed vacuum, fluctuations undergo phase amplification in number of photons generated per mode and phase sensitivity also modifies the spontaneous decay rate. The inelastic scattering pictured by resonance fluorescence spectrum is generated by an electric dipole under the influence of the coherent pumping and bath fluctuations. Here bath fluctuations are expressed by spontaneous decay rates and therefore, a dipole embedded in squeezed fluctuations manifest phase-sensitive decay rate and the central peak of resonance fluorescence spectrum can be made sharper, achieving a smaller width in comparison to the one set by ordinary vacuum fluctuations.

Nevertheless, the interaction of an optical field with a two-level system operating in the weak excitation regime has continued to require emergent experimental conditions for the observation of squeezing with atoms. In this context Schulte et al.[94] used an artificial atom possessing a large optical dipole which allows the enhancement of the photon detection rate comparing to the natural atom and achieve the required conditions for the detection of quadrature squeezing in single resonance fluorescence photons. They proved that electric field quadrature fluctuations of resonance fluorescence is a bit lower the fundamental limit determined by vacuum fluctuations, while keeping the photon statistics antibunched. Thus, the presence of squeezing and antibunching simultaneously is a non-classical result of wave-particle duality of photons.

Optical emission features of solid-state and molecular systems are influenced by vibrational modes of the environment, limiting their quantum dynamical features. Thus it is important to turn the detrimental influence of vibrational environments into advantage. Iles-Smith et al. [95] shown that vibrational interactions combined with resonance fluorescence to create optical states with a higher degree of quadrature squeezing in comparison to single atoms. Using the setup based on a driven quantum dot interacting with phonons, it was proved the possibility to enhance the level of squeezing above the predicted theoretical level obtained in single atomic systems, outperforming the single mode squeezed vacuum states.

Comparing with single atoms and bulk materials, the two-level systems observed in quantum dots are more convenient for the manipulation of the two-level system and field interaction, which opens new opportunities of exploring light squeezing in resonance fluorescence and allows to use the outcomes in various quantum optical devices based on artificial atoms-quantum dots.

1.3 Cooling phenomena in quantum dipolar systems

The importance of cooling effects is based on its wide range of potential applications in the microscale and nanoscale devices. As well, many experiments involving the generation and manipulation atomic systems require a precise control of the system of interest. It is a crucial tool for probing quantum properties of the matter. Also it is an important factor in a wide range of experiments ranging from Bose-Einstein condensation to quantum computing and quantum computational modeling based on atoms and ions. Currently, there are known several cooling schemes ranging from Doppler cooling for free particles [96], sideband cooling for bound particles [97], dark-state cooling setups for free [98] and bound particles [99]. Additionally, beginning with the first observation of laser cooling, many fundamental applications have been developed employing laser cooling, as in the following examples: the direct experimental observation of quantum jumps, the preparation of atoms in the motional ground state, high-precision spectroscopy.

Earliest methods to cool quantum optical systems to very low temperatures using coherent light were proposed about 40 years ago. The motivation standing behind these researches was to improve the atomic spectroscopic measurements, but later advances proved the extended range of applications of laser cooling. Ultra cold few level atomic systems are reformatting constantly the physics research. They are employed in determination of constants, investigation of ultracold collisions, study quantum phase transitions, quantum information processing. Laser cooling methods of polar molecular systems are studied within applications of these cold molecules to a various range of topics. Heavy polar molecules are used to measure the electric dipole moment and in other experiments since their polar nature improves the interaction between the electric dipole moment and applied electric field. Also experimental precision can be enhanced by using ultracold molecules in order to expand the observation time and improve the overall experimental control. Additionally laser cooled molecules can advance quantum science since quantum molecular systems possessing a large electric dipole moment can be easily controlled through the long-range dipole-dipole interaction. Thus quantum information processing is another area where cooled quantum optical systems possessing a dipole moment can have an impact and integrated in real quantum computing schemes. The rotational states of the quantum optical systems can be considered as qubits, individual qubits are manipulated by microwave fields, and the dipolar interactions are used for the building of multi-qubit gates. Thus fundamental questions arising in physics can be explored within cooling of quantum molecular systems to low temperatures and bringing them into single quantum states. In this regime, the wave characteristics of the quantum molecular systems and the interference between these waves is changing. The diverse applications of cooled quantum molecu-

lar systems as quantum computing, quantum tunneling in reactions, generation of multi-qubit gates have motivated the worldwide research community to develop and model situations for producing the cooled quantum molecular systems. An important technique in this context is the laser cooling in quantum molecular systems [100].

Further quantum optical molecular systems placed in a room temperature environment face a lot of difficulties in practical implementation due to the high speed limits of the observation time, the wide range of Doppler shifts displacing their spectral lines and many vibrational and rotational states, which hinders their quantum-mechanical properties. In order, to have quantum control of the system over the mechanical motion, thermal fluctuations following inevitably the interaction with the surrounding environment need to be overcome. Because most nano- and micromechanical setups typically have resonance frequencies below 10 MHz, cooling the system employing a dilution refrigerator can be not enough to achieve groundstate cooling of the mechanical motion of the system. Thus to get over this, laser cooling techniques are being developed [101].

Advances in the control and measurement of quantum mechanical oscillators has facilitated tests of fundamental physics, and applications in quantum information processing and sensing. Nevertheless, the output of these experiments is frequently reduced by thermal motion of the mechanical mode. Though the most advanced cooling technologies are enough to cool high-frequency quantum mechanical structures to the ground state, monitoring quantum behaviour in lower-frequency quantum mechanical systems demands another cooling methods. In this context, laser cooling techniques controlling coherently the atomic systems allow the lowest possible cooling and vacuum fluctuations can improve this kind of cooling technique specially suitable for macroscopic oscillators.

Modern progresses have advanced significantly the manufacturing, measuring and controlling diverse mechanical systems at micro- and nano-level. The experiments involving such mechanical devices include generation of non-classical states, entanglement, quantum measurements, establishing quantum information channels and storage, measuring weak forces as the Casimir force, and many others. The above mentioned experiments demand the system to be cooled to its ground state, i. e., in the temperature range from 20 to ~ 100 mK for 1 GHz resonators. This is difficult to be achieved employing bulk cooling methods, but it may be possible to achieve using nonequilibrium cooling techniques as laser-cooling setups for trapped ions and neutral atoms. However, in some applications like a macroscopic mechanical oscillator with quantum-level motion, cooling with lower frequencies is more required due to its greater zero point motion level and less control required. Even at cryogenic temperature, thermal oscillation are still present at frequency $\lesssim 100$

MHz. Thus motional excitation can be reduced using supplementary cooling processes, such as feedback cooling, sideband cooling, ultrafast pulsed laser cooling, or laser cooling with a dissipative multilevel system. Also, via quantum enhanced cooling by a squeezed field [102], an oscillator can be steered towards the ground state with real-time feedback. Squeezing improves the cooling of the quantum mechanical system and thereby simplifies the preparation of the quantum mechanical system in its motional ground state, which is achieved by increasing the power of the probe beam. Thus, by adjusting the quantum state of the laser beam and reducing the measurement noise, an improved cooling rate is observed. Nevertheless, cooling rates enough for ground state cooling are challenging to be achieved due to bulk heating generated by absorption of the probe field.

Laser cooling in a finite-level system is especially useful for quantum information processing because of the dissipative finite-level system can be integrated in real devices by inherent quantum memory initialization mechanism. If the initial temperature of the oscillator is low enough, satisfying the Lamb-Dicke regime, a real quantum mechanical oscillator setup can be cooled to the ground state by coupling with a quantum dot, or a superconducting circuit. In this context, Lau et al. [103] presented the laser cooling of mechanical oscillator by coupling with a dissipative three-level system. Considering the environment temperature exceeding the Lamb-Dicke regime, they have extended the laser cooling analysis. They proved that in low-temperature mode efficient cooling can be engineered by properly driving a multilevel system, namely a three-level ladder system, in which quantum coherence between multiple metastable states are inducing cooling effects different from two-level system cooling. In the high-temperature regimes, electromagnetic induced transparency (EIT) cooling with Λ -type system exhibits both cooling and phonon-lasing effects.

Applications in high precision detection of mass, mechanical displacement and quantum information processing attract considerable interest towards ground state state cooling in micromechanical and nanomechanical resonant devices. In order, to entirely make use of nanomechanical resonators properties and observe a wide range of quantum phenomena within them, it is required to cool the nanomechanical resonator to the ground state. In their paper, Li et. al [104] presented a new setup for ground-state cooling of a mechanical resonator consisting of a two coupled quantum dots which has an effective Λ -type three-level system structure. The cooling process in this setup occurs through phonon absorption when the electrons tunnel through the coupled dots. Consequently, the cooling rate and its efficiency is possible to be achieved in realistic experimental setups. Additionally, Xia et al. [105] discussed the cooling of a Λ -type three-level system placed in a nanomechanical resonator, where the ground state cooling occurs due to induced quantum

interference canceling the heating excitations.

In this context laser cooling has a major impact in the generation of fundamental quantum mechanical atomic systems, for example: in experiments concerning the quantum statistical properties of atoms, trapped ions for quantum information processing. Under this aspect, laser cooling of trapped ions is an important step regarded for the construction of a quantum computer based on trapped ions. Supplementary, ground state cooling techniques are fundamental for quantum computation schemes with trapped ion and quantum gate operations, because higher quantum computational speed involves remove of decoherence in the system due the coupling to the environment and reducing the perturbation of the desired processes. The fundamental requirement for quantum computing operations with trapped ions is the generation of the ions in the quantum mechanical ground state of their motion by laser cooling. However, for quantum gate computing consisting of multiple ion string cooling is required and high fidelity manipulation of the qubits demands the other modes to satisfy the Lamb-Dicke regime, where the residual amplitude of motion is much smaller in comparison to the wavelength of the laser that generates optical transitions. Raman cooling has a disadvantage for quantum computing as it allows the cooling of one mode at a time, while other modes remain heated by spontaneous radiation processes. Thus, electromagnetic induced transparency (**EIT**) is an efficient cooling technique for quantum computation because it allows a larger cooling bandwidth. Several modes are cooled at the same time by suppressing through quantum interference a large number of the heating processes [106].

The most often ground state laser cooling of trapped ions is achieved through the two-level sideband cooling and Raman sideband cooling, which is designed for Λ -type three-level system by Raman coupling. These cooling techniques are based on laser pumping of an atom, which has two internal levels: ground and excited, correspondingly. In both cases, sideband cooling has to fulfill several conditions, namely: (a) the system must have equidistant levels, which is possible to achieve when the particle or particles are placed or trapped in a harmonic oscillator; (b) the system must work in the Lamb-Dicke regime, which means that the amplitude of the oscillations of the system's particles is less than the wavelength of the driving cooling laser; (c) the strong confinement condition has to be satisfied, according to which the spontaneous decay rate is less then the distance between any pair of energy levels. In this context, G. Moriggi et al. [107] proposed a method for ground state cooling of multilevel quantum atomic systems, excluding the carrier excitation by electromagnetically induced transparency.

Electromagnetically induced transparency (**EIT**) appears in three-level or multilevel systems and consists of cancellation of the absorption of the transition induced by synchronous laser driving

of another transition. The cooling method is based on continuous coherent light driving and has been proved to be more effective than two-level and Raman sideband cooling. Thus, unlike the sideband cooling in two-level systems, the strong confinement regime is no more required. Instead, are used two dipole-allowed transition, which don't satisfy the strong confinement limitation and two lasers are required, unlike Raman sideband cooling which involves a supplementary re-pumping laser. Finally, they proved a more efficient ground state cooling than sideband cooling methods, particularly cooling of several vibration modes. Electromagnetically induced transparency (EIT) [108] achieved in three-level system irradiated by Raman lasers with strong blue detuning that couple the ground and a metastable state to an excited dissipation state and between the dressed states of the system is one dark state which cancels the carrier transition. Properly selected parameters can place the red sideband corresponding to a peak of *Fano*-like absorption spectrum, thus reaching low final temperatures. Unlike cooling on dipole-forbidden transitions and cooling due to Raman transitions, cooling obtained through electromagnetically induced transparency (EIT) is an encouraging modern technique to achieve the mechanical ground state of trapped atoms or ions. Hence Evers J. [109] et al. proposed a double electromagnetically induced transparency cooling scheme based on three-level Λ -setup, which in the ordinary electromagnetically induced transparency scheme employ a supplementary-third ground state that is coupled strongly by laser to the upper state. Thus are obtained two independent electromagnetically induced structures, which are controlled by the two coupling laser fields delaying the carrier-transitions and the blue-sideband transitions, correspondingly. In many cooling schemes, single electromagnetically induced transparency demands supplementary repumping fields since the upper level state decays to the other two lower states. In this context, the proper choice of the parameters as frequency, intensity of the pumping laser field generates the double electromagnetically induced transparency improving the cooling performances. This in double electromagnetically induced transparency setups additional decay paths offer an advantage for cooling. Also, these supplementary decay paths allow multiple electromagnetically induced transparency cooling with multiple lower states.

Sideband cooling is method of selection of trapped ions and it is required for efficient cooling of the motional sidebands. Cooling takes place when a red sideband transition excites the atom electronically and at the same time annihilates a phonon to fulfill the energy conservation condition. Also, it requires that Rabi frequency of the laser to be much smaller than the motional frequency of the sideband. On the other side, a blue transition can heat the system through recoil after spontaneous decay or coherent generation of a phonon. Further suppression of blue sideband transitions employs destructive interference observed in the dark state. Thus, the electromagneti-

cally induced transparency (**EIT**) has become an important laser cooling schemes for trapped ions as Stark-shift cooling [122] and some others: feedback cooling [110], ultrafast pulsed laser cooling [111, 112, 113], laser cooling with a dissipative finite-level system [108, 114]. In electromagnetically induced transparency (**EIT**), quantum interference excludes the carrier transition to enhance cooling performance while the Stark-shift cooling is achieved through Rabi frequency tuning [115].

The concept of sideband cooling is based on the cancellation of mechanical energy by scattering incident photons to higher frequencies. However, the photon up-conversion, namely anti-Stokes process, is exceeded by down-conversion or Stokes process, which adds energy to the system. In optomechanical cavities, the light-matter interaction emerges due to a parametric change of the resonance frequency of an optical cavity with the location of a mechanical oscillator. If the quantum optical cavity is pumped at laser detuning frequency below its resonance frequency, the discrepancy in the density of states of the cavity at the sideband frequencies drives to an anti-Stokes scattering rate. The distinction between Stokes and anti-Stokes scattering rates increases as function of linewidth of the cavity reduction relative to the frequency of the oscillator. Subsequently, optomechanical systems in the the above mentioned resolved sideband limit can be cooled with coherent light to low temperatures. However, a full quantum analysis brings out that vacuum fluctuations constantly stimulate some degree of Stokes scattering [111, 116], which inhibits deep ground-state cooling.

Consequently, there were stated many proposals to cool the quantum optical systems below the sideband cooling threshold, which include various schemes as: pulsed cooling schemes [117, 118], dissipative coupling [119], optomechanically induced transparency [101] and nonlinear interactions [120]. For setups built on atomic laser cooling, squeezed light can bring an advantage in comparison to laser cooling with coherent states. In this context, Clark et al.[121] proposed the implementation of an enhanced quantum cooling scheme for cavity optomechanical systems. They have shown that irradiating an optomechanical cavity with squeezed coherent light can annihilate the Stokes scattering process, as well the sideband cooling threshold can be excluded. Thus squeezing-enhanced cooling implemented in cavity optomechanical system can reach cooling below the traditional quantum threshold.

Another method of cooling is the *Stark-shift cooling* [122] which takes place when transitions between ground and metastable state are determined by one laser and another two Raman lasers coupled to the superposition of ground, metastable and excited state. The first laser generated Rabi flips between the dark state and the orthogonal light state. In case of proper coupling strength tuning, the flips also include neighboring levels so that dark and bright states coupled with carrier

transitions are excluded. It is important to highlight, that both Stark-shift and **EIT** cooling reach a final temperature independent of the Lamb-Dicke parameter. Additionally, Borkje et al. [123] presented a setup for cooling mechanical motion to the ground state in an optomechanical system exploiting the effect of *optomechanically induced transparency*. This cooling setup is an outcome of a destructive interference effect and is associated to the electromagnetically induced transparency cooling, where **EIT** is used to cancel unneeded transitions while laser cooling of atoms. Particularly, the optomechanical induced transparency is similar of **EIT**, as it is changing the the photon number fluctuation in the cavity and consequently the rate of Stokes and anti-Stokes scattering. Unlike **EIT**, optomechanically induced transparency has a priority as it requires only optomechanical interactions. Consequently, the cavity-assisted ground-state cooling of mechanical motion in the unresolved sideband regime is generated in systems exhibiting dissipative optomechanical coupling, which means that Stokes processes are annihilated by a destructive interference effects and in ordinary optomechanical systems annihilation occurs through time-dependent optical driving.

In conclusion, one has presented here various cooling technique setups implemented in various devices built on the base of few-level atomic or molecular systems embedded in optical cavities or placed in nano-mechanical resonators. The growing interest for novel quantum systems exhibiting enhanced cooling in a wider parameter range in microscale and nanoscale devices is an interesting topic for investigation.

1.4 Terahertz lasing in quantum dipolar systems

Terahertz radiation is a type of electromagnetic radiation whose frequency is situated between microwave and infrared regions of the spectrum. This kind of radiation cannot be seen, however we can feel this radiation since its spectrum is situated in the vicinity of far-infrared radiation. THz radiation generated naturally is present everywhere, nevertheless this range of electromagnetic spectrum is still the least explored because of difficulties related to making proper and compact THz sources and detectors. The absence of any suitable technology or setup functioning in the THz band led it to be called "THz" gap. However, this gap has been reducing quickly for last several decades. This gap has been minded by tremendous technological progresses in the high frequency side and microwave technologies functioning from the low frequency side.

In this paragraph we are going to give the basic perspectives over the THz radiation: properties, applications and progresses of THz science and technologies subsequently. The most often used term referring to this frequency band is "Terahertz radiation", which is similar to referring microwaves, infrared radiation, and X-rays. Alternatively, we can refer to Terahertz radiation using the term "T-rays", where "T" stands for the frequency unit of the spectral band. By now, researchers from several different disciplines are working independently in the development of THz technologies. This resulted into distinct descriptions of THz radiation by different communities. Beside the universal unit referring to THz radiation (10^{12} Hz), other units can be also used appropriately and below one is giving the conversion of 1 THz as follows:

- Frequency: $\nu = 1 \text{ THz} = 1000 \text{ GHz}$
- Angular frequency: $\omega = 2\pi\nu = 6.28 \text{ THz}$
- Period: $\tau = \frac{1}{\nu} = 1 \text{ ps}$
- Wavelength: $\lambda = \frac{c}{\nu} = 0.3 \text{ mm} = 300 \mu\text{m}$
- Wavenumber: $\bar{k} = \frac{k}{2\pi} = \frac{1}{\lambda} = 33.3 \text{ cm}^{-1}$
- Photon energy: $h\nu = \hbar\omega = 4.14 \text{ meV}$
- Temperature: $T = \frac{h\nu}{k_B} = 48 \text{ K}$

where c is the speed of light in vacuum, \hbar is Planck's constant, and k_B is Boltzmann's constant [124]. Usually defining the THz band, one makes reference to the spectral region 0.1 and 30 THz. However the range of 10 – 30 THz trespasses the mid-infrared band and exceeds the far-infrared band, where certain well-functioning optical technologies exist. The ultrabroadband THz band comprises the band 0.1 – 10 THz, which is used as a general definition of THz band. From the electromagnetic spectrum of the THz, it is evident that it intersects with neighboring spectral bands like the millimeter wave-band, which possesses the highest radio frequency band named as

Extremely High Frequency (**EHF**), additionally the submillimeter-wave band also the far-infrared band. Characteristic technologies correspond to these bands, for example: solid-state devices, sensors and millimeter wave emitters are built using microwave technologies [125].

Further, one is going to describe briefly the setups employed for THz generation and detection, classified by functioning concepts. A method of generation THz radiation is to use a nonlinear medium in which the incident wave is converted by nonlinear frequency. Optical rectification and difference frequency generation are methods of THz photon generation by second order nonlinear optical processes at two different frequencies, so that their difference corresponds to the frequency of a THz photon. Broadband THz pulses are generated by femtosecond lasers, which possess a broad spectral bandwidth ~ 10 THz and it is similar to the optical pulse envelope obtained via optical rectification. Two continuous wave (**CW**) optical beams can generate THz frequencies by difference frequency generation (**DFG**). In solid-state devices based on microwave technology, THz wave frequencies are generated from conversion of the incoming microwave into harmonic wave using diodes with nonlinear intensity-voltage characteristics. THz radiation is obtained by laser beam excitation of a biased photo-conductive (**PC**) antenna. In this technological method, the photo-conductive (**PC**) antenna, which consists of two metal electrodes, is deposited on a semiconductor substrate. The optical beam creates photo-carriers by irradiating the gap between the electrodes and the static bias field contributes to the acceleration of the free carriers. Since the generated photo-current alternates in time simultaneously with the incident laser beam intensity, then the femtosecond laser pulses are transformed into THz pulses. Continuous wave (**CW**) THz radiation is generated by applying simultaneously or mixing two laser beams with different frequencies and forming an optical beat. This method of THz waves generation is named photo-mixing. Another method of generating extremely bright THz radiation uses relativistic electrons produced by electron accelerators. In this method, a femtosecond laser irradiates an electron source and generates ultrashort pulses of electrons. After the relativistic speed acceleration of electrons, they are directed into a metal target or are manipulated to move circularly by a magnetic field. Consequently, this transient electron acceleration generates THz radiation [126, 127].

Various experimental facilities are employed by now to generate THz radiation. One will mention some of them, as follows: backward wave oscillators (**BWO**'s) are laboratory level equipment, free-electron lasers (**FEL**'s), small scale electron accelerators, as well. Despite the difference in dimension of these devices, there is a certain resemblance in their THz generation mechanism. In both backward wave oscillators (**BWO**s) and free-electron lasers (**FEL**'s), the electron beam oscillates due periodic structures embedded in the construction of these devices, namely: the **BWO**

posses a metal grid and the **FEL** is build from magnetic array [128].

It is well-known that two-level quantum lasers require population inversion. In the far-infrared lasers, transitions between molecular rotation energy levels are used to generate frequencies in the THz region. In the electrically pumped solid-state lasers namely germanium lasers, the lasing takes place due to the population inversion of two Landau levels generated by hot-carriers influenced by crossed electric and magnetic fields. Quantum cascade lasers (**QCLs**) are classified as semiconductor heterostructure built from periodically alternating layers of heterogeneous semiconductors. In these semiconductor nanostructure lasers, THz photons are generated by transitions between subbands. Also in quantum cascade lasers (**QCLs**), the electrons go through consecutive intersubband transitions which practically generate coherent THz radiation [111, 129].

Beside THz generation schemes, it is important to ascertain the obtained frequencies to THz band. The detection setups are organized into coherent and incoherent detection. Coherent measurement method detects the amplitude and the phase of the field, whereas incoherent measurements detects the field intensity. Coherent methods are based on generation techniques because they share same functioning mechanism and the key assembly components, for example: optical detection setups use the same light sources for generation and detection.

In the following, we present some commonly used coherent detection techniques. Free-space electro-optic (**EO**) technique detects the electric field broadband THz pulses in time by using the Pockels effect. This type of measurement technique is based on optical rectification principles. Since the THz field generates birefringence in a nonlinear optical medium which is proportional to the field amplitude, then the waveform is detected by measuring the field generated birefringence of the relative time delay between the THz and optical pulses. Broadband THz pulses are measured by a photoconductive setup in time domain. This method of measurement is based on the following principle: the THz field injects a current in the photoconductive gap simultaneously when an optical probe pulse injects photo-carriers. The THz field amplitude is proportional to the induced photocurrent. By detecting the photocurrent the THz pulse spectrum shape is measured in time while changing the time delay between the THz pulse and the optical sample [130, 131]. The broadband generated THz pulses are detected by a combine setup named THz time-domain spectroscopy, which measure both the amplitude and the phase of THz pulses induced by a probe, which offers enough data to measure at the same time the dispersion and the absorption of the sample. Incoherent detectors mostly used are thermal sensors as: Golay cells, bolometers and pyroelectric devices.

Certainly, THz band has innumerable applications exploring the features of material responses

to THz radiation because this frequency region is related to the fundamental physical processes, for example: rotational transitions of molecules, vibrational motions of organic chemical compounds, lattice oscillations in solids, transitions detected in the intrabands of semiconductors, and energy gaps in semiconductors. THz spectroscopy is able to analyze the spectral signatures and dynamics of organic and biological molecules in this spectral region. Therefore it can be used to detect explosives, illegally transported prohibited substances, testing new pharmaceutical substances etc. Many materials exposed to THz radiation are transparent, like: nonpolar materials, dielectrics such as paper, plastic, clothes and wood that are usually opaque at optical wavelength. This stark property is specially useful for many imaging techniques because THz imaging is a nondestructive detection technique to check sealed packages, identification of metal objects like weapons [132, 133].

Indeed, laser sources generating coherent light in the THz region of electromagnetic spectrum are a subject of ongoing research in fundamental and applied physics. The THz region represents a technological gap which one can get over it with electronic devices functioning at lower frequencies or with lasing devices operating at higher frequencies. In this context some attempts have extended the semiconductor quantum lasers to the THz region. Therefore, multiple quantum-well structures are designed and within the quantized subbands in the conduction band transitions occur. In quantum cascade laser THz transitions are limited because the radiative lifetimes of excited electronic states are much greater in comparison to the fast recombination arising from electron-phonon scattering or from incoherent electronic excitation. Intersubband transitions occur when there is strong light-matter coupling regime achieved by embedding a multiple doped quantum well into a microcavity resonator and creating intersubband cavity polariton modes. In such systems, the applied electric field is generating the hybridization of the exciton states with different parity. This makes possible transitions between exciton-polariton states thus creating integrated THz sources [134, 135].

The growing inquiry for high-energy broadband pulses functioning in the THz frequency range, situated from tens to thousands of micrometers for respective wavelengths, has emerged into many new advances in this field such as the development of the optic rectification technique, which was intensively researched by many groups. Optical rectification is used for intensive efficient THz conversion in lithium niobate crystal through pumping with high-energy picosecond pulses. Efficient generation of THz waves has to fulfill the Manley-Rowe conversion threshold, which allows a conversion rate of at least $\sim 10^{-2}$ from a wavelength of 1 to 100 μm [136, 137]. Several solutions have been proposed to overcome this threshold, such as: quasi-phase-matched materials with, THz generation through cascading processes and self-induced transparency (SIT) [138].

Also, there have been performed attempts to generate THz waves using nonlinear wave mixing in non-centrosymmetric media, which possess permanent dipole moments. However, centrosymmetric media like quantum dots are also favorable for applications in mid- and long-infrared photonic setups [139].

High-power lasers operating in the THz frequency domain are of special interest, because tunable coherent THz sources are employed in quantum optics and informatics, control and manipulation of quantum systems, contemporary sensing and visualization systems. Several promising techniques have been already proposed for the realization of high-intensity THz sources, such as accelerator-based lasers, ionizing gas targets via ultrashort laser pulses and the most promising out of them is THz generation based on the difference between optical frequencies in bound-bound transitions. Also, resonant excitation of the atoms with Rabi oscillations generates the radiation at the Rabi frequency, which for strong laser fields may be in the THz region. The Rabi frequency depending on the driving field alongside with dipolar moment are used to tune the intensity of the generated electromagnetic waves. Therefore, the generation of electromagnetic field with frequency lying in the THz is specially challenging for traditional methods, which appear to be inefficient and failing. Since this frequency region is situated between radio and optical frequency ranges, optical and microwave techniques are not applicable for THz waves generation. Consequently, nanostructures as THz emitters and detectors are the most proper candidates to fill this gap. A solution might be the quantum cascade THz transitions in quantum dot systems, THz emission from carbon nanotubes, array of quantum dots with broken inversion symmetry, which is currently actively explored because it provides smooth control of frequency tuning by adjusting the driving field intensity. Besides generation, amplification of THz waves in quantum dot arrays is possible to achieve and can be employed for THz detection [140, 141, 142].

In certain semiconductor structures, namely the ones possessing broken inversion symmetry, strong light-matter coupling creates Rabi splitting for moderate intensities of the dressing field. This fact makes them attractive candidates for implementation of THz laser sources. Among the most auspicious candidates are asymmetric quantum dots (QDs) obtained from semiconducting materials with crystal structure of wurtzite type, for example GaN quantum dots, which exhibit giant piezoelectric effects and possess a static dipolar moment. The permanent dipole moment in asymmetric quantum dots while interaction with externally driving fields generates a row of unusual optical phenomena, such as spontaneous emission at Rabi frequency, dynamically controllable fluorescence. On the basis of these peculiar properties of asymmetric quantum dots possessing a dipole moment, THz lasing can be generated in asymmetric QDs dressed an intense lasing field

inside the THz optical cavity. On the other side, the emission spectrum of symmetric and asymmetric QDs, which are a standard example of two-level systems, are different if they are driven by a strong laser field because of violation of symmetry inversion leading to the emission of electromagnetic waves at Rabi frequency. Since the Rabi frequency depends of the intensity of the lasing field, this effect is suggested for frequency-tuned generation of electromagnetic waves. This effect, can be observed III-nitride QDs with broken inversion symmetry and strong dipole moment ~ 10 Debye, which makes them emit coherent light at Rabi frequency, which lies in the THz range for the pumping field $\sim 10^7$ V/m [143, 144]. Also transitions in the THz range were observed in an asymmetric two-level systems realized in quantum wells and other kind of two-level systems. Based on this considerations, two-level systems with broken inversion symmetry pumped by an off-resonant coherent electromagnetic field were investigated [145, 146]. By proper adjustment of laser frequency, one has generated at a frequency situated in the range between the laser frequency and transition frequency also a subsequent photon with transition frequency, which can be in THz and optical spectra range. The major advantage of this setup is the opportunity to change the longer-wavelength photons using the proper selected detuning. This aspect is specially useful in the control of quantum networks consisting of different modes of various frequencies embedding quantum wells or dots with transition frequency in the THz range. Also that model exhibits flexibility in applications unlike cascade three-level systems or other down-conversion processes especially in the emerging quantum information science where entangled photon pairs of different frequencies are of great interest for the implementation of quantum networks [41, 69].

It is important to bring here this data and prove the importance terahertz spectroscopy and imaging recalling for the better knowledge of matter and material spectroscopy. Many reliable THz radiation sources have been proposed, yet some of these sources have operational restraints, for example, quantum cascade lasers are functioning at cryogenic temperatures, on the other side free electron based sources are quite bulky [147, 148, 149]. Nevertheless, the design and development of new ones implemented on few level systems possessing a permanent dipole moment is the endeavoring field of research.

In one of the previous paragraphs, we have presented the feature specific for three-level systems as the observation of electromagnetic induced transparency (EIT) in different experimental setups, such as coupled resonators, various optomechanic circuits, plasmonic structures and etc. Widely explored electromagnetic induced transparency (EIT) has its analogue observed in metamaterial structures have drawn a huge research interest because of their effective medium features. Electromagnetic induced transparency (EIT) in metamaterials can work in the terahertz regime and

can be used to build and design chip-scale optical devices. In their paper Bai Zh. et al. [150] proposed a method to construct a new type of optical metamaterial that can function as a multilevel atomic system exhibiting electromagnetic induced transparency (**EIT**). In their setup the transition from single **EIT** to a double **EIT** in the THz range is achieved by actively adjusting the intensity of infrared driving field or changing the geometrical structure of resonator. Supplementary, in this setup the group velocity of the terahertz radiation is adjusted by the driving field intensity. Consequently, the suggested setup may be used to construct chip-scale devices which can switch quickly from subluminal to superluminal terahertz radiation at room temperature.

Consequently the importance of THz technologies towards sensing, imaging, spectroscopy, or quantum data communication is highly appreciated. Based on the above explored background, quantum systems possessing permanent dipoles and able to generate THz frequencies are a special area of interest for quantum optics [151]. More over, these systems exhibit bare-state population inversion and multiple spectral lines in resonance fluorescence spectra and squeezing [30, 152]. In this sense, there is a growing interest for new quantum optical devices manifesting in a wider range of parameters lasing or cooling. From this perspective, the investigation of laser-driven Λ -type three level system with the upper level coupled with a quantized single- mode boson field is of edge-cutting interest. More exactly this theoretical model can be employed for the modeling of experimental schemes consisting of a nanomechanical resonator containing a three-level emitter or an electromagnetic cavity with a three-level sample embedded inside it and the the upper state of the sample has a permanent dipole moment. Further, the both situations will be considered separately as well the mechanism explaining the lasing and cooling effects for them.

1.5 Multiphoton dynamics of quantum dipolar systems

The photon is the building block of the light. Particular combinations of photon-ranging from more stringent distribution to entangled superpositions-are required to power quantum technology. The ultimate technological advances in handling light-matter interactions, basically the few-level atoms and photons, were implemented in quantum information protocols. Such interactions implemented on different platforms have disapproved the mistrust towards the quantum computer becoming real. Quantum computing protocols have been already embedded on certain setups. Photons can fulfill the requirement of quantum information coding. A single photon encodes a single qubit in various ways, for example, the horizontal and vertical polarization can be employed as a computational basis, while arbitrary qubits can be generated and managed using available waveplates. Photons are known to interact very well with environment, which lead to photons decoherence. However, photons do not interact with each other this makes challenging the criteria of acquiring two qubit entangled gates.

In the early 2000's, Knill et al. [153] demonstrated that linear optical components altogether with single photon sources and single photon detectors can generate the nonlinearity required to generate, an optical quantum computer possible to be build following the laws of quantum mechanics. In the same way, photonics technologies have been implemented in quantum metrology for the super-resolved images and hyper-sensitive interferometric experiments using single photons. Photons have always proven to be the most appropriate tool in observing, verifying and understanding the major quantum mechanical phenomena on which quantum information science is based, particularly the entanglement phenomenon. Entanglement was experimentally tested using photons emitter from atomic cascades and entangled photons generated from spontaneous parametric down conversion. These experiments served as a demonstration of quantum coding protocols dependence on entanglement, specially the compression of multiple classical bits into a single qubit [154].

In a classical representation, an atom contains a permanent dipole moment and if it is negatively charged electrons vibrate relative to the positively charged ionic nucleus. The dipole moment results from the superposition of energetically bound states, allowing specific discrete energies and the corresponding dipole oscillations emit light with certain frequencies [155]. Properly adjusted coherent light sources are able to excite dipole oscillations in the resonant regime with specific dipole oscillation frequencies. Particularly speaking, optical excitation is able to induce transitions between the atomic eigenstates. It was shown that an isolated atomic system generates an oscillating dipole if it is an appropriate superposition of hydrogen-like eigenstates. In the perspective of classical optics an oscillating dipole emits light. This quantum-optical set up is computed by

deriving the equations of motion for the light-matter system. Quantum mechanical consideration of light generates a wider range of problems analogous to the one arising in the many-body interactions in complex systems. One, considering a system possessing a permanent dipole, will presume a set of approximations in order to derive a solution and explore the quantum dynamics.

A two-level system coupled with a harmonic oscillator is a simple model which contributed to the development of the modern physics ranging from quantum optics to condensed matter physics. The Jaynes-Cummings model accurately describes a two-level atom resonantly coupled to a single electromagnetic radiation mode [156]. Trapped ion experiments in quantum informatics, graphene placed in the magnetic field, quantized single mode radiation field, quantum dots coupled with photonic cavities, superconducting qubits coupled with microwave cavities are the few experimental realization of Jaynes-Cummings model. Since cavity quantum electrodynamics functions in several coupling regimes: weak, strong, and ultrastrong allow the control of the spontaneous emission rate as function of vacuum level by tuning the discrete cavity modes. The strong coupling regime occurs when the emitter-photon interaction is much greater than the combined decay rate. Due to the recent advances in solid-state semiconductor or superconductor systems, ultrastrong coupling is achieved. Also, in these setups is possible to include new interaction terms in the Jaynes-Cummings model, which was not available in conventional cavity quantum electrodynamics setups. Another term included in the Jaynes-Cummings model is an inversion-symmetry-breaking term. In this way, the well-known Jaynes-Cummings model and Rabi model with classical radiation field assumes that the dipolar moment operator's diagonal matrix elements are zero.

Quantum systems possessing a permanent dipole moment in the steady state can exhibit multiphoton dynamics while pumping the system with a strong laser field. The main advantage of this system is the generation of Rabi frequencies. The inversion-symmetry-breaking on dynamics of a two-level system coupled with a quantized harmonic oscillator. Especially, it was explored and proved the negative impact of the inversion-symmetry-breaking on the eigenvalues and eigenfunctions of the generalized Jaynes-Cummings Hamiltonian and the Rabi oscillations dynamics. In comparison to the quasiclassical case, multiphoton transitions can be adjusted and there are Rabi oscillations with periodic exchange of several photons between emitter and the bosonic field [29].

The Jaynes-Cummings model can be used for the theoretical modeling of non-dipolar light-matter interaction, particularly the multiphoton Jaynes-Cummings model which considers multiphoton interaction. The investigation of multiphoton interaction through the Jaynes-Cummings Hamiltonian is frequently applied in quantum information science. In this context J. Villas-Boas et al.[157] have investigated the Hamiltonian describing a multiphoton interaction in the Jaynes-

Cummings framework for the future employment in quantum information. The proposed setup by them functioning in the strong coupling regime was transformed using arbitrary rotations defined in the Fock space involving vacuum and multiphoton rates. The implementation of a quantum device allowing the channeling of a field only in a finite superposition or mixture of Fock states was proved by [17]. Particularly the two-photon interaction is applied for single-photon generation comparing to existing quantum computing protocols involving standard Jaynes-Cummings interactions. Theory of a two-level system interacting with a lasing field is important for a wide range of applications due to its very general formalism: laser science, fluorescent spectroscopy, imaging, efficient light emitting setups, quantum information theory. In this row of ideas, one has to remind again the theoretical description of light-matter interaction assumes the dynamics of the system governed by non-diagonal matrix element of the dipole moment operator. Systems with permanent dipole radiate at Rabi frequency as an emitter in the THz range.

Multiphoton states generation has become an ultimate research field in quantum cryptography and quantum metrology. Atomic ensembles coupled to waveguide quantum electrodynamic system and cavity quantum electrodynamic systems are the basic experimental setups on which were implemented several quantum information protocols. Teng Zhao et al.[158] in their paper proposed a scheme to generate the multiphoton nonclassical states in which single-photon and two-photon states are suppressed by cavity induced transparency effects. Cavity induced transparency was investigated with a three-level atom in free space, which was employed for the preparation of entangled states with a pair of identical atoms. Cavity induced transparency is a tool for the observation of Dicke superradiance in a system of two qubits coupled to a single coplanar waveguide resonator. Namely, they are considering a system consisting of two identical qubits coupled to a single-mode cavity where the coupling strength is comparable to the cavity decay rate. In comparison to other papers, they are exploring the abnormal region of hyperradiance that used to be considered as subradiance. Particularly, they have proved the photon-number distribution is switched to the near-resonance states via the weak coupling between symmetric and antisymmetric Dicke states. These states undergoing a particular physical process and have the Poissonian photon-number statistics. Additionally, the nonclassical behavior of photon distribution was verified according to Klyshko criterion and they figured out multiphoton nonclassical states in which higher-order distribution exhibit nonclassical behavior. Unlike them J. Z. Lin et al.[159] have considered the multiphoton behavior of the two-cascade three-level systems strongly coupled with a cavity, in which two identical atoms interact with the lasing field and a control field simultaneously. They explored the possibilities to manipulate the multiphoton blockade through the dressed states of the system by

adding a strong lasing field. Thus the multiphoton blockade can be manipulated and improved by controlling the lasing field intensity. In this sense, the two-photon blockade can be switched to the three-photon by increasing the control field Rabi frequency, when two atoms emit coherent light in the same phase. If the radiated light is out of phase, then the three-photon blockade can be substantially improved by the control field. Then optical switching is possible to be achieved from three-photon blockade to the super-Poissonian by increasing the control field Rabi frequency. This important result is achieved in atom-cavity quantum electrodynamics, also in systems embedded in quantum electrodynamical circuits for quantum networking and telecommunications. On the other side Baranov et al.[160] have investigated the Rabi oscillations in a two-level system possessing a permanent dipole moment. One of the main results of this research proved that permanent dipole moment enables multiphoton Rabi oscillations and strongly influences the Rabi frequency for single photon processes. The quantum picture of light interacting with two-level system possessing a permanent dipole allowed to observe the collapse of Rabi oscillations in the few photon regimes, by means of numerical simulations and theoretical analysis, demonstrating previously unexplored regime of light-matter interaction.

Modern technological progresses in engineering of light-matter interaction, especially for the atoms possessing few-levels allow the implementation of various applications involving multiphoton states, which have become an active research field in quantum information, quantum cryptography, quantum metrology, implementation of quantum processing protocols based on atomic ensembles coupled to waveguide quantum electrodynamical systems.

The engineering of such interactions on various platforms such as a few level atomic ensembles coupled to a waveguide quantum electrodynamic system are proving the possibility of building a real scheme for a quantum computer. In this context, multiphoton nonclassical light possess unique features as it presents a bundle of indistinguishable photons with highlighted particle behavior. The nonclassical light with higher number of photons is generated quite easy through squeezing. Also the interpretation of nonclassical multiphoton states is a challenging theoretical subject.

Interaction of high power electromagnetic fields with atomic systems is proved to have multiphoton features. As well, recent advances in quantum electrodynamics allow us to achieve multiphoton effects, which occur when atom-photon coupling rate is in the range of the oscillator frequency. Current laser technology requires generation of electromagnetic fields comparable with and larger than internal atomic fields. Also, advances in laser technologies enable the generation of laser sources functioning in high-frequencies ranges. In this circumstances, transitions in atomic systems are required to have multiphoton features. Thus the increasing interest for strong atom-

laser interaction is due to the possibility of high harmonic generation via multiphoton transitions. It is widely known that strong laser fields generate multiphoton resonant excitation of atomic levels. If the laser frequency is in the same range with frequency associated with two-level system, then applying proper laser pulses one can generate superposition states. Nevertheless, generation of superposition states is a challenging process due to the energy gap between states, which has to be comparable with the optical transitions. In this situation, generation of multiphoton excitation will enable one to explore cooperative effects in the high frequency region [33, 64].

The two-level atomic system is an efficient and simple model to describe the resonant interaction regime and high efficiency of harmonic generation. In some few-level atomic and molecular system multiphoton excitation based on the two-level model is more effective when the system has a permanent dipole moment in the excited states. Otherwise, the energies of the excited states of a two-level atom has to be close enough to each other and the transition dipole moment between the state must be non-zero. These systems have an advantage, enabling the generation of frequencies much lower than laser frequency. The generation of high order harmonics is possible to achieve within systems with the bound-bound transitions and, as a consequence, a two-level system possessing permanent dipole moment exposed to multiphoton excitations is of special interest [161].

Quantum systems possessing permanent dipole moment in the steady state are exhibiting new multiphoton quantum dynamical features in the strong laser field. In this circumstance, the dipolar system can generate waves of Rabi frequency. Thus systems with permanent dipole moment are widely investigated in the context of multiphoton quantum dynamics. The permanent dipole in such systems changes the multiphoton absorption rates, emission spectrum features, transforming them into systems able to emit at Rabi frequency and generate THz waves. Also, it facilitates multiphoton Rabi oscillations. Permanent dipole moment influences laser-molecule interplay, especially absorption of radiation through single- and multiphoton interactions [28, 33].

Various fundamental and experimental research papers cover the issues of multiphoton transitions. Multiphoton resonant transitions occur when atoms are placed in strong laser field. Periodic multiphoton exchange between the atom and the radiation field is possible to achieve at the breaking inversion symmetry in two-level systems. Additionally, one highlights that exploring multiphoton dynamics of a two-level system, which possesses a permanent dipole, placed in a quantized photonic field is a special area of interest [162].

Recently has increased the interest towards studies involving multiphoton laser pumping of ground state of molecules through absorption of two or several photons [163]. The mechanism standing behind the two-photon excitation involves one virtual excited state, which is dipole bounded

to the initial and final excitation state simultaneously. The latest researches explored another mechanism responsible for direct two-photon excitation. This one involves both permanent dipoles of the initial and final states as well the transition dipoles between them can influence the two-photon absorption. Another discussion of excitation mechanism in the two- and three-photon of dipolar molecules proves the impact of permanent molecular dipoles for the design of molecules with a certain multiphoton excitation cross section [164, 165].

The growing interest towards the study of multiphoton excitation of molecules relies in the applications which involve various processes such as fluorescence microscopy, for example, the study of biological systems requiring wavelengths, which avoid unwanted absorption [166, 167]. Microscopy based on two- or three absorption has many benefits which are associated with the reduced scattering of longer-wavelength photons, separation of excitation and fluorescence wavelengths, three-dimensional optical data storage and other applications. Therefore, the mechanism responsible for two- and three-photon excitation of dipolar molecules demonstrated the impact of permanent molecular dipole moment for the design of molecules with a certain multiphoton excitation cross section in [168].

Nowadays due to various feasible quantum applications, frequency conversion processes where the pumping light beam can be converted into an output beam with another frequency [169, 170]. One of the first experimental proofs of this effect is the experiment reported by [171], which is promising and well-developed source of quantum tunable light. From this perspective, single-photon upconversion from a quantum dot keeping preserving the quantum features was proved in [172]. Practical confirmation of strong coupling between telecom (1500 nm) and visible (775 nm) optical modes on an aluminum nitride photonic chip was proved as well in [173]. Even greater frequency differences can be obtained. For example, an experimental confirmation of converting a microwave field into an optical field via frequency mixture in a cloud of cold ^{87}Rb atoms was reported in [174]. Earlier theoretical researches have proved frequency downconversion in laser-driven two-level systems with broken inversion symmetry [146, 152]. Moreover, single- and multiphoton frequency conversion via ultra-strong coupling regime between the two-level qubit and the two resonators was theoretically foreseen in [175]. Multiple quantum processes have been investigated for a long period of time. Despite that this subject has attracted again a certain solid research interest due to its potential experimental and industrial applications of multi-quanta processes in quantum lithography [176] or novel coherent light sources [177, 178, 179]. As well, optomechanically induced multiphoton induced transparency of X-Rays through optical control was proved by [180] and the strongly correlated multiphonon emission in an acoustical cavity coupled to a laser pumped

two-level quantum dot demonstrated by [181] respectively .

Nevertheless, the majority of investigations regarding frequency conversion refer to resonant processes. In this row of ideas, the demonstration of photon conversion scheme including non-resonant multiphoton effects is an endeavoring subject of investigation for future industrial applications.

1.6 Conclusions to Chapter 1

It is obvious to say that modern quantum optics is built on the concept of a few level atom. The most important and general concept introduced in this field is the two-level atom and three-level atom, which is a particular extension of two-level atom model. The physics of two- and three-level systems constitutes the basis for quantum optics and quantum electrodynamics. A considerable impact is observed in the field of photonic quantum technologies, where it enables secure exchange of information via single and multiple photon states. In connection with the development of quantum informatics, squeezing in resonance fluorescence processes of laser-driven few-level molecule possessing permanent dipole has been recognized as crucial resource for quantum information processing. The potential applications with artificial atomic systems have renewed interest towards resonance fluorescence and squeezing of the field quadratures within them.

Furthermore, artificial atomiclike systems exhibit an advantage with respect to engineering of their dipole moments and transition frequencies, which makes them extremely sensitive to ultra-weak perturbations and cooling or lasing these systems is of fundamental interest as well. Moreover, quantum systems with permanent dipoles are shown to generate terahertz waves required in high-precision sensing, imaging, spectroscopy and data communication. From this perspective, the investigation of a laser driven three-level system possessing a non-zero dipole moment and coupled to a quantum oscillator is an emerging research topic, because of possibility to create novel quantum system showing lasing or cooling in a wider range of parameters.

Developing sources of quantum tunable light is another relevant nowadays emerging application, such as quantum lithography, novel light sources or quantum computing protocols. This is the reason why multi-photon processes are considered under attention as well. Furthermore, the single- and multiple photon conversion process in strongly coupled two-level qubit to a resonator was predicted before. In this context, frequency conversion processes of input light into an output beam of a different frequency is very relevant nowadays to do the above mentioned feasible applications. However, the majority of frequency conversion researches regard only resonant processes. Thus, demonstration of non-resonant multiphoton conversion scheme will fill the gap in the subject of frequency down-conversion processes.

2 PROPERTIES OF NON-CLASSICAL LIGHT SCATTERED BY LASER-PUMPED MOLECULES POSSESSING PERMANENT DIPOLES

The phenomenon of resonance fluorescence offers a wide amount of information about light-matter interaction, as well, it is an iconic illustration of quantum optics in opened systems. During this phenomenon, a two-level atom is pumped by a resonant continuous wave coherent light source and the spectral and quantum statistical properties of the emitted fluorescent light emitted by the atom are detected. If the two-level atom is pumped by a low intensity monochromatic laser field, then the two-level atom absorbs a photon of the excitation frequency and re-emits it at the same frequency. Therefore, the spectral width of the fluorescent light is narrow. When the excitation frequency intensity increases and the Rabi frequency characterizing the driving field is comparable to the atomic linewidth, then the Rabi oscillations modulate the dipole moment and sidebands begin to occur in the spectrum of the emitted radiation—the Mollow triplet, which in classically consists of three lines. The central one arises at the frequency of the driving field and the symmetrically placed sidebands are arising from the Rabi frequency flopping. Due to the dynamic Stark splitting some unusual characteristics of light-matter interaction are highlighted in the fluorescent light spectrum.

Additionally, the fluorescent light possesses some nonclassical features like squeezing, which is a quantum-mechanical effect and is described by a field state in which the fluctuation value of one of the two non commuting observables is less than one-half of the absolute of their commutator. Due to this special feature of reducing the quantum noise in one quadrature phase, squeezing has a potential to be integrated in various optical communication systems and detection of gravity waves. Squeezing in resonance fluorescence arising from coherently pumped two-level system is discussed widely in many sources, beside quantum like features of photon antibunching, sub-Poissonian statistics, which were proved experimentally. However, these studies assumed collections of many stationary two-level atoms manifesting squeezing, taking into account additionally the collective effects, but not considering the solid impact of permanent dipole moment. It is expected that the consideration of permanent dipole moment will visibly modify the squeezing features of resonance fluorescence considerably. The squeezing phenomenon in resonance fluorescence spectrum for a two-level system possessing a permanent dipole will be treated as an important resource for continuous applications in various fields of quantum optics and quantum information. By modulating the fluctuations of the electric field with respect to some phase below that of the vacuum, squeezing in resonance fluorescence can be employed to improve the accuracy in interferometric measurements

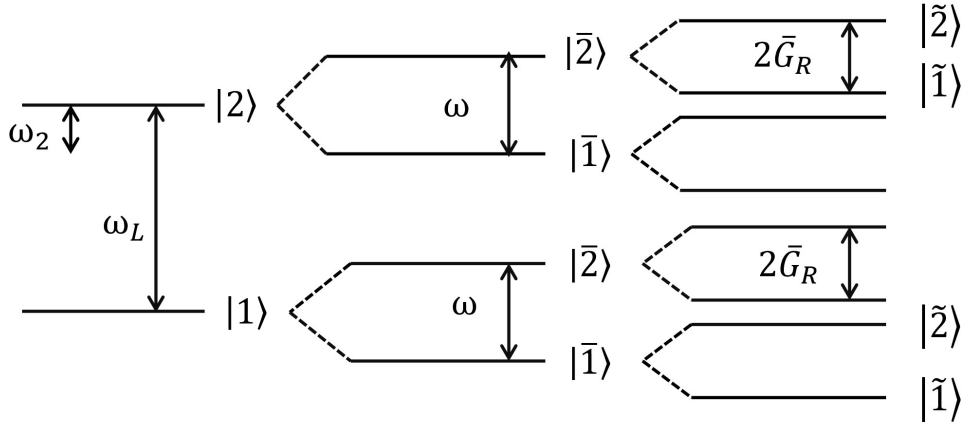


Fig. 2.1: The energy diagram of a two-level system possessing a permanent dipole. A laser of a moderate intensity with frequency ω_L is interacting with the molecular system, generating the dynamical Stark splitting. The second laser of frequency $\omega = \omega_2$ close to the value of Rabi frequency due to the first laser is leading to transition between double dressed-states. The double dressed-states correspond to the Rabi splitting frequency $2\bar{G}_R$.

for metrology applications, for secret encodings in quantum key distribution, and are an important resource in continuous variable generation for quantum computing schemes.

In this chapter, one studies squeezing in resonance fluorescence and total quantum fluctuations processes from a two-level system possessing all dipole matrix elements are considered nonzero. We shall begin by defining the system Hamiltonian consisting of all terms describing all types of interactions within the system. We are considering a strong coherent field is pumping the sample near resonance. The second weak laser field is driving the dressed two-level transition due to a dynamical Stark-splitting. In comparison to the similar problem yet in the absence of the permanent dipoles, one will compute the fluorescence spectrum, which will have additional scattered spectral lines and supplementary squeezing regions are found.

We shall consider a two-level system with permanent dipoles interacting with two external coherent laser fields. The first laser is near resonance with the transition frequency of the two-level sample while the second one is close to resonance with the dressed-frequency splitting due to the first laser, respectively, see Fig.2.1.

2.1 The theoretical framework

Hamiltonian describing the above mentioned setup is developed in the rotating frame at the first laser frequency ω_L and in the dipole approximation is the following:

$$\begin{aligned}
H = & \sum_k \hbar\omega_k a_k^\dagger a_k + \hbar\omega_0 S_z + \hbar\Omega_1(S^+ e^{-i\omega_L t} + S^- e^{i\omega_L t}) + \hbar\Omega_2(S^+ + S^-) \cos(\omega t) + \\
& + \hbar G S_z \cos(\omega t) + \hbar G_1 S_z \cos(\omega_L t) + i\hbar \sum_k (\vec{g}_k \cdot \vec{d}) \{a_k^\dagger S^- + a_k S^+\}. \quad (2.1)
\end{aligned}$$

In Hamiltonian (2.1), the first four components are the free energies of the environmental vacuum modes and molecular subsystems together with the laser-molecule interaction Hamiltonian, respectively. Here, $\Omega_1 \equiv \Omega = dE_1/(2\hbar)$ is the corresponding Rabi frequency with $d \equiv d_{21} = d_{12}$ being the transition dipole moment while E_1 is the amplitude of the first laser field. The fifth term accounts the interaction of the second laser at frequency ω and amplitude E_2 with the molecular system due to the presence of the permanent dipoles incorporated in G , i.e., $G = (d_{22} - d_{11})E_2/\hbar$, while the sixth terms is due to the interaction of the first laser with permanent dipoles. The last term describes the interaction of the molecular subsystems with the experimental vacuum modes of the electromagnetic field reservoir. Further, $\vec{g} = \sqrt{2\pi\hbar\omega k/V}\vec{e}_\lambda$ is the molecule-vacuum coupling strength with \vec{e}_λ being the photon polarization vector and $\lambda \in 1, 2$ whereas V is the quantization volume; $\Delta = \omega_{21} - \omega_L$ is the laser field detuning from the molecular transition frequency ω_{21} . The molecule bare-state operators $S^+ = |2\rangle\langle 1|$ and $S^- = [S^+]^\dagger$ obey the commutation relations $[S^+, S^-] = 2S_z$ and $[S_z, S^\pm] = \pm S^\pm$. Here, $S_z = (|2\rangle\langle 2| - |1\rangle\langle 1|)/2$ is the bare-state inversion operator. $|2\rangle$ and $|1\rangle$ are the excited and the ground state of the molecule, respectively a_k^\dagger and a_k are the creation and the annihilation operators of the k_{th} electromagnetic field mode and satisfy standard bosonic commutation relations, namely $[a_k, a_{k'}^\dagger] = \delta_{kk'}$ and $[a_k, a_{k'}] = [a_k^\dagger, a_{k'}^\dagger] = 0$.

We reduce the exponential terms present in the Hamiltonian (2.1) by transforming it into the Schrödinger picture and applying an affine transformation according to Rotating Wave Approximation (**RWA**). This is required to adopt the presented Hamiltonian (2.1) of the model to realistic conditions assuming that $\Omega \ll \omega_L \pm \omega$ as well as $\{G, \omega\} \ll \omega_L$ and consequently rapid oscillating terms are dropped off. These assumptions are necessary to derive a linear Hamiltonian as presented in eq.(2.2):

$$\begin{aligned}
H = & \sum_k \hbar(\omega_k - \omega_L) a_k^\dagger a_k + \hbar\Delta S_z + \hbar\Omega_1(S^+ + S^-) + \hbar G S_z \cos(\omega t) + \\
& + i \sum_k (\vec{g}_k \cdot \vec{d}) \{a_k^\dagger S^- + a_k S^+\} \quad (2.2)
\end{aligned}$$

where $\hbar GS_z \cos(\omega t)$ is a slowly oscillating term and we shall keep it. In this case it is more convenient to describe the system in semi-classical laser-molecule picture in the dressed-states base, due to the first laser pumping:

$$\begin{aligned} |2\rangle &= -\sin\theta|\bar{1}\rangle + \cos\theta|\bar{2}\rangle, \\ |1\rangle &= \cos\theta|\bar{1}\rangle + \sin\theta|\bar{2}\rangle, \end{aligned} \quad (2.3)$$

where the angle θ is defined as:

$$\tan 2\theta = \frac{2\bar{\Omega}}{\Delta}. \quad (2.4)$$

Additionally after one has defined the new projection base, the new Rabi frequency depends as function of Rabi frequency of the first laser pumping and the laser detuning:

$$\bar{\Omega} = \sqrt{\Omega^2 + \left(\frac{\Delta}{2}\right)^2}.$$

Therefore the new atomic operators defined in the dressed-state base: $R^+ = |\bar{2}\rangle\langle\bar{1}|$, $R^- = [R^+]^\dagger$ and the inversion operator $R_z = |\bar{2}\rangle\langle\bar{2}| - |\bar{1}\rangle\langle\bar{1}|$ satisfy the commutation relations: $[R^+, R^-] = 2R_z$ and $[R_z, R^\pm] = \pm 2R^\pm$.

Using the new atomic operators, the effective Hamiltonian (2.5) is projected in the new dressed-states base in the following way:

$$\begin{aligned} H_0 &= \hbar\Delta S_z + \hbar\Omega_1(S^+ - S^-) = \\ &= \hbar\left\{\frac{\Delta}{2}\cos 2\theta + \hbar\Omega_1\sin 2\theta\right\}R_z + \hbar(R^+ - R^-)\left\{\cos 2\theta - \frac{\Delta}{2}\sin 2\theta\right\}. \end{aligned} \quad (2.5)$$

Substituting in the effective Hamiltonian H_0 (2.5), the eigenfunctions and the eigenvalues of the dressed state-base (2.4), then we derive the new effective Hamiltonian (2.6) in the dressed-state base:

$$H_0 = \hbar\bar{\Omega}R_z. \quad (2.6)$$

Introducing the dressed-state base transformation (2.3) into the system Hamiltonian (2.2), the system Hamiltonian is projected in the dressed-state base:

$$\begin{aligned} H &= \sum_k \hbar(\omega_k - \omega_L)a_k^\dagger a_k + \hbar\bar{\Omega}R_z + \frac{\hbar}{4}G\{\cos 2\theta R_z - \sin 2\theta(R^+ + R^-)\}\{e^{i\omega t} + e^{-i\omega t}\} \\ &+ i \sum_k (\vec{g}_k \cdot \vec{d}) \left\{ a_k^\dagger \left(\frac{1}{2} \sin 2\theta R_z + \cos^2 \theta R^- + \sin^2 \theta R^+ \right) - H.c. \right\}. \end{aligned} \quad (2.7)$$

Since the laser frequency is greater than the permanent dipole moment $\omega \gg G$, as well as the dressed-state Rabi frequency and the laser frequency overcome the value of permanent dipole moment $2\bar{\Omega} + \omega \gg G$, rapid oscillating terms $\frac{\hbar G}{4} \cos 2\theta R_z \{e^{i\omega t} + e^{-i\omega t}\}$ are excluded from Hamiltonian (2.7), within rotating wave approximation (**RWA**) and is obtained the following Hamiltonian:

$$H = \sum_k (\omega_k - \omega_L) a_k^\dagger a_k + \hbar \left(\bar{\Omega} - \frac{\omega}{2} \right) R_z - \hbar \bar{G} (R^+ + R^-) + i \sum_k (\vec{g}_k \cdot \vec{d}) \left\{ a_k^\dagger \left(\frac{1}{2} \sin 2\theta R_z + \cos^2 \theta R^- e^{-i\omega t} - \sin^2 \theta R^+ e^{i\omega t} \right) - H.c. \right\}. \quad (2.8)$$

We shall denote the laser detuning $\bar{\Delta} = \bar{\Omega} - \frac{\omega}{2}$ and the permanent dipole moment $\bar{G} = \frac{1}{4} G \sin 2\theta$. In the next, one is going to solve the master equation in the dressed-state base, as follows:

$$\begin{aligned} \frac{d}{dt} \langle Q \rangle &= \frac{i}{\hbar} \langle [\hbar \bar{\Delta} R_z - \hbar \bar{G} (R^+ - R^-), Q] \rangle \\ &- \sum_k \frac{(\vec{g}_k \cdot \vec{d})}{\hbar} \left\{ \left\langle a_k^\dagger \left[\frac{1}{2} \sin 2\theta R_z + \cos^2 \theta R^- e^{-i\omega t} - \sin^2 \theta R^+ e^{i\omega t} \right] \right\rangle - H.c. \right\}. \end{aligned} \quad (2.9)$$

Before proceeding to the lengthy computation of master equation, we present the differential form of the equation necessary to derive the generation and annihilation operators:

$$\frac{d}{dt} a_k^\dagger(t) = i(\omega_k - \omega_L) a_k^\dagger + (\vec{g}_k \cdot \vec{d}) \left\{ \frac{1}{2} \sin 2\theta R_z + \cos^2 \theta R^+ e^{i\omega t} - \sin^2 \theta R^- e^{-i\omega t} \right\}. \quad (2.10)$$

The generation operator is obtained from the integral equation:

$$\begin{aligned} a_k^\dagger &= a_k^\dagger(0) e^{i(\omega_k - \omega_L)t} + (\vec{g}_k \cdot \vec{d}) \\ &\times \int_0^t dt' e^{i(\omega_k - \omega_L)t'} \left\{ \frac{1}{2} \sin 2\theta R_z(t') + \cos^2 \theta R^+(t') e^{i\omega t'} - \sin^2 \theta R^-(t') e^{-i\omega t'} \right\}. \end{aligned} \quad (2.11)$$

According to the Markov Approximation, we are neglecting the memory effects $t' = t - \tau$, thus we can approximate the atomic operators included in the eq.(2.11) :

$$\begin{aligned} R_z(t - \tau) &\approx R_z(t), \\ R^-(t - \tau) &= R^-(t) e^{i(2\bar{\Omega} - \omega)t}, \\ R^+(t - \tau) &= R^+(t) e^{-i(2\bar{\Omega} - \omega)t}, \end{aligned} \quad (2.12)$$

and using the integration method for complex exponential functions, from which the imaginary

terms will be dropped of keeping the real terms:

$$\begin{aligned} \int_0^t d\tau e^{i(\omega_k - \omega_L \pm 2\bar{\Omega})\tau} &= \pi \delta(\omega_k - \omega_L \pm 2\bar{\Omega}) + iP \frac{1}{(\omega_k - \omega_L \pm 2\bar{\Omega})} \\ &\approx \xi(\omega_k - \omega_L \pm 2\bar{\Omega}) \end{aligned} \quad (2.13)$$

is derived the analytical form of the generation operator in the dressed-state base:

$$\begin{aligned} a_k^\dagger &= a_k^\dagger(0) e^{i(\omega_k - \omega_L)t} + \pi \sum_k \frac{(\vec{g}_k \cdot \vec{d})^2}{\hbar^2} \left\{ \frac{1}{2} \sin 2\theta R_z(t) \xi(\omega_k - \omega_L) \right. \\ &\quad \left. + \sin^2 \theta R^-(t) \xi(\omega_k - \omega_L - 2\bar{\Omega}) e^{-i\omega t} + \cos^2 \theta R^+(t) \xi(\omega_k - \omega_L + 2\bar{\Omega}) e^{i\omega t} \right\}. \end{aligned} \quad (2.14)$$

From the generation operator (2.14), we have derived the spontaneous emission coefficients in the dressed-state base:

$$\begin{aligned} \gamma_0 &= \frac{2d^2 \omega_L^3}{3\hbar c^3}, \\ \gamma_{\pm} &= \frac{2d^2 (\omega_L \pm 2\bar{\Omega})^3}{3\hbar c^3}. \end{aligned} \quad (2.15)$$

The next step is to derive the average values of the atomic operators. For this purpose, following the Born-Markov Approximation (**BMA**) and the secular approximation, according to which $\omega \approx 2\bar{\Omega}$ rapid oscillating terms with frequency $\pm\omega$, $\pm 2\omega$ are dropped off and is obtained the Heisenberg equation in the dressed-state base, which includes the spontaneous decay rates (2.15):

$$\begin{aligned} \frac{d}{dt} \langle Q(t) \rangle &= i \langle [\bar{\Delta} R_z - \bar{G}(R^+ - R^-), Q] \rangle - \frac{\gamma_0}{4} \sin^2 2\theta \{ \langle R_z [R_z, Q] \rangle + \langle [Q, R_z] R_z \rangle \\ &\quad - \gamma_+ \cos^4 \theta \{ \langle R^+ [R^-, Q] \rangle + \langle [Q, R^+] R^- \rangle \\ &\quad - \gamma_- \sin^4 \theta \{ \langle R^- [R^+, Q] \rangle + \langle [Q, R^-] R^+ \rangle \}. \end{aligned} \quad (2.16)$$

Taking into account the medium values of the atomic operators:

$$\begin{aligned} \langle R^+ R^- \rangle &= \frac{1}{2} (1 + R_z), \\ \langle R^- R^+ \rangle &= \frac{1}{2} (1 - R_z), \end{aligned} \quad (2.17)$$

one derives the master equation for average values of atomic operators $\langle R^-(t) \rangle$, $\langle R^+(t) \rangle$ and $\langle R_z(t) \rangle$. These equations are a system of linear differential equations or optical Bloch equations, which are solved in stationary case: $t \rightarrow \infty \Rightarrow \frac{d}{dt} \langle R^-(t) \rangle = 0$, $\frac{d}{dt} \langle R^+(t) \rangle = 0$, $\frac{d}{dt} \langle R_z(t) \rangle = 0$.

$$\begin{aligned}
\frac{d}{dt}\langle R_z(t) \rangle &= -2i\bar{G}(\langle R^- \rangle - \langle R^+ \rangle) - 2\Gamma_+ \langle R_z \rangle - 2\Gamma_-, \\
\frac{d}{dt}\langle R^+(t) \rangle &= (2i\Delta - \Gamma)\langle R^+ \rangle + i\bar{G}\langle R_z \rangle, \\
\frac{d}{dt}\langle R^-(t) \rangle &= -(2i\Delta + \Gamma)\langle R^- \rangle - i\bar{G}\langle R_z \rangle.
\end{aligned} \tag{2.18}$$

in the above eq.(2.18), Γ_+ , Γ_- and Γ are:

$$\begin{aligned}
\Gamma_+ &= \gamma_- \sin^4 \theta + \gamma_+ \cos^4 \theta, \\
\Gamma_- &= \gamma_- \sin^4 \theta - \gamma_+ \cos^4 \theta, \\
\Gamma &= \Gamma_+ + \gamma_0 \sin^2 2\theta,
\end{aligned} \tag{2.19}$$

are the spontaneous emission rates in the dressed-state base and the average values of the atomic operators in the stationary case are the following [188, 189, 190, 191]:

$$\begin{aligned}
\langle R_z \rangle &= \frac{2\Gamma_-}{2\Gamma_+ + \frac{(2\bar{G})^2\Gamma}{\Gamma+(2\Delta)^2}}, \\
\langle R^+ \rangle &= \frac{2i\bar{G}\Gamma_-(\Gamma + 2i\bar{\Delta})}{2\Gamma_+(\Gamma^2 + (2\bar{\Delta})^2) + (2\bar{G})^2\Gamma}, \\
\langle R^- \rangle &= \frac{-2i\bar{G}\Gamma_-(\Gamma - 2i\bar{\Delta})}{2\Gamma_+(\Gamma^2 + (2\bar{\Delta})^2) + (2\bar{G})^2\Gamma}.
\end{aligned} \tag{2.20}$$

Due to the second laser of the frequency ω another dynamic Stark splitting takes place, we have to simplify once more the system Hamiltonian (2.7) in the double dressed-state base and have to perform the same calculations of the generation and annihilation operators, which lead us to the value of single molecule decay rate in double dressed-state base, according to the algorithm exposed above in eqs. (2.10)-(2.14). First of all, we have to compute the new base of system Hamiltonian (2.8) given below and use it for later projection.

$$\begin{aligned}
H &= \sum_k \hbar(\omega - \omega_k) a_k^\dagger a_k - \hbar\Delta R_z - \hbar\bar{G}(R^+ + R^-) \\
&+ i \sum_k a_k^\dagger \left(\frac{1}{2} \sin 2\theta R_z + \cos^2 \theta R^- e^{-i\omega t} - \sin^2 \theta R^+ e^{i\omega t} \right).
\end{aligned} \tag{2.21}$$

We diagonalize the dressed-state Hamiltonian (2.21), considering the following effective Hamiltonian:

$$H_0 = \hbar\bar{\Delta} - \hbar\bar{G}(R^+ + R^-). \tag{2.22}$$

We obtain the eigenfunctions of the double dressed-state base as follows:

$$\begin{aligned} |\bar{2}\rangle &= \sin \bar{\theta} |\tilde{1}\rangle + \cos \bar{\theta} |\tilde{2}\rangle, \\ |\bar{1}\rangle &= \sin \bar{\theta} |\tilde{1}\rangle + \cos \bar{\theta} |\tilde{2}\rangle. \end{aligned} \quad (2.23)$$

These eigenfunctions embed the eigenvalues depending on the two-level system parameters as the permanent dipole moment \bar{G} and new generalized Rabi frequency \bar{G}_R projected in the double dressed-state base:

$$\begin{aligned} \cos 2\bar{\theta} &= \frac{\bar{\Delta}}{\bar{G}_R}, \\ \sin 2\bar{\theta} &= \frac{\bar{G}}{\bar{G}_R}, \\ \cot 2\bar{\theta} &= \frac{\bar{\Delta}}{\bar{G}}. \end{aligned} \quad (2.24)$$

where the generalized Rabi frequency are functions of laser detuning and dipole moment value $\bar{G}_R = \sqrt{\bar{\Delta}^2 + \bar{G}^2}$.

The new operators, i.e, $\tilde{R}^+ = |\tilde{2}\rangle\langle\tilde{1}|$, $\tilde{R}^- = [\tilde{R}^+]^\dagger$ and $\tilde{R}_z = |\tilde{2}\rangle\langle\tilde{2}| - |\tilde{1}\rangle\langle\tilde{1}|$, are operating in the double dressed-state picture obeying the following commutation relations: $[\tilde{R}^+, \tilde{R}^-] = \tilde{R}_z$ and $[\tilde{R}_z, \tilde{R}^\pm] = \pm 2\tilde{R}^\pm$. Also, the operators projected in the double dressed-state base depend on the laser detuning in the double dressed-state $\bar{\Delta}$, dipole moment \bar{G} and Rabi frequency \bar{G}_R .

We substitute the double dressed-state operators, in order to project the system Hamiltonian (2.21) into the double dressed-state base:

$$\begin{aligned} H &= \sum_k \hbar(\omega_k - \omega_L) a_k^\dagger a_L + \hbar \bar{G}_R \tilde{R}_z + i \sum_k (\vec{g}_k \cdot \vec{d}) \\ &\times \left\{ a_k^\dagger \left(\left[\frac{1}{2} \sin 2\theta \cos 2\bar{\theta} - \frac{1}{2} \sin 2\bar{\theta} \cos^2 \theta e^{-i\omega t} - \frac{1}{2} \sin 2\bar{\theta} \sin^2 \theta e^{i\omega t} \right] \tilde{R}_z \right. \right. \\ &+ \left. \left[\frac{1}{2} \sin 2\theta \sin 2\bar{\theta} - \cos^2 \theta \sin^2 \bar{\theta} e^{-i\omega t} - \sin^2 \theta \cos^2 \bar{\theta} e^{i\omega t} \right] \tilde{R}^+ \right. \\ &+ \left. \left[\frac{1}{2} \sin 2\bar{\theta} \sin 2\theta + \cos^2 \bar{\theta} \cos^2 \theta e^{-i\omega t} + \sin^2 \theta \sin^2 \bar{\theta} e^{i\omega t} \right] \tilde{R}^- \right) - H.c. \left. \right\}. \end{aligned} \quad (2.25)$$

The further step is to solve the Heisenberg (2.26) equation in double dressed-state base. The obtained solutions are the generation operators defined in the double dressed-state base, containing also the spontaneous decay rates. As well, employing this equation one will derive the average values of the new atomic operators.

$$\begin{aligned}
\frac{d}{dt}\langle Q(t) \rangle &= i\bar{G}_R\langle[\tilde{R}_z, Q]\rangle - \bar{\Gamma}_0\{\langle\tilde{R}_z[\tilde{R}_z, Q]\rangle + \langle[Q, \tilde{R}_z]\tilde{R}_z\rangle \\
&- \bar{\Gamma}_+\{\langle\tilde{R}^+[\tilde{R}^-, Q]\rangle + \langle[Q, \tilde{R}^+]\tilde{R}^-\rangle \\
&- \bar{\Gamma}_-\{\langle\tilde{R}^-[\tilde{R}^+, Q]\rangle + \langle[Q, \tilde{R}^-]\tilde{R}^+\rangle.
\end{aligned} \tag{2.26}$$

Below are presented the analytical forms of the spontaneous decay rates in the double dressed-state base and included in the above eq.(2.26) [188, 189, 190, 191]:

$$\begin{aligned}
\bar{\Gamma}_0 &= \frac{1}{4}\gamma(\omega_L)\sin^2 2\theta\cos^2 2\bar{\theta} + \frac{1}{4}\gamma(\omega_L + \omega)\sin^2 2\bar{\theta}\cos^4 \theta + \frac{1}{4}\gamma(\omega_L - \omega)\sin^2 2\bar{\theta}\sin^4 \theta, \\
\bar{\Gamma}_+ &= \frac{1}{4}\gamma(\omega_L + 2\bar{G}_R)\sin^2 2\bar{\theta}\sin^2 2\theta + \frac{1}{4}\gamma(\omega_L + \omega + 2\bar{G}_R)\sin^4 \bar{\theta}\cos^4 \bar{\theta} \\
&+ \frac{1}{4}\gamma(\omega_L - \omega + 2\bar{G}_R)\sin^4 \theta\sin^4 \bar{\theta}, \\
\bar{\Gamma}_- &= \frac{1}{4}\gamma(\omega_L - 2\bar{G}_R)\sin^2 2\theta\sin^2 2\bar{\theta} + \frac{1}{4}\gamma(\omega_L + \omega - 2\bar{G}_R)\cos^4 \theta\sin^4 \bar{\theta} \\
&+ \frac{1}{4}\gamma(\omega_L - \omega - 2\bar{G}_R)\sin^4 \theta\cos^4 \bar{\theta},
\end{aligned} \tag{2.27}$$

which depend of eigenvalues of dressed-state base and double dressed-state base, also the above presented decay rates embed the single molecule decay rate $\gamma(x)$, the generalized Rabi frequency \bar{G}_R and laser detuning $\bar{\Delta}$

$$\begin{aligned}
\gamma(x) &= \frac{2d^2x^3}{3\hbar c^3}, \\
\bar{G}_R &= \sqrt{\bar{\Delta}^2 + \bar{G}^2}, \\
\bar{\Delta} &= \bar{\Omega} - \frac{\omega}{2}.
\end{aligned} \tag{2.28}$$

The master equation (2.26) contains slowly varying terms in the spontaneous emission damping. Thus, we have assumed that $\bar{G}_R \gg \gamma(\omega_{21})$, with $\gamma(\omega_{21}) = \frac{2d^2\omega_{21}^3}{3\hbar c^3}$. With the help of the master equation (2.26), we obtain the Bloch system of differential equations, describing our sample, which is solved first in stationary case, i.e., we consider that $\frac{d}{dt}\langle\tilde{R}^-(t)\rangle = 0$, $\frac{d}{dt}\langle\tilde{R}^+(t)\rangle = 0$, $\frac{d}{dt}\langle\tilde{R}_z(t)\rangle = 0$ in order

$$\begin{aligned}
\frac{d}{dt}\langle\tilde{R}_z(t)\rangle &= -2(\bar{\Gamma}_+ + \bar{\Gamma}_-)\langle\tilde{R}_z\rangle + 2(\bar{\Gamma}_- - \bar{\Gamma}_+), \\
\frac{d}{dt}\langle\tilde{R}^+(t)\rangle &= (2i\bar{G}_R - 4\bar{\Gamma}_0 - \bar{\Gamma}_+ - \bar{\Gamma}_-)\langle\tilde{R}_+\rangle, \\
\frac{d}{dt}\langle\tilde{R}^-(t)\rangle &= -(2i\bar{G}_R + 4\bar{\Gamma}_0 + \bar{\Gamma}_+ + \bar{\Gamma}_-)\langle\tilde{R}_-\rangle,
\end{aligned} \tag{2.29}$$

to arrive at the average values of the atomic operators in the double dressed-state base: $\langle\tilde{R}_z\rangle_s =$

$\frac{\bar{\Gamma}_- - \bar{\Gamma}_+}{\bar{\Gamma}_- + \bar{\Gamma}_+}$, while $\langle \tilde{R}^+ \rangle_s = \langle \tilde{R}^- \rangle_s = 0$. Here, we took into account the relations: $\langle \tilde{R}^+ \tilde{R}^- \rangle = \frac{1}{2}(1 + \tilde{R}_z)$, $\langle \tilde{R}^- \tilde{R}^+ \rangle = \frac{1}{2}(1 - \tilde{R}_z)$. The time dependence of the mean-values of operators \tilde{R}^\pm and \tilde{R}_z in the double dressed-state basis follows immediately from eq.(2.29):

$$\begin{aligned}
\langle \tilde{R}^+ \rangle &= \langle \tilde{R}^+(0) \rangle e^{(2i\bar{G}_R - \bar{\Gamma}_s)\tau}, \\
\langle \tilde{R}^- \rangle &= \langle \tilde{R}^-(0) \rangle e^{-(2i\bar{G}_R + \bar{\Gamma}_s)\tau}, \\
\langle \tilde{R}_z \rangle &= \langle R_z(0) \rangle e^{-2(\bar{\Gamma}_- + \bar{\Gamma}_+)\tau} + \langle \tilde{R}_z \rangle_s (1 - e^{-2(\bar{\Gamma}_- + \bar{\Gamma}_+)\tau}),
\end{aligned} \tag{2.30}$$

where the spontaneous decay rate is $\bar{\Gamma}_s = 4\bar{\Gamma}_0 + \bar{\Gamma}_+ + \bar{\Gamma}_-$ [188, 190].

In the current paragraph, one has presented the detailed description of the theoretical model of a two-level system with permanent dipole possessing a permanent dipole moment pumped by a weak and a low frequency coherent field near resonance. The second stronger laser field driving the main two-level transition induces a dynamical Stark-splitting in the system. One has developed the algorithm required to monitor the population dynamics in the manifolds. These results are employed for further computation of new features of the model in the next paragraph.

2.2 Resonance fluorescence spectrum of a two-level system

The phenomenon of resonance fluorescence is the process in which a laser pumped two-level atom scatters photons both coherently and incoherently. If the driving field is monochromatic, at low excitation intensities, the atom absorbs a photon and re-emits it at the frequency as a consequence of energy conservation. The spectral width of the fluorescent light is very narrow. The situation is considerably more complex when the laser intensity increases and the Rabi frequency associated with the laser field is comparable or greater than the width of the energy bands of the quantum emitter. Under these circumstances the atom can coherently interact several times with the field before spontaneously emitting a photon. In this case, Rabi oscillations appear as a modulation of the dipolar quantum moment and the side bands appear in the spectrum of the emitted radiation. Due to the dynamic Stark splitting, which is a specially interesting feature of the atom-field interaction, the fluorescent light exhibits unusual features including photon antibunching and squeezing.

In this paragraph, we derive the resonance fluorescence for a two-level system possessing a non-zero permanent dipole and explain the phenomena occurring in such theoretical system. We shall begin by relating the atomic operators required to derive the characteristics of the fluorescent light to the atomic permanent dipole moment, in the strong driving field approximation. As well, we evaluate the complete power spectrum of the fluorescent light scattered by a two-level system by an incident lasing field.

Generally, the power $S(\mathbf{r}, \nu)$ spectrum of the fluorescent light at some suitably chosen point \mathbf{r} in the far field is derived by employing the Fourier transform of the normally ordered correlation function $\langle E^{(-)}(\mathbf{r}, t)E^{(+)}(\mathbf{r}, t + \tau) \rangle$, with respect to τ [186]:

$$S(\mathbf{r}, \nu) = \frac{1}{\pi} \text{Re} \int_0^{\infty} d\tau e^{i(\nu - \omega_L)\tau} \langle E^{(-)}(\mathbf{r}, t)E^{(+)}(\mathbf{r}, t + \tau) \rangle. \quad (2.31)$$

Here we have approximated that the field is statistically stationary and the field correlation function does not depend of the origin so the correlation function $\langle E^{(-)}(\mathbf{r}, t)E^{(+)}(\mathbf{r}, t + \tau) \rangle$ depends only on the time difference τ . According to Weisskopf-Wigner approximation, then field operator $E^{(+)}$ at a certain observation point \mathbf{r} is determined by:

$$\begin{aligned} E^{(+)}(\mathbf{r}, t) &= \Phi(\mathbf{r})S^-\left(t - \frac{|\mathbf{r} - \mathbf{r}_0|}{c}\right), \\ E^{(-)}(\mathbf{r}, t) &= \Phi(\mathbf{r})S^+\left(t - \frac{|\mathbf{r} - \mathbf{r}_0|}{c}\right). \end{aligned} \quad (2.32)$$

The above equations (2.32) that the positive frequency part of the field and the negative frequency part of the field operator is proportional to the corresponding atomic operators at a retarded time.

It follows that the correlation function is computed according to the below given expression:

$$\langle E^{(-)}(\mathbf{r}, t)E^{(+)}(\mathbf{r}, t + \tau) \rangle = \Phi(\mathbf{r})\langle S^+(t)S^-(t + \tau) \rangle. \quad (2.33)$$

The two-time correlation function $\langle S^+(t)S^-(t + \tau) \rangle$ is computed using the quantum regression theorem if we project the single-time correlation function in double-dressed state base. Additionally, we consider below the field correlation independent of the vector of distance to the detector, then $\Phi(\mathbf{r})$ will be considered as numerical constant.

Thus, following the Wigner-Khntchine theorem [187], the power spectrum S_ν is given through the integration of the two-time correlation function of the fluorescent field by:

$$S(\nu) = \frac{1}{2\pi} \lim_{T \rightarrow \infty} \frac{1}{T} \int_0^T dt \int_0^T dt' \langle E^{(-)}(t)E^{(+)}(t') \rangle e^{-i(\nu - \omega_L)(t - t')}. \quad (2.34)$$

According to the stationary condition, the correlation function $\langle E^{(-)}(t)E^{(+)}(t') \rangle$ is depending only on the time $\tau = t - t'$ and (2.34) is transformed into:

$$\begin{aligned} S(\nu) &= \frac{1}{2\pi} \lim_{T \rightarrow \infty} \int_0^T dt \left(\int_0^t dt' + \int_t^T dt' \right) \times \langle E^{(-)}(t)E^{(+)}(t') \rangle e^{-i(\nu - \omega_L)(t - t')} = \\ &= \frac{1}{2\pi} \lim_{T \rightarrow \infty} \int_0^T dt \left[\int_0^t d\tau \langle E^{(-)}(\tau)E^{(+)}(0) \rangle e^{-i(\nu - \omega_L)\tau} \right. \\ &\quad \left. + \int_0^{T-t} d\tau \langle E^{(-)}(0)E^{(+)}(\tau) \rangle e^{i(\nu - \omega_L)\tau} \right]. \end{aligned} \quad (2.35)$$

Taking into account that the field operators are correlated over a short time difference, then the upper limit of the τ -integrations to infinity without any perceptible changes. Thus we have

$$\langle E^{(-)}(\tau)E^{(+)}(0) \rangle = \langle E^{(-)}(0)E^{(+)}(\tau) \rangle. \quad (2.36)$$

Taking into account the equality (2.36), it follows from the (2.35) that the power spectrum of resonance fluorescence is expressed through the Riemann-Stieltjes integral

$$S(\nu) = \frac{1}{\pi} Re \int_0^\infty d\tau \langle E^{(-)}(0)E^{(+)}(\tau) \rangle e^{i(\nu - \omega_L)\tau}. \quad (2.37)$$

The resonance fluorescence spectrum is represented via the terms of the double-correlated functions of the emitted field [186]:

$$S(\nu) = \Phi(r) \int_0^\infty d\tau e^{i(\nu - \omega_L)\tau} \lim_{t \rightarrow \infty} \langle S^+(t)S^-(t - \tau) \rangle, \quad (2.38)$$

where $\Phi(r) = \frac{2d^2\omega_{21}^4}{3r^2c^4}$, r is the distance to the detector. In the double dressed picture, we found the

following expression for the correlation function entering in (2.38):

$$\begin{aligned}
& \lim_{t \rightarrow \infty} \langle S^+(t) S^-(t - \tau) \rangle = \\
& \langle \tilde{R}^- \tilde{R}^+(\tau) \rangle \left(\frac{1}{4} \sin^2 2\theta \sin^2 2\bar{\theta} + \cos^4 \theta \sin^4 \bar{\theta} e^{-i\omega\tau} + \sin^4 \theta \cos^4 \bar{\theta} e^{i\omega\tau} \right) + \\
& \langle \tilde{R}^+ \tilde{R}^-(\tau) \rangle \left(\frac{1}{4} \sin^2 2\bar{\theta} \sin^2 2\theta + \cos^4 \bar{\theta} \cos^4 \theta e^{-i\omega\tau} + \sin^4 \bar{\theta} \sin^4 \theta e^{i\omega\tau} \right) + \\
& \langle \tilde{R}_z \tilde{R}_z(\tau) \rangle \left(\frac{1}{4} \sin^2 2\theta \cos^2 2\bar{\theta} + \frac{1}{4} \sin^2 2\bar{\theta} \cos^4 \theta e^{-i\omega\tau} + \frac{1}{4} \sin^2 2\bar{\theta} \sin^4 \theta e^{i\omega\tau} \right).
\end{aligned} \tag{2.39}$$

Using the time-dependence of the qubit operators (2.39) and integrating the corresponding expressions according to Sokhotskyi-Plemelj formula [187], given as follows:

$$\int_0^t dt' e^{\pm(\nu - \omega_j)(t-t')} = \pi \delta(\nu - \omega_j) \pm iP \left(\frac{1}{\nu - \omega_j} \right), \tag{2.40}$$

we derive the following terms

$$Re \int_0^\infty d\tau e^{i(\nu - \omega_L)\tau} \langle \tilde{R}_z \tilde{R}_z(\tau) \rangle = \pi \langle R_z \rangle_s^2 \delta(\nu - \omega_L) + (1 - \langle R_z \rangle_s^2) \frac{\Gamma_\parallel}{\Gamma_\parallel^2 + (\nu - \omega_L)^2},$$

$$\begin{aligned}
& Re \int_0^\infty d\tau e^{i(\nu + \omega_L)\tau} e^{-i\omega\tau} \langle \tilde{R}_z \{ \langle \tilde{R}_z \rangle_s (1 - e^{-\Gamma_\parallel \tau}) + \tilde{R}_z e^{-\Gamma_\parallel \tau} \} \rangle = \\
& = \pi \langle R_z \rangle_s^2 \delta(\nu - \omega_L - \omega) + (1 - \langle R_z \rangle_s^2) \frac{\Gamma_\parallel}{\Gamma_\parallel^2 + (\nu - \omega_L - \omega)^2},
\end{aligned}$$

$$\begin{aligned}
& Re \int_0^\infty d\tau e^{i(\nu - \omega_L + \omega)\tau} \langle \{ e^{-\Gamma_\parallel \tau} (1 - \langle \tilde{R}_z \rangle_s^2) + \langle \tilde{R}_z \rangle_s^2 \} \rangle = \\
& = \pi \langle \tilde{R}_z \rangle_s^2 \delta(\nu - \omega_L + \omega) + (1 - \langle \tilde{R}_z \rangle_s^2) \frac{\Gamma_\parallel}{\Gamma_\parallel^2 + (\nu - \omega_L + \omega)^2},
\end{aligned}$$

$$Re \int_0^\infty d\tau e^{i(\nu - \omega_L)\tau} \langle \tilde{R}^- \tilde{R}^+(\tau) \rangle = \langle \tilde{R}^- \tilde{R}^+ \rangle_s \frac{\Gamma_s}{\Gamma_s^2 + (\nu - \omega_L + 2\bar{G}_R)^2},$$

$$Re \int_0^\infty d\tau e^{i(\nu - \omega_L - \omega)\tau} \langle \tilde{R}^- \tilde{R}^+(\tau) \rangle = \langle \tilde{R}^- \tilde{R}^+ \rangle_s \frac{\Gamma_s}{\Gamma_s^2 + (\nu - \omega_L - \omega + 2\bar{G}_R)^2},$$

$$Re \int_0^\infty d\tau e^{i(\nu - \omega_L + \omega)\tau} \langle \tilde{R}^- \tilde{R}^+(\tau) \rangle = \langle \tilde{R}^- \tilde{R}^+ \rangle_s \frac{\Gamma_s}{\Gamma_s^2 + (\nu - \omega_L + \omega + 2\bar{G}_R)^2},$$

$$Re \int_0^\infty d\tau e^{i(\nu - \omega_L)\tau} \langle \tilde{R}^+ \tilde{R}^-(\tau) \rangle = \langle \tilde{R}^+ \tilde{R}^- \rangle_s \frac{\Gamma_s}{\Gamma_s^2 + (\nu - \omega_L - 2\bar{G}_R)^2},$$

$$\begin{aligned}
\text{Re} \int_0^\infty d\tau e^{i(\nu - \omega_L - \omega)\tau} \langle \tilde{R}^+ \tilde{R}^-(\tau) \rangle &= \langle \tilde{R}^+ \tilde{R}^- \rangle_s \frac{\Gamma_s}{\bar{\Gamma}_s^2 + (\nu - \omega_L - \omega - 2\bar{G}_R)^2}, \\
\text{Re} \int_0^\infty d\tau e^{i(\nu - \omega_L + \omega)\tau} \langle \tilde{R}^+ \tilde{R}^-(\tau) \rangle &= \langle \tilde{R}^+ \tilde{R}^- \rangle_s \frac{\Gamma_s}{\bar{\Gamma}_s^2 + (\nu - \omega_L + \omega - 2\bar{G}_R)^2}.
\end{aligned} \tag{2.41}$$

We obtain the final expression of resonance fluorescence spectra in the steady-state [188]:

$$\begin{aligned}
S(\nu) &= \frac{1}{4} \sin^2 2\theta \cos^2 \bar{\theta} \left\{ \pi \langle \tilde{R}_z \rangle_s^2 \delta(\nu - \omega_L) + (1 - \langle \tilde{R} \rangle_s^2) \frac{\Gamma_{\parallel}}{\bar{\Gamma}_{\parallel}^2 - (\nu - \omega_L)^2} \right\} \\
&+ \frac{1}{4} \sin^2 2\bar{\theta} \cos^4 \theta \left\{ \pi \langle \tilde{R}_z \rangle_s^2 \delta(\nu - \omega_L - \omega) + (1 - \langle \tilde{R} \rangle_s^2) \frac{\Gamma_{\parallel}}{\bar{\Gamma}_{\parallel}^2 - (\nu - \omega_L - \omega)^2} \right\} \\
&+ \frac{1}{4} \sin^2 2\bar{\theta} \sin^4 \theta \left\{ \pi \langle \tilde{R}_z \rangle_s^2 \delta(\nu - \omega_L + \omega) + (1 - \langle \tilde{R} \rangle_s^2) \frac{\Gamma_{\parallel}}{\bar{\Gamma}_{\parallel}^2 - (\nu - \omega_L + \omega)^2} \right\} \\
&+ \langle \tilde{R}^- \tilde{R}^+ \rangle_s \left[\frac{1}{4} \sin^2 2\theta \sin^2 2\bar{\theta} \frac{\bar{\Gamma}_s}{\bar{\Gamma}_s^2 + (\nu - \omega_L + 2\bar{G}_R)^2} + \right. \\
&+ \left. \cos^4 \theta \sin^4 \bar{\theta} \frac{\bar{\Gamma}_s}{\bar{\Gamma}_s^2 + (\nu - \omega_L - \omega + 2\bar{G}_R)^2} + \sin^4 \theta \cos^4 \bar{\theta} \frac{\bar{\Gamma}_s}{\bar{\Gamma}_s^2 + (\nu - \omega_L + \omega + 2\bar{G}_R)^2} \right] \\
&+ \langle \tilde{R}^+ \tilde{R}^- \rangle_s \left[\frac{1}{4} \sin^2 2\bar{\theta} \sin^2 2\theta \frac{\bar{\Gamma}_s}{\bar{\Gamma}_s^2 + (\nu - \omega_L - 2\bar{G}_R)^2} + \right. \\
&+ \left. \cos^4 \bar{\theta} \cos^4 \theta \frac{\bar{\Gamma}_s}{\bar{\Gamma}_s^2 + (\nu - \omega_L - \omega - 2\bar{G}_R)^2} + \sin^4 \theta \sin^4 \bar{\theta} \frac{\bar{\Gamma}_s}{\bar{\Gamma}_s^2 + (\nu - \omega_L + \omega - 2\bar{G}_R)^2} \right],
\end{aligned} \tag{2.42}$$

note that: $\Gamma_{\parallel} = 2(\bar{\Gamma}_- + \bar{\Gamma}_+)$.

The spectrum of *resonance fluorescence* describes the light scattered by a two-level system with permanent dipole that is driven by a laser of frequency ω_L and a second laser of frequency ω . The spectrum is sketched in Fig.2.2(a) and exhibits for a sufficiently large laser intensity three triplets whose width in frequency is of the order of the atomic decay rate Γ_{\parallel} and $\bar{\Gamma}_s$. Additionally, the central line of the central triplet is an elastic line at the laser frequency whose width is limited by the frequency width of the laser. The Mollow spectra presented in Fig.2.2(a) is an example of inelastic scattering since the frequency of laser is changing due to the double dressed-state formalism. We shall consider this aspect in this paragraph. The correlation function for resonance fluorescence contains components proportional to the dipole moment itself. According to the Glauber theory of photodetection [1, 187], which proves that the observed signal involves *normally ordered* correlation functions of the electric field, thus the resonance fluorescence spectrum is related to the

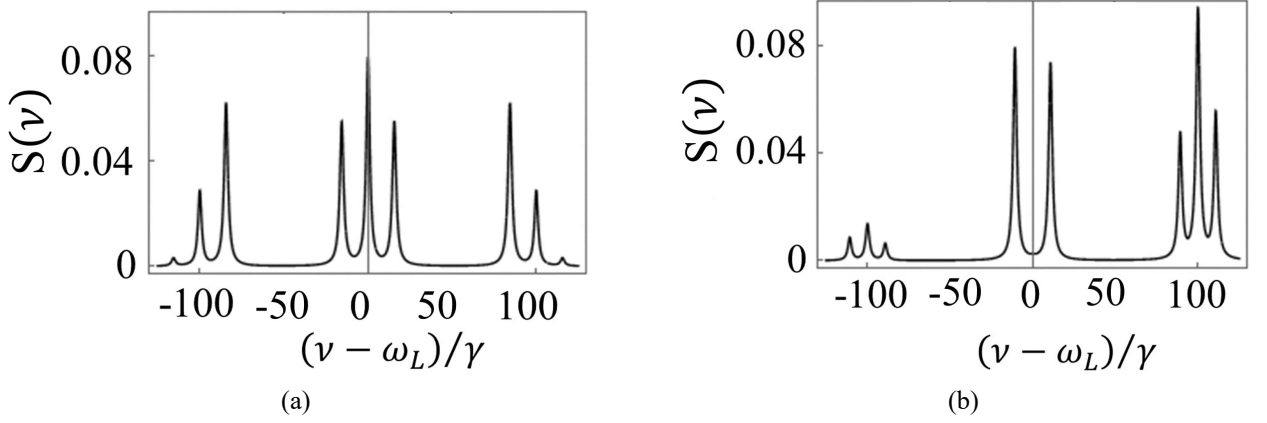


Fig. 2.2: Resonance fluorescence spectra computed for the non-zero permanent dipole moment $G \neq 0$ and the laser detuning ratio over the Rabi frequency: (a) $\frac{\Delta}{2\Omega} = 0$; (b) $\frac{\Delta}{2\Omega} = 0, 5$. Here $\frac{\Omega}{\gamma} = 45$ is a parameter representing the ratio between Ω the Rabi frequency and the spontaneous decay rate γ and $\Omega \gg \gamma$, whereas $\frac{\omega}{\gamma} = 100$ corresponds to the ratio between the frequency of dynamical Stark splitting ω and the spontaneous decay rate [191].

normally ordered dipole autocorrelation. Due to the transformation into the frame rotating at the laser frequency ω_L appears the exponential $e^{i\omega_L\tau}$ and this factor explains the position of the central peak in the spectrum is located near the laser frequency. Also it shows that the two-level system has reached a stationary state determined by the laser field and its radiative decay.

The explicit solutions of the master equation involves cumbersome algebraic calculations, and we shall mention the most important aspect of those manipulations. One of the main ideas is to rewrite the solutions of the master equations. Each of these functions evolves in time with exponential $e^{-i\nu\tau}$ and gives a contribution to the spectrum that consists of Lorentzian peaks. The real part of the integrals give the Lorentz-like profile and the frequency shift with respect to the detector frequency. Also since the stationary solutions of the master equation are reached at long times, we can conclude that all eigenvalues of the master equation must have positive real part.

Analyzing the resonance fluorescence spectrum given in eq.(2.42), one can observe that there are three coherently scattered spectral lines at ω_L , and $\omega_L \pm \omega$ and up to nine incoherently scattered spectral bands, i.e., at $\nu - \omega_L = 0, \nu - \omega_L - \omega = 0, \nu - \omega_L + \omega = 0$, etc., in agreement with double-dressed state picture. Particularly, Fig.2.2(a) and Fig.2.2(b), depicts the resonance fluorescence spectrum for certain parameters. In the strong driving approximation, the two additional side triplets, displaced by the generalized Rabi frequency in the double-dressed state formalism $2\bar{G}_R$. This spectral structure is similar to the Mollow triplet. More specifically, one can observe the cancellation of the central spectral band due to interference effects among the induced double dressed-state transitions. Asymmetrical behaviors in the scattered light spectrum are observed as well. This is because of the population inversion in the bare state and it differs from usual resonance

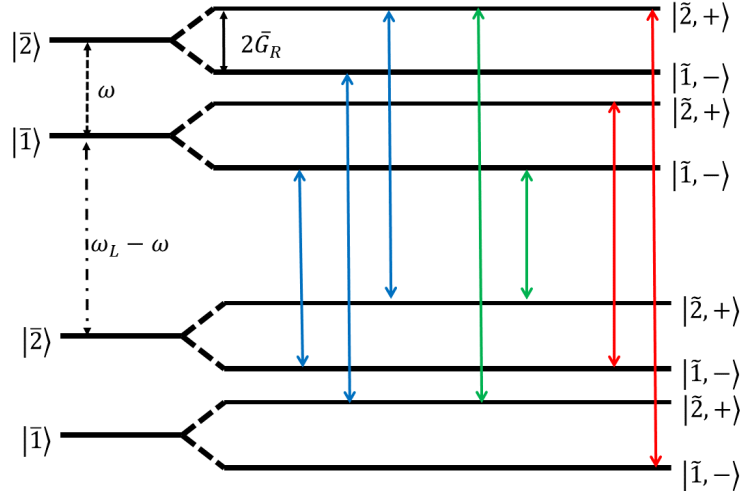


Fig. 2.3: Dressed-state and double dressed-states atom diagrams showing some of the nine optical transitions indicated by arrows and corresponding to the spectra presented in Fig.2.2(a).

fluorescence spectrum obtained in the absence of permanent dipoles.

Notice, in the resonance fluorescence spectrum presented in eq.(2.42) the first three terms represent the coherent part of the spectrum, whereas the last three terms correspond to the incoherent Mollow spectra line emission. The relative height of the red shifted triplet side-bands: central triplet: blue shifted triplet sidebands is 1:3:1, the relative area ratio is 1:2:1 and the width of in angular frequencies is found to be Γ_{\parallel} for the central Mollow triplet and $\bar{\Gamma}_s$ for the side-bands respectively, which is evident in the Fig.2.2(a).

Using the optical Bloch equations, one has calculated the resonance fluorescence spectrum at high intensity or large detuning this spectrum consists of three triplets. We will try to discuss the various features of the Mollow fluorescence spectra consisting of nine lines, which can be related to the existence of doublets of the dressed states. Since the dipolar two-level system is resonant due to the first laser ω_L so it degenerates the bare states $|1\rangle, |2\rangle$. When the atom-field coupling is taken into account and the pumping of the second laser ω , one gets series of doublets of double-dressed states represented in the right part of Fig.2.3, where the splitting of the each doublet equals to $2\bar{G}_R$, which is the generalized Rabi frequency corresponding to the field associated with the cavity. By the strong coupling regime, we mean that the damping rate of the field in the cavity also the damping rate of the atom are small enough in comparison to $2\bar{G}_R$ that the two dressed states of each double-dressed doublet are well resolved.

The left part of Fig.2.3 represent two adjacent manifolds of uncoupled dressed-states, similar to the ones shown in Fig.2.5. Since the distance between the upper two and lower two manifolds is ω_L . When the coupling is taken into consideration, one gets the four doublets of double-dressed states represented, $|\bar{2}, +\rangle$ and $|\bar{1}, +\rangle$ in the right part of Fig.2.3. In each doublet the splitting is $2\bar{G}_R$ and the

distance between the upper doublets and lower doublets is $\omega_L - \omega - 2\bar{G}_R$. The allowed spontaneous transitions that take place between double-dressed states levels for which the dipole moment has a nonzero value. One immediately understands in this way why the resonance fluorescence spectrum consists of nine lines with frequencies $\omega_L, \omega_L + \omega, \omega_L - \omega, \omega_L - 2\bar{G}_R, \omega_L + \omega - 2\bar{G}_R, \omega_L - \omega - 2\bar{G}_R, \omega_L + 2\bar{G}_R, \omega_L + \omega + 2\bar{G}_R, \omega_L - \omega + 2\bar{G}_R$, associated with transitions between the four doublets $|\tilde{1}, -\rangle \rightarrow |\tilde{1}, -\rangle, |\tilde{1}, -\rangle \rightarrow |\tilde{2}, +\rangle, |\tilde{2}, +\rangle \rightarrow |\tilde{2}, +\rangle, |\tilde{2}, +\rangle \rightarrow |\tilde{1}, -\rangle$, respectively considering the strong field approximation.

The peaks in the resonance fluorescence spectrum, see Fig.2.2(a) can be interpreted in terms of transitions between the double-dressed states of Jaynes-Cummings model. Following this analysis, the emission at the laser frequency ω_L come from transition $|\tilde{1}, -\rangle \rightarrow |\tilde{1}, -\rangle$ and $|\tilde{2}, +\rangle \rightarrow |\tilde{2}, +\rangle$. The transitions on the sidebands of the central triplet occur when the atom changes $|\tilde{1}, -\rangle \rightarrow |\tilde{2}, +\rangle$ at $\omega_L - \omega$ or $\omega_L + \omega$, corresponding to the blue arrows in Fig.2.3. Here the fluorescence photon is shifted because of the splitting between the double-dressed states. The transitions on the left triplet are associated in the following way $|\tilde{1}, -\rangle \rightarrow |\tilde{2}, +\rangle$ at $\omega_L - 2\bar{G}_R$; $|\tilde{2}, +\rangle \rightarrow |\tilde{2}, +\rangle$ at $\omega_L - \omega - 2\bar{G}_R$; $|\tilde{1}, -\rangle \rightarrow |\tilde{2}, +\rangle$ at $\omega_L - \omega + 2\bar{G}_R$ and are corresponding the green arrows in Fig.2.3. Additionally, the right triplet is associated to the atomic changes from the following states $|\tilde{2}, +\rangle \rightarrow |\tilde{1}, -\rangle$ at $\omega_L + 2\bar{G}_R$; $|\tilde{2}, +\rangle \rightarrow |\tilde{1}, -\rangle$ at $\omega_L - \omega + 2\bar{G}_R$; $|\tilde{2}, +\rangle \rightarrow |\tilde{1}, +\rangle$ at $\omega_L + \omega + 2\bar{G}_R$. Alternatively, the occurrence of the nine lines in the fluorescence spectrum is explained by the two-level system flops at the Rabi frequency $2\bar{G}_R$ between the ground and the excited state and its emission is amplitude and frequency modulated. Therefore, the emission spectrum contains bands at $\omega_L \pm \omega, \omega_L \pm 2\bar{G}_R$ and side triplets at $\omega_L - \omega \pm 2\bar{G}_R, \omega_L + \omega \pm 2\bar{G}_R$. Unlike the spectrum represented in Fig.2.2(a), the fluorescence spectrum in Fig.2.2(b) exhibits cancellation of the central line at laser frequency ω_L and the increase in the amplitude of the right sided triplet and the decrease of the left sided triplet. These changes occur due to the interference effects among the double-dressed states and in non-resonant case when the laser detuning has non-zero values.

Additionally, we have computed the resonance fluorescence spectra assuming the zero value of the dipolar moment, $G = 0$. We have obtained the Mollow spectra Fig.2.4 in the strong field approximation. This means the spectrum contains three peaks. The two additional peaks are displaced by the generalized $\bar{\Omega}$ Rabi frequency from the laser frequency.

The triplet describing the two-level system as dressed by the laser is generated by the new eigenstates, formed from a combination of bare states of the two level system. A family of such states whose total energy is the same, forms a manifold of excitation. In every manifold, the eigenstates are split by the generalized Rabi frequency $\bar{\Omega}$, while the energy difference between two manifolds

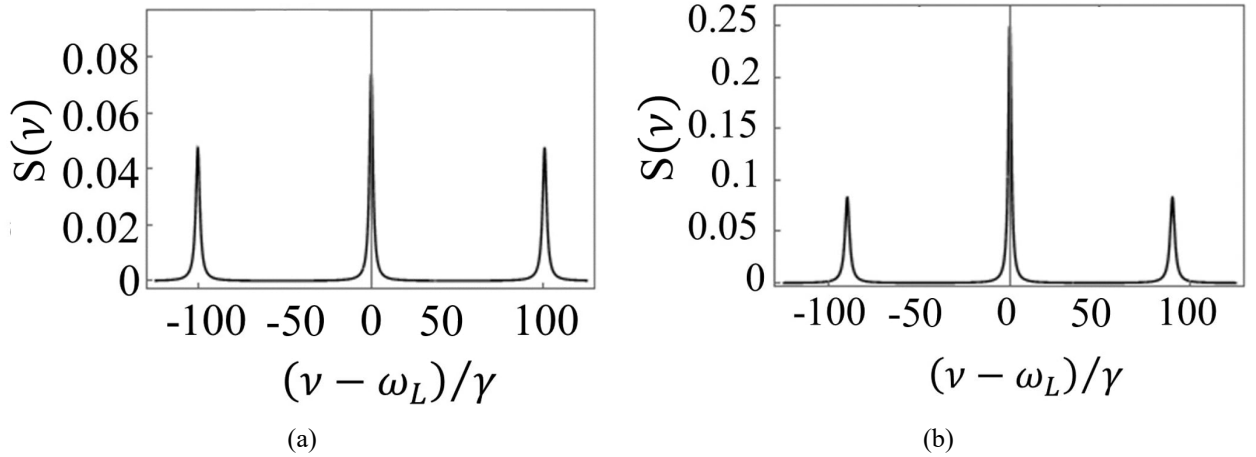


Fig. 2.4: Resonance fluorescence spectra computed for the zero value of the permanent dipole moment $G = 0$. Here (a) $\frac{\Delta}{2\Omega} = 0.5$ and (b) $\frac{\Delta}{2\Omega} = 0$ are the ratio between the laser detuning and the Rabi frequency. Other parameters are the ratio between the Rabi frequency Ω and spontaneous decay rate γ , namely $\frac{\Omega}{\gamma} = 45$ and $\Omega \gg \gamma$ [191].

is that of bare states. The transitions taking place between manifolds exhibit the main features: a triplet in which the integrated spectral intensities of its peaks have 1:2:1 proportions, when the laser is resonant with the two-level system. This spectral shape is readily derived by solving the master equation, and it is better understood from the physics perspective as transitions between the eigenstates $|\bar{1}\rangle$ and $|\bar{2}\rangle$ introduced earlier. The level structure of the ladder of manifolds, separated by the energy of the of difference between the first and the second laser $\omega - \omega_L$ and each split by ω , proves the phenomenology of resonance fluorescence in the high-excitation regime. The central peak of the spectrum is twice high unlike the neighboring peaks due to the four degenerate transitions. The dressed-state description of the transitions and the quantitative results can be obtained by the master equations for the transitions between the states. The transitions that yield the central peak, highlighted by *red arrows* in Fig.2.5, leave the two-level system unchanged, while those yielding the side peaks, *green arrow* and *light-blue arrow* change the state of the two-level system. In this configuration, changes in the populations of the particular dressed state via one-photon transitions can occur in the following ways: relaxation into a given level involves two transitions down from the upper manifold and relaxation out of the level occurs by two transitions down to the lower neighboring manifold.

Using the quantum mechanical treatment of resonantly pumped two-level system in the framework *dressed state*, which is particularly important to explain the non-classical features of resonance fluorescence spectra computed for the case when the dipolar moment is zero $G = 0$, namely the photon correlations on the Mollow triplet spectra. The excitation laser represented by coherent

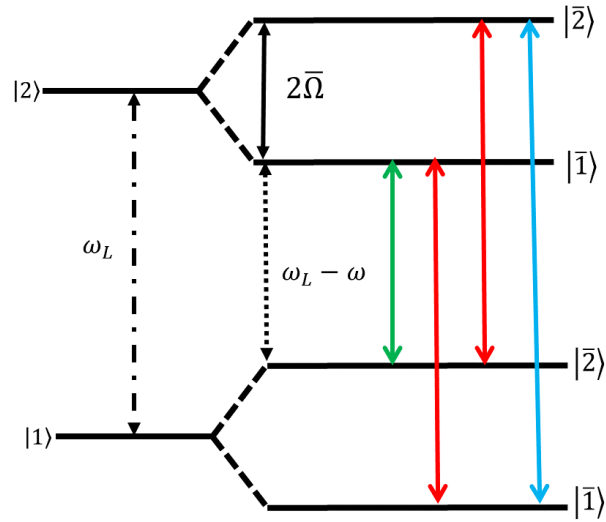


Fig. 2.5: Dressed-state atom diagram showing the three optical transitions indicated by arrows and corresponding to the spectra presented in Figs.2.4(a) and (b).

light states, which are a superposition of photon number states, interacts with the two-level system, consisting of uncoupled states. Via the dynamic Stark interaction the uncoupled states are transformed into a new combination of eigenstates named as before in this chapter *dressed states*, which are now coupled. Taking into account the energetic separation of the dressed states for all manifolds unlike the classic Jaynes-Cummings ladder, the properties of a strongly driven two-level system can be interpreted using the reduced part of only two neighbouring doublets of the whole ladder structure as depicted in Fig.2.5. The four optically allowed transitions are indicated in the Fig.2.5 via arrows. In the spectra shown in Fig.2.4(a) and (b) these transitions are reflected by the characteristic Mollow triplet. The transitions from \$|\bar{2}\rangle \rightarrow |\bar{2}\rangle\$ and \$|\bar{1}\rangle \rightarrow |\bar{1}\rangle\$, highlighted by the red arrows give, rise to the emission at the two-level system resonance corresponding to as Rayleigh line. The two sidebands are generated by the transitions \$|\bar{2}\rangle \rightarrow |\bar{1}\rangle\$ and \$|\bar{1}\rangle \rightarrow |\bar{2}\rangle\$. The lower energetic sideband is associated with the fluorescence line since it is the nearest to the two-level system resonance for laser detuning \$\Delta \geq 0\$. Taking into account, that there are two possible transitions corresponding to the central band, compared to the probability of photon transitions arising from the sidebands, then the central peak has twice the area of the individual sidebands. Additionally, it is important to mention that the resonance fluorescence spectra shown in Fig.2.4(a) computed when \$\frac{\Delta}{2\Omega} = 0.5\$ manifests lower amplitude Mollow triplet spectra unlike the resonance fluorescence spectra in Fig.2.4(b), proving the impact of the ratio of laser detuning over the Rabi frequency \$\frac{\Delta}{2\Omega}\$.

Finalizing this part, one has studied the resonance fluorescence properties of this system and we figure out new properties of the resonance fluorescence spectra due to the permanent dipole

moment. Particularly, one has studied the resonance fluorescence spectra for certain parameters. One has observed the changes in spectra due to interference effects induced by double-dressed state transitions. As well, asymmetrical behaviors in the scattered light spectrum are noticed as well, due to the different population inversion in the bare state unlike the usual resonance fluorescence spectrum computed in the absence of permanent dipole.

One has shown in this paragraph that the positions of the spectral lines are determined by the splitting of the dressed states, which in our case is dependent on the Rabi frequency and the heights of the spectra are proportional to the populations of the corresponding dressed state and numerically expressed by the spontaneous decay rates. In this context, one mention that the dressed-state populations in a such system might be associated with Bessel functions of argument $\frac{\Delta}{2\Omega}$ [205] and for certain values of Rabi frequency, the function gets zero value, resulting in disappearance of the corresponding spectral line evident in Fig.2.2(b). Since the dressed-state population is symmetrically distributed about the central dressed state in each manifold. Thus the resonance fluorescence spectrum in Figs.2.2(a), 2.4(a) and (b) are symmetric about the laser frequency ω_L . In the following, one shall calculate the squeezing effects in the resonance fluorescence processes of laser-pumped molecules with permanent dipoles [187, 188].

2.3 Squeezing spectra and quantum fluctuations

Before embarking on the detailed calculation, we will introduce the basics of squeezing, and how it can occur in a two-level system possessing a permanent dipole. The minimum variance in any quantum measurement involving some canonical conjugates variables, for example the position and momentum are restricted by the Heisenberg uncertainty principle. Though this principle cannot be disregarded, the fluctuations of a single variable can be minimized below the minimal value taking the advantage of improving the fluctuations of the conjugate variable. The most extensively researched implementation of this non-classical phenomenon is the squeezed light, where the quadrature operators \hat{X}_1 and \hat{X}_2 of the electric field are canonically conjugated operators. Based on the quadratic dependence on the bosonic creation and annihilation operators in the Hamiltonian, squeezed light can be generated using intense laser fields and other nonlinear optical source. Additionally, we mention the practical importance of the squeezed light as it is employed in interferometry with reduced quantum noise.

Having motivated the study and nature of squeezed states, we shall consider A and B which satisfy the commutation relation, which verify the commutation relation

$$[A, B] = iC. \quad (2.43)$$

Following the Heisenberg uncertainty principle, the product of the uncertainties in determining the expectation values of the two variables A and B is determined by

$$\Delta A \Delta B \geq \frac{1}{2} |\langle C \rangle|. \quad (2.44)$$

Therefore, we consider that the state system is named squeezed if the uncertainty in one observable, for example A verifies the relation

$$(\Delta A)^2 < \frac{1}{2} |\langle C \rangle| \quad (2.45)$$

Beside the condition (2.45), the variances verify the minimum-uncertainty relation, i. e.,

$$\Delta A \Delta B = \frac{1}{2} |\langle C \rangle|, \quad (2.46)$$

then the state is defined as an ideal squeezed state. Consequently, in a squeezed state, the quantum fluctuations of one variable are smaller than their value in a symmetric minimum-uncertainty state $(\Delta A)^2 = (\Delta B)^2 = \frac{|\langle C \rangle|}{2}$ from the corresponding increased fluctuations in the conjugated variable, maintaining the uncertainty relation non-violated [187].

As we mentioned above, the most proper illustration of state squeezing condition are the quadrature operators of a quantized single-mode electric field of frequency ν

$$\mathbf{E}(t) = \mathcal{E}\hat{\epsilon}(ae^{-i\nu t} + a^\dagger e^{i\nu t}), \quad (2.47)$$

in the above formula the a and a^\dagger verify the commutation relation

$$[a, a^\dagger] = 1. \quad (2.48)$$

We introduce the Hermitian quadrature operators, describing the quantized single-mode electric field:

$$\begin{aligned} X_1 &= \frac{1}{2}(a + a^\dagger), \\ X_2 &= \frac{1}{2i}(a - a^\dagger), \end{aligned} \quad (2.49)$$

Since both single-mode electric field quadrature operators are functions of generation and annihilation operators, they obey the following commutation relation

$$[X_1, X_2] = \frac{i}{2}. \quad (2.50)$$

Rewriting the expression of the single-mode electric field, one substitutes the Hermitian quadrature operators in (2.47) and derives the following expression:

$$\mathbf{E}(t) = 2\mathcal{E}\hat{\epsilon}(X_1 \cos \nu t + X_2 \sin \nu t) \quad (2.51)$$

The Hermitian operators X_1 and X_2 are now evidently to be the amplitudes of the quantized single-mode electric field having a phase difference $\frac{\pi}{2}$. The uncertainty relation for the two amplitudes is:

$$\Delta X_1 \Delta X_2 \geq \frac{1}{4}. \quad (2.52)$$

Thus, a squeezing of the lasing field occurs when:

$$\langle \Delta X_i \rangle^2 < \frac{1}{4}, (i = 1, 2) \quad (2.53)$$

The ideal, squeezed state is generated if is verified the relation

$$\Delta X_1 \Delta X_2 = \frac{1}{4} \quad (2.54)$$

The steady-state spectrum of squeezing is a phase-sensitive effect, which is evident from the

expression of the slowly varying part of the radiated field at the detector [32]:

$$S_\varphi(\nu) = \frac{\gamma}{|\mu|^2} \int_0^\infty [e^{i\nu\tau} + e^{-i\nu\tau}] \times \lim_{t \rightarrow \infty} \Gamma_\varphi(t + \tau, t) d\tau, \quad (2.55)$$

where $\Gamma_\varphi(t + \tau), t = \langle : \Delta E_\varphi(t + \tau) \Delta E_\varphi(t) : \rangle$ is the normally ordered variance of the electric field. The reduced quantum fluctuations are phase dependent due to the weak oscillating terms of the filed emitted to the detector:

$$E_\varphi(t) = \frac{E^+(t)e^{i\varphi} + E^-(t)e^{-i\varphi}}{2}, \quad (2.56)$$

where φ is the phase reference and $E^{(\pm)}$ are the negative and positive amplitudes of the filed, and the quadrature variance is $\Delta E_\varphi(t)^2 = \langle E_\varphi(t)^2 \rangle - \langle E_\varphi(t) \rangle^2$. The Heisenberg uncertainty relation connects to variances in two out of phase quadratures via the following manner $\Delta E_\varphi(t) \Delta E_{\varphi+\frac{\pi}{2}}(t) \geq \frac{1}{2} |\langle [E_\varphi(t), E_{\varphi+\frac{\pi}{2}}(t)] \rangle|$. We consider the state of the field is a minimal uncertainty state when the reference state is saturated, and then the filed becomes squeezed if there is a quadrature that verifies the following inequality $\Delta E_\varphi(t)^2 < \frac{1}{2} |\langle [E_\varphi(t), E_{\varphi+\frac{\pi}{2}}(t)] \rangle|$.

The spectrum of squeezing is related to the normal-order variance:

$$\begin{aligned} \Gamma_\varphi(t + \tau, t) &= \langle : \Delta E_\varphi(t + \tau) \Delta E_\varphi(t) : \rangle \\ &= \frac{1}{4} [e^{2i\varphi} \langle \Delta E^{(+)}(t + \tau) \Delta E^{(+)}(t) \rangle + e^{-2i\varphi} \langle \Delta E^{(-)}(t) \Delta E^{(-)}(t + \tau) \rangle \\ &\quad + \langle \Delta E^{(-)}(t + \tau) \Delta E^{(+)}(t) \rangle + \langle \Delta E^{(-)}(t) \Delta E^{(+)}(t + \tau) \rangle]. \end{aligned} \quad (2.57)$$

Here, the fluctuations presented by eq.(2.57) $\Delta A = A - \langle A \rangle$ and the angular brackets denote the averages with respect to the atomic density operator ρ .

Particularly, one can show that the normally ordered variance of the radiated field:

$$\begin{aligned} \Gamma_\varphi(t + \tau, t) &= \frac{1}{4} \times \\ &\left\langle : \left(E^+(t + \tau)e^{i\varphi} - E^-(t + \tau)e^{-i\varphi} - \langle E^+(t + \tau) \rangle e^{i\varphi} - \langle E^-(t + \tau) \rangle e^{-i\varphi} \right) \right. \\ &\quad \left. \times \left(E^+(t)e^{i\varphi} - E^-(t)e^{-i\varphi} - \langle E^+(t) \rangle e^{i\varphi} - \langle E^-(t) \rangle e^{-i\varphi} \right) : \right\rangle \end{aligned} \quad (2.58)$$

or the fluctuations of the normally ordered variance of the electric field is

$$\begin{aligned} \Gamma_\varphi(t + \tau, t) &= \\ &\frac{1}{4} \times \left\{ e^{2i\varphi} \langle E^+(t + \tau) E^+(t) \rangle + e^{-2i\varphi} \langle E^-(t + \tau) E^-(t) \rangle \right. \\ &\quad \left. + \langle E^-(t + \tau) E^+(t) \rangle + \langle E^-(t) E^+(t + \tau) \rangle \right\}. \end{aligned} \quad (2.59)$$

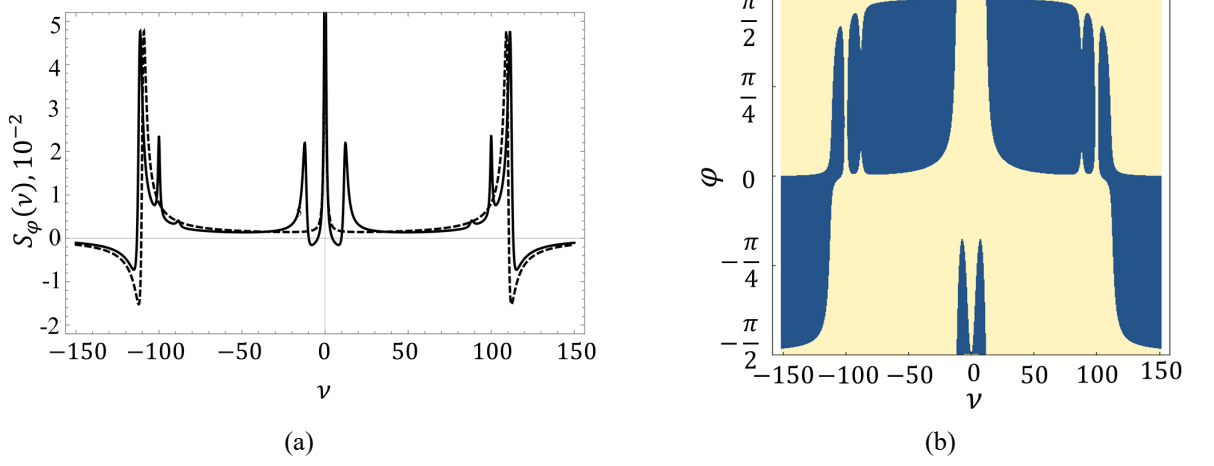


Fig. 2.6: Squeezing spectrum $S_\varphi(\nu)$ as function of ν : (a) in the absence of permanent dipole moment $\frac{g}{\gamma} = 0$ it corresponds to the dashed line and in the presence of dipole moment, $\frac{g}{\gamma} = 16$ it corresponds to the solid line while the observation angle is $\varphi = -\frac{\pi}{4}$; (b) the projection of squeezing spectrum function in the system of coordinates defined by the observation angle φ and frequency ν [191].

In the strong field approximation and in the absence of the free field, the radiated field $E^+(t)$ can be substituted by $\mu S_-(t)$ [186]. Since $E^+ \sim a \sim S^-$, $E^- \sim a^\dagger \sim S^+$, in this way, we can assume

$$\begin{aligned}
\langle \Delta E^+(t + \tau) \rangle &= S^-(t + \tau) - \langle S^-(t + \tau) \rangle, \\
\langle \Delta E^+(t) \rangle &= S^-(t) - \langle S^-(t) \rangle, \\
\langle \Delta E^-(t + \tau) \rangle &= S^+(t + \tau) - \langle S^+(t + \tau) \rangle, \\
\langle \Delta E^-(t) \rangle &= S^+(t) - \langle S^+(t) \rangle.
\end{aligned} \tag{2.60}$$

In this way we get the normal ordered correlation function, consisting of atomic operators:

$$\begin{aligned}
\Gamma_\varphi(t + \tau, t) &= \frac{|\mu|^2}{4} \times \\
&\left\{ e^{2i\varphi} (\langle S^-(t + \tau) S^-(t) \rangle - \langle S^-(t + \tau) \rangle \langle S^-(t) \rangle) + \right. \\
&+ e^{-2i\varphi} (\langle S^+(t) S^+(t + \tau) \rangle - \langle S^+(t) \rangle \langle S^+(t + \tau) \rangle) + \\
&+ (\langle S^+(t + \tau) S^-(t) \rangle - \langle S^+(t + \tau) \rangle \langle S^-(t) \rangle) + \\
&\left. + (\langle S^+(t) S^-(t + \tau) \rangle - \langle S^+(t) \rangle \langle S^-(t + \tau) \rangle) \right\}.
\end{aligned} \tag{2.61}$$

Next step involves substitution of the atomic operators in the double dressed-state derived in previous paragraph (2.2) base in equation corresponding to the normal ordered variance (2.61). Thus, we obtain the normal ordered variance which includes the fluctuations of the atomic operators

from their steady-state mean value and the relative phase of the applied field φ :

$$\begin{aligned}
\Gamma_\varphi(t + \tau, t) &= \frac{|\mu|^2}{4} \times \\
&\frac{1}{2} \sin^2 2\theta \cos 2\varphi \left(\cos^2 2\bar{\theta} - \frac{1}{2} \sin^2 2\bar{\theta} \cos \omega\tau \right) (\langle \tilde{R}_z \tilde{R}_z(\tau) \rangle - \langle \tilde{R}_z \rangle \langle \tilde{R}_z(\tau) \rangle) \\
&+ \frac{1}{4} \sin^2 2\theta (\sin^2 2\theta - \sin^4 \bar{\theta} e^{-i\omega\tau} - \cos^4 \bar{\theta} e^{i\omega\tau}) (\langle \tilde{R}^+(\tau) \tilde{R}^- \rangle e^{2i\varphi} + \langle \tilde{R}^- \tilde{R}^+(\tau) \rangle e^{-2i\varphi}) \\
&+ \frac{1}{4} \sin^2 2\theta (\sin^2 2\theta - \cos^4 \bar{\theta} e^{-i\omega\tau} - \sin^4 \bar{\theta} e^{i\omega\tau}) (\langle \tilde{R}^-(\tau) \tilde{R}^+ \rangle e^{2i\varphi} + \langle \tilde{R}^+ \tilde{R}^-(\tau) \rangle e^{-2i\varphi}) \\
&+ \left(\frac{1}{4} \sin^2 2\theta \cos^2 2\bar{\theta} + \frac{1}{4} \sin^2 2\bar{\theta} \cos^4 \theta e^{i\omega\tau} + \frac{1}{4} \sin^2 2\bar{\theta} \sin^4 \theta e^{-i\omega\tau} \right) (\langle \tilde{R}_z(\tau) \tilde{R}_z \rangle - \langle \tilde{R}_z(\tau) \rangle \langle \tilde{R}_z \rangle) \\
&+ \left(\frac{1}{4} \sin^2 2\theta \sin^2 2\bar{\theta} + \sin^4 \bar{\theta} \cos^4 \theta e^{i\omega\tau} + \cos^4 \bar{\theta} \sin^4 \theta e^{-i\omega\tau} \right) \langle \tilde{R}^-(\tau) \tilde{R}^+ \rangle \\
&+ \left(\frac{1}{4} \sin^2 2\theta \sin^2 2\bar{\theta} + \cos^4 \bar{\theta} \cos^4 \theta e^{i\omega\tau} + \sin^4 \bar{\theta} \sin^4 \theta e^{-i\omega\tau} \right) \langle \tilde{R}^+(\tau) \tilde{R}^- \rangle \\
&+ \left(\frac{1}{4} \sin^2 2\theta \cos^2 2\bar{\theta} + \frac{1}{4} \sin^2 2\bar{\theta} \cos^4 \theta e^{i\omega\tau} + \frac{1}{4} \sin^2 2\bar{\theta} \sin^4 \theta e^{-i\omega\tau} \right) (\langle \tilde{R}_z \tilde{R}_z(\tau) \rangle - \langle \tilde{R}_z \rangle \langle \tilde{R}_z(\tau) \rangle) \\
&+ \left(\frac{1}{4} \sin^2 2\theta \sin^2 2\bar{\theta} + \sin^4 \bar{\theta} \cos^4 \theta e^{i\omega\tau} + \cos^4 \bar{\theta} \sin^4 \theta e^{-i\omega\tau} \right) \langle \tilde{R}^- \tilde{R}^+(\tau) \rangle \\
&+ \left(\frac{1}{4} \sin^2 2\theta \sin^2 2\bar{\theta} + \cos^4 \bar{\theta} \cos^4 \theta e^{i\omega\tau} + \sin^4 \bar{\theta} \sin^4 \theta e^{-i\omega\tau} \right) \langle \tilde{R}^+ \tilde{R}^-(\tau) \rangle. \tag{2.62}
\end{aligned}$$

We substitute the stationary solutions of the of the Bloch equations in the normally ordered variance expressed by eq.(2.62) showing the fluctuations of the atomic operators containing the parameters of interest as the the generalized Rabi frequency \bar{G}_R and the decay rate $\bar{\Gamma}_S$. Also it is convenient to rewrite the two-time correlation functions from eq. (2.62) determined by the coupled Bloch equations solutions, also making a contribution to the central component as well as to the sidebands:

$$\begin{aligned}
\langle \tilde{R}^-(\tau) \tilde{R}^+ \rangle &= \frac{1}{2} (1 - \langle \tilde{R}_z \rangle_s) e^{-(2i\bar{G}_R + \bar{\Gamma}_s)\tau}, \\
\langle \tilde{R}^+ \tilde{R}^-(\tau) \rangle &= \frac{1}{2} (1 + \langle \tilde{R}_z \rangle_s) e^{-(2i\bar{G}_R + \bar{\Gamma}_s)\tau}, \\
\langle \tilde{R}^+(\tau) \tilde{R}^- \rangle &= \frac{1}{2} (1 + \langle \tilde{R}_z \rangle_s) e^{(2i\bar{G}_R - \bar{\Gamma}_s)\tau}, \\
\langle \tilde{R}^- \tilde{R}^+(\tau) \rangle &= \frac{1}{2} (1 - \langle \tilde{R}_z \rangle_s) e^{(2i\bar{G}_R - \bar{\Gamma}_s)\tau}. \tag{2.63}
\end{aligned}$$

Substituting (2.63) in (2.62) one sets:

$$\begin{aligned}
\Gamma_\varphi(t + \tau, t) &= \frac{|\mu|^2}{4} \times \\
&\frac{1}{2} \sin^2 2\theta \cos 2\varphi \left[\cos^2 2\bar{\theta} - \frac{1}{2} \sin^2 2\bar{\theta} \cos(\omega\tau) \right] \{ \langle \tilde{R}_z^2 \rangle_s - \langle \tilde{R}_z \rangle_s^2 \} e^{-\bar{\Gamma}_\parallel \tau} \\
&+ \frac{1}{4} \sin^2 2\theta \sin^2 \bar{\theta} \cos 2\varphi [e^{-i(2\bar{G}_R - i\bar{\Gamma}_s)\tau} + e^{i(2\bar{G}_R + i\bar{\Gamma}_s)\tau}]
\end{aligned}$$

$$\begin{aligned}
& + \frac{i}{4} \sin^2 2\theta \sin^2 2\bar{\theta} \sin 2\varphi \langle \tilde{R}_z \rangle_s [e^{i(2\bar{G}_R+i\bar{\Gamma}_s)\tau} - e^{-i(2\bar{G}_R-i\bar{\Gamma}_s)\tau}] \\
& - \frac{1}{4} \sin^2 2\theta \sin^4 \bar{\theta} \cos 2\varphi [e^{-i(\omega-2\bar{G}_R-i\bar{\Gamma}_s)\tau} + e^{i(\omega-2\bar{G}_R+i\bar{\Gamma}_s)\tau}] \\
& + \frac{i}{4} \sin^2 2\theta \sin^4 \bar{\theta} \sin 2\varphi \langle \tilde{R}_z \rangle_s [e^{-i(\omega-2\bar{G}_R-i\bar{\Gamma}_s)\tau} + e^{i(\omega-2\bar{G}_R+i\bar{\Gamma}_s)\tau}] \\
& - \frac{1}{4} \sin^2 2\theta \sin^4 \bar{\theta} \cos 2\varphi [e^{i(\omega+2\bar{G}_R+i\bar{\Gamma}_s)\tau} + e^{-i(\omega-2\bar{G}_R+i\bar{\Gamma}_s)\tau}] \\
& + \frac{i}{4} \sin^2 2\theta \cos^2 2\bar{\theta} \sin 2\varphi \langle \tilde{R}_z \rangle_s [e^{-i(\omega+2\bar{G}_R-i\bar{\Gamma}_s)\tau} - e^{i(\omega+2\bar{G}_R+i\bar{\Gamma}_s)\tau}] \\
& + \frac{1}{2} \left(\sin^2 2\theta \cos^2 \bar{\theta} + \sin^2 2\bar{\theta} \cos \omega\tau (\cos^4 \theta + \sin^4 \theta) \right) \{ \langle \tilde{R}_z^2 \rangle_s - \langle \tilde{R}_z \rangle_s^2 \} e^{-\bar{\Gamma}_\parallel \tau} \\
& + \frac{1}{4} \sin^2 2\theta \sin^2 \bar{\theta} [e^{i(2\bar{G}_R+i\bar{\Gamma}_s)\tau} + e^{-i(2\bar{G}_R-i\bar{\Gamma}_s)\tau}] \\
& + \frac{1}{2} \sin^4 \bar{\theta} (\cos^4 \theta + \sin^4 \theta - \langle \tilde{R}_z \rangle_s \cos 2\theta) [e^{i(\omega-2\bar{G}_R+i\bar{\Gamma}_s)\tau} + e^{-i(\omega-2\bar{G}_R-i\bar{\Gamma}_s)\tau}] \\
& + \frac{1}{2} \cos^4 \bar{\theta} (\sin^4 \theta + \cos^4 \theta - \langle \tilde{R}_z \rangle_s \cos 2\theta) [e^{i(\omega+2\bar{G}_R+i\bar{\Gamma}_s)\tau} + e^{-i(\omega+2\bar{G}_R-i\bar{\Gamma}_s)\tau}]. \quad (2.64)
\end{aligned}$$

The enhancement and appearance of some new squeezing peaks can be explained using the double-dressed state picture. In order to understand the influence of permanent dipole on the spectral features of the squeezing spectra shown in Fig.2.6(a), below we present the final analytical formula for the squeezing spectra in double-dressed state formalism:

$$\begin{aligned}
S_\varphi(\nu) &= \frac{\gamma}{4} \times \left\{ (\langle \tilde{R}_z^2 \rangle_s - \langle \tilde{R}_z \rangle_s^2) [\sin^2 2\theta \cos^2 2\bar{\theta} (1 + \cos 2\varphi)] \chi_1(\nu) \right. \\
&+ \frac{1}{2} \sin^2 2\bar{\theta} \left(\cos^4 \theta + \sin^4 \theta + \frac{1}{2} \sin^2 2\theta \cos 2\varphi \right) \chi_2(\nu) \\
&+ \frac{1}{2} \sin^2 2\theta \sin^2 2\bar{\theta} (1 + \cos 2\varphi) \chi_3(\nu) \\
&+ \sin^4 \bar{\theta} \left(\cos^4 \theta + \sin^4 \theta - \langle \tilde{R}_z \rangle_s \cos 2\theta - \frac{1}{2} \sin^2 2\theta \cos 2\varphi \right) \chi_4(\nu) \\
&+ \cos^4 \bar{\theta} \left(\cos^4 \theta + \sin^4 \theta + \langle \tilde{R}_z \rangle_s \cos 2\theta - \frac{1}{2} \sin^2 2\theta \cos 2\varphi \right) \chi_5(\nu) \\
&+ \frac{1}{2} \sin^2 2\theta \sin^2 2\bar{\theta} \sin 2\varphi \langle \tilde{R}_z \rangle_s \chi_6(\nu) + \frac{1}{2} \sin^2 2\theta \sin^4 \bar{\theta} \sin 2\varphi \langle \tilde{R}_z \rangle_s \chi_7(\nu) \\
&\left. + \frac{1}{2} \sin^2 2\theta \cos^4 \bar{\theta} \sin 2\varphi \langle \tilde{R}_z \rangle_s \chi_8(\nu) \right\}, \quad (2.65)
\end{aligned}$$

where the terms χ_1 - χ_8 represent the squeezing peaks enhanced by the presence of permanent dipole:

$$\begin{aligned}
\chi_1(\nu) &= \frac{2\bar{\Gamma}_\parallel}{\bar{\Gamma}_\parallel^2 + \nu^2}, \\
\chi_2(\nu) &= \frac{\bar{\Gamma}_s}{\bar{\Gamma}_s^2 + (\nu - \omega)^2} + \frac{\bar{\Gamma}_s}{\bar{\Gamma}_s^2 + (\nu + \omega)^2},
\end{aligned}$$

$$\begin{aligned}
\chi_3(\nu) &= \frac{\bar{\Gamma}_s}{\bar{\Gamma}_s^2 + (\nu - 2\bar{G}_R)^2} + \frac{\bar{\Gamma}_s}{\bar{\Gamma}_s^2 + (\nu + 2\bar{G}_R)^2}, \\
\chi_4(\nu) &= \frac{\bar{\Gamma}_s}{\bar{\Gamma}_s^2 + (\nu - \omega + 2\bar{G}_R)^2} + \frac{\bar{\Gamma}_s}{\bar{\Gamma}_s^2 + (\nu + \omega - 2\bar{G}_R)^2}, \\
\chi_5(\nu) &= \frac{\bar{\Gamma}_s}{\bar{\Gamma}_s^2 + (\nu + \omega + 2\bar{G}_R)^2} + \frac{\bar{\Gamma}_s}{\bar{\Gamma}_s^2 + (\nu - \omega - 2\bar{G}_R)^2}, \\
\chi_6(\nu) &= \frac{\nu - 2\bar{G}_R}{\bar{\Gamma}_s^2 + (\nu - 2\bar{G}_R)^2} - \frac{\nu + 2\bar{G}_R}{\bar{\Gamma}_s^2 + (\nu + 2\bar{G}_R)^2}, \\
\chi_7(\nu) &= \frac{\nu - \omega + 2\bar{G}_R}{\bar{\Gamma}_s^2 + (\nu - \omega + 2\bar{G}_R)^2} - \frac{\nu + \omega - 2\bar{G}_R}{\bar{\Gamma}_s^2 + (\nu + \omega - 2\bar{G}_R)^2}, \\
\chi_8(\nu) &= \frac{\nu + \omega + 2\bar{G}_R}{\bar{\Gamma}_s^2 + (\nu - \omega + 2\bar{G}_R)^2} - \frac{\nu - \omega - 2\bar{G}_R}{\bar{\Gamma}_s^2 + (\nu + \omega - 2\bar{G}_R)^2}. \tag{2.66}
\end{aligned}$$

Here, $\chi_1 - \chi_5$ exhibit Lorentzian-like while $\chi_6 - \chi_8$ represent dispersion-like terms. On the other hand, the total normally ordered quantum fluctuation of the radiated field presented by eq. (2.67) expression can be obtained after frequency integration of eq.(2.65), i.e.,

$$\begin{aligned}
\langle : (\Delta E_\varphi)^2 : \rangle &= \frac{d^2}{2\gamma} \times \\
&\left\{ \left(\langle \tilde{R}_s^z \rangle_s - \langle \tilde{R}_z \rangle_s^2 \right) \left[4 \sin^2 2\theta \cos^2 \bar{\theta} \cos^2 \varphi + \sin^2 2\bar{\theta} \left(\cos^4 \theta + \sin^4 \theta + \frac{1}{2} \sin^2 2\theta \cos 2\varphi \right) \right. \right. \\
&+ \left. \left. \sin^2 2\theta \sin^2 2\bar{\theta} (1 + \cos 2\varphi) \right] \right. \\
&+ 2 \sin^4 \bar{\theta} \left(\cos^4 \theta + \sin^4 \theta - \langle \tilde{R}_z \rangle_s \cos 2\theta - \frac{1}{2} \sin^2 2\theta \cos 2\varphi \right) \\
&+ 2 \cos^4 \bar{\theta} \left(\cos^4 \theta + \sin^4 \theta + \langle \tilde{R}_z \rangle_s \cos 2\theta - \frac{1}{2} \sin^2 2\theta \cos \varphi \right) \\
&\left. + \sin 2\varphi \sin^2 2\theta (\sin^2 2\bar{\theta} + \sin^4 \bar{\theta} + \cos^4 \bar{\theta}) \langle \tilde{R}_z \rangle_s \right\}. \tag{2.67}
\end{aligned}$$

In Fig.2.6(a) is presented the squeezing spectrum for some parameters of interest. Specially, we would like to highlight that squeezing is observed at negative values, which is evident through the solid line in the Fig.2.6(a) and the dark-blue areas shown in Fig.2.6(b). This is a straightforward prove that permanent dipole generates occurrence of new squeezing intervals near the zero value of the detector's frequency ν , which are missing in the squeezing spectra shown by the dashed line.

Additionally, in Fig.2.7, we depict the normally ordered variance of the radiated $\langle : (\Delta E_\varphi)^2 : \rangle$, proceeding from the resonance fluorescence processes of laser-pumped two-level systems possess-

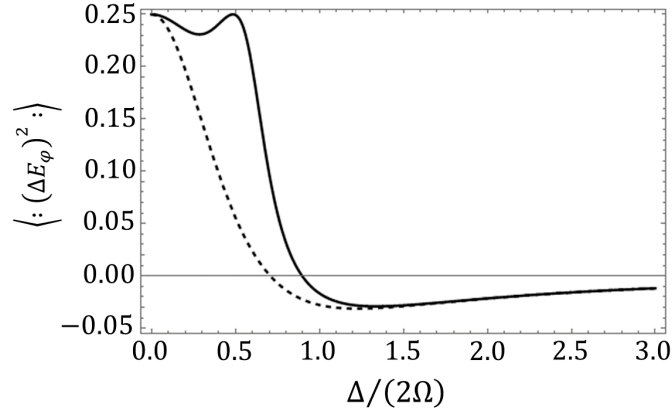


Fig. 2.7: The variance $\langle (\Delta E_\varphi)^2 \rangle$ in units of $|d|^2$ as function of $\frac{\Delta}{2\Omega}$ for $\frac{G}{\gamma} = 0$ (dashed line), $\frac{G}{\gamma} = 16$ (solid line) [191].

ing permanent dipoles. We have found distinct quantum fluctuations features, which are due to permanent dipoles, which is evident from the comparison of the solid and dashed curves, see also [189]. The variance curve shown in Fig.2.7 with dashed line was computed for the case when the permanent dipole moment of the two-level system is zero. The presence of the permanent dipole changes the aspect of the normally ordered variance of the radiated field expanding the variance range, though it keeps the same amplitude as compared with dashed line of the normally ordered variance spectra.

In Fig.2.6(b), we plot the squeezing spectrum for certain parameters of interest. Particularly, squeezing occurs for negative values (dark are in Fig.2.6(b)) and broader squeezing ranges takes place because of permanent dipoles (see also [190]). Especially, squeezing around ν is due to permanent dipoles and will not be observed in the absence of it.

2.4 Conclusions of Chapter 2

In this chapter one has investigated the resonance fluorescence and squeezing in resonance fluorescence processes observed in a two-level system possessing all dipole matrix elements nonzero. One has presented the detailed description of the theoretical model of a two-level system with permanent dipole possessing a permanent dipole moment pumped by a weak and a low frequency coherent field near resonance. The second stronger laser field driving the main two-level transition induces a dynamical Stark-splitting in the system. The particularity of the current model, consists in evaluating the impact of non-zero permanent dipole moment on the resonance fluorescence spectrum of the spontaneous emission of photons during the laser pumping processes of two-level system. One has described the system using semi-classical laser-molecule dressed-state picture due to the first laser. Applying the dressed-state centrally symmetric transformation to the system Hamiltonian one arrived at the effective system Hamiltonian represented in a frame rotating at the second laser field frequency. Performing the rotating wave approximation with the respect to the second laser ω , one eliminated the vacuum modes of the electromagnetic field reservoir in the usual way by adopting the Born-Markov approximations. One has computed the elastic photon scattering spectrum consisting of three lines at $\{\omega_L, \omega_L \pm \omega\}$, considering a non-zero dipole moment. The inelastic photon scattering contains up to nine spectral lines at $\omega_L, \{\omega_L \pm \omega\}, \{\omega_L \pm 2\bar{G}_R\}, \{\omega_L - \omega \pm 2\bar{G}_R\}, \{\omega_L + \omega \pm 2\bar{G}_R\}$. Suppression of a spectral line at the frequency of the strongly driven laser occurs due to interference effects among the induced double dressed-state transitions. Asymmetrical behaviors in the scattered light spectrum are observed as well. This is because of the population inversion in the bare state and it differs from the ordinary resonance fluorescence spectrum computed in the absence of permanent dipoles, which also modifies the squeezing spectrum for certain parameters of interest. Particularly, squeezing occurs for negative values (dark area in Fig. 2.6(b)) and broader ranges because of the permanent dipoles. In the absence of permanent dipoles squeezing around detectors frequency ν is not observed. Additionally, the dipole moment expands slightly the range of quantum fluctuations. Summarizing, we have investigated the steady-state quantum dynamics of laser pumped two-level system possessing non-zero permanent dipole moment. We have plotted the resonance fluorescence spectrum of spontaneously emitted photons, squeezing spectrum and total quantum fluctuations, during the laser pumping processes of the system. Features differing from those in the case of similar processes yet in the absence of permanent dipoles have been found. In particular, additional spectral lines are emitted and extra squeezed frequency domains are observed. The corresponding study is published in the following scientific papers [189, 190, 191].

3 DYNAMICS OF A QUANTUM OSCILLATOR COUPLED WITH A THREE-LEVEL Λ -TYPE EMITTER

The interest for novel quantum systems exhibiting lasing in a wider parameter range, lasing and cooling in microscale and nanoscale devices is growing. From this perspective, here, we research out a laser pumped Λ -type three-level system the upper state of which is being coupled with a quantum oscillator described by a quantized single-mode boson field. More exactly, as quantum oscillator can be considered a vibrational mode of a nanomechanical resonator incorporating the three-level emitter or, correspondingly, an electromagnetic cavity mode field if the upper state of the three-level sample, embedded in the cavity, possesses a permanent dipole.

The frequency of the quantum oscillator is smaller than all other frequencies involved to describe the model; on the other hand, it is of the order of the generalized Rabi frequency identifying the laser-pumped three-level qubit. In accordance to the dressed-state base of the three-level system, we have derived two resonance conditions regulating the oscillator's quantum dynamics, specifically, when the quantum oscillator's frequency is near to the doubled generalized Rabi frequency or to the generalized Rabi frequency, correspondingly. In this way, we consider these two situations as distinct cases. We have derived the stationary lasing or cooling regimes in both cases for the quantum oscillator's field mode, nevertheless, for asymmetrical spontaneous decay rates corresponding to each of the three-level qubit's transition. The mechanisms determining these effects are totally different for the two cases.

In this circumstance when the double generalized Rabi frequency is close to the oscillator's one, the model is in some way similar to a two-level system interacting with a quantum field mode where the spontaneous decay pumps both levels. On the other side, if the oscillator's frequency tends to the value of the generalized Rabi frequency, which is near resonance, then the sample is associated with an equidistant three-level system where the single-mode quantum oscillator interacts with both qubit's transitions. The latter case includes single- or two-quanta processes occurring simultaneously with quantum interference effects among the involved dressed states leading to more profound cooling regimes and flexible ranges for lasing effects. This is contrasting from other similar experimental schemes based on electromagnetically induced transparency processes. In this instance the model consists of an electromagnetic cavity mode, which describes the quantum oscillator, then its frequency can be in the terahertz domain and, thus, we prove an effective coherent electromagnetic field source of such photons. While lasing or cooling effects are possible within two-level system as well, three-level system may possess an advantage apparently they exhibit improved features for the same parameters involved, which is a benefit when there are only certain

accessible parameter ranges. Furthermore, certain realistic novel systems are explored employing the three-level model. For example, as a particular Λ -type system may be considered laser pumped color center embedded on a vibrating membrane, where strong coupling strengths can be achieved via vacuum dispersive forces [192]. Few coupled quantum dots are appropriate systems too. Also, alternative systems can be asymmetrical real or artificial few-level molecules possessing permanent dipoles. If $d_{11} \gg \{d_{22}, d_{33}\}$, then an electromagnetic resonator mode can couple with the upper state of the Λ -type system via its permanent dipole.

In this chapter, one investigates the quantum dynamics of a quantum oscillator coupled with most upper state of a three-level Λ -type system. The both transitions of three-level emitter, possessing orthogonal dipole moments, are coherently pumped with a single or two electromagnetic field sources, respectively. One has determined ranges for flexible lasing and cooling phenomena related to the quantum oscillator's degrees of freedom. Due to the asymmetrical decay rates and quantum interference effects, population transfer takes place among relevant dressed states of the emitter's subsystem with which the quantum oscillator is coupled. The most appropriate system can be a nano-mechanical resonator coupled with the most highly energetic state of the three-level emitter place on it. On the other side, if the upper state of the Λ -type system has a permanent dipole it can couple with a cavity electromagnetic field mode oscillating in the terahertz domain, for instance. Furthermore, we demonstrate an effective electromagnetic field source of terahertz photons.

3.1 The theoretical framework

In this paragraph, we are going to discuss the system Hamiltonian which includes the surrounding damping phenomena and permanent dipole moment and allows us to model the quantum dynamics of a nanomechanical resonator and a quantum oscillator simultaneously. One will develop and present in this paragraph the analytical approximation allowing to consider in further computations, the proposed model proper to explore the quantum dynamics of a nanomechanical resonator and quantum oscillator. The Hamiltonian describing a quantum oscillator of frequency ω coupled with a laser-pumped Λ -type three-level system, see figure, in a frame rotating at $\frac{\omega_{12}+\omega_{13}}{2}$, is:

$$H = \hbar\omega b^\dagger b + \frac{\hbar\omega_{23}}{2}(S_{22} + S_{33}) + \hbar g S_{11}(b + b^\dagger) - \hbar \sum_{\alpha \in \{2,3\}} \Omega_\alpha (S_{1\alpha} + S_{\alpha 1}). \quad (3.1)$$

One has presumed here that as a pumping electromagnetic field source acts a single laser of frequency ω_L exciting both arms of the emitter or, respectively, two lasers fields $\{\omega_{L1}, \omega_{L2}\}$ each driving separately the two transitions of the Λ -type system possessing orthogonal transition dipoles. Supplementary, one has also considered that $\omega_{L1} = \omega_{L2} \equiv \frac{\omega_{12}+\omega_{23}}{2}$, see Fig.3.1(a). Here $\omega_{\alpha\beta}$ are the frequencies of transitions $|\alpha\rangle \longleftrightarrow |\beta\rangle$ between three-level qubit's, $\{\alpha, \beta \in 1, 2, 3\}$. The terms entering the Hamiltonian (3.1) have the following meaning, specifically, the first and the second terms describe the free energies of the quantum oscillator and the atomic subsystem. The third term accounts the mutual interaction of the quantum oscillator and the atomic subsystem via the most upper-state energy level with g being the respective coupling strength. The last term corresponds to the atom-laser interaction and $\{\Omega_2, \Omega_3\}$ are the corresponding Rabi frequencies associated with a particular driven transitions. Remark that if the upper state of the investigated model contains a permanent dipole moment then the external coherent light sources interact with the upper state as well. The corresponding Hamiltonian is:

$$H_{pd} = \hbar S_{11} \sum_{i \in \{2,3\}} G_i \cos(\omega_{Li} t), \quad (3.2)$$

where $G_i = \frac{d_{11} E_i}{\hbar}$ is the dipole moment, with E_i being the lasers amplitudes. Nevertheless, the Hamiltonian H_{pd} can be considered as fast oscillating function, since $\omega_{Li} \gg G_i$, being further dropped off. Consequently, the Hamiltonian (3.1) and the analytical approximation developed here allow considering simultaneously both situations, basically, when either a nanomechanical resonator or an electromagnetic cavity is considered as a quantum oscillator.

The three-level qubit's operators, $S_{\alpha\beta} = |\alpha\rangle\langle\beta|$, obey the commutation relation $[S_{\alpha\beta}, S_{\beta'\alpha'}] = \delta_{\beta\beta'} S_{\alpha,\alpha'} - \delta_{\alpha',\alpha} S_{\beta'\beta}$, whereas the operators describing the quantum oscillators operators satisfy

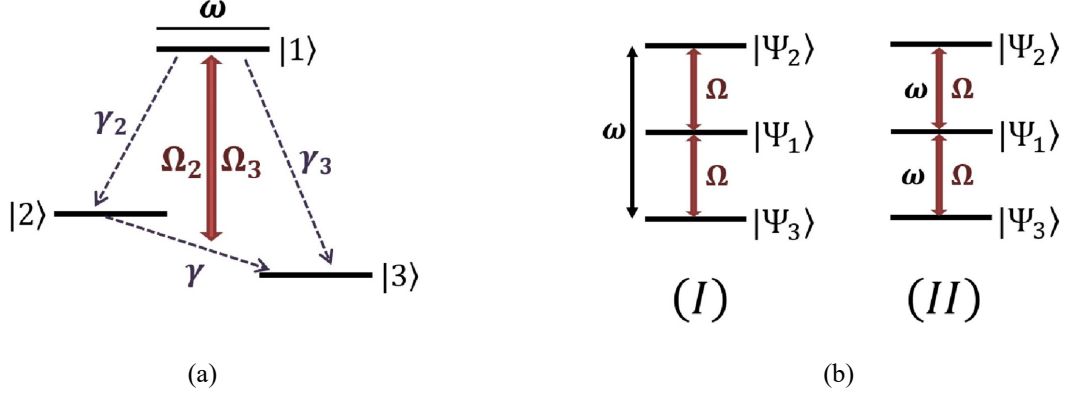


Fig. 3.1: (a) The schematic set up of the model: a laser-pumped three-level Λ -type system. In this system the upper state, $|1\rangle$ is coupled with a quantum oscillator mode of frequency ω . The oscillator can be associated with a single mode of a nanomechanical resonator containing the three-level emitter. On the other side, if the upper state of the three-level system possesses a permanent dipole then the coupling with an electromagnetic cavity mode occurs in the terahertz ranges of waves, for instance. In this situation, the coupling of the resonator with the lower two levels is insignificant small or, otherwise, the cavity resonant frequency should be out of this resonance with this transition. Additionally, the pumping lasers frequencies are equal to the average transitions frequency of three-level emitter $\frac{\omega_{12} + \omega_{13}}{2}$. Ω_2 and Ω_3 are the frequencies corresponding to laser-qubit coupling strength, i.e., the Rabi frequency and γ 's are the particular spontaneous decay rates. (b) The semi-classical laser-qubit dressed-state picture where each bare-state level is dynamically split in three dressed states $\{|\Psi_2\rangle, |\Psi_1\rangle, |\Psi_3\rangle\}$. Resonance occur at (I) $\omega = 2\Omega$ or at (II) $\omega = \Omega$, respectively, where Ω is the generalized Rabi frequency [34].

the following commutation relations $[b, b^\dagger] = 1$ and $[b, b] = [b^\dagger, b^\dagger] = 0$, respectively. In the Born-Markov approximation [7, 79], the quantum dynamics of the proposed complex model can be explored via the following master equation:

$$\begin{aligned} \dot{\rho} + \frac{i}{\hbar}[H, \rho] &= - \sum_{\alpha \in \{2,3\}} \gamma_\alpha [S_{1\alpha}, S_\alpha \rho] \\ &- \gamma [S_{23}, S_{32} \rho] - \kappa(1 + \bar{n})[b^\dagger, b\rho] - \kappa\bar{n}[b, b^\dagger\rho] + H.c. \end{aligned} \quad (3.3)$$

The terms situated on the right side of the eq. (3.3) corresponds to the emitter's damping due to spontaneous emission as well it accounts the quantum oscillator's damping effects with

$$\bar{n} = \frac{1}{\exp \frac{\hbar\omega}{k_B T} - 1},$$

being the mean oscillator's quanta number due to the environmental thermostat temperature T . Note that here k_B is the Boltzmann constant, while γ_2 and γ_3 are the spontaneous decay rates corresponding to $|1\rangle \longleftrightarrow |2\rangle$ and $|1\rangle \longleftrightarrow |3\rangle$ transitions, respectively see Fig. 3.1 (a). γ coefficient depicts the spontaneous two-photon decay rate on the $|2\rangle \longleftrightarrow |3\rangle$ transition of the three-level

qubit, the collisional decay rate etc., while κ describes the quantum oscillator's leaking rate, respectively. The physical phenomena standing behind our model can easier understood if we project the three-level qubit-laser in another base, dressed-state basically, which is given below:

$$\begin{aligned}
|1\rangle &= \sin\theta|\Psi_1\rangle - \frac{\cos\theta}{\sqrt{2}}(|\Psi_2\rangle + |\Psi_3\rangle), \\
|2\rangle &= \frac{\cos\theta}{\sqrt{2}}|\Psi_2\rangle + \frac{1}{2}(1 + \sin\theta)|\Psi_2\rangle - \frac{1}{2}(1 - \sin\theta)|\Psi_3\rangle, \\
|3\rangle &= -\frac{\cos\theta}{\sqrt{2}}|\Psi_1\rangle + \frac{1}{2}(1 - \sin\theta)|\Psi_2\rangle - \frac{1}{2}(1 + \sin\theta)|\Psi_3\rangle,
\end{aligned} \tag{3.4}$$

where

$$\begin{aligned}
\sin\theta &= \frac{\omega_{23}}{2\Omega}, \\
\cos\theta &= \frac{\sqrt{2}\Omega_0}{\Omega},
\end{aligned}$$

with

$$\Omega = \sqrt{2\Omega_0^2 + \left(\frac{\omega_{23}}{2}\right)^2},$$

being the generalized Rabi frequency whereas $\Omega_2 = \Omega_3 \equiv \Omega_0$. Projecting the Hamiltonian (3.1) in the new base (3.4), one arrives to the corresponding Hamiltonian's expression in the dressed-state picture, i.e,

$$H = H_0 + H_d + H_1 + H_2,$$

where

$$\begin{aligned}
H_0 &= \hbar\omega b^\dagger b + \hbar\Omega R_z, \\
H_d &= \hbar g \left(\sin^2\theta R_{11} + \cos^2\theta \frac{(R_{22} + R_{33})}{2} \right) (b + b^\dagger), \\
H_1 &= \hbar \cos^2\theta (R_{32} + R_{23}) \frac{(b + b^\dagger)}{2}, \\
H_2 &= -\hbar \frac{\sin 2\theta}{2\sqrt{2}} (R_{21} + R_{13} + H.C.) (b + b^\dagger),
\end{aligned} \tag{3.5}$$

where $R_z = R_{22} - R_{33}$. Here the dressed-state three-level system operators are $R_{\alpha\beta} = |\Psi_\alpha\rangle\langle\Psi_\beta|$ and they satisfy the same commutation relations as the old ones. In the interaction picture, H_d can be canceled as a fast oscillating term, which can be dropped off the dynamics, while the last two

Hamiltonians can be represented as:

$$\begin{aligned}
H_{1I} &= \bar{g}(R_{23}e^{2i\Omega t} + H.C.)(b^\dagger e^{i\omega t} + H.c.), \\
H_{2I} &= -\tilde{g}((R_{21} + R_{13})e^{i\Omega t} + H.C.)(b^\dagger e^{i\omega t} + H.c.),
\end{aligned} \tag{3.6}$$

where

$$\bar{g} = \hbar g \frac{\cos^2 \theta}{2},$$

whereas

$$\tilde{g} = \hbar g \frac{\sin 2\theta}{2\sqrt{2}},$$

with the unitary transformation:

$$U(t) = \exp\left(\frac{iH_0 t}{\hbar}\right). \tag{3.7}$$

According to the above mentioned Hamiltonians one can notice straightforward that the quantum dynamics of the proposed model is determined by two resonant cases, see Fig. 3.1 (b), more exactly (I) at

$$2\Omega = \omega,$$

and (II) at

$$\Omega = \omega.$$

Consequently, in what follows, we will consider these two cases separately. Thereby, the Hamiltonian for the first case (I) is:

$$H = \bar{\delta} b^\dagger b + \bar{g}(R_{32}b^\dagger + bR_{23}), \tag{3.8}$$

while for the second case (II), it is

$$H = \tilde{\delta} b^\dagger b - \tilde{g}((R_{12} + R_{31})b^\dagger + b(R_{21} + R_{13})), \tag{3.9}$$

where, respectively, $\bar{\delta} = \omega - 2\Omega$ whereas $\tilde{\delta} = \omega - \Omega$. Supplementary, applying the dressed-state transformation equations (3.4) one will arrive at a master equation, which will allow to obtain

a precise system of equations monitoring the quantum dynamics of the examined system. Note that rapidly oscillating terms in the above Hamiltonians (3.6) were dropped off, meaning that $\Omega \gg \{g, \gamma, \gamma_2, \gamma_3\}$, which corresponds to the definition of the secular approximation, according to which the Rabi frequency is much greater than the spontaneous decay rates and the coupling constant of the most energetic level coupled with an electromagnetic cavity.

In the following, we will compare the two cases, i.e., (I) and (II), for the same parameters range and the physical phenomena behind them will be discussed, as well the mechanism behind them.

The ideas of lasing and cooling of a quantum oscillator by coupling it to a non-resonantly two-level atom has been studied extensively. The novelty of the model proposed in this chapter is the investigation of a laser-pumped Λ -type three-level system with the upper state of which is being coupled with a quantum oscillator described by a quantized single-mode boson field. However, we will try to discuss more detailed the advantages of using a three-level system instead of a two-level system. Thus, in order to clarify the issues regarding similarities and differences of a three-level system with a two-level system possessing the transition frequency ω_{21} , we bring below the Hamiltonian describing a laser pumped two-level qubit the upper state of which interacts with a boson mode is:

$$H = \hbar\omega b^\dagger b + \hbar\Delta S_z + \hbar\Omega_0(S^+ - S^-) + \hbar g S_{22}(b + b^\dagger). \quad (3.10)$$

Here, the first two components in the Hamiltonian (3.10) describe the free energies of the boson mode of frequency ω and the qubit's one, respectively, where the laser detuning is $\Delta = \omega_{21} - \omega_L$. The last two terms depict the laser-qubit and the qubit-boson mode interactions, respectively, where Ω_0 is the standard Rabi frequency while g is the coupling among the boson mode and the two-level emitter. The qubit's operators are defined in the usual way, i.e., $S_{\alpha\beta} = |\alpha\rangle\langle\beta|$, with $\{\alpha, \beta \in 1, 2\}$ and $S_z = (S_{22} - S_{11})/2$, satisfying the commutation relations for $SU(2)$ algebra. In the following, we describe the whole system in the semi-classical dressed-state defined by the transformations:

$$\begin{aligned} |2\rangle &= \cos\phi|\bar{2}\rangle - \sin\phi|\bar{1}\rangle, \\ |1\rangle &= \sin\phi|\bar{2}\rangle + \cos\phi|\bar{1}\rangle, \end{aligned} \quad (3.11)$$

with $\cot 2\phi = \frac{\Delta}{2\Omega_0}$. The semi-classical dressed state transformation involves the diagonalization of the Hamiltonian describing the laser-qubit subsystem defined via the free qubit Hamiltonian term of equation (3.10) and the qubit-laser interaction term of the same equation, where the laser is treated classically. The derived dressed-states are defined via a linear transformation of the initial, so called bare states. Thus the eigenstates of this subsystem are called dressed-states and define a

new Hilbertian basis for the atomic states. In this representation, the Hamiltonian (3.10) transforms as follows:

$$H = \hbar\omega b^\dagger b + \hbar\Omega R_z + \hbar g \left(\cos^2 \phi R_{22} + \sin^2 \phi R_{11} - \frac{1}{2} \sin 2\phi (R_{21} + R_{12}) (b + b^\dagger) \right), \quad (3.12)$$

where $\Omega = \sqrt{\Omega_0^2 + \left(\frac{\Delta}{2}\right)^2}$ is the generalized Rabi frequency. The qubit's operators in the dressed-state picture are defined as follows: $R_{\alpha\beta} = |\alpha\rangle\langle\beta|$, $\{\alpha, \beta \in \bar{1}, \bar{2}\}$ and $R_z = R_{\bar{2}\bar{2}} - R_{\bar{1}\bar{1}}$, satisfying the standard commutation relations for $SU(2)$ algebra. In the interaction picture defined by the unitary operator

$$U = \exp\left(\frac{iH_0 t}{\hbar}\right), \quad (3.13)$$

with $H_0 = \hbar\omega b^\dagger b + \hbar\Omega R_z$, one derives the following expression for the interaction Hamiltonian,

$$H_i = \hbar g \left(\cos^2 \phi R_{22} + \sin^2 \phi R_{11} - \frac{1}{2} \sin 2\phi (R_{21} e^{2i\Omega t} + R_{12} e^{-2i\Omega t}) \right) (b e^{-i\omega t} + b^\dagger e^{i\omega t}). \quad (3.14)$$

Based on the interaction Hamiltonian (3.14), one can conclude that the resonance occur at

$$\omega = 2\Omega, \quad (3.15)$$

and without having an additional resonance condition at $\omega = \Omega$ which is distinct from the three-level qubit case in this chapter.

Thus, the three-level system exhibits additional features in comparison to the two-level one. Furthermore, the second resonance condition $\omega = \Omega$, which exists in the three-level system, improves the lasing or cooling phenomena in comparison to $\omega = 2\Omega$ case while keeping the same parameters. This can be an advantage when there are only certain accessible ranges for the involved parameters. Also, when $\omega = \Omega$ the mean quanta number shows a dip while $\langle R_z \rangle = 0$. These differences occur because of the quantum decay interference effects among the involved dressed-states which are not proper to the case of a two-level system. Additionally, there are certain realistic systems which are described by a three-level Λ -type system, see for instance references [32, 34, 192]. Thus, reducing the three-level system to a two-level one may not always work.

3.2 The dressed-state master equation of the three-level Λ -type system

In this paragraph, the master equation (3.16), with Hamiltonians (3.8) and (3.9) is solved by projecting the both Hamiltonians into the system's states basis. The solving technique involves the use of interaction picture.

Below, we are going to present the master equation used to derive the equations of motion modeling the quantum dynamics of both the quantum oscillator as well as the three-level Λ -type emitter, as [34, 35, 36]:

$$\begin{aligned}
\dot{\rho} + \frac{i}{\hbar}[H, \rho] &= -\gamma_2 [R^{(+)}, R^{(+)}\rho] - \gamma_3 [R^{(-)}, R^{(-)}\rho] - \frac{\sin^2 \theta}{4} \gamma^{(+)} [R_{12}, R_{21}\rho] \\
&- \frac{\sin^2 \theta}{4} \gamma^{(-)} [R_{13}, R_{31}\rho] - \gamma_0^{(0)} ([R_{21}, R_{12}\rho] + [R_{31}, R_{13}\rho]) \\
&- \Gamma^{(+)} [R_{32}, R_{23}\rho] - \Gamma^{(-)} [R_{23}, R_{32}\rho] - \frac{\gamma_0^{(+)}}{2} ([R_{12}, R_{13}\rho] + [R_{31}, R_{21}\rho]) \\
&- \frac{\gamma_0^{(-)}}{2} ([R_{21}, R_{31}\rho] + [R_{13}, R_{12}\rho]) - \frac{\gamma}{4} \cos^4 \theta \\
&\times \left[\frac{1}{2} (R_{22} + R_{33}) - R_{11}, \left(\frac{1}{2} (R_{22} + R_{33}) - R_{11} \right) \right] \\
&- \frac{\gamma}{8} \cos^2 \theta (1 - \sin \theta)^2 [R_{12} + R_{31}, (R_{21} - R_{13})\rho] \\
&- \frac{\gamma}{8} \cos^2 \theta (1 + \sin \theta)^2 [R_{21} + R_{13}, (R_{12} - R_{31})\rho] \\
&- \kappa(1 + \bar{n})[b^\dagger, b\rho] - \kappa\bar{n}[b, b^\dagger\rho] + H.c.
\end{aligned} \tag{3.16}$$

where $R^{(+)}$ and $R^{(-)}$ are the atomic operators in the dressed states

$$\begin{aligned}
R^{(+)} &= \frac{\sin 2\theta}{2\sqrt{2}} R_{11} - \frac{\cos \theta}{2\sqrt{2}} (1 + \sin \theta) R_{22} + \frac{\cos \theta}{2\sqrt{2}} (1 - \sin \theta) R_{33}, \\
R^{(-)} &= \frac{\sin 2\theta}{2\sqrt{2}} R_{11} + \frac{\cos \theta}{2\sqrt{2}} (1 - \sin \theta) R_{22} - \frac{\cos \theta}{2\sqrt{2}} (1 + \sin \theta) R_{33}.
\end{aligned} \tag{3.17}$$

The terms $[R_{12}, R_{13}\rho]$, $[R_{31}, R_{21}\rho]$, $[R_{21}, R_{31}\rho]$ and $[R_{13}, R_{12}\rho]$ within master equation (3.16), as well as their Hermitian conjugate ones, describe the cross-damping effects arising from quantum interference phenomena [195, 196, 197]. Also, we present the equations of motion for the dressed-state populations of the three-level emitter in the absence of the quantum oscillator, when the coupling constant is $g = 0$:

$$\begin{aligned}
\langle \dot{R}_{22} \rangle &= \gamma_{11}^{(+)} \langle R_{22} \rangle - \gamma_{22}^{(+)} \langle R_{22} \rangle + \gamma_{33}^{(+)} \langle R_{33} \rangle, \\
\langle \dot{R}_{33} \rangle &= \gamma_{11}^{(-)} \langle R_{11} \rangle + \gamma_{22}^{(-)} \langle R_{22} \rangle - \gamma_{33}^{(-)} \langle R_{33} \rangle, \\
\langle \dot{R}_{11} \rangle &= 1 - \langle R_{22} \rangle - \langle R_{33} \rangle,
\end{aligned} \tag{3.18}$$

The stationary solution of the above system (3.18) of equations are

$$\begin{aligned}\langle R_{22} \rangle &= \frac{\gamma_{11}^{(+)}\gamma_{22}^{(-)} + \gamma_{11}^{(-)}\gamma_{33}^{(-)}}{\gamma_{11}^{(+)}(\gamma_{22}^{(-)} + \gamma_{33}^{(-)}) + \gamma_{22}^{(+)}(\gamma_{11}^{(-)} + \gamma_{22}^{(-)}) + \gamma_{33}^{(+)}(\gamma_{11}^{(-)} - \gamma_{33}^{(-)})}, \\ \langle R_{33} \rangle &= \frac{\gamma_{11}^{(-)}\gamma_{22}^{(+)} + \gamma_{11}^{(+)}\gamma_{33}^{(+)}}{\gamma_{11}^{(-)}(\gamma_{22}^{(+)} + \gamma_{33}^{(+)}) + \gamma_{22}^{(-)}(\gamma_{11}^{(+)} + \gamma_{22}^{(+)}) + \gamma_{33}^{(-)}(\gamma_{11}^{(+)} - \gamma_{33}^{(+)})}.\end{aligned}\quad (3.19)$$

Here in (3.19) the average values of the atomic operators in the dressed-state base include the following spontaneous decay rates, where $\gamma^{(\pm)}$, $\Gamma^{(\pm)}$ are presented later:

$$\begin{aligned}\gamma_{11}^{(+)} &= \gamma^{(+)}\frac{\sin^2\theta}{2} + \gamma\cos^2\theta\frac{(1-\sin\theta)^2}{4}, \\ \gamma_{11}^{(-)} &= \gamma^{(-)}\frac{\sin^2\theta}{2} + \gamma\cos^2\theta\frac{(1+\sin\theta)^2}{4}, \\ \gamma_{22}^{(+)} &= 2\gamma_0^{(0)} + \frac{\Gamma^{(-)}}{2} + \gamma\cos^2\theta\frac{(1+\sin\theta)^2}{4}, \\ \gamma_{22}^{(-)} &= 2\gamma_0^{(0)} + \frac{\Gamma^{(+)}}{2} + \gamma\cos^2\theta\frac{(1-\sin\theta)^2}{4}, \\ \gamma_{33}^{(+)} &= \gamma^{(+)}\frac{\cos^2\theta}{4} + \gamma\frac{(1-\sin\theta)^4}{8}, \\ \gamma_{33}^{(-)} &= \gamma^{(-)}\frac{\cos^2\theta}{4} + \gamma\frac{(1+\sin\theta)^4}{8}.\end{aligned}\quad (3.20)$$

In the following, we get an explicit solution of the master equation in the form (3.16) and substituting the Hamiltonian for the case (I) (3.21), given below

$$H = \bar{\delta}b^\dagger b + \bar{g}(R_{32}b^\dagger + bR_{23}), \quad (3.21)$$

by projecting in into the system base, which is required for the derivation of the density matrix elements. In this way, if we project the master equation we derive a system of differential equations define by density matrix elements. This system consists of linear first order differential equations, which dimensions are determined by the number of the quantum oscillator states multiplied by the number of all possible phonon states. Further, we have to employ a proper solving method, taking into account the phonon state basis in order to derive a system of equations which can be truncated. We will use the Fock states basis, which is the phonon field basis of any other single-mode boson field defined through the eigenfunctions of the Hamiltonian of the free field in the second quantization. The eigenstate $|n\rangle$ are called Fock states or phonon number states, which form a complete set of states. Though the energy eigenvalues are discrete, which is different from the classical electromagnetic theory where energy can take any value, then the energy expectation can take any value since the state vector is an arbitrary superposition of energy states. The phonon probability dis-

tribution corresponds to the diagonal elements of the reduced density matrix of the phonon field. The whole system of density matrix elements is defined in the Hilbert space, where the basis is considered the quantum oscillator-phonon state basis $\{|i, n\rangle\} \equiv \{|i\rangle \otimes |n\rangle\}$, which is a vectorial product of the three-level system dressed-state basis $\{|i\rangle, i \in \{|1\rangle, |2\rangle, |3\rangle\}\}$ and the Fock state basis $\{|n\rangle, n \in \mathbb{N}\}$. Within Hilbert space, the phonon field is defined by a vectorial sub-space of the system, thus the reduced density matrix is computed by tracing the system density matrix over the qubit state basis, i. e., $\rho_{phonon} = Tr_{Qubit}[\rho]$. As the laser pumped qubit is considered as a quantum field with a discrete average number of phonons, then its quanta probability distribution asymptotically tends to zero when $n \rightarrow \infty$. This means that phonon probability to be in a certain Fock states tends to zero, but never gets zero value, for a very high Fock states. The solutions treating the model's dynamics are derived taking into account various analytical conditions as the asymptotic features of the phonon distribution necessary for the truncation of reduced density matrix elements defined by equations of motion. This necessary condition can be applied only to the diagonal matrix elements and quantities regarding them. Nevertheless, the projection of the diagonal elements may involve the off-diagonal elements, which cannot be canceled if $n \rightarrow \infty$. The purpose of the solving method is to build an asymptotically stable system of non-linear differential equations of first order by rearranging and combining the off-diagonal elements. In this manner, we form a closed system of equations of motion, further will provide only the quantities obeying the asymptotic behavior. The projection of master equation for the resonant case (I) into the qubit's dressed-state basis, we arrive to a system of seven equations of motion, which are the elements of the reduced qubit density matrix $\rho_{i,j} = \langle i|\rho|j\rangle$, where $\{i, j \in |1\rangle, |2\rangle, |3\rangle\}$. The projection within qubit's basis has canceled the qubit operators from the equation of motion $\rho_{i,j}$, which is defined only through the field operators. The further projection in the phonon basis, one will derive a system of equations defined only through the scalar values of the projected quantities. Combining the off-diagonal matrix elements appearing in the equations of motion of $\dot{\rho}_{11}, \dot{\rho}_{22}, \dot{\rho}_{33}$, one derives the hermitian variables, which contain the cross-correlation terms of the qubit-phonon interaction. Thus we arrive to the corresponding system of equations for variables describing the (I) resonant case:

$$\begin{aligned}
\rho^{(0)} &= \rho_{11} + \rho_{22} + \rho_{33}, \\
\rho^{(1)} &= \rho_{22} + \rho_{33}, \\
\rho^{(2)} &= \rho_{22} - \rho_{33}, \\
\rho^{(3)} &= b^\dagger \rho_{23} - \rho_{32} b,
\end{aligned}$$

$$\begin{aligned}
\rho^{(4)} &= b^\dagger \rho_{23} + \rho_{32} b, \\
\rho^{(5)} &= \rho_{23} b^\dagger - b \rho_{32}, \\
\rho^{(6)} &= \rho_{23} b^\dagger + b \rho_{32}.
\end{aligned} \tag{3.22}$$

Deriving the new set of Hermitian variables, we have excluded the oscillating part of the off-diagonal elements that doesn't vanish asymptotically. The further projection within the phonon basis derives a system which may be numerically computed. The later projection within the phonon Fock basis $|n\rangle$ determines a new infinite system of differential equations where the variables are defined by the scalar values $P_n^{(i)} = \langle n | \rho^{(i)} | n \rangle$, $i \in \{0..6\}$ and the general form of the equations mentioned above is

$$\rho_{\alpha\beta} = \langle \alpha | \rho | \beta \rangle. \tag{3.23}$$

The dimension of the new system of equations is $7 \times \infty$. The infinite dimension occurs when the system of equations is projected into the infinite amount of the Fock states. Later, only a certain amount of first n_{max} Fock states is considered and thus the dimension of the system used for numerical computation evolves into $7 \times n_{max}$. The presented projection method has numerous advantages in comparison to the direct projection mechanism, which incorporate the analytical accuracy of the approximations applied for its truncation, but also in terms of computational efficiency of numerical computation. From the programming perspective, the direct projection generates a system of $\infty \times \infty$, which after truncation leads to an algorithm employing a set of n_{max}^2 equations. This is a strict numerical constraint regarding the number of operations, comparing to the method exposed above which employs a system of only $7 \times n_{max}$ dimension. It is important to mention that the truncation threshold n_{max} is based on the mean number of the field bosons and their distribution statistics. The enforced threshold is checked empirically, by applying a higher calculation threshold, which will not change significantly the estimated statistic distribution. The impact of a further threshold increment is controlled in order to test the asymptotic behavior. Nevertheless, any threshold incrementation also extends the number of numerical operations and reduces the computation efficiency of the implemented algorithm. Remark, the plots presented in this chapter computed by varying some of the system parameters, which obviously change the mean quanta number of the quantum oscillator. Thus, a constant test check of the applied threshold is highly necessary in order to validated the results. Since we concentrate our attention on the steady-state behaviour of the statistics, thus the time derivatives of the system variables are dropped off. This is available to be done, since the system variables were derived by excluding the exponential, or rapid oscillating

elements of the off-diagonal terms. In this way, within the steady-state regime, the differential system of equations is simplified to a linear system of coupled equations.

The analytical approach developed in this chapter allows us to derive an exact system of equations describing the quantum dynamics of a system consisting of laser pumped spontaneously damped qubit and leaking phonon mode within Rotating Wave Approximation, Born-Markov, and secular approximations, respectively, and to extract the variables of interest, applying the traced density operator over the corresponding degrees of freedom. In order to solve the infinite system of eqs.(3.25), we have to truncate it at a certain maximum value $n = n_{max}$ checking to not modify the obtained results in the case of a further increase of value n_{max} . In the same way, the stationary mean value of the dressed-state inversion operator, $\langle R_z \rangle = \langle R_{22} \rangle - \langle R_{33} \rangle$, can be derived as follows:

$$\langle R_z \rangle = \sum_{n=0}^{n_{max}} P_n^{(2)}. \quad (3.24)$$

Thus, the equations of motion for the first situation (I), analyzing the oscillator's quantum dynamics, (i.e, mean quanta number and its quantum statistics, qubit's populations, etc.), are derived using the master equation (3.16):

$$\begin{aligned} \dot{P}_n^{(0)} &= i\bar{g}(P_n^{(5)} - P_n^{(3)}) - 2\kappa\bar{n}((1+n)P_n^{(0)} - nP_{n-1}^{(0)}) \\ &\quad - 2\kappa(1+\bar{n})(nP_n^{(0)} - (n+1)P_{n+1}^{(0)}), \\ \dot{P}_n^{(1)} &= i\bar{g}(P_n^{(5)} - P_n^{(3)}) - 2\kappa\bar{n}((n+1)P_n^{(1)} - nP_{n-1}^{(1)}) \\ &\quad - 2\kappa(1+\bar{n})(nP_n^{(1)} - (n+1)P_{n+1}^{(1)}) + \gamma_0^{(1)}P_n^{(0)} - \gamma_1^{(1)}P_n^{(1)}, \\ \dot{P}_n^{(2)} &= i\bar{g}(P_n^{(5)} + P_n^{(3)}) - 2\kappa\bar{n}((n+1)P_n^{(2)} - nP_{n-1}^{(2)}) \\ &\quad - 2\kappa(1+\bar{n})(nP_n^{(2)} - (n+1)P_{n+1}^{(2)}) + \gamma_0^{(2)}P_n^{(0)} - \gamma_1^{(2)}P_n^{(1)} - \gamma_2^{(2)}P_n^{(2)}, \\ \dot{P}_n^{(3)} &= i\bar{\delta}P_n^{(4)} - i\bar{g}(P_n^{(1)} - P_n^{(2)} - P_{n-1}^{(1)} - P_{n-1}^{(2)}) \\ &\quad - \kappa(1+\bar{n})((2n-1)P_n^{(3)} - 2(n+1)P_{n+1}^{(3)} + 2P_n^{(5)}) \\ &\quad - \kappa\bar{n}((2n+1)P_2^{(3)} - 2nP_{n-1}^{(3)}) - \gamma_3^{(3)}P_n^{(3)}, \\ \dot{P}_n^{(4)} &= i\bar{\delta}P_n^{(3)} - \kappa(1+\bar{n})((2n-1)P_n^{(4)} + 2P_n^{(6)} - 2(n+1)P_{n+1}^{(4)}) \\ &\quad - \kappa\bar{n}((2n+1)P_n^{(4)} - 2nP_{n-1}^{(4)}) - \gamma_4^{(4)}P_n^{(4)}, \\ \dot{P}_n^{(5)} &= i\bar{\delta}P_n^{(6)} + i\bar{g}(n+1)(P_n^{(1)} + P_n^{(2)} - P_{n+1}^{(1)} + P_{n+1}^{(2)}) \\ &\quad - \kappa(1+\bar{n})((2n+1)P_n^{(5)} - 2(n+1)P_{n+1}^{(5)}) \\ &\quad - \kappa\bar{n}((2n+3)P_2^{(5)} - 2nP_{n-1}^{(5)} - 2P_n^{(3)}) - \gamma_5^{(5)}P_n^{(5)}, \end{aligned}$$

$$\begin{aligned}
\dot{P}_n^{(6)} &= i\bar{\delta}P_n^{(5)} - \kappa\bar{n}((2n+3)P_n^{(6)} - 2nP_{n-1}^{(6)} - 2P_n^{(4)}) \\
&- \kappa(1+\bar{n})((2n+1)P_n^{(6)} - 2(n+1)P_{n+1}^{(6)}) - \gamma_6^{(6)}P_n^{(6)}.
\end{aligned} \tag{3.25}$$

Below are presented the spontaneous decay rates for the resonant case (I) derived from the master equation (3.16):

$$\begin{aligned}
\gamma_0^{(1)} &= \frac{1}{2}(\gamma^{(-)} + \gamma^{(+)} \sin^2 \theta + \gamma \cos^2 \theta (1 + \sin^2 \theta)), \\
\gamma_1^{(1)} &= \frac{1}{2}(2\gamma_0^{(0)} + (\gamma^{(-)} + \gamma^{(+)} \sin^2 \theta) + \frac{1}{4}3\gamma \cos^2 \theta (1 + \sin^2 \theta)), \\
\gamma_0^{(2)} &= \frac{1}{2}((\gamma^{(+)} - \gamma^{(-)}) \sin^2 \theta - 2\gamma \sin \theta \cos^2 \theta), \\
\gamma_1^{(2)} &= 2(\Gamma^{(-)} - \Gamma^{(+)}) + \frac{1}{2}(\gamma^{(+)} - \gamma^{(-)}) \sin^2 \theta - \frac{1}{2}\gamma \sin \theta \cos^2 \theta, \\
\gamma_2^{(2)} &= 2\left(\gamma_0^{(0)} + \Gamma^{(-)} + \Gamma^{(+)} + \gamma \cos^2 \theta \frac{(1 + \sin^2 \theta)}{8}\right), \\
\gamma_3^{(3)} &= \frac{1}{2}(\gamma_2 + \gamma_3) \cos^2 \theta + 2\gamma_0^{(0)} + \Gamma^{(-)} + \Gamma^{(+)} + \frac{1}{4}\gamma \cos^2 \theta (1 + \sin^2 \theta), \\
\gamma_4^{(4)} &= \gamma_5^{(5)} = \gamma_6^{(6)} = \gamma_3^{(3)}.
\end{aligned} \tag{3.26}$$

additionally,

$$\begin{aligned}
\gamma^{(+)} &= \gamma_2(1 + \sin \theta)^2 + \gamma_3(1 - \sin \theta)^2, \\
\gamma^{(-)} &= \gamma_2(1 - \sin \theta)^2 + \gamma_3(1 + \sin \theta)^2, \\
\Gamma^{(+)} &= \frac{1}{8}\gamma^{(+)} \cos^2 \theta + \frac{1}{16}\gamma(1 - \sin \theta)^4, \\
\Gamma^{(-)} &= \frac{1}{8}\gamma^{(-)} \cos^2 \theta + \frac{1}{16}\gamma(1 + \sin \theta)^4, \\
\gamma_0^{(+)} &= \frac{1}{2}(\gamma_3(1 - \sin \theta) - \gamma_2(1 + \sin \theta)) \sin \theta \cos^2 \theta, \\
\gamma_0^{(-)} &= -\frac{1}{2}(\gamma_3(1 + \sin \theta) - \gamma_2(1 - \sin \theta)) \sin \theta \cos^2 \theta, \\
\gamma_0^{(0)} &= \frac{1}{4}(\gamma_2 + \gamma_3) \cos^4 \theta.
\end{aligned} \tag{3.27}$$

Further, we shall present the derivation of equations of motion when $\omega \approx \Omega$ for the second case (II), obtained with the help of master equation (3.16) in which we have substituted the corresponding Hamiltonian for the second case (II):

$$H = \tilde{\delta}b^\dagger b - \tilde{g}((R_{12} + R_{31})b^\dagger + b(R_{21} + R_{13})), \tag{3.28}$$

Similar to the case (I), we have employed the same projection algorithm in the Fock state base, as it is important for us to bring forward the amount of reasonable calculations standing behind the second case (II).

In this system of new Hermitian variables as in the (I) resonant case, we have dropped off the rapid oscillating part of the non-diagonal elements. Further, the system was projected within the phonon base until the system of equation closes and we receive a set of seventeen equations of motion, corresponding to new variables, which build the system of $17 \times \infty$ equations. The infinite dimension is limited later to a certain amount of first n_{max} . This truncation threshold is verified empirically through the numerical computation for higher thresholds, which did not change the hypothetical statistic distribution and do not modify the obtained results in the case of increase of values n_{max} . Further extension of threshold verifies the asymptotic stability of equations solutions, meaning that system's solutions are converging to certain fixed values as system dimensions approach to infinity. Asymptotic stability appears to be a reasonable requirement, but it only involves how long it takes to converge. Thus, the corresponding system of equations of motion describing the resonant case (II) (A-2) presented in 4.3 ANNEXES was derived from the master equations derived for the resonant case (II) (A-1). In the next paragraph, one is presenting the results and discussions of the above computed equations, regarding the novel quantum-optical features of the three-level Λ -type system. The differences of the light statistics between the resonant situations (I) and (II) will be the special scope of the upcoming paragraph.

3.3 Lasing and cooling effects in the three-level Λ -type system

The focus of this study is stressed on the quantum dynamic statistics of three-level Λ -type system coupled with a quantum oscillator mode. We shall compare the two resonant situations, i.e., (I) and (II), for the same parameters range and discuss the mechanisms behind them. Before, one shall give some basic insights into the second order correlation functions $g^{(2)}$ and their role in the interpretation of quantum optical features of the three-level Λ -type system.

Statistical properties of the light are investigated through field measurements at different locations in time and space. Therefore, the first generalized concept of first-order degree of coherence included correlations between field intensities measured at different space-time points. In classical interference experiments, the first-order coherence contributes and governs the formation of fringes. On the other hand, the intensity correlation yield the the second-order coherence function, which made possible to obtain statistical information on the field correlations without requiring the interferometric stability. However $g^{(2)}$ contains only information about energy dynamics of the field, photon generation times unlike $g^{(1)}$ yielding no information regarding the phase fluctuation. The second-order coherence $g^{(2)}$ is computed through the products of field operators and their hermitian conjugates, which makes $g^{(2)}$ be positively defined, as given below:

$$g^{(2)}(\tau) = \frac{\langle I(t)I(t+\tau) \rangle}{\langle I(t) \rangle^2} = \frac{\langle \hat{E}^\dagger(t)\hat{E}^\dagger(t+\tau)\hat{E}(t+\tau)\hat{E}(t) \rangle}{\langle \hat{E}^\dagger(t)\hat{E}(t) \rangle^2}, \quad (3.29)$$

with $I \propto |E(t)|^2$ and $I(t+\tau)$ being the averaged intensities of the mode at a given time. According to this definition the $g^{(2)}(\tau)$ function describes the correlation between two temporally separated intensity signals with time difference $\tau = t_2 - t_1$ from one light source. Applying the transformation formalism from classical field quantities into equivalent quantum mechanical operators using the second quantization, we can present the electric field $E(t)$ as function of annihilation \hat{a} and creation \hat{a}^\dagger operators:

$$\hat{E}_k(t) = \hat{E}_k^{(+)}(t) + \hat{E}_k^{(-)}(t),$$

with

$$\begin{aligned} \hat{E}_k^{(+)}(t) &\propto \hat{a}_k \cdot \exp(-i(\omega_k t - \vec{k} \cdot \vec{r})), \\ \hat{E}_k^{(-)}(t) &\propto (\hat{a}_k)^\dagger \cdot \exp(-i(\omega_k t - \vec{k} \cdot \vec{r})), \end{aligned}$$

representing the *negative* and *positive* ω_k frequency parts of the mode [7, 8, 187]. For a single mode we can rewrite the second-order correlation function $g^{(2)}(\tau)$ using the commutator relations,

as follows [7, 8, 187]:

$$\begin{aligned}
g^{(2)}(\tau) &= \frac{\langle \hat{E}_k^{(-)}(t) \hat{E}_k^{(-)}(t+\tau) \hat{E}_k^{(+)}(t+\tau) \hat{E}_k^{(+)}(t) \rangle}{\langle \hat{E}_k^{(-)}(t) \hat{E}_k^{(+)}(t) \rangle^2} \\
&\stackrel{(\tau \rightarrow 0)}{=} \frac{\langle \bar{b}^\dagger \bar{b}^\dagger \bar{b} \bar{b} \rangle}{\langle \bar{b}^\dagger \bar{b} \rangle^2}.
\end{aligned} \tag{3.30}$$

An important difference between the classical and quantum mechanical description is that in the latter case the detection of a photon at t reduces the amount of photons detected at $t + \tau$, since the photons are the smallest quanta of electromagnetic field and cannot be divided [187]. The steady-state second-order correlation $g^{(2)}(0)$ function presents a special interest, since it represents the conditional probability how likely is it to detect a second photon at the same time while one photon has been already detected. Thus it is a measure tool of the temporal photon coincidences, required to distinguish and classify different light states. In this sense, we have to remind that in quantum statistics we can describe the fluctuations in the photon number n of a single mode by the variance $(\Delta n)^2$ defined as the weighted sum of the squared deviations of the photon number n with respect to the mean occupation $\langle n \rangle$ [8, 187]:

$$(\Delta n)^2 = \sum_{n=0}^{\infty} (n - \langle n \rangle)^2 \cdot P(n) = \langle n^2 \rangle - \langle n \rangle^2. \tag{3.31}$$

This expression (3.31) can be further derived according to the general definition of k -th order factorial moment:

$$\begin{aligned}
\langle n(n-1)(n-2) \dots (n-k+1) \rangle &= \sum_{n=0}^{\infty} n(n-1)(n-2) \dots \\
&\quad \cdot (n-k+1) P(n).
\end{aligned} \tag{3.32}$$

Particularly, for the second order factorial we calculate:

$$\langle n(n-1) \rangle = \sum_{n=0}^{\infty} n(n-1) \cdot P(n) = \sum_{n=0}^{\infty} n^2 \cdot P(n) - \sum_{n=0}^{\infty} n \cdot P(n) = \langle n^2 \rangle - \langle n \rangle. \tag{3.33}$$

Using the second factorial (3.33) and the variance definition we get the simplified steady-state second-order correlation function [8, 187]:

$$g^{(2)}(0) = \frac{\langle n^2 \rangle - \langle n \rangle}{\langle n \rangle^2} = \frac{(\Delta n)^2 + \langle n \rangle^2 - \langle n \rangle}{\langle n \rangle^2} = 1 + \frac{(\Delta n)^2 - \langle n \rangle}{\langle n \rangle^2}. \tag{3.34}$$

According to the steady-state value of second-order correlation function $g^{(2)}(0)$, light states are

divided into three categories:

$$\begin{aligned} (\Delta n)_{thermal}^2 &= \langle n^2 \rangle + \langle n \rangle \Rightarrow g^{(2)}(0) = 2, \\ (\Delta n)_{coherent}^2 &= \langle n \rangle \Rightarrow g^{(2)}(0) = 1, \\ (\Delta n)_{Fock}^2 &= 0 \Rightarrow g^{(2)}(0) = 1 - \frac{1}{n} \quad (n \geq 1). \end{aligned}$$

It is evident from the above equations, the thermal state has a higher probability to emit more than one photon at the same time [187]. However, this occurs for shorter time periods than coherence times, which is specific usually for thermal or chaotic light and it is named photon bunching. In the opposite side, Fock states occur when $g^{(2)} < 1$ and in this circumstance the probability to emit two photons at the same time is reduced, generating photon antibunching. Fock states occur when the photon number $n = 1$ and if in this state a single photon is annihilated, then the second photon cannot be detected. Therefore these states are defined as non-classical states and exhibit photon anti-bunching. The single photon sources are important for the realization of different applications in quantum photonics. Nevertheless, sources of multiple photons would be a significant step towards the development of an optical quantum computer, which uses photons as qubits. Consequently, the proposals for the generation of multiple photon states or streams of photons have been recently put forward. For example, multiphoton states are built up by placing a semiconductor quantum dot (**QD**) embedded in an optical microcavity and placed in a magnetic field. In this set-up, photons are generated by resonant scattering from the quantum dot (**QD**), while the charge spin is used to detect the encoding of the photons [193].

The quantum oscillator's statistics is explored through the mean phonon number $\langle n \rangle$ and the phonon-phonon second-order correlation function $g^{(2)}(0) = \frac{\langle b^\dagger b^\dagger bb \rangle}{\langle b^\dagger b \rangle^2}$. The second-order correlation function and the mean phonon number are derived from the reduced quantum oscillator's density matrix. For a proper explanation, we are going to consider a system consisting of two entities or two subsystems A and B , and \mathcal{O} -an operator acting over sub-system A . Basically, the average value of any random operator is computed through the density matrix operator as follows $\langle \mathcal{O} \rangle = Tr[\rho \mathcal{O}]$. Since the operator \mathcal{O} acts over the sub-system A , applying the trace over the states of the sub-system B , i.e, $\langle \mathcal{O} \rangle = Tr[\rho \mathcal{O}] = Tr_B[Tr_A[\rho \mathcal{O}]]$. In context of the a laser pumped spontaneously damped qubit and leaking phonon mode, then the operator \mathcal{O} corresponds to the field operator and sub-systems A and B are the qubit and the leaking phonon mode, consequently is derived as follows:

$$\langle \mathcal{O} \rangle = Tr_{Qubit}[Tr_{phonon}[\rho \mathcal{O}]] = Tr_{Qubit} \left[\sum_{n=0}^{\infty} \langle n | \rho \mathcal{O} | n \rangle \right]. \quad (3.35)$$

From the above equation, it follows that the phonon mean number $\langle n \rangle$ is derived in the following

way:

$$\langle n \rangle = \langle b^\dagger b \rangle = Tr_{Qubit} \left[\sum_{n=0}^{\infty} \langle n | \rho b^\dagger b | n \rangle \right] = Tr_{Qubit} \left[\sum_{n=0}^{\infty} n \langle n | \rho | n \rangle \right], \quad (3.36)$$

where one has expressed the field operators in the ket base as $b^\dagger b | n \rangle = n | n \rangle$. Computing the trace sum over the system states we get:

$$\langle n \rangle = \sum_{i=1,2,3} \sum_{n=0}^{\infty} n \langle n, i | \rho | n, i \rangle = \sum_{n=0}^{\infty} \langle n | \rho_{11} + \rho_{22} + \rho_{33} | n \rangle = \sum_{n=0}^{\infty} \langle n | \rho^{(0)} | n \rangle, \quad (3.37)$$

where we have swapped the sum over the system states, performing in this way the trace over the qubits states first. According to the computation method explained in the last equality, we substitute the variables (3.22), i.e, $P_n^{(0)}$ and truncate the sum over the infinite Fock states for the numerical computation:

$$\langle n \rangle = \sum_{n=0}^{\infty} n P_n^{(0)} \simeq \sum_{n=0}^{n_{max}} n P_n^{(0)}. \quad (3.38)$$

with

$$\sum_{n=0}^{n_{max}} P_n^{(0)} = 1, \quad (3.39)$$

while the stationary second-order correlation function is defined as:

$$\begin{aligned} g^{(2)}(0) &= \frac{\langle b^\dagger b^\dagger b b \rangle}{\langle b^\dagger b \rangle^2} = \frac{1}{\langle n \rangle^2} Tr_{Qubit} \left[\sum_{n=0}^{\infty} \langle n | \rho b^\dagger b^\dagger b b | n \rangle \right] = \frac{1}{\langle n \rangle^2} Tr_{Qubit} \left[\sum_{n=0}^{\infty} n(n-1) \langle n | \rho | n \rangle \right] \\ &= \frac{1}{\langle n \rangle^2} \sum_{i=1,2,3} \sum_{n=0}^{\infty} n(n-1) \langle n, i | \rho | n, i \rangle = \frac{1}{\langle n \rangle^2} \sum_{n=0}^{\infty} n(n-1) \langle n | \rho^{(0)} | n \rangle \\ &= \frac{1}{\langle n \rangle^2} \sum_{n=0}^{\infty} n(n-1) P_n^{(0)} \simeq \frac{1}{\langle n \rangle^2} \sum_{n=0}^{n_{max}} n(n-1) P_n^{(0)}. \end{aligned} \quad (3.40)$$

These parameters are used to describe the quanta distribution of quantum oscillator's vibrations. In another perspective, statistical distribution of the mean phonon number is used for the interpretation of the field intensity and the distribution parameter. Second-order correlation functions define the type of the distribution we observe. If the $g^{(2)}(0) = 1$ then the coherent field has Poissonian distribution. In the case of the narrow distribution, then the second-order correlation function is $g^{(2)}(0) = \frac{1}{n}$ corresponds to a narrow distribution similar to the Dirac delta function with maximum at n [187]. The fields exhibiting narrower distribution are named sub-Poissonian fields and the Dirac peak corresponds to a pure Fock state. Fields with a broader distribution are generated when

$g^{(2)}(0) > 1$ or $g^{(2)}(0) = 2$. The last value of the second-order correlation function corresponds to a thermal field with an exponential distribution. Fields exceeding the value $g^{(2)}(0) \geq 2$ are named super-Poissonian showing more evidenced exponential-like distribution in comparison to the thermal fields. Considering eqs.(3.38)-(3.40), one obtained the complete and closed system of quantities of interest, more exactly, the mean quanta's number of the quantum oscillator, in other words the system's quantum statistics described by the second-order correlation function, as well the qubit's populations.

3.3.1 Lasing and cooling in the resonant case (I)

In the following subparagraphs, we present the results computed for both resonant case (I) and (II), which involve similar lasing and cooling processes. One is going to demonstrate the different mechanisms generating lasing and cooling in the three-level Λ -type system and the novel properties embedded in the model. One is going to present the results for both cases separately in order to avoid confusion and give a distinct interpretation to each particular process.

The stationary values of the dressed-state inversion operators $\langle R_z \rangle$ computed for the resonant case (I) in the presence $g \neq 0$ and in the absence $g = 0$ of optical cavity is shown in Fig.3.2. The solid and the dashed lines highlight the difference between the presence and absence of the optical cavity. Fig.3.2(a) presents the lasing regime in the resonant case (I) and Fig.3.2(b) corresponds to the cooling regime in the resonant case (I).

One can notice that there is an evident difference between the cases with $g = 0$ and $g \neq 0$ in the lasing regimes and cooling regimes, which is evident from the comparison of Fig.3.2(a) and 3.2(b).

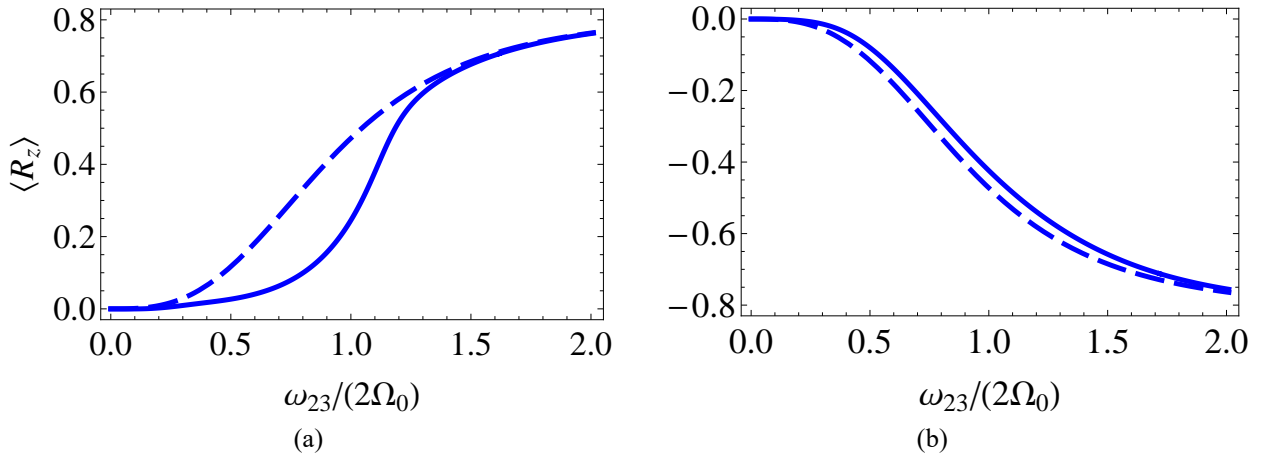


Fig. 3.2: Mean dressed-state inversion operator $\langle R_z \rangle = \langle R_{22} \rangle - \langle R_{33} \rangle$ as a function of $\frac{\omega_{23}}{(2\Omega_0)}$, derived in the steady state for the first situation (I). (a) $\frac{\gamma_2}{\gamma_3} \ll 1$ corresponds to lasing whereas (b) $\frac{\gamma_2}{\gamma_3} \ll 1$ corresponds to cooling. The solid lines are obtained with the full system of equations (3.25), while the dashed lines in the absence of the quantum oscillator, i.e., with eq.(3.19) [34].

Analyzing the equations of motion (3.18) one can notice that the spontaneous decay transitions takes place between all involved dressed-states $|\Psi_2\rangle \longleftrightarrow |\Psi_3\rangle$, $|\Psi_2\rangle \longleftrightarrow |\Psi_1\rangle$ and $|\Psi_1\rangle \longleftrightarrow |\Psi_3\rangle$. Additionally, later we will highlight the impact of ratio $\frac{\gamma_2}{\gamma_3}$ on the population inversion between the dressed states. As well, the cross-correlation terms embedded in eq.(3.16) do not change the population dynamics given by eq. (3.18). Their impact is evident in the presence of the quantum oscillator, i.e., when $g \neq 0$, and this is evident here, compare Figs.3.2(a) and 3.2(b).

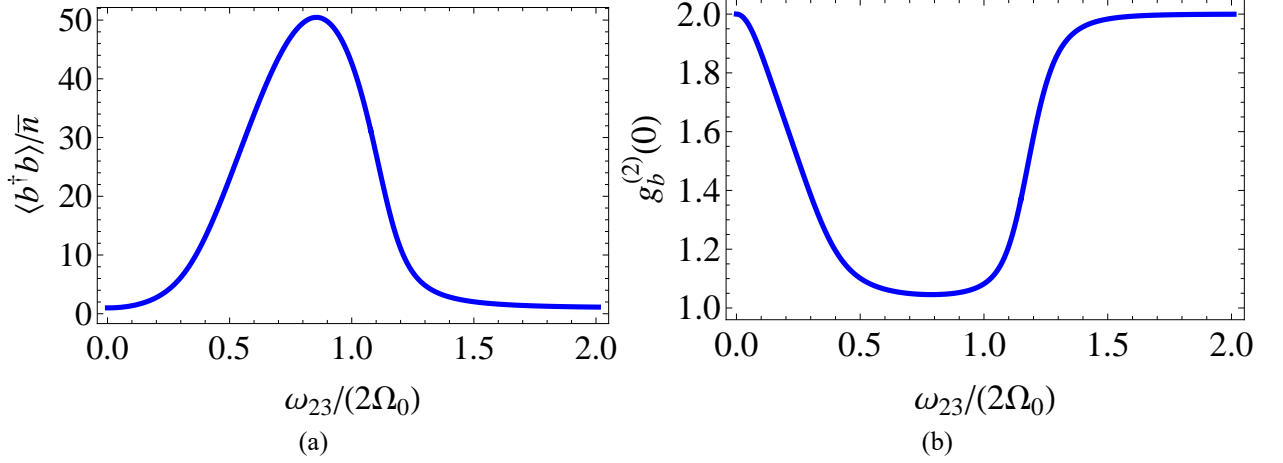


Fig. 3.3: (a) Mean quanta number of the quantum oscillator $\frac{\langle b^\dagger b \rangle}{\bar{n}}$ for the situation (I). (b) Presents the second-order correlation function $g_b^{(2)}(0)$ as function of $\frac{\omega_{23}}{2\Omega_0}$ for the situation (I). Here the parameters of interest are $\frac{g}{\gamma_2} = 4, \frac{\gamma_3}{\gamma_2} = 0.1, \frac{\gamma}{\gamma_2} = 0, \frac{\kappa}{\gamma_2} = 10^{-3}, \frac{\omega}{\gamma_2} = 20, \frac{\Omega_0}{\gamma_2} = 20$ and $\bar{n} = 1$ [34].

In the next step, one is presenting the quantum statistics and the mean quanta number computed with eqs.(3.25) and (3.38)-(3.40) is shown in Fig.3.3. Here, one can observe the maximum value for $\langle b^\dagger b \rangle$ occurs around $\bar{\delta} = 0$, i.e., at the resonance when the quanta's frequency ω is equal to the dressed-state splitting frequency 2Ω due to pumping laser. It is important to mention here that the quanta's statistics is near Poissonian, which means that we have determined lasing regimes in our system. This result is evident from Fig.3.3(a) and (b). Also, lasing takes place if is satisfied the following condition $\frac{\gamma_3}{\gamma_2} \ll 1$. In this case $\langle R_{22} \rangle > \langle R_{33} \rangle$, this means we have population inversion of the dressed-states, which means we have the lasing effect in our system and evident in Fig.3.2(a). To avoid any misunderstandings via *lasing* we mean *generation of the quantum oscillator's quanta possessing Poissonian statistics*, i.e., $g_b^{(2)}(0) = 1$.

Subsequently, Fig.3.4(a) and 3.4(b) brings out the cooling regimes in this system in the context of resonant case (I). This takes place when $\frac{\gamma_2}{\gamma_3} \ll 1$, which means more exactly that $\langle R_{22} \rangle < \langle R_{33} \rangle$ leading to quanta's absorption processes, which is evident in the Fig.3.2(b). The minimum value in the mean quanta number followed by an increased second-order correlation function $g_b^{(2)}(0)$ is observed at $\bar{\delta} = 0$, which is the resonance condition noticeable in Fig.3.4(a) and 3.4(b).

Here, one can draw some important conclusions regarding the cooling and lasing phenomena mechanisms standing behind resonant case (I). If $\gamma_2 \neq \gamma_3$ and $\gamma = 0$, the first situation (I) corresponds to a two-level system $\{|\Psi_2\rangle, |\Psi_3\rangle\}$ of frequency 2Ω interacting, correspondingly, with a quantum oscillator of frequency ω , we mean here that $2\Omega \approx \omega$, see also [194]. The spontaneous decay functions in both directions, i. e., $|\Psi_2\rangle \longleftrightarrow |\Psi_3\rangle$, with a reciprocal impact on cooling or lasing effects.

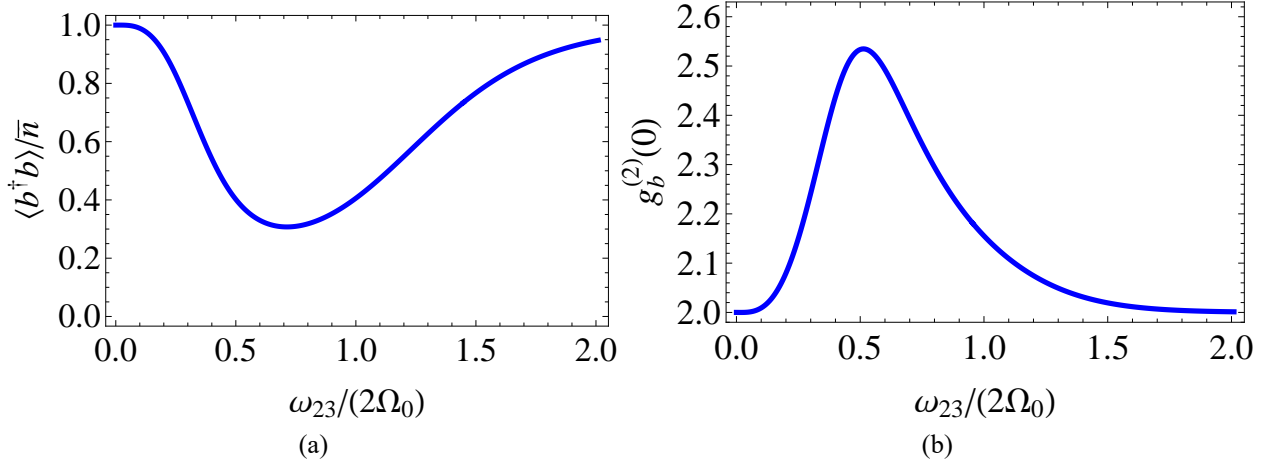


Fig. 3.4: (a) Scaled mean quanta number of the quantum oscillator $\frac{\langle b^\dagger b \rangle}{\bar{n}}$ for the situation (I). (b) The corresponding second-order correlation function $g_b^{(2)}(0)$ against the scaled parameter $\frac{\omega_{23}}{2\Omega_0}$ for the situation (I). Here $\frac{g}{\gamma_3} = 4$, $\frac{\gamma_2}{\gamma_3} = 0.1$, $\frac{\gamma}{\gamma_3} = 0$, $\frac{\kappa}{\gamma_3} = 10^{-3}$, $\frac{\omega}{\gamma_3} = 50$, $\frac{\Omega_0}{\gamma_3} = 20$ and $\bar{n} = 15$ [34].

3.3.2 Lasing and cooling in the resonant case (II)

Here, we present the results of the cumbersome calculus performed to determine the quantum optical statistics and mechanisms of lasing and cooling in the second resonant case (II). As well, one is going to prove the differences and the advantages of the resonant case (II) in comparison to resonant case (I). The stationary mean value of dressed-state inversion operator $\langle R_z \rangle$, in the lasing regime, behaves in another way as in this resonant case (I), compare Fig.3.5(a) with Fig.3.2(a). In the second situation (II), $\langle R_z \rangle$ approaches zero values, while the mean quanta's number is large, although has a minimum, which is straightforward from Fig.3.6(a). These new distinct features are due to quantum interference effects. Nonetheless, cooling phenomena occurs when $\langle R_{22} \rangle < \langle R_{33} \rangle$ facilitating quanta's absorption processes, see Fig.3.5(b). Note that we have discreetly checked the convergence of our results with respect to various values for n_{max} .

In Fig.3.5(a) $\langle R_z \rangle$ approaches the zero value, depicted by the solid curve, highlights the presence of a minimum value in the stationary population of the dressed state, i.e., $|2\rangle$. Equivalently, in the cooling regimes the quantum oscillator's impact on the steady-state mean values of the qubit inversion operator is not quite significant, though still evident via weak oscillations, which is specific for the second case (II). One arrives to the conclusion that the cross-correlation terms defining the interference effects induce a different behave of population in the dressed state, which is depicted by the solid curves in Figs.3.2(a), 3.5(a) as well as in Figs.3.2(b) and 3.5(b), respectively.

To a greater extent, for the sake of comparison, one will keep the same parameters and shall explore the quantum dynamics for the second situation, i.e., (II). The corresponding equations of

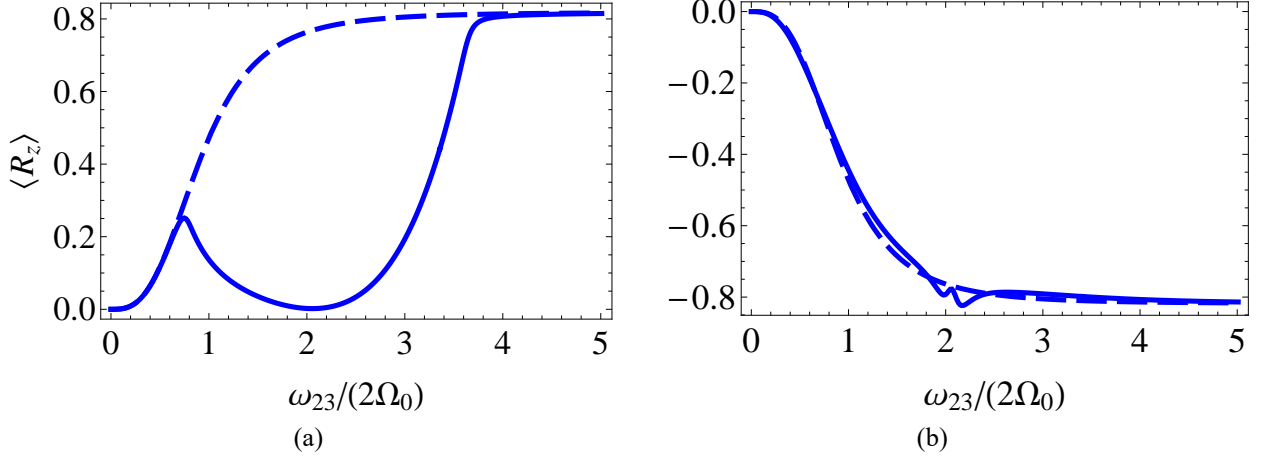


Fig. 3.5: Mean dressed-state inversion operator $\langle R_z \rangle = \langle R_{22} \rangle - \langle R_{33} \rangle$ as a function of $\frac{\omega_{23}}{(2\Omega_0)}$, derived in the steady state for the first situation (II). (a) $\frac{\gamma_3}{\gamma_2} \ll 1$ corresponds to lasing whereas (b) $\frac{\gamma_2}{\gamma_3} \ll 1$ determines cooling. The solid lines are obtained with the full system of equations (A-2), while the dashed lines are computed for the equations (3.19). All other parameters are as in Fig.3.2, respectively [34].

motion analyzing the quantum oscillator's dynamics as well as the quantum emitter's one were given in previous paragraph (3.2), i.e., eqs. (A-2).

In the following, Fig. 3.6(a) shows the means quanta's number of the quantum oscillator in this case. The mean oscillator's quanta number, reproduced in Fig. 3.6(a), exhibits an asymmetric shape, in a certain point of view it is related to a *Fano-like* profile, forecasting the interference effects to exhibit a major role here. Reciprocally, Fig. 3.6(b) displays the comparable behavior of the second order quanta's correlation function depending on $\frac{\omega_{23}}{2\Omega_0}$ when $\frac{\gamma_3}{\gamma_2} \ll 1$. It is important to mention that one can notice a wide plateau where quanta's statistics is Poissonian at the same time its quantum oscillator's mean quanta numbers range from small to larger values. Thus, we have an evident lasing effect in this theoretical setup.

Unlike the resonant case (I), i.e., Fig. 3.3(a) in this paragraph, one has demonstrated the generation more quanta of the quantum oscillator followed by a broader lasing regime, which is more suitable for potential industrial applications, see Figs. 3.6(a) and 3.3(a).

In this conditions, if the upper state $|1\rangle$ of the three-level emitter has a permanent dipole then it can couple with a single-cavity electromagnetic field mode of terahertz frequency, for instance. In this case, we have retrieved a coherent electromagnetic field source generating terahertz photons. Moreover, the externally applied field intensities are moderate, preventing the samples degradation. Correspondingly, Fig.3.7(a) highlight the cooling regime in the studied system, and for the situation (II), which takes place when $\frac{\gamma_2}{\gamma_3} \ll 1$. The second-order correlation function increases appropriately, see Fig.3.7(b), proving enhanced phonon-phonon or photon-photon correlations ap-

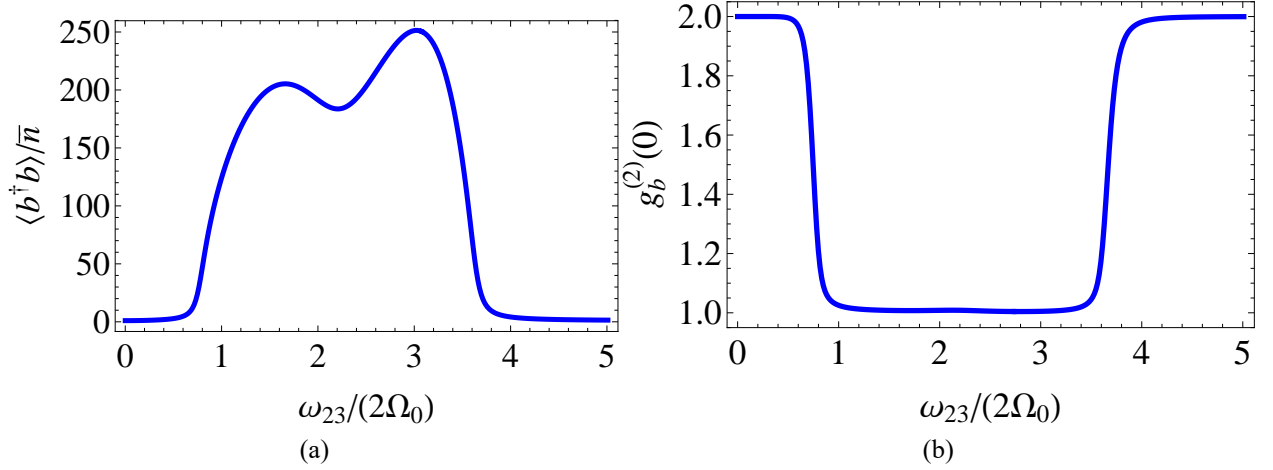


Fig. 3.6: (a) The mean quanta number of the quantum oscillator $\frac{\langle b^\dagger b \rangle}{\bar{n}}$ for the situation (II). (b) Second-order correlation function $g_b^{(2)}(0)$ versus $\frac{\omega_{23}}{2\Omega_0}$ for the situation (II). Here the parameters of interest are $\frac{g}{\gamma_2} = 4$, $\frac{\gamma_3}{\gamma_2} = 0.1$, $\frac{\gamma}{\gamma_2} = 0$, $\frac{\kappa}{\gamma_2} = 10^{-3}$, $\frac{\omega}{\gamma_2} = 20$, $\frac{\Omega_0}{\gamma_2} = 20$ and $\bar{n} = 1$ [34].

plicable for both models. Compared with Fig.3.4(a) describing the same phenomenon but for the first situation (I), the cooling process is rather improved in the second case (II) at the same time keeping the identical parameters, see Fig. 3.4(a) and 3.7(a).

Here, one can observe that according to the resonant case (II), see Fig.3.1(b), the three-level Λ -type system is similar to an equidistant three-level system $|\Psi_2\rangle \longleftrightarrow |\Psi_1\rangle \longleftrightarrow |\Psi_3\rangle$, where each transition occurs at frequency Ω , interacting as well with the quantum oscillator possessing the frequency $\omega \approx \Omega$. In this circumstance, transitions may emerge via a single oscillator's quanta processes among the dressed-state $|\Psi_2\rangle \longleftrightarrow |\Psi_1\rangle \longleftrightarrow |\Psi_3\rangle$, or, correspondingly involving two-quanta effects among the dressed-states $|\Psi_2\rangle \longleftrightarrow |\Psi_3\rangle$. This also implies that cross-correlation terms within master equation (3.16) do determine the quantum dynamics in this case.

This is certainly demonstrated also if one goes through the variable $\rho^{(i)}$, $\{i \in 0 \dots 16\}$, presented in 4.3 ANNEXES and see eqs.A-2, since they consist of single- or two-quanta processes emerging simultaneously. The diversified decay paths among the dressed states involved $|\Psi_2\rangle \longleftrightarrow |\Psi_1\rangle \longleftrightarrow |\Psi_3\rangle$ lead to quantum interference, see also eq.(3.16), although the dipole moments corresponding to the two bare transitions of the Λ -type sample are orthogonal to each other. These cross correlations terms [195, 196, 197] among the dressed state reinforce a more flexible range of lasing and deeper cooling regimes in comparison with the situation (I) and for the same parameters employed in the computation. Thus, one can draw the conclusion that quantum interference effects via single-or two-quanta processed identifies the situation (II), described by Hamiltonian given by the eq.(3.9), from the respective one characterized by the Hamiltonian given by the eq.(3.8), i. e., the case (I). This is also the reason for which the three-level emitter's population dynamics act

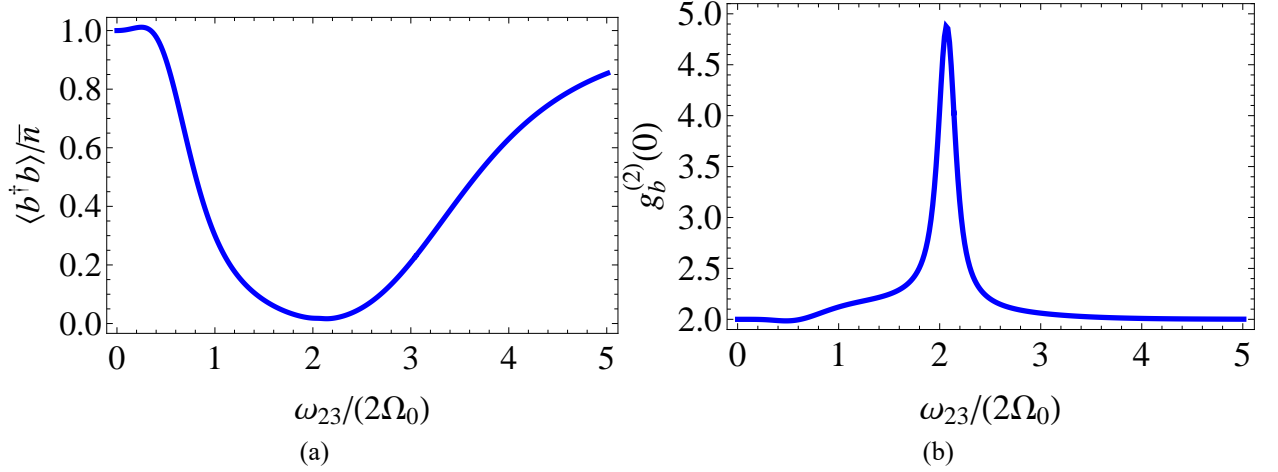


Fig. 3.7: (a) Scaled mean quanta number of the quantum oscillator for the situation (II) $\frac{\langle b^\dagger b \rangle}{\bar{n}}$. (b) The second-order correlation function for the situation (II) $g_b^{(2)}(0)$ versus $\frac{\omega_{23}}{2\Omega_0}$ and the parameters of interest are $\frac{g}{\gamma_3} = 4$, $\frac{\gamma_2}{\gamma_3} = 0.1$, $\frac{\gamma}{\gamma_3} = 0$, $\frac{\kappa}{\gamma_3} = 10^{-3}$, $\frac{\omega}{\gamma_3} = 50$, $\frac{\Omega_0}{\gamma_3} = 20$ and $\bar{n} = 15$ [34].

uniquely as well in these two cases, compare Fig.3.2 and 3.5.

Notice, when $\frac{\omega_{23}}{2\Omega} \rightarrow 0$ then the quantum emitter lies in the state $|\Psi\rangle = \frac{|3\rangle - |2\rangle}{\sqrt{2}}$, whereas $\frac{\langle b^\dagger b \rangle}{\bar{n}} = 1$ and $g_b^{(2)}(0) = 2$, see Figs. 3.3(a)-3.7(b), which means that the quantum oscillator's mode is in a thermal state and no cooling or lasing effects occur, respectively. Here, these phenomena occur for $\frac{\omega_{23}}{2\Omega_0} \neq 0$, when some population is located on the higher upper state $|1\rangle$, which is different from other similar based schemes on coherent population trapping effects or electromagnetically induced transparency phenomenon [103, 104, 192, 198]. Another important result is that we have observed the lack of cooling phenomenon for both cases described in this paragraph, (I) or (II), if $\gamma_2 = \gamma_3$, while $\gamma = 0$. Anyhow, the cooling phenomenon will occur with the increase of γ while maintaining $\gamma_2 = \gamma_3$. Finally, the temperatures considered here are within several Kelvins for phonon cooling effects to few hundreds of Kelvins for coherent terahertz photon generation, correspondingly [34].

3.4 Conclusions to Chapter 3

In conclusion, one has investigated the quantum dynamics of a quantum oscillator coupled with the most upper state of a three-level Λ -type system. Additionally, one has specified that as a quantum oscillator can serve a vibrational mode of a nanomechanical resonator containing the three-level emitter or, equivalently, an electromagnetic cavity mode field, unless the upper state of the three-level sample is embedded within the cavity, possesses permanent dipole. Also it was taken into consideration, the frequency of the quantum oscillator is significantly smaller than all other frequencies involved to describe the model. Nevertheless, is of the order of the generalized Rabi frequency describing the laser-pumped three-level qubit.

Following, the dressed-state picture of the three-level system, one has identified the two-resonance conditions operating the oscillator's quantum dynamics. According to the first resonant condition, the quantum oscillator's frequency is close to the double generalized Rabi frequency and in the second resonant condition the qubit frequency is close to the generalized Rabi frequency, respectively. For both resonant cases, one has computed the average inversion operators, the mean quanta number of the qubit and second-order correlation function analyzing the lasing and cooling phenomena occurring in the three-level system. However, one has identified the different mechanisms behind the lasing and cooling in each resonant situation. In the first resonant case, the three-level system resembles a two-level system of frequency 2Ω interacting with a quantum oscillator of frequency ω . On the other side, in the second resonant case the qubit functions as an equidistant three-level system, where each transition is of frequency Ω interacting as well the quantum oscillator possessing the frequency ω .

Particularly, we have proved that the exchange between single- or two-quanta processed followed by quantum interference effects among the induced emitter's dressed states are in charge of flexible lasing or deeper cooling effects, correspondingly. This generates also reciprocal interplay between the quantum oscillator's dynamics and the three-level emitter's quantum dynamics respectively. Additionally, if the upper state of the three-level emitter has a permanent dipole that it could couple with a single-cavity electromagnetic field mode of terahertz frequency. In this case, the coherent terahertz photons generation is identified as one of the possible applications resulting from this study.

4 MICROWAVE MULTIPHOTON CONVERSION VIA COHERENTLY DRIVEN PERMANENT DIPOLE SYSTEMS

In this chapter, our purpose is the investigation of the multiphoton quantum dynamics of a leaking single-mode quantized cavity field coupled with a resonantly laser pumped two-level system or qubit possessing permanent dipole moment. The frequencies of interacting subsystems, namely the cavity and the emitter, are situated in different frequency domains, respectively, and in this way the latter one couples to the resonator via its parallel dipole moments. Also, the generalized Rabi frequency arising from the external coherent driving field of the two-level qubit is considered to have another values unlike the resonator's frequency. Consequently, this highly dispersive interaction regime has an impact on the cavity multiphoton quantum dynamics and photon conversion from optical to microwave ranges.

One is considering a single-mode quantized cavity with a resonantly driven two-level qubit possessing permanent dipoles. This setup can serve for the implementation of light-matter quantum interface required for quantum information transfer using photons. One of the most studied quantum mechanical models is the two-level system interacting with a quantum oscillator, a quantum optical cavity or quantum mechanical resonator. It is used in a wide range of phenomena, especially in atomic physics, where it describes a two-level atom coupled to a quantized electromagnetic field. Controlling the output of the light emitter is one of the basic tasks in photonics, with landmarks such as the development of the laser and single-or multiphoton sources. The ever growing range of quantum applications is making it increasingly important to diversify the available quantum sources [177]. It is known, however, that multiphoton processes are realized in a two-level system, for a number of physically important cases. Such situation occurs when there is a dipole forbidden transition in the system [199].

In this chapter, one has identified the Hamiltonian defining the quantum dynamical processes of the model. Each part of the two-level system and every type of interaction among the system's components is considered. Furthermore, one has searched and identified the proper set of basis transformations to be applied to the Hamiltonian, in order to prepare its implementation in the master equation. The final form of the Hamiltonian and its transformation technique will be shown further.

Quantum frequency conversion (QFC) is a process in which an input beam light is converted into an output beam of a different frequency while keeping the quantum state to generate quantum tunable states of light, which is relevant nowadays to various feasible quantum applications. Namely, frequency conversion can be used to transduce one photon at a given wavelength to a

photon at another wavelength, which could be used to couple different quantum system possessing different energies or it is embedded in quantum information schemes, which use photons as a communication channel for quantum information over long distances [170]. Among the first demonstrations of quantum frequency conversion effect (QFC) is the experiment reported by [171] promising developments of tunable sources of quantum light. From this perspective, single-photon upconversion from a quantum dot preserving the quantum features was proved in [172]. Experimental demonstration of strong coupling between telecom (1550 nm) and visible (775 nm) optical modes on an aluminum nitride photonic chip was proved as well, in [173]. Even greater frequency differences can be generated. For example, and experimental demonstration of converting a microwave field to an optical field via frequency mixing in a cloud of cold ^{87}Rb atoms was reported in [174]. Earlier theoretical researches have proved frequency downconversion in driven two-level systems with broken inversion symmetry [152, 146]. Additionally, single-and multiphoton frequency conversion via ultrastrong coupling of a two-level emitter to two resonators was theoretically proposed in [175]. Although, multi-quanta processes have been already explored for a long period of time, recently have attracted a renewed considerable attention as well, due to feasible application of these processes to quantum technologies related to quantum lithography [176], novel light sources [177], etc. Supplementary, optomechanically multiphonon-induced transparency of X-Rays via optical control was proved in [180], while strongly correlated multiphonon emission in an acoustical cavity coupled to a driven two-level quantum dot was demonstrated in [181], respectively. Nevertheless, most of the frequency conversion investigations are related to resonant processes. In this context, here we will demonstrate a photon conversion scheme involving non-resonant multiphoton effects.

Coherent conversion from microwave radiation and terahertz radiation into optical range and vice versa has a huge potential of application: detection and imaging, security screening. Superconducting qubit coupled to optical photons is an example of implementation of a quantum hybrid system, where optical photons can be transported with low noise. The main problem in achieving microwave-optical and optical-microwave conversion is to build a suitable platform that couples strongly to both frequency and assures a proper connection between them. Experimentally microwave-optical conversion was explored on the a variety of systems included in microcavities to enhance the coupling to microwaves, such as: Λ -type atomic systems, nanomechanical oscillators, Rydberg atoms possessing strong electric dipole transitions in a wide range of frequencies from microwaves to terahertz and other microcavity based devices with enhanced photon-photon interactions [171, 172, 173, 174].

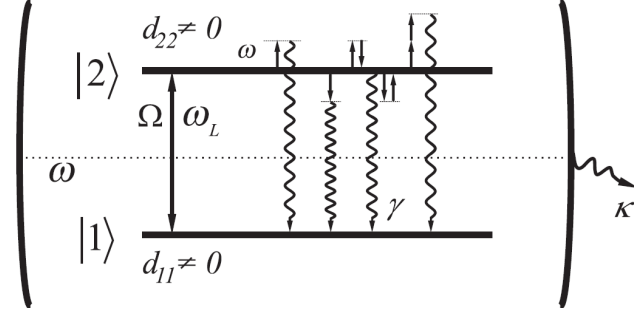


Fig. 4.1: The scheme of the investigated model. It consists of a coherently pumped two-level system interacting with a single-mode resonator of frequency ω through its non-zero parallel components of the permanent dipole moment, $d_{\alpha\alpha}$, with $\alpha \in \{1, 2\}$. In this schematic setup, Ω is the corresponding Rabi frequency due to the off-diagonal dipole moment d_{21} whereas $\omega_L, \omega_L \gg \omega$, is the frequency of the resonantly applied external field. The two-level qubit-resonator coupling strength is denoted by g , while κ is the resonator's decay rate. Also are sketched some processed which may occur, namely, emission or absorption of cavity photon (or two, three etc.) followed by spontaneous decay γ [204].

Most of the well-known frequency conversion investigations involve resonant processes. For this reason, we are going to prove a photon conversion setup exhibiting non-resonant multiphoton effects, respectively. In this context, we are conducting an investigation about frequency down-conversion processes through a resonantly laser-driven emitter possessing a non-zero permanent diagonal dipole moment, $d_{\alpha\alpha} \neq 0$ with $\alpha \in \{1, 2\}$ and placed in a quantized cavity presented in Fig.4.1. The frequencies of the two-level qubit and the single-mode cavity are remarkably different from each other, namely optical and microwave ranges. Consequently, the two-level emitter couples by default to the resonator only through its permanent parallel components of the dipole moment. The cavity's frequency has a different value from the generalized Rabi frequency that arises due to resonant and coherent external pumping of the two-level emitter.

As a consequence, this highly dispersive interaction regime generates multiphoton absorption and emission processes in the resonator mode mediated by the corresponding damping effects, namely qubit's spontaneous emission and the photon leaking through the cavity, as it is shown in Fig.4.1. One has obtained the corresponding cavity photon quantum dynamics in the steady state and demonstrated the feasibility to generate a certain multiphoton superposition state with high probability, and at different frequencies than that of the input external coherent pumping. The multi-quanta nature of the final cavity state can be demonstrated via the second-order photon-photon correlation function.

In this chapter, one is going to derive the corresponding cavity photon quantum dynamics in the steady state and prove the feasibility to generate a certain multiphoton superposition state with high probability, and at different frequencies than that of the external lasing field. The main advantage

of the proposed setup are the features of its components, which have different values of the parallel dipole moments, namely $d_{22} \neq d_{11}$, such as asymmetrical two-level quantum dots and molecules, or, correspondingly, spin or quantum circuits, altogether with the technological advances towards their coupling to various resonators. As feasible applications of our results one may consider the possibility to couple distant real or artificial atoms having transition frequencies in the microwave domain via multiphoton state generated by our setup. Various entangled states [182, 183, 184, 185] of distant emitters can be generated then. Another opportunity, for example, would be to study the quantum thermodynamic performances of distant qubit systems interconnected through the microwave multiphoton field described here.

Before that, many theoretical and experimental studies have been proposed in the framework of symmetric quantum emitters where inversion symmetry is presumed. However, the violation of this presumption is evident in many quantum systems and is evolving into a nonzero permanent dipole moment of the ground and excited states. The presence of a nonzero permanent dipole moment in the system considerably changes the optical output of the system generating changes in single- or multiphoton interactions of a laser with two-level systems. The impact of the dipole is substantial as it manipulates the laser-molecule coupling and is used as a selection tool of transitions.

4.1 The theoretical framework

In this paragraph of the chapter, one will present the main steps in derivation of master equation adopted to the framework of our investigation, which is a differential equation describing the evolution of the probabilities for Markov processes for systems that changes from one to another state in a continuous time. The quantum optical setup considered in this chapter is an important tool for the development of ultimate quantum technologies. Furthermore, the Lindblad master equation plays a major role as it is the most general equation for describing the Markovian dynamics in quantum systems. Open quantum system techniques are the key systems for many studies in quantum mechanics. One particular case is the study of the multiphoton dynamics of a two-level system possessing a permanent dipole that couples the system to an optical cavity.

The master equation analyzing the interaction of a two-level qubit, possessing permanent diagonal dipole moment, with a classical coherent electromagnetic field of frequency ω_L as well as with a quantized single mode resonator frequency $\omega \ll \omega_L$ see Fig.4.1 and is being damped via the corresponding environmental bath in the Born-Markov approximations is:

$$\frac{d}{dt}\rho(t) + \frac{i}{\hbar}[H, \rho] = -\frac{\gamma}{2}[S^+, S^-\rho] - \frac{\kappa}{2}(1 + \bar{n})[b^\dagger, b\rho] - \frac{\kappa}{2}\bar{n}[b, b^\dagger\rho] + H.c. \quad (4.1)$$

In this master equation (4.1), γ is the single-qubit spontaneous decay rate, whereas κ is the corresponding boson's leaking mode with $\bar{n} = \left[\exp\left(\frac{\hbar\omega}{k_B T}\right) - 1 \right]^{-1}$ is the mean resonator's photon number due to thermal bath temperature T , and k_B is the Boltzmann constant. The two-level qubit might have transition frequency in the optical range of frequencies, while the single-mode cavity frequency is situated in the microwave range of frequencies, respectively. The wavevector of the coherent applied field is perpendicular to the cavity axis. As well, in eq.(4.1) the bare-state qubit's operators are defined as follows: $S^+ = |2\rangle\langle 1|$ and $S^- = [S^+]^\dagger$ are verifying the commutation relations defined in $SU(2)$ algebra, as follows: $[S^+, S^-] = 2S_z$ and $[S_z, S^\pm] = \pm S^\pm$, where $S_z = \frac{(|2\rangle\langle 2| - |1\rangle\langle 1|)}{2}$ is the bare state inversion operator. Note that, $|2\rangle$ and $|1\rangle$ are corresponding to the excited and ground state of the qubit, respectively, while b^\dagger and b are the creation and annihilation operator of the electromagnetic field (**EMF**) in the resonator, are satisfying the standard bosonic commutation relation, i.e., $[b, b^\dagger] = 1$, and $[b, b] = [b^\dagger, b^\dagger] = 0$.

Next, one is going to presents the derivation of Hamiltonian describing the coherent evolution of the considered system. The Hamiltonian describing completely the interaction of a two-level system possessing permanent dipoles with an external resonant coherent field as well as with a

single-mode resonator, in the dipole and rotating wave approximations, is:

$$\begin{aligned}
H = & \hbar\omega b^\dagger b + \hbar\omega_{21} S_z - \hbar\Omega(S^+ e^{i\omega_L t} + S^- e^{-i\omega_L t}) + \hbar g_0 (d_{22} S_{22} + d_{11} S_{11}) (b^\dagger + b) \\
& + \hbar\bar{g}_0 (S^+ + S^-) (b^\dagger + b) - E_L (d_{22} S_{22} + d_{11} S_{11}) \cos(\omega_L t). \tag{4.2}
\end{aligned}$$

In this Hamiltonian (4.2), the first two terms correspond to the free energies of the resonator and the two-level subsystem. The third and the sixth terms of this Hamiltonian (4.2) describes the interaction of the external laser field with the two-level emitter through its off-diagonal dipole moments d_{21} , $d_{21} = d_{12}$, as well as the diagonal dipole moments d_{22} and d_{11} , correspondingly. The fourth and the fifth terms of the Hamiltonian account for the interactions of the cavity mode with the two-level system via diagonal and off-diagonal dipole moments. Also, E_L is the amplitude of the external driving field, while $g_0 = \sqrt{\frac{2\pi\omega}{\hbar V}}$ where V is the quantization volume, and $\bar{g}_0 = g_0 d_{21}$. $S_{\alpha\alpha}, \{\alpha = 1, 2\}$ are the population operators respectively. One can notice that the fifth's Hamiltonian's term is a rapidly oscillating since ω_L is bigger than the corresponding coupling strength, i.e., $\omega_L \gg \bar{g}_0$ and $\omega_L \gg \omega$, and with respect to this term we have performed the unitary transformation $\bar{U} = \exp(i\omega_L S_z t)$. The last term in the Hamiltonian (4.2) is neglected for the similar reason since $\omega_L \gg \left\{ \frac{E_L d_{22}}{\hbar}, \frac{E_L d_{11}}{\hbar} \right\}$ for moderate assumed external pumping strengths. After the above mentioned assumptions and transformations, the following Hamiltonian is derived:

$$H = \hbar\omega b^\dagger b + \hbar\Delta S_z - \hbar\Omega(S^+ - S^-) + \hbar g S_z (b^\dagger + b) + \hbar g_0 (d_{11} + d_{22}) \frac{(b^\dagger + b)}{2}, \tag{4.3}$$

where $g = g_0 (d_{22} - d_{11})$, and we have also considered the relations $S_{22} = \frac{1}{2} + S_z$, and $S_{11} = \frac{1}{2} - S_z$. Later, applying a unitary transformation $V = \exp(\zeta b - \zeta^* b^\dagger)$, with $\zeta = g_0 \frac{(d_{11} + d_{22})}{2(\omega + i\frac{\kappa}{2})}$, in the whole master equation (4.1), embedding the Hamiltonian (4.3) one derives the same form of the master equation with, however, the Hamiltonian (4.5) given below, and where $\Delta \equiv \Delta - g_0^2 \frac{(d_{22}^2 - d_{11}^2)}{\omega}$, where $\omega \gg \kappa$. The last term from the detuning's expression is used for the redefinition of the emitter's frequency, i.e., $\omega_{21} \equiv \omega_{21} - g_0^2 \frac{(d_{22}^2 - d_{11}^2)}{\omega}$, so one finally has derived $\Delta = \omega_{21} - \omega_L$. Further, if we perform the unitary transformation in the Hamiltonian (4.5), $\bar{V}(t) = \exp(i\omega b^\dagger b t)$, the one derives the following Hamiltonian:

$$H = \hbar\Delta S_z - \hbar\Omega(S^+ + S^-) + \hbar g S_z (b^\dagger e^{i\omega t} + b e^{-i\omega t}). \tag{4.4}$$

If one avoids any resonances in the system with respect to the resonator's frequency or its multiples, as it is the considered in this chapter, then the last term in the above Hamiltonian (4.4) is a rapidly oscillating one, if ω is significantly greater then g , and may be dropped off. Below, one develops

an approach where the contribution of this term is perturbatively computed for moderately intense externally applied fields and appropriate parameters ranges, i.e., $\omega > 2\Omega \gg \{g, \gamma, \kappa\}$, respectively.

The Hamiltonian characterizing the respective coherent evolution of the leaking single-mode quantized cavity field coupled with a resonantly driven two-level qubit possessing permanent dipoles is:

$$H = \hbar\omega b^\dagger b + \hbar\Delta S_z - \hbar\Omega(S^+ + S^-) + \hbar g S_z(b^\dagger + b). \quad (4.5)$$

In the Hamiltonian (4.5), the first two terms describe the free energies of the cavity electromagnetic field and the two-level qubit, respectively, with $\Delta = \omega_{21} - \omega_L$ is the detuning of the two-level qubit transition frequency ω_{21} from the laser one. The last two terms are describing, respectively, the laser interaction with the two-level qubit and the qubit-cavity interaction. In the corresponding way, Ω and g are the respective coupling strengths, according to the model scheme presented in Fig.4.1. It is important to highlight at this point that Rabi frequency Ω is proportional to the off-diagonal dipole moment d_{21} , the qubit-cavity coupling is proportional to the diagonal dipole moments, i.e. $g \propto (d_{22} - d_{11})$. The interaction of the external coherent electromagnetic field with permanent dipoles are dropped off as being rapidly oscillating terms. From the same reason, the qubit-cavity interaction described by the Hamiltonian defined in the Jaynes-Cummings framework, proportional to d_{21} are dropped off as well.

In what follows, we perform a spin rotation:

$$U(\chi) = \exp[2i\chi S_y], \quad (4.6)$$

where

$$S_y = \frac{S^+ - S^-}{2i}, \quad (4.7)$$

and

$$2\chi = \arctan\left[\frac{2\Omega}{\bar{\Delta}}\right], \quad (4.8)$$

with

$$\bar{\Delta} = \Delta + g(b^\dagger + b), \quad (4.9)$$

diagonalizing the last three terms presented in Hamiltonian (4.5). This transformation will lead to new quasi-spin operators, i.e., R_z and R^\pm , defined via the old emitter's operators in the following

way:

$$\begin{aligned} R_z &= S_z \cos 2\chi - \frac{1}{2}(S^+ - S^-) \sin 2\chi, \\ R^+ &= S^+ \cos^2 \chi - S^- \sin^2 \chi + S_z \sin 2\chi, \\ R^- &= [R^+]^\dagger. \end{aligned}$$

The new emitter operators $R^+ = |\bar{2}\rangle\langle\bar{1}|$, $R^- = |\bar{1}\rangle\langle\bar{2}|$, and $R_z = \frac{(|\bar{2}\rangle\langle\bar{2}| - |\bar{1}\rangle\langle\bar{1}|)}{2}$, describing the transitions and populations among the dressed-state $\{|\bar{2}\rangle, |\bar{1}\rangle\}$, will obey the commutation relations $[R^+, R^-] = 2R_z$ and $[R_z, R^\pm] = \pm R^\pm$, similarly to the old-basis ones. Respectively, the Hamiltonian (4.5) is transformed into:

$$H = \hbar\omega b^\dagger b + 2\hbar\bar{\Omega}R_z, \quad (4.10)$$

where the operator $\bar{\Omega}$ is the new generalized Rabi frequency

$$\bar{\Omega} = \sqrt{\frac{\bar{\Delta}^2}{4} + \Omega^2}, \quad (4.11)$$

whereas the bosonic annihilation operator b is expanded in power series

$$b = \bar{b} - i\eta S_y \sum_{k=0}^{\infty} \frac{\eta^k}{k!} (\bar{b}^\dagger + \bar{b})^k \frac{\partial^k}{\partial \xi^k} \frac{1}{1 + \xi^2}, \quad (4.12)$$

with bosonic operators being rotated as well, according to the unitary transformation $b^\dagger = [b]^\dagger$, $\bar{b} = UbU^{-1}$, $\bar{b}^\dagger = [\bar{b}]^\dagger$, and the small parameters defined for further derivation

$$\begin{aligned} \eta &= \frac{g}{2\Omega}, \\ \xi &= \frac{\Delta}{2\Omega}. \end{aligned}$$

In the next step, one has to insert eqs.(4.10)-(4.12) in master equation (4.1) getting a cumbersome final equation and laborious to be derived. To avoid supplementary complicated calculations, one is going to perform a secular approximation, namely, one is going to drop off all terms from the master equation oscillating at the generalized Rabi frequency $2\Omega_0$, $\Omega_0 = \Omega\sqrt{1 + \xi^2}$ and higher one. Consequently, will dropped off all terms satisfying the following condition if $2\Omega_0 \gg \{\omega, g, \gamma\}$, which is the situation considered here.

Thus in the following, we are expanding the generalized Rabi frequency $\bar{\Omega}$ defined in (4.11) in

the Taylor series using the small parameter η , as it is presented below,

$$\bar{\Omega} = \Omega_0 \left\{ 1 + \frac{\xi \hat{\eta}}{1 + \xi^2} + \frac{\hat{\eta}^2}{2(1 + \xi^2)^2} - \frac{\xi \hat{\eta}^3}{2(1 + \xi^2)^3} + \dots \right\}, \quad (4.13)$$

in this series expansion (4.13) the small parameter $\hat{\eta} = \eta(\bar{b}^\dagger + \bar{b})$ is directly proportional to the bosonic generation and annihilation operators, as well expanded in power series according to (4.12).

Another important step is to get the Heisenberg equation modeling the multiphoton interactions of the system described in this chapter:

$$\begin{aligned} \frac{d}{dt} \langle Q(t) \rangle &= \frac{i}{\hbar} \langle [H, Q] \rangle = -\frac{\gamma}{8(1 + \xi^2)} \left\{ \langle R_z [R_z, Q] \rangle + \frac{\xi^2}{(1 + \xi^2)^2} \langle \hat{\eta} R_z [\hat{\eta} R_z, Q] \rangle \right. \\ &- \frac{1 - 2\xi^2}{2(1 + \xi^2)^2} \left(\langle R_z [\hat{\eta}^2 R_z, Q] \rangle + \langle \hat{\eta}^2 R_z [R_z, Q] \rangle \right) \left. \right\} \\ &- \frac{\gamma}{8} \left\{ \left(1 + \frac{\xi}{\sqrt{1 + \xi^2}} \right)^2 \langle R^+ [R^-, Q] \rangle + \frac{1}{(1 + \xi^2)^2} \langle \hat{\eta} R^+ [\hat{\eta} R^-, Q] \rangle \right. \\ &- \left(1 + \frac{\xi}{\sqrt{1 + \xi^2}} \right) \frac{3\xi}{2(1 + \xi^2)^{\frac{5}{2}}} \left(\langle R^+ [\hat{\eta}^2 R^-, Q] \rangle + \langle \hat{\eta}^2 R^+ [R^-, Q] \rangle \right) \left. \right\} \\ &- \frac{\gamma}{8} \left\{ \left(1 - \frac{\xi}{\sqrt{1 + \xi^2}} \right) \langle R^- [R^+, Q] \rangle + \frac{1}{(1 + \xi^2)^3} \langle \hat{\eta} R^- [\hat{\eta} R^+, Q] \rangle \right. \\ &- \left(1 + \frac{\xi}{\sqrt{1 + \xi^2}} \right) \frac{3\xi}{2(1 + \xi^2)^{\frac{5}{2}}} \left(\langle R^- [\hat{\eta}^2 R^+, Q] \rangle + \langle \hat{\eta}^2 R^- [R^+, Q] \rangle \right) \left. \right\} \\ &- \frac{\kappa}{2} (1 + \bar{n}) \langle \bar{b}^\dagger [\bar{b}, Q] \rangle - \frac{\kappa}{2} \bar{n} \langle \bar{b} [\bar{b}^\dagger, Q] \rangle + H.c. \end{aligned} \quad (4.14)$$

The above presented Heisenberg (4.14) form of the master equation derived for the first three terms of the Taylor series, in which was expanded the generalized Rabi frequency (4.13) including as well $\hat{\eta}$ expanded correspondingly in the power series, as presented below:

$$\hat{\eta}^2 = \eta^2 (\bar{b}^\dagger \bar{b} + \bar{b} \bar{b}^\dagger + \bar{b}^2 + \bar{b}^{\dagger 2}). \quad (4.15)$$

In this context, we present the master equation derived discretely for $\hat{\eta}^2$ expanded in power series as presented above, where the rapid oscillating terms were dropped of:

$$\begin{aligned} \rho(t) &= -\frac{\gamma}{8(1 + \xi^2)} \left\{ [R_z, R_z \rho] + \frac{\xi^2 \eta^2}{(1 + \xi^2)^2} \left([\bar{b} R_z, R_z \bar{b}^\dagger \rho] + [\bar{b}^\dagger R_z, R_z \bar{b} \rho] \right) \right. \\ &- \frac{(1 - 2\xi^2) \eta^2}{2(1 + \xi^2)^2} \left([R_z, (\bar{b} \bar{b}^\dagger + \bar{b}^\dagger \bar{b}) R_z \rho] + [(\bar{b} \bar{b}^\dagger + \bar{b}^\dagger \bar{b}) R_z, R_z \rho] \right) \left. \right\} \\ &- \frac{\gamma}{8} \left\{ \left(1 + \frac{\xi}{\sqrt{1 + \xi^2}} \right)^2 [R^+, R^- \rho] + \frac{\eta^2}{(1 + \xi^2)^3} \left([\bar{b} R^+, R^- \bar{b} \rho] + [\bar{b}^\dagger R^+, R^- \bar{b} \rho] \right) \right. \end{aligned}$$

$$\begin{aligned}
& - \left(1 + \frac{\xi}{\sqrt{1+\xi^2}} \right) \frac{3\xi}{2(1+\xi^2)^{\frac{5}{2}}} \left([R_z, (\bar{b}\bar{b}^\dagger + \bar{b}^\dagger\bar{b})R_z\rho] + [R_z(\bar{b}\bar{b}^\dagger + \bar{b}^\dagger\bar{b}), R_z\rho] \right) \Big\} \\
& - \frac{\gamma}{8} \left\{ \left(1 - \frac{\xi}{\sqrt{1+\xi^2}} \right)^2 [R^-, R^+\rho] + \frac{\eta^2}{(1+\xi^2)^3} \left([\bar{b}R^+, \bar{b}^\dagger R^-\rho] + [\bar{b}^\dagger R^+, \bar{b}R^-\rho] \right) \right. \\
& - \left. \left(1 - \frac{\xi}{\sqrt{1+\xi^2}} \right) \frac{3\xi}{2(1+\xi^2)^{\frac{5}{2}}} \left([R^-, (\bar{b}\bar{b}^\dagger + \bar{b}^\dagger\bar{b})R^+\rho] + [R^-(\bar{b}\bar{b}^\dagger + \bar{b}^\dagger\bar{b}), R^+\rho] \right) \right\} \\
& - \frac{\kappa}{2}(1+\bar{n})\langle \bar{b}^\dagger [\bar{b}, Q] \rangle - \frac{\kappa}{2}\bar{n}\langle \bar{b} [\bar{b}^\dagger, Q] \rangle + H.c. \tag{4.16}
\end{aligned}$$

In the next step, one is performing a unitary transformation $U(t) = \exp [2i\Omega_0 R_z t]$ of the whole master equation. This way, we will neglect the rapid oscillating terms at the Rabi frequency $2\Omega_0$ or higher. Afterwards, we project the obtained master equation in the dressed-state base in the following manner: $\rho_{\bar{\alpha}\bar{\alpha}} = \langle \bar{\alpha} | \rho | \bar{\alpha} \rangle$, $\alpha \in \{1, 2\}$, and one is arriving to the following generalized master equation describing the cavity degrees of freedom only:

$$\begin{aligned}
\frac{d}{dt}\bar{\rho}(t) & + \frac{i}{\hbar} [\bar{H}, \bar{\rho}] - \frac{\gamma}{4} \{ \cos 2\chi \bar{\rho} \cos 2\chi + \sin 2\chi \bar{\rho} \sin 2\chi - \bar{\rho} \} = \\
& - \frac{\kappa}{2}(1+\bar{n}) [\bar{b}^\dagger, \bar{\rho}] - \frac{\kappa}{2}\bar{n} [\bar{b}, \bar{\rho}] \\
& - \frac{\kappa\eta^2}{8}(1+2\bar{n}) \sum_{k_1, k_2}^{\infty} f_{k_1}(\eta, \xi) f_{k_2}(\eta, \xi) \\
& \times \left[(\bar{b}^\dagger + \bar{b})^{k_1}, (\bar{b}^\dagger + \bar{b})^{k_2} \bar{\rho} \right] + H.c., \tag{4.17}
\end{aligned}$$

where the final master equation was computed as a sum of two master equations projected in the Fock states base to determine the dynamics of the population $\bar{\rho} = \rho_{\bar{1}\bar{1}} + \rho_{\bar{2}\bar{2}}$. As well, in the master eq.(4.17) functions $f_k(\eta, \xi)$, $\sin 2\chi$, $\cos 2\chi$ are defined in the corresponding power series:

$$\begin{aligned}
f_k(\eta, \xi) & = \frac{\eta^k}{k!} \frac{\partial^k}{\partial \xi^k} \frac{1}{1+\xi^2}, \\
\sin 2\chi & = \frac{\Omega}{\bar{\Omega}} = \sum_{k=0}^{\infty} \frac{\eta^k (\bar{b} + \bar{b}^\dagger)^k}{k!} \frac{\partial^k}{\partial \xi^k} \frac{1}{\sqrt{1+\xi^2}}, \\
\cos 2\chi & = \frac{\bar{\Delta}/2}{\bar{\Omega}} = \sum_{k=0}^{\infty} \frac{\eta^k (\bar{b} + \bar{b}^\dagger)^k}{k!} \frac{\partial^k}{\partial \xi^k} \frac{\xi}{\sqrt{1+\xi^2}}. \tag{4.18}
\end{aligned}$$

According to the above presented power series (4.18), one can recognize the multiphoton dynamics of the cavity electromagnetic quantum field quantum dynamics.

Additionally, one has used the sum of bosonic operators expanded in power series:

$$(A+B)^n = \sum_{k'}^n \frac{n!}{k'! \left(\frac{n-k'}{2}\right)!} \left(-\frac{C}{2}\right)^{\frac{n-k'}{2}} \sum_{r=0}^{k'} \frac{k'!}{r!(k'-r)!} \times A^r B^{k'-r}, \tag{4.19}$$

where the operators A and B verify the operator's identities $[A, B] = C$ and $[A, C] = [B, C] = 0$, whereas $\{n, k', r\} \in \mathbb{Z}^*$ are integer non-zero numbers. These properties of power series indexes are used to reduce the master equation (4.1) to a time-independent equation, unless a supplementary unitary transformation is performed:

$$V(t) = \exp [i\omega \bar{b}^\dagger \bar{b} t], \quad (4.20)$$

and all terms rotating at frequency ω and higher are dropped off. Also, these transformation neglects the resonance cases in the system, i. e., $2\Omega_0 - s\omega \neq 0$, $s \in \{1, 2, \dots\}$.

In the result, one obtains a diagonal equation for $P_n = \langle n | \bar{\rho} | n \rangle$, with $|n\rangle$ being the Fock state base and $n \in \{0, 1, 2, \dots\}$, describing the cavity multiphoton quantum dynamics, in the presence of the corresponding damping effects, which is modeled then numerically here. Notice that the coherent part of the master equation (4.17), i.e., $[\bar{H}, \bar{\rho}]$ does not contribute to the final expression for the photon distribution function P_n . The reason is that, after the performed approximations the Hamiltonian \bar{H} would contain photonic correlators such that $\langle n | [\bar{H}, \bar{\rho}] | n \rangle = \bar{H}_n P_n - P_n \bar{H}_n = 0$. herefore, the cavity photon dynamics has a multiphoton output because of the highly dispersive or non-resonant properties of the interaction among the asymmetrical two-level emitter and cavity field mode. According to this judgment, one obtains an output multiphoton beam of microwave photons, although the two-level is coherently pumped at a different frequency, i.e. with optical photons.

4.2 Results and discussions

Statistics of light is of great importance for many applications in metrology, material probing, biomedical optics, and optical communications and etc. Light's statistics features are described by correlations between the electric field amplitudes at different locations or times. Due to the variance of light sources, one calculates the first-order correlation function of the field, which after normalization calculation is named the degree of first-order temporal coherence. The value of the first-order correlation function is indirectly determined by the power spectrum of the light, according to Wiener-Khintchine theorem.

In this paragraph, we will present the cavity multiphoton quantum dynamics computed according to the master equation (4.17) presented in the paragraph 4.1. The analytical solving method presented in this paragraph allows us to derive a finite system of equations describing the multiphoton quantum dynamics of a system consisting of a leaking single-mode quantized cavity field coupled with resonantly pumped two-level qubit possessing permanent dipoles. Applying the Rotating Wave Approximation, Born-Markov and secular approximations, one has derived the variables of interest, applying supplementary the traced density operator over the corresponding equations of interest. In order to solve the infinite system of equations presented by eq.(4.17), we have truncated it at certain value $n = n_{max}$, which assures the asymptotic stability threshold of system's solutions so that further increase of n_{max} will not modify the result.

Below, we shall describe the cavity multiphoton quantum dynamics defined by eq.(4.17). Here, we highlight some processes occurring in our setup in more details, namely, the single- and two-photon effects. Let us write down the time-independent damping part of the master equations (4.17), taking into account expansion terms up to η^4 , namely,

$$\begin{aligned}
\frac{d}{dt}\bar{\rho} &= -\frac{\gamma\eta^2}{8(1+\xi^2)^2} \{ [\bar{b}, \bar{b}^\dagger\bar{\rho}] + [\bar{b}^\dagger, \bar{b}\bar{\rho}] \} - \frac{\gamma\eta^4(1+4\xi^2)}{32(1+\xi^2)^4} \\
&\times \{ [(\bar{b}\bar{b}^\dagger + \bar{b}^\dagger\bar{b}), (\bar{b}\bar{b}^\dagger + \bar{b}^\dagger\bar{b})\bar{\rho}] + [\bar{b}^2, \bar{b}^{\dagger 2}\bar{\rho}] + [\bar{b}^{\dagger 2}, \bar{b}^2]\bar{\rho} \} \\
&+ \frac{3\gamma\eta^4(1-2\xi^2)}{8(1+\xi^2)^4} \{ [\bar{b}^\dagger(1+\bar{b}^\dagger\bar{b}), \bar{b}\bar{\rho}] + [(1+\bar{b}^\dagger\bar{b})\bar{b}, \bar{b}^\dagger\bar{\rho}] \} \\
&- \frac{\kappa}{2}(1+\bar{n})[\bar{b}^\dagger, \bar{b}\bar{\rho}] - \frac{\kappa}{2}\bar{n}[\bar{b}, \bar{b}^\dagger\bar{\rho}] + H.c.
\end{aligned} \tag{4.21}$$

where smaller contributions, proportional to $\kappa\eta^4$, were dropped off since we have considered that $\frac{\kappa}{\gamma} \ll 1$. One can notice that terms proportional to η^2 describe single-photon processes; that is, the photon number in the distribution function $P_n (P_n = \langle n|\bar{\rho}|n\rangle$ with $n \in \{0, 1, 2, \dots\})$ will change by ± 1 , i.e., $P_{n\pm 1}$. Respectively, the terms proportional to η^4 express the two-photon effects. For example, the last two commutators from the second term of eq.(4.21) will change the photon

number in the distribution function P_n by ± 2 , i.e., $P_{n\pm 2}$ see also eq.(4.28) and Fig.4.1. Concluding this part, one can generalize that terms proportional η^{2N} , in the master equation (4.17), account for N -photon processes, respectively. Considering then $\eta^4 \rightarrow 0$, we derive the eq. (4.26), accounting for single-photon processes only since

$$P_n = Z^{-1} e^{-\alpha n}, \quad (4.22)$$

where the normalization Z is determined by the requirement $\sum_{n=0}^{\infty} e^{-\alpha n}$, whereas $\alpha = \ln \beta$ and $\beta = \frac{\kappa_1}{\kappa_2}$ with $\kappa_1 = \frac{\kappa(1+\bar{n}+\gamma\eta^2)}{[4(1+\xi^2)]^2}$, and $\kappa_2 = \kappa\bar{n} + \frac{\gamma\eta^4}{[4(1+\xi^2)]^2}$. The mean-photon number is determined via

$$\langle \bar{b}^\dagger \bar{b} \rangle = \sum_{n=0}^{\infty} n P_n = \frac{1}{\beta - 1} = \bar{n} + \frac{\gamma\eta^2}{4\kappa(1 + \xi^2)^2}, \quad (4.23)$$

which is mentioned below again. Note that, unfortunately, finding the analytic solution of eq. (4.21) or eq. (4.27), incorporating both single- and two-photon processes, is not a trivial task.

Once again, for single-photon non-resonant processes one can derive equation for the photon distribution function:

$$\frac{d}{dt} P_n(t) = -P_n^{(1)}, \quad (4.24)$$

where

$$P_n^{(1)} = \left\{ \kappa(1 + \bar{n}) + \frac{\gamma\eta^2}{4(1 + \xi^2)^2} \right\} \left(n P_n - (n + 1) P_{n+1} \right) + \left\{ \kappa\bar{n} + \frac{\gamma\eta^2}{4(1 + \xi^2)^2} \right\} \left((n + 1) P_n - n P_{n-1} \right). \quad (4.25)$$

The first line of the above expression for the $P_n^{(1)}$ (4.25) describes the photon generation processes, i.e., photons that leave the cavity. The second line corresponds to processes describing photons pumping the cavity mode due to the environmental thermostat and non-resonant external driving, respectively. One can observe that both processes are influenced by the resonant laser driving of the two-level emitter possessing permanent dipoles. As a consequence, the stationary mean-photon number in the resonator mode is

$$\langle \bar{b}^\dagger \bar{b} \rangle = \bar{n} + \frac{\gamma\eta^2}{4\kappa(1 + \xi^2)^2}, \quad (4.26)$$

whereas its second-order photon-photon correlation function is $g^{(2)}(0) = 2$. Correspondingly, for

two-photon non-resonant processes one derives:

$$\frac{d}{dt}P_n(t) = -P_n^{(2)}, \quad (4.27)$$

where

$$\begin{aligned} P_n^{(2)} &= P_n^{(1)} - \frac{3\gamma(1-2\xi^2)\eta^4}{4(1+\xi^2)^4} \left((1+n)^2(P_n - P_{n+1}) + n^2(P_n - P_{n-1}) \right) \\ &+ \frac{\gamma(1+4\xi^2)\eta^4}{16(1+\xi^2)^4} \left(n(n-1)P_n - (n+1)(n+2)P_{n+2} \right) \\ &+ \frac{\gamma(1+4\xi^2)\eta^4}{16(1+\xi^2)^4} \left((n+1)(n+2)P_n - n(n-1)P_{n-2} \right), \end{aligned} \quad (4.28)$$

where terms proportional to $\kappa\eta^4$ have been dropped off since we have assumed that $\kappa/\gamma \ll 1$. Here, the first two lines of the expression for $P_n^{(2)}$ (4.28) describe the photon depopulation and population of the cavity mode due to single-photon processes. Notice that the single-photon effects are influenced by the second-order one, see the second term proportional to η^4 in the first line of $P_n^{(2)}$. The last two lines of the same expression consider the resonator photon depopulation and population effects via two-photon processes, correspondingly. In this way, eq.(4.27) describes the photon processes where single-photon and two-photon effects occur simultaneously. In the next paragraph, we will show the mean-photon number in the cavity mode change correspondingly. Thus, we have explicitly shown the equations for the photon distribution for single-and two-photon processes, namely eqs.(4.25) and (4.28). For instance, eq.(4.25) is due to terms in the master eq.(4.17), like $[\bar{b}^\dagger, \bar{b}\rho]$ and $[\bar{b}, \bar{b}^\dagger\rho]$ and their Hermitian conjugates, respectively, whereas eq.(4.28) results from terms $[\bar{b}^{\dagger 2}, \bar{b}^2\rho]$ and $[\bar{b}^2, \bar{b}^{\dagger 2}\rho]$ in eq.(4.17). This proves a clear two-photon process in eq. (4.28) and the final cavity is a multiphoton one as it will be discussed below.

Similarly, additional N - photon non-resonant processes with $N \in \{3, 4, \dots\}$ can be included by reducing the eq.(4.1) to terms up to η^{2N} . In order to solve the infinite system of equations for P_n , see eq. (4.28) for two-photon processes, we truncate it at a certain maximum value $n = n_{max}$ so that increasing this value, i.e. n_{max} , the calculated results do not change, keeping the the parameters of interest fixed. Thus, the cavity photon dynamics has multiphoton dynamics due to the highly dispersive (non-resonant) features of the interaction between the asymmetrical two-level qubit and cavity field mode. This way, one generates an output multiphoton beam of microwave photons, although the two-level system is coherently driven at a different frequency, i.e. with optical photons.

Thus, generally the resonator's steady-state mean quanta number can be expressed as:

$$\langle n \rangle = \langle \bar{b}^\dagger \bar{b} \rangle = Tr_{Qubit} \left[\sum_{n=0}^{\infty} \langle n | \rho \bar{b}^\dagger \bar{b} | n \rangle \right] = Tr_{Qubit} \left[\sum_{n=0}^{\infty} n \langle n | \rho | n \rangle \right], \quad (4.29)$$

here we expressed the bosonic field operators in the ket basis $\bar{b}^\dagger \bar{b} | n \rangle = n | n \rangle$. Deriving the trace sum over the system states, we get:

$$\langle n \rangle = \sum_{i=1,2} \sum_{n=0}^{\infty} n \langle n, i | \rho | n, i \rangle = \sum_{n=0}^{\infty} \langle n | \rho_{11} + \rho_{22} | n \rangle = \sum_{n=0}^{\infty} n \langle n | \bar{\rho}^{(1)} | n \rangle, \quad (4.30)$$

here we have swapped the sum over the system states, computing in this way the trace over the two-level qubits states first. Following the computation algorithm brought here, one substitutes the master equation 4.17, i.e., $P_n^{(1)}$ and truncate the sum over the infinite Fock states, getting the suitable equations for the numerical calculations:

$$\langle \bar{b}^\dagger \bar{b} \rangle = \sum_{n=0}^{n_{max}} n P_n^{(1)}, \quad (4.31)$$

with

$$\sum_{n=0}^{n_{max}} P_n^{(1)} = 1, \quad (4.32)$$

while the steady-state second-order photon-photon correlation function is defined as:

$$\begin{aligned} g^{(2)}(0) &= \frac{\langle \bar{b}^\dagger \bar{b}^\dagger \bar{b} \bar{b} \rangle}{\langle \bar{b}^\dagger \bar{b} \rangle^2} = \frac{1}{\langle \bar{b}^\dagger \bar{b} \rangle^2} Tr_{Qubit} \left[\sum_{n=0}^{\infty} \langle n | \rho \bar{b}^\dagger \bar{b}^\dagger \bar{b} \bar{b} | n \rangle \right] = \frac{1}{\langle \bar{b}^\dagger \bar{b} \rangle^2} Tr_{Qubit} \left[\sum_{n=0}^{\infty} n(n-1) \langle n | \rho | n \rangle \right] \\ &= \frac{1}{\langle \bar{b}^\dagger \bar{b} \rangle^2} \sum_{i=1,2} \sum_{n=0}^{\infty} n(n-1) \langle n, i | \rho | n, i \rangle = \frac{1}{\langle \bar{b}^\dagger \bar{b} \rangle^2} \sum_{n=0}^{\infty} n(n-1) \langle n | \bar{\rho}^{(1)} | n \rangle \\ &= \frac{1}{\langle \bar{b}^\dagger \bar{b} \rangle^2} \sum_{n=0}^{\infty} n(n-1) P_n^{(1)} \simeq \frac{1}{\langle \bar{b}^\dagger \bar{b} \rangle^2} \sum_{n=0}^{n_{max}} n(n-1) P_n^{(1)}. \end{aligned} \quad (4.33)$$

Particularly, Fig.4.2 presents the steady-state mean photon numbers and their second-order photon-photon correlation functions for single-photon and two-photon processes computed using eqs.(4.24) and (4.27). One can notice here that these quantities are distinct from each other for single- and two-photon effects, correspondingly. In order to compare and understand the difference between single- and two-photon processes, Fig.4.3 presents similar effects for two- and three-photon processes, respectively. Here, it is evident that the mean-photon numbers almost overlap for the two cases under consideration, whereas their second-order correlation function is different from each other. One can proceed in the same vein with higher order photon processes. Neverthe-

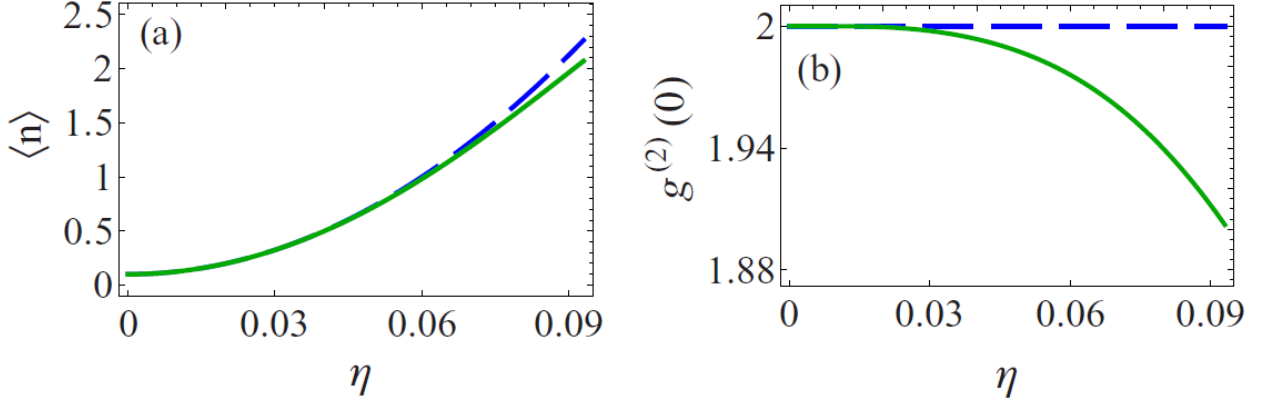


Fig. 4.2: In the right side (a) of the figure is presented the steady-state mean cavity photon number $\langle n \rangle \equiv \langle \bar{b}^\dagger \bar{b} \rangle$ as well as in the left side (b) its second-order correlation function $g_s^{(2)}(0)$ as a function of $\eta = \frac{g}{2\Omega}$. The blue lines are plotted for single-photon processes $N = 1$, while the green ones for two-photon processes, $N = 2$, respectively. Here, $\bar{n} = 10^{-1}$, $\frac{\kappa}{\gamma} = 10^{-3}$ and $\xi = 0$ [204].

less, for similar considered parameters, their probabilities are small and the mean photon numbers are basically identical with ones mentioned in the description of left side of Fig.4.3. Further, the photon statistics changes from super-Poissonian and thermal features, subsequently, as η increases with other parameters kept constant. The main conclusion drawn here is that single-, two- and three-photon processes are most feasible when other parameters are maintained constant, whereas the final cavity steady state is a quantum superposition of all those photons.

Note, values different from 2 for $g_s^{(2)}(0)$ occur typically for higher values of η 's with $\eta < 1$, ensure the creation of this final cavity state. Remark that generally the surrounding thermal mean-photon number will count linearly to the final photon flux as presented in eq.(4.26) for single-photon processes, so that an increase in the environmental temperature will lead to more output photons for the considered parameter ranges. To prove supplementary this statement, Fig.4.4 displays the photon distribution function $P_n = \langle n | \bar{\rho} | n \rangle$ for the same parameters considered for the computation in Fig.4.2 and 4.3, however, for five-photon processes, i.e. $N = 5$. One can observe here that larger ratios of $\eta = \frac{g}{2\Omega}$, with $\eta < 1$ lead to population of higher photon states, compare the green and the blue curves plotted for $\eta = 0.09$ and $\eta = 0.07$, respectively facilitating the generation of multiphoton states when $\frac{\kappa}{\gamma} \ll 1$. Correspondingly, P_n small for larger n and smaller η , while $\eta < 1$, assuring convergence of the results computed by eq.(4.17). One can notice that the probability of a two-photon state, that is $n = 2$, is almost the same for $\eta = 0.07$ and $\eta = 0.09$, respectively, and it is higher than 0.1. One may conjecture then that a multiphoton superposition state around $n = 2$ is generated when other parameters are maintained constant. Furthermore, same results, presented in the Figs. 4.2, 4.3, 4.4 will strive for moderate detunings, i.e., would not change significantly if $\xi \ll 1$.

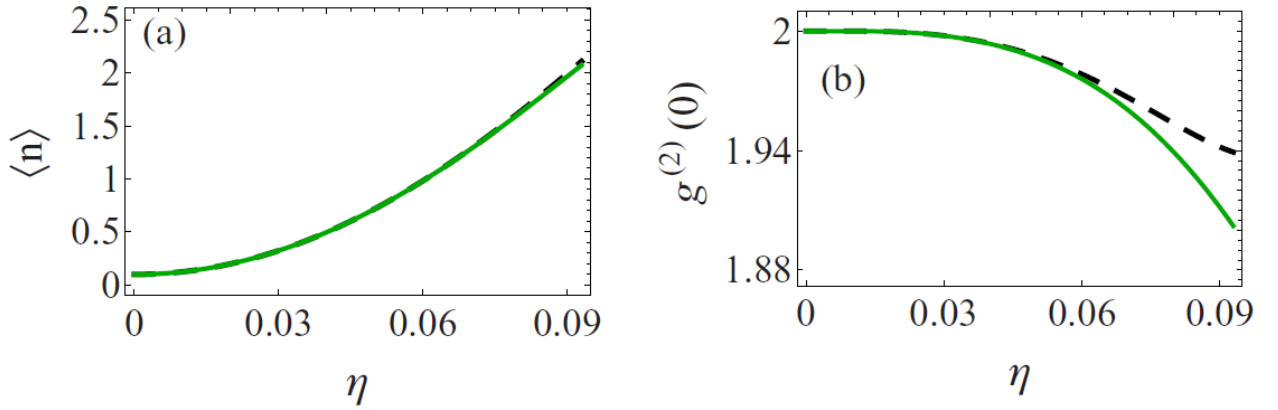


Fig. 4.3: In the left side (a) of the figure is presented the steady-state mean cavity photon number $\langle n \rangle \equiv \langle \bar{b}^\dagger \bar{b} \rangle$ as well as the right side (b) its second-order correlation function $g^{(2)}(0)$ as a function of $\eta = \frac{g}{2\Omega}$. The green curves are plotted for two-photon processes, $N = 2$, while the short-dashed black ones are computed for three-photon processes, $N = 3$, respectively and keeping the same parameters as in Fig. 4.2 [204].

Here, we can conclude that the presence of diagonal dipole moments, in a resonance coherently driven two-level qubit, makes achievable the coupling to the resonator mode at a completely different frequency than the input one which pumps the two-level quantum emitter, and cavity multiphoton state generation, respectively. Notice, the experimental generation of multiple photon states with tunable correlation properties using quantum dots was proved by [203]. Also, the photon statistics in their case varied by the excitation rate from a sub-Poissonian one, where photons are temporally antibunched, to super-Poissonian, demonstrating a multiply populated quantum light source emitting temporally bunched photons. Additionally, the proposed approach here may be applied equally to a laser driven two-level quantum dot incorporated in an acoustical phonon cavity. In these circumstances, the manipulation of quantum states namely photons and phonons continues to be one of the main topics of modern science. The increasing research interest towards multiphoton engineering is raised due to multiphoton lasing effect, embedded in hypersensitive metrological systems. Setups enabled to generate bundles of photon states was proposed under the platform of cavity quantum electrodynamics (**cQED**). Beside them, phonons, which are mechanical waves, are emerging as proper states for the engineering of solid-state based quantum mechanical devices, as on-chip embedded quantum communications systems. Since the speed of acoustic waves is rather reduced than the speed of light, it suggests phonon based setups to be more suitable for communication over short distances, in the range of few hundred micrometers or even less. As well, phonons can be used as radiation loss communication channels in vacuum. Beyond that another fascinating advantage is the possibility to manufacture greatly tunable phonon cavities within the resonant frequency ranges from gigahertz (GHz) to terahertz (THz). The phonon

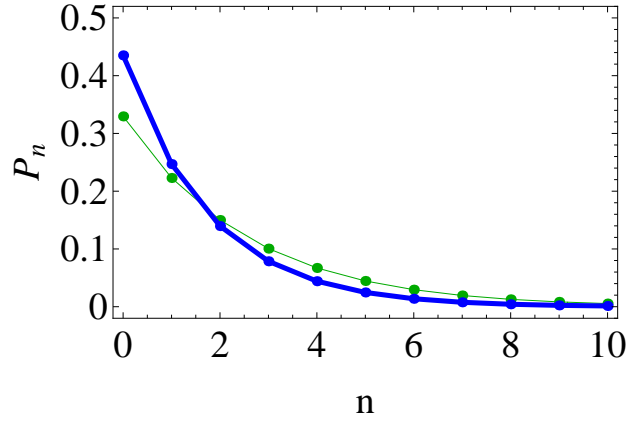


Fig. 4.4: The cavity photon distribution function P_n in the steady state. The green curve is plotted for $\eta = 0.09$, while the blue one for $\eta = 0.07$, respectively $\eta < 1$ is a small parameter considered by default. Other parameters are maintained as in Fig.4.2 [204].

generated THz waves are comparable to the crystal lattice constants, which makes them significant for sensing and nanoscale imaging, atomic precision detection. Thus, progresses in quantum phononics emerged further into multiphonon quantum states generation, setting them milestone towards acoustic quantum devices. The special interest present the antibunched bundles of phonon states, used as multi-phonon sources for acoustic quantum precision measurement and applications in ultrasensitive biodetection. A method of implementing multiphoton bundle emission from a quantum dot (QD) coupled to an acoustic cavity with electron-phonon interaction and coherently pumped by a coherent light source at a certain order phonon side band was presented by [181]. The optically driven Stokes processes generate super-Rabi oscillations between the states. Particularly, the quantum dot (QD) flips are assisted by multiphoton generation in the cavity, induced by electron-phonon interaction. In contrast to them [181] a multi-photon emitter was realized by [177] relying on cavity quantum electrodynamics paradigm of a two-level system placed in a cavity and feasible in a wide range of physical systems, which include atoms in optical cavities, superconducting qubits placed in microwave resonators and quantum dots placed in microcavities. They have shown the realization multiphoton emitters-sources that generate multiple photon grouped in bundles of photons, excluding the dipolar interaction between the two-level system and the cavity. Thus the feasibility of light composed of building blocks that are no longer single photons is proved. Such non-classical emitters present the new generation of light sources for quantum lithography, metrology, medical applications, allowing greater penetration lengths and better resolution without harming the tissue [36].

4.3 Conclusions to Chapter 4

In conclusion, one has investigated the quantum multiphoton dynamics of a two-level system possessing unequal permanent dipoles, placed in a leaking single-mode quantized cavity field and coupled to it. In this setup, we considered the frequencies of the interacting subsystems, namely the cavity and the emitter, are considered to belong to different frequencies range: microwave and optical domain, correspondingly, and therefore the two-level qubit couples to the resonator via its parallel dipole moments. Also, the generalized Rabi frequency generated by the external coherent pumping of the two-level qubit was considered different from the resonator's frequency. Consequently, the highly dispersive interaction regime is responsible for the cavity multiphoton quantum dynamics and photon conversion from optical to microwave range, as it was proved above in the chapter.

The interaction of driving laser field with a two-level system, which has a nonzero permanent dipole moment and its impact on the multiphoton transitions were computed in the Rotating Wave Approximation. Numerical calculations within Rotating Wave Approximation for the steady-state populations of the two-level system states are derived and used to discuss the impact of permanent dipole moments on the multiphoton transitions problem proposed in this chapter.

One has identified and described the Hamiltonian terms required to solve multiphoton dynamics of the quantum model, as well as, the terms required to deduce the master equation with an adapted approach for the characterization of the multiphoton emission processes, which have been presented in this chapter. As well, one has defined the complete dynamics of the system by deriving the required master equation, substituting the transformed Hamiltonian. The master equation has been simplified in order to obtain a solvable numerical expression. The required transformations and approximations have been applied, as well, the final analytical form of the master equation has been presented.

As a result, one has demonstrated the possibility to convert photons from optical to microwave frequency domains, via resonantly pumped asymmetrical two-level quantum optical emitter placed in a quantized single-mode resonator. The accompanying damping effects due to qubit's spontaneous emission and cavity's photon leakage were considered as well in the calculations. The transition frequency of the two-level qubit is several orders different from the cavity's one, specifically, it can lay in the optical range while resonator's frequency in the microwave range of frequencies. Consequently, the two-state quantum cavity emitter couples to the cavity mode through its parallel dipole moments. As well, the cavity's frequency is regarded as far off-resonance from the generalized Rabi frequency resulting from the coherent laser driving of the two-level qubit via

its non-diagonal dipole. In these state of affairs, multiphoton absorption-emission processes are relating to the cavity quantum dynamics.

It was proved that cavity's multiphoton characteristics and demonstrated the feasibility for a certain output multiphoton superposition of the generated states. The corresponding photon statistics feature changes from super-Poissonian to quasi-Poissonian photon statistics. These change arises from the increase of pumping parameter η from zero. Actually, values different from 2 for the second-order photon-photon correlation function $g^{(2)}(0)$ ensures the creation of the cavity superposition state. Finally, as a certain system, where the developed approach in this chapter can apply, can serve asymmetrical two-level quantum dots coupled to microwave resonators as well as polar biomolecules, spin or quantum circuit systems respectively. Additionally, the analytical approach can be employed for the study of non-resonant multiphoton quantum dynamics when two-level dot is interacting with an acoustical phonon resonator, respectively. Also, coupling to THz or even higher-frequency resonators will allow photon conversion in these photon ranges as well. Finally, it can be generalized to an ensemble of two-level emitters having permanent dipoles.

CONCLUSIONS AND RECOMMENDATIONS

The objectives of the thesis have been fulfilled and various new features of light-matter interaction and enhanced properties of molecular dipolar systems have been identified while studying the two-level and Λ -type three-level systems possessing a permanent non-zero dipole moment placed in quantum oscillator and interacting with external laser fields.

In correspondence with objectives stated in the introduction chapter, three different setups have been modeled in order to explain more exhaustively the impact of permanent dipole moment in all three setups and highlight the new quantum optical features of molecular dipolar systems, which were not discussed in similar researches. In the first case, one is considering a two-level system possessing permanent dipole moments and interacting with two external coherent laser fields. The first laser is near resonance with the transition frequency of the two-level system, while the second laser is close to resonance with the dressed-frequency splitting due to the first laser. In the second case, one studies the quantum dynamics of a quantum oscillator coupled with the most upper state of a three-level Λ -type system. Transitions within the three-level emitter possess orthogonal dipole moments and are coherently pumped with a single or two electromagnetic field sources, correspondingly. As a quantum oscillator in this case can serve a vibrational mode of a nanomechanical resonator embedding the three-level emitter or an electromagnetic cavity mode field if the highest energetic level of the Λ -type system incorporated in the cavity possesses a permanent dipole. In the third case, one investigates the frequency downconversion processes via a resonantly laser-pumped two-level emitter possessing non-zero permanent diagonal dipoles and is placed in a quantized microwave resonator.

The main scientific results presented in this thesis are summarized as follows:

1) The investigation of a steady-state quantum dynamics of a laser pumped two-level system possessing a non-zero permanent dipole moment involved the application of semi-classical laser-molecule dressed-state picture due to the first laser. The further dressed-state centrally symmetric transformation of the system Hamiltonian was derived.

One has plotted the resonance fluorescence spectrum of spontaneously emitted photons, squeezing spectrum and total quantum fluctuations, during the laser pumping processes of the system. New features differing from those in the case of two-level systems yet in the absence of permanent dipoles have been found. In particular, additional spectral lines are emitted and extra squeezed frequency domains are observed. The corresponding study is published in [190, 191].

2) The investigation of a laser-pumped three-level Λ -type system with highest energetic level coupled with a quantum oscillator described by a single quantized leaking mode, has led ones to

the identification of two distinct regimes leading to cooling and lasing effects of the quantum oscillator's degrees of freedom and have described the mechanisms determining them. Additionally, one has specified that as a quantum oscillator can serve a vibrational mode of a nanomechanical resonator containing the three-level emitter or, equivalently, an electromagnetic cavity mode field, unless the upper state of the three-level sample is embedded within the cavity, possesses permanent dipole. Also it was taken into consideration, the frequency of the quantum oscillator is significantly smaller than all other frequencies involved to describe the model [34, 35].

3) One has identified the two-resonance conditions operating the oscillator's quantum dynamics. According to the first resonant condition, the quantum oscillator's frequency is close to double generalized Rabi frequency and in the second resonant condition the qubit frequency is close to generalized Rabi frequency, respectively. For both resonant cases, one has computed the average inversion operators, the mean quanta number of the qubit and second-order correlation function analyzing the lasing and cooling phenomena occurring in the three-level system. One has identified the different mechanisms behind the lasing and cooling in each resonant situation [36].

4) One has proved that the exchange between single- or two-quanta processed followed by quantum interference effects among the induced emitter's dressed states are in charge of flexible lasing or deeper cooling effects, correspondingly. Additionally, if the upper state of the three-level emitter has a permanent dipole then it could couple with a single- cavity electromagnetic field mode of terahertz frequency. Another important result identified from this model is the coherent terahertz photons generation assigned as one of the possible applications resulting from this study. The first complete study on this model is published in [34], while the cooling regime in the three-level system was lately presented in [36].

5) One has investigated the quantum multiphoton dynamics of a two-level system possessing unequal permanent dipoles, placed in a leaking single-mode quantized cavity field and coupled to it. In this setup, we considered the frequencies of the interacting subsystems, namely the cavity and the emitter, are considered to belong to different frequencies range: microwave and optical domain, correspondingly, and therefore the two-level qubit couples to the resonator via its parallel dipole moments. One has demonstrated the possibility to convert photons from optical to microwave frequency domains, via resonantly pumped asymmetrical two-level quantum optical emitter placed in a quantized single-mode resonator. It was proved that cavity's multiphoton characteristics and demonstrated the feasibility for a certain output multiphoton superposition of the generated states. The present result is published in [36]

Considering the conclusions above, one would propose the following recommendations:

1) The particularity of the current model, consists in evaluating the impact of non-zero permanent dipole moment on the resonance fluorescence spectrum of the spontaneous emission of photons during the laser pumping processes of two-level system. Finally, one has observed the elastic photon scattering spectrum consists of three lines at $\{\omega_L, \omega_L \pm \omega\}$ computed for the case when the permanent dipole is non zero. The inelastic photon scattering contains to nine spectral lines at $\omega_L, \{\omega_L \pm \omega\}, \{\omega_L \pm 2\bar{G}_R\}, \{\omega_L - \omega \pm \bar{G}_R\}, \{\omega_L + \omega \pm 2\bar{G}_R\}$. Suppression of a spectral line at the frequency of the strongly driven laser occurs due to interference effects among the induced double dressed-state transitions. One has shown that squeezing occurs for negative values (dark area in Fig.2.6(b)) and broader ranges because of the permanent dipoles. In the absence of permanent dipoles squeezing around detectors frequency ν is not observed. Additionally, the dipole moment expands slightly the range of quantum fluctuations, which makes the considered system specially useful for hyperfine measurements and is valid for integration in certain quantum optical and mechanical devices.

2) In Λ -type three-level system possessing permanent dipole moment and embedded in an optical cavity, the frequency of the quantum oscillator is quite smaller than all other frequencies involved to describe the model; on the other hand, it is of the order of the generalized Rabi frequency identifying the laser-pumped three-level qubit. In accordance to the dressed-state base of the three-level system, one has derived two resonance conditions regulating the oscillator's quantum dynamics, specifically, when the quantum oscillator's frequency is near to the doubled generalized Rabi frequency or to the generalized Rabi frequency, correspondingly. Therefore, one recommends considering these two situations as distinct cases leading to the stationary lasing or cooling regimes for the quantum oscillator's field mode, with different mechanisms behind them.

3) If the double generalized Rabi frequency is close to the oscillator's one, then the model is similar to a two-level system interacting with a quantum field mode where the spontaneous decay pumps both levels. Also, if the oscillator's frequency tends to the value of the generalized Rabi frequency, then the sample is associated with an equidistant three-level system. The latter case includes single- or two-quanta processes occurring simultaneously with quantum interference effects among the involved dressed states leading to more profound cooling regimes and flexible ranges for lasing effects. In this instance the model consists of an electromagnetic cavity mode, which describes the quantum oscillator, then its frequency can be in the terahertz domain and, thus, we prove an effective coherent electromagnetic field source of such photons. Thus one recommend the further extensive study of quantum interference in three-level systems.

4) It is known that lasing or cooling effects are possible within two-level system. However, the

three-level system may possess an advantage as it exhibit improved features for the same parameters involved, which is a benefit when there are only certain accessible parameter ranges. Furthermore, certain realistic novel systems are explored employing the three-level model and recommended for further integration in industrial manufacturing. One recommends the developed model proper to study few coupled quantum dots and alternative systems as asymmetrical real or artificial few-level molecules possessing permanent dipoles.

5) One would suggest the further investigation of the presence of diagonal dipole moments, in a resonance coherently driven two-level qubit, because it makes achievable the coupling to the resonator mode at a completely different frequency than the input one which pumps the two-level quantum emitter, and cavity multiphoton state generation, respectively. Additionally, the proposed approach is suitable for a laser driven two-level quantum dot incorporated in an acoustical phonon cavity. In these circumstances, the manipulation of quantum states namely photons and phonons continues to be one of the main topics of modern science.

The limitation of the presented results is related to the exclusive theoretical aspect of the overall thesis, referring to already existing experimental setups.

In Chapter 2, one has presented the theoretical framework related to the dynamics of a two-level system possessing a permanent non-zero dipole moment interacting with two-laser fields. One has applied several approximations to define and explain each term of the Hamiltonian and assign it to a certain type of interaction. The main purpose was to derive the parameters of interest containing the terms responsible for the impact of permanent dipole moment. The developed approach was consequently extended in chapters 3 and 4, where rotating wave, Born-Markov, the secular approximations were used to derive valid results plotted in corresponding graphs. Chapters 3 and 4 required certain truncation approximations due to the infinite number of quantum state, while computing the photon statistics and second order correlation function. Nevertheless, these assumptions did not affect the overall results but propose solutions to improve the parameters of existing quantum optical models.

The personal contribution of the author to the presented results: The author has directly contributed to the definition of research objectives, tasks and models. She has been advised about the theoretical treatment applied to the quantum dynamics of the studied systems. She has contributed to the writing of publications drafts related to the results presented in this thesis and at various conferences.

References

- [1] GLAUBER, R. J. Photon Correlations. In: *Phys. Rev. Lett.*, 1963, vol. 10, pp. 84-86.
- [2] SPRING, J. B., METCALF, B. J., HUMPHREYS, P. C., KOLTHAMMER, W. S. Boson sampling on a photonic chip. In: *Science*, 2013, vol. 339, pp. 798-801.
- [3] LOUDON, R., KNIGHT, P. L. Squeezed light. In: *J. Mod. Opt.*, 1987, vol. 34, pp. 709-759.
- [4] ASASI, J. Enhanced sensitivity of LIGO gravitational wave detector by using squeezed state of light. In: *Nature Photonics*, 2013, vol. 7, pp. 613-619.
- [5] YUEN, H., SHAPIRO, J. H. Optical communications with two-photon coherent states-part I: Quantum state propagation and quantum noise reduction. In: *IEEE Transactions on Information Theory*, 1978, vol. 24, pp. 657-668.
- [6] BURNHAM, D. C., WEINBERG, D. L. Observation of simultaneity in parametric production of optical photon pairs. In: *Phys. Rev. Lett.*, 1970, vol. 25, pp. 84-87.
- [7] AGARWAL, G.S. *Quantum Optics*, Cambridge University, 2014.
- [8] LOUDON, R. *The quantum theory of light*, Oxford University Press, 1983.
- [9] BENNETT, C. H., BRASSARD, G. "Quantum Cryptography" Public key distribution and coin tossing. In: *Proc. IEEE International Conference on Computers, Systems and Processing*, 1984, vol. 175, pp. 7-11.
- [10] PLENIO, M. B., KNIGHT, P. L. The quantum-jump approach to dissipative dynamics in quantum optics. In: *Rev. Mod. Phys.*, 1998, vol. 70, pp. 101-144.
- [11] SARGEANT, M., SCULLY, M. O., LAMB, W. E. *Laser Physics*, Addison-Wisley Pub. Co., 1974.
- [12] LAKOWICZ, J. R., RAY, K., CHOWDHURY, M., SZMANCINSKI, H. Plasmon-controlled fluorescence: a new paradigm in fluorescence spectroscopy In: *The Analyst*, 2008, vol. 133, pp. 1308-1346.
- [13] ACUNA, G. P., MOELLER, F. M., HOLZMEISTER, P., BEATER, S.. Fluorescence enhancement at docking Sites of DNA-directed self-assembled nanoantennas. In: *Sciences*, 2012, vol. 338, pp. 506-510.
- [14] LODHAL, P., MAHMOODIAN, S., STOBBE, S. Interfacing single photons and single quantum dots with photonic nanostructures. In: *Rev. Mod. Phys.*, 2015, vol. 87, pp. 347-400.
- [15] HOANG, T. B., AKSELROD, G. M., MIKKELSEN, M. H. Ultrafast room-temperature single photon emission from quantum dots coupled to plasmonic nanocavities. In: *Nano. Lett.*, 2016, vol. 16, pp. 270-275.
- [16] OKAMOTO, K., NIKI, I., SHVARTSER, A., NARUKAWA, Y., MUKAI, T. Surface-plasmon-enhanced light emitters based on InGaN quantum wells. In: *Nat. Mater.*, 2004, vol. 3, pp. 601-605.
- [17] KREINBERG, S., GRBEŠIĆ, T., STRAUß, M. Quantum-optical spectroscopy of a two-level system using an electrically driven micropillar laser as a resonant excitation source. In: *Light Sci. Appl.*, 2018, vol. 41, pp. 1-9.

- [18] COHEN-TANNOUDJI, C., REYNAUD, S. Atoms in strong light-fields: photon antibunching in single atom fluorescence In: *Phil. Trans. R. Soc. Lond. A*, 1979, vol. 223, pp. 223-237.
- [19] FRASCA, M. A modern review of two-level approximation. In: *Annals of Physics*, 2003, vol. 306, pp. 193-208.
- [20] HE, Y.-L. Multiphoton Rabi oscillations between highly excited Stark states of potassium. In: *Phys. Rev. A.*, 2011, vol. 84, pp. 053414/1-7.
- [21] TAMINIAU, T. H., KARAVELI, S., VAN HULST, N. F., ZIA, R. Quantifying the magnetic nature of light emission. In: *Nat. Commun.*, 2012, vol. 3, pp. 9791/1-6.
- [22] AIGOUY, L., CAZE, A., GREDIN, P., MORTIER, M., CARMINATI, R. Mapping and quantifying electric and magnetic dipole luminescence at the nanoscale. In: *Phys. Rev. Lett.*, 2014, vol. 113, pp. 076110/1-5.
- [23] CALDERON, O. G., GUTIERREZ-CASTREJON, R., GUERRA, J. M. High harmonic generation induced by permanent dipole moment. In: *IEEE J. Quantum Electron.*, 1999, vol. 35, pp. 47-52.
- [24] KONDO, A. E., BLOKKER, V. M., MEATH, W. J. Permanent dipole moments and two-color multiphoton resonances in the two-level molecule: the rotating wave approximations versus exact results. In: *J. Chem. Phys.*, 1992, vol. 96, pp. 2544-2555.
- [25] BESSEGA, M. C., PAZ, J. L., HERNANDEZ, A. J., CARDENS, A. E. Study of additional resonances in frequency space and permanent dipole effects on non-degenerate four-wave mixing signals. In: *Phys. Lett. A.*, 1995, vol. 206, pp. 305-310.
- [26] HOERNER, C., LAVINE, J. P., VILLAYES, A. A. Theoretical description of two-photon phase conjugation in polar molecules. In: *Phys. Rev. A*, 1993, vol. 48, pp. 1564-1572.
- [27] SAVENKO, I. G., KIBIS, O. V., SHLEYKH, I. A. Asymmetric quantum dot in a microcavity as a nonlinear optical element. In: *Phys. Rev. A*, 2012, vol. 85, pp. 053815/1-6.
- [28] AVETISSIAN, H. K., MKRTCHIAN, G. F., POGOSYAN, M. G. Creation of coherent superposition states in hydrogenlike ions via multiphoton resonant photonic field. In: *Phys. Rev. A.*, 2006, vol. 73, pp. 063413/1-7.
- [29] AVETISSIAN, H. K., MKRTCHIAN, G. F. Two-level system with broken inversion symmetry coupled to a quantum harmonic oscillator. In: *Phys. Rev. A.*, 2013, vol. 88, pp. 043811/1-6.
- [30] MACOVEI, M., MISHRA, M., KEITEL, C.H. Population inversion in two-level systems possessing permanent dipoles. In: *Phys. Rev. A.*, 2015, vol. 92, pp. 013846/1-5.
- [31] BAVLI, R., BAND, Y. B. Nonlinear absorption and dispersion in a two-level system with permanent dipole moments. In: *Phys. Rev. A.*, 1991, vol. 43, pp. 5039-5043.
- [32] ANTON, M. A., MAEDE - RAZAVI, S., CARRENO, F., THANOPOULOS, I., PASPALAKIS, E. Optical and microwave control of resonance fluorescence and squeezing spectra in a polar molecule. In: *Phys. Rev. A.*, 2017, vol. 96, pp. 063812/1-16.
- [33] BROWN, A., MEATH, W. J. Two-color pulsed-laser phase control in dipolar molecules: Rotating-wave approximation versus exact results. In: *Phys. Rev. A.*, 2002, vol. 65, pp. 063401/1-12.
- [34] MÎRZAC, A., MACOVEI, M. Dynamics of a quantum oscillator coupled with a three-level Λ -type emitter. In: *J. Opt. Soc. Am. B*, 2019, vol. 36, pp. 2473-2480.

- [35] MÎRZAC, A.. Dinamica răcirii cuantice a unui oscilator cuplat cu un atom artificial. In: *Revista de Știință, Inovare, Cultură și Artă "Akademos"*, 2019, vol. 4(55), pp. 16-19.
- [36] MIRZAC, A. Steady-state behaviors of a quantum oscillator coupled with a three-level emitter. In: *Tiginyanu I., Sontea V., Railean S. (eds) 4th International Conference on Nanotechnologies and Biomedical Engineering. ICNBME 2019. IFMBE Proceedings, Springer, Cham., 2020, vol 77, pp. 677-680.*
- [37] KOCINAC, S., IKONIC, Z., MILANOVIC, V. Second harmonic generation at the quantum - interference induced transparency in semiconductor quantum wells: the influence of permanent dipole moments. In: *IEEE Journal of Quantum Electronics*, 2001, vol. 37, pp. 873-876.
- [38] LEE, M., WANKE, M. Searching for a solid-state terahertz technology. In: *Science*, 2007, vol. 64, pp. 64-65.
- [39] ALLEN, L., EBERLY J.H. *Optical Resonance and two-Level Atoms*, Wiley, 1975.
- [40] YARIV, A. *Quantum electronics*, 3rd edition, Wiley, 1989
- [41] MIRI, M., ZAMANI, F., ALIPOOR, H. Two tunneling-coupled two-level systems with broken inversion symmetry: tuning the terahertz emission. In: *JOSA B*, 2016, vol. 33, pp. 1873-1880.
- [42] RABI, I.I. Space quantization in gyrating magnetic field. In: *Phys. Rev. A*, 1937, vol. 51, pp. 652-654.
- [43] CLARKE, J., WILHELM, F. K. Superconducting quantum bits. In: *Nature*, 2008, vol. 453, pp. 1031-1042.
- [44] DEVORET, M. H., MARTINIS, J. M. Implementing qubits with superconducting integrated circuits. In: *Quant. Inform. Process.*, 2004, vol. 3, pp. 163-203.
- [45] DEVORET, M. H., SCHOELKOPF, R. J. Superconducting circuits for quantum information: an outlook. In: *Science*, 2013, vol. 339, pp. 1169-1174.
- [46] NAKAMURA, Y., PASHKIN, Yu. A., TSAI, J.-S. Coherent control of macroscopic quantum states in single-Cooper-pair box. In: *Nature*, 1999, vol. 398, pp. 786-788.
- [47] DUTTA, P., HORN, P.M.. Low-Frequency Fluctuations in solids-1-F Noise. In: *Rev. Mod. Phys*, 1981, vol.53, pp. 497-516.
- [48] MÜLLER, C., COLE, J. H., LISENFELD, J. Towards understanding two-level-systems in amorphous solids: insights from quantum circuits. In: *Reports on Progress in Physics*, 2019, vol. 82, pp. 124501-124535.
- [49] PALADINO, E., GALPERIN, Y. M., FALCI, G., ALTSHULER, B. L. 1/f noise: Implications for solid-state quantum information. In: *Rev. Mod. Phys.*, 2014, vol. 86, pp. 361-418.
- [50] LI, L.-Sh., ALIVISATOS, P. Origin and scalling of the permanent dipole moment in CdSe nanorods. In: *Phys. Rev. Lett*, 2003, vol. 90, pp. 097402-097405.
- [51] WIERSIG, J., GIES, C., JAHNKE, F. et al. Direct observation of correlations between individual photon emission events of a microcavity laser. In: *Nature*, 2009, vol. 460, pp. 245-249.
- [52] LINDNER, N.H., RUDOLPH, T. Proposal for pulsed on-demand sources of photonic cluster state strings. In: *Phys. Rev. Let.*, 2009, vol. 103, pp. 113602/1-4.

- [53] ANTON, M. A., GONZALO, I. Two-photon optical bistability in polar molecules: vibrational coupling effects. In: *IEEE J. Quantum. Electron.*, 1995, vol. 31, pp. 1088-1097.
- [54] FRY, P. W., ITSKEVICH, I. E.; MOWBRAY D.J., SKOLNICK, J.J. et al. Inverted electron-Hole alignment in InAs-GaAs self-assembled quantum dots. In: *Phys. Rev. Lett.*, 2000, vol. 84, pp. 733-736.
- [55] KOTHARI, N. C., KOBAYASHI, T. Single beam two-photon optical bistability in a submicron size Fabry-Perot cavity. In: *IEEE J. Quantum Electron.*, 1984, vol. 20, pp. 418-423.
- [56] PATANE, A., LEVIN, A., POLIMENI, A., SCHINDLER, F. et al. Piezoelectric effects in In_{0.5}Ga_{0.5}As self-assembled quantum dots grown on (311)B GaAs substrates. In: *Appl. Phys. Lett.*, 2000, vol. 77, pp. 2979-2981.
- [57] WARBURTON, R. J., SCHULHAUSER, D., HAFT, D., SCHAFLEIN, C., KARRAI, K., GARCIA, J. M., SCHOENFELD, W., PETROFF, P.M. Giant permanent dipole moments of excitons in semiconductor nanostructures. In: *Phys. Rev. B.*, 2002, vol. 65, pp. 113303/1-4.
- [58] SCHULHAUSER, C., HAFT, D., SCHÄFLEIN, C., KARRAI, K., WARBURTON, R. J., GARCIA, J. M., SCHÖNFELD, W., PETROFF, P.M. Giant permanent dipole moments of excitons in semiconductor nanostructures. In: *Physica E*, 2002, vol. 13, pp. 161-164.
- [59] OSTAPENKO, I. A., HONIG, G., KINDEL C., RODT, A., et al. Large internal dipole moment in InGaN/GaN quantum dots. In: *Appl. Phys. Lett.*, 2010, vol. 97, pp. 063103/1-5.
- [60] SUGISAKI, M., REN, H.-W., NAIR, S. S., NISHI, K., MASUMOTO, Y. External-field effects on the optical spectra of self-assembled InP quantum dots. In: *Phys. Rev. B.*, 2002, vol. 66, pp. 235309/1-10.
- [61] KOVARSKY, V. A., PHILIPP, B.S., KOVARSKY, E. V. The generation of the short-wave UV light in cells under the action of ultrashort of intense visible radiation. In: *Phys. Lett. A.*, 1997, vol. 226, pp. 321-322.
- [62] DICK, B., HOHLNEICHER, G. Importance of initial and final as intermediate states in two-photon spectroscopy of polar molecules. In: *J. Chem. Phys.* vol. 76, pp. 5755-5760.
- [63] KOCINAC, S., IKONIC, Z., MILANOVIC, V. The influence of permanent dipole moments on second harmonic generation in asymmetric semiconductor quantum wells. In: *Opt. Commun.*, 1997, vol. 140, pp. 89-92.
- [64] GAVRILENKO V. P., OKS, E. A significant enhancement of high-order harmonic generation by using a dipole gas. In: *J. Phys. B: At. Mol. Opt. Phys.*, 2000, vol. 33, pp. 1629-1643.
- [65] LAGMAGO KAMTA, G., BANDARUK, A.D.. Phase dependence of enhanced ionization in asymmetric molecules. In: *Phys. Rev. Lett.*, 2005, vol. 94, pp. 203003-203006.
- [66] YANG, W., GONG, Sh., XU, Zh. Enhancement of ultrafast four-wave mixing in a polar molecule medium. In: *Optics Express*, vol. 14, pp. 7216-7222.
- [67] CHEN, Hs.-T., LI, E. T., NITZAN, A., SUBOTNIK, J. Predictive semiclassical model for coherent and incoherent emission in the strong field regime: the Mollow triplet revised. In: *J. Phys. Chem. Lett.*, 2019, vol. 10, pp. 1331-1336.
- [68] KRYUCHKYAN, G. Yu., SHAHNAZARYAN, V., KIBIS, O. V., SHELYKH, I. A. Resonance fluorescence from an asymmetric quantum dot dressed by a bichromatic electromagnetic field. In: *Phys. Rev. A.*, 2017, vol. 95, pp. 013834/1-7.

- [69] CHESTNOV, I. Yu., SHAHNAZARYAN, V. A., ALDOJANTS, A. P., SHELYKH, I. A. Terahertz lasing in ensemble of asymmetric quantum dots. In: *ACS Photonics*, 2017, vol. 4, pp. 2726-2737.
- [70] CARRENO LOPEZ, J. C., VALLE, E., LAUSSY, F. Photon correlations from the Mollow triplet. In: *Laser Photonics*, vol. 11, pp. 1700090/1-10.
- [71] MOLLOW, B. R. Power spectrum of light scattered by two-level systems. In: *Phys. Rev.*, 1969, vol. 188, pp. 1969-1975.
- [72] APANASEVICH, P. A., KILIN, S.Y. Photon bunching and antibunching in resonance fluorescence. In: *J. Phys. B.: At. Mol.*, 1979, vol. 12, pp. L83-L86.
- [73] SCHRAMA, C. A., NIENHUIS G., DIJKERMAN, H. A., STEIJSIGER, C., HEIDEMAN, M. Intensity correlations between the components of the resonance fluorescence triplet. In: *Phys. Rev. A*, 1992, vol. 45, pp. 8045-8055.
- [74] ULHAQ, A., WEILER, S., ULRICH, S. M., ROSSBACH, R., JETTER, M., MICHLER, P. Cascaded single-photon emission from the Mollow triplet sidebands of a quantum dot. In: *Nat. Photon*, 2012, vol. 6, pp. 238-242.
- [75] FLORESCU, M., SAJEEV, J. Resonance fluorescence in photonic band gap waveguide architectures: Engineering the vacuum for all-optical switching. In: *Phys. Rev. A*, 2004, vol. 69, pp. 053810/1-21.
- [76] ZHOU, P., SWAIN, S., FICEK, Z. Resonance fluorescence spectrum of a two - level atom driven by a bichromatic field in a squeezed vacuum. In: *Phys. Rev. A*, 1997, vol. 55, pp. 2340-2346.
- [77] WALLS, D. F., ZOLLER, P. Reduced quantum fluctuations in resonance fluorescence. In: *Phys. Rev. Lett.*, 1981, vol. 47, pp. 709-711.
- [78] GARDINER, C. W., ZOLLER, P. *Quantum Noise*, Springer, 2004.
- [79] WALLS, D.F., MILBURN, G. J. *Quantum Optics*, Springer, 2008.
- [80] TOYLI, D. M., EDDINS, A. W., BOUTIN, S., PURI, S., HOVER, D., BOLKHOVSKY, W. D., BLAIS, A., SIDDIQI, I. Resonance fluorescence from an artificial atom in squeezed vacuum. In: *Phys. Rev. X*, 2016, vol.6, pp. 031004/1-5.
- [81] MIRZAC, A., MIHAESCU, T., MACOVEI, M., ISAR, A. Interferometric power of Gaussian systems in a squeezed thermal bath. In: *Rom. J. Phys.*, 2020, vol. 65, pp. 1-12.
- [82] ANDERSEN, U. L., GEHRING, T., MARQUARDT, C., LEUCHS, G. 30 years of squeezed light generation. In: *Phys. Scr.*, 2016, vol.91, pp. 053001-053011.
- [83] MAREK, P., JEONG, H., KIM, M. S. Generating "squeezed" superpositions of coherent states using photon addition and subtraction. In: *Phys. Rev. A*, 2008, vol. 78, pp. 063811-063818.
- [84] ZAHEER, K., ZUBAIRY, M. S. Squeezed states of the radiation field, In: *Adv. At. Mol. Phys.*, 1990, vol. 142, pp. 142-235.
- [85] MILBURN, G. J., WALLS, D. F. Production of squeezed states in a degenerate parametric amplifier. In: *Opt. Commun.*, 1981, vol. 39, pp. 401-404.
- [86] MILBURN, G. J., WALLS, D. F., LEVENSON, M. D. Quantum phase fluctuations and squeezing in degenerate four-wave mixing. In: *J. Opt. Soc. Am. B*, 1984, vol. 1, pp. 390-394.

- [87] LUGIATO, L. A. Atomic correlations in driven optical systems. In: *Phys. Rev. A.*, 1986, vol. 33, pp. 4079-4084.
- [88] DALTON, B. J., FICEK, Z., KNIGHT, P. L. Optimum field squeezing from atomic sources: three-level atoms. In: *Phys. Rev. A.*, 1994, vol. 50, pp. 2646-2666.
- [89] MEYSTRE, P., ZUBAIRY, M. S. Squeezed states in the Jaynes-Cummings model. In: *Phys. Lett.*, 1982, vol. 89 A, pp. 390-392.
- [90] WODKIEWICZ, K., KNIGHT, P. L., BUCKLE, S. J., BARNETT, S. M. Squeezing and superposition states. In: *Phys. Rev. A*, 1987, vol. 35, pp. 2567-2577.
- [91] BARNETT, S. M., DUPERTIUS, M. A. Multiatom squeezed states: a new class of collective atomic states. In: *J. Opt. Am. B*, 1987, vol. 4, pp. 505-511.
- [92] HEIDMAN, A., RAIMOND, J. M., REYNAUD, S. Squeezing in a Rydberg Atom Maser. In: *Phys. Rev. Lett.*, 1985, vol. 54, pp. 326-328.
- [93] BUTLER, M., DRUMOND, P. D. Squeezed states in a cooperative Dicke system. In: *Opt. Acta*, 1986, vol. 33, pp. 1-5.
- [94] SCHULTE, C. H., HANSOM, J., JONES, A. E., MATTHIESEN, Cl., LE GALL, Cl., ATATURE, M. Quadrature squeezed photons from a two-level system. In: *Nature*, 2015, vol. 525, pp. 222-225.
- [95] ILES-SMITH, J., NAZIR, A., MCCUTCHEON, D. P. S. Vibrational enhancement of quadrature squeezing and phase sensitivity in resonance fluorescence. In: *Nature Communications*, 2019, vol. 10, pp. 3034/1-7.
- [96] HÄNSCH, T., SCHAWLOW, A. Cooling of gases by laser radiation. In: *Opt. Commun.*, 1975, vol. 13, pp. 68-69.
- [97] WINELAND, D., DRULLINGER, R. E., WALLS, F. L. Radiation-pressure cooling of bound resonant absorbers. In: *Phys. Rev. Lett.*, 1978, vol. 40, pp. 1639-1642.
- [98] ASPECT, A., ARIMONDO, E., KAISER, R., VANSTEENKISTE, N., COHEN-TANNOUDJI, C. Laser cooling below the one-photon recoil energy by velocity-selective coherent population trapping. In: *Phys. Rev. Lett.*, 1988, vol. 61, pp. 826-826.
- [99] DUM, R., MARTE, P., PELLIZZARI, T., ZOLLER, P. Laser cooling to a single quantum state in a trap. In: *Phys. Rev. Lett.*, 1994, vol. 73, pp. 2829-2832.
- [100] TAR BUTT, M.R. Laser cooling of molecules. In: *Contemporary Physics*, 2018, vol. 59, pp. 356-376.
- [101] OJANEN, T., BORKJE, K. Ground-state cooling of mechanical motion in the unresolved sideband regime by use of optomechanically induced transparency. In: *Phys. Rev. A.*, 2014, vol. 90, pp. 013824/1-14.
- [102] SCHLAFERMEIER, Cl., KERDONCUFF, H., HOFF, U. B. Quantum enhanced feedback cooling of a mechanical oscillator using nonclassical light. In: *Nature*, 2016, vol. 7, pp. 13628/1-6.
- [103] LAU, H.K., PLENIO, M.B. Laser cooling of a high-temperature oscillator by a three-level system. In: *Phys. Rev. B.*, 2016, vol. 94, pp. 054305/1-10
- [104] LI, G.-X., ZHU, J.-P. Ground-state cooling of a mechanical resonator coupled to two coupled quantum dots. In: *J. Phys. B. At. Mol. Opt. Phys.*, 2011, vol. 44, pp. 1995502/1-10.

- [105] XIA, K., EVERS, J. Ground state cooling of a nanomechanical resonator in the nonresolved regime via quantum interference. In: *Phys. Rev. Lett.*, 2009, vol. 103, pp. 227203/1-4.
- [106] WINELAND, D. J., MONROE, C., ITANO, W. M., LEIBFRIED, D., KING, B.E., MEEKHOF, D.M. Experimental issues in coherent quantum-state manipulation of trapped atomic ions. In: *J. Res. Natl. Inst. Stand. Technol.*, 1998, vol. 103, pp. 259-328.
- [107] MORIGI, G., ESCHNER, J., KEITEL, C. H. Ground state laser cooling using electromagnetically induced transparency. In: *Phys. Re. Lett.*, 2000, vol. 85, pp. 4458-4461.
- [108] MORIGI, G., ARIMONDO, E. Two-photon and electromagnetically-induced-transparency-assisted Doppler cooling in a three-level cascade system. In: *Phys. Rev. A.*, 2007, vol. 75, pp. 051404(R)/1-4.
- [109] EVERS, J., KEITEL, C.H. Double-EIT ground-state laser cooling without blue-sideband beating. In: *Europhys. Lett.*, 2004, vol. 68, pp. 370-376.
- [110] HOPKINS, A., JACOBS, K., HABIB, S., SCHWAB, K. Feedback cooling of a nanomechanical resonator. In: *Phys. Rev. B.*, 2003, vol. 68, pp. 235328/1-10.
- [111] WILSON-RAE, I., NOOSHI, N., ZWERGER, W., KIPPENBERG, T. J. Theory of ground state cooling of a mechanical oscillator using dynamical backaction. In: *Phys. Rev. A.*, 2007, vol. 99, pp. 093901/1-4.
- [112] MANCHES, S., PLENIO, M. B., REZNIK, B., STEANE, A. M., RETZKER, A. Superfast laser cooling. In: *Phys. Rev. Lett.*, 2010, vol. 104, pp. 183001/1-4.
- [113] MARTIN, I., SHNIRMAN, A., TIAN, L., ZOLLER, P. Ground-state cooling of mechanical resonators. In: *Phys. Rev. B.*, 2004, vol. 69, pp. 125339/1-12.
- [114] ROGHANI, M. Trapped-atom cooling beyond the Lamb-Dicke limit using electromagnetically induced transparency. In: *Phys. Rev. A.*, 2008, vol. 77, pp. 043418/1-8.
- [115] FLEISCHHAUER, M., IMMAMOGLU, A., MATAGANOS, J.P. Electromagnetically induced transparency: Optics in coherent media. In: *Rev. Mod. Phys.*, 2005, vol. 77, pp. 633-673
- [116] MARQUARDT, F., CHEN, J., CLERK, A. A., GIRVIN, S. M. Quantum theory of the cavity-assisted sideband cooling of mechanical motion. In: *Phys. Rev. Lett.*, 2007, vol. 99, pp. 093902/1-4.
- [117] VANNER, D. J., PIKOVSKI, I., COLE, G.D., KIM, M. S., BRUKENER, C., HAMMERER, K., MILBURN, G. J., ASPELMEYER, M. In: *Proc. Natl. Acad. Sci. USA*, 2011, vol. 108, pp. 16182-16187.
- [118] LIU, Y.-C., XIAO, Y.-F., LUAN, X., WONG, C. W. Dynamic dissipative cooling of a mechanical resonator in strong coupling optomechanics. In: *Phys. Rev. Lett.*, 2013, vol. 110, pp. 153606/1-5.
- [119] ELSTE, F., GIRVIN, S. M., CLERK, A. A. Quantum noise interference and backaction cooling in cavity nanomechanics. In: *Phys. Rev. Lett.*, 2009, vol. 102, pp. 207209/1-6.
- [120] HUANG, S., AGARWAL, G. S. Enhancement of cavity cooling of a micromechanical mirror using parametric interactions. In: *Phys. Rev. A.*, 2009, vol. 79, pp. 013821/1-6.
- [121] CLARK, J. B, LECOCQ, Fl., SIMMONDS, R. W., AUMENTADO, J., TEUFEL, J. D. Sideband cooling beyond the quantum backaction limit with squeezed light. In: *Nature*, vol. 541, 2017, pp. 191-195.

- [122] RETZKER, A., PLENIO, M. B. Fast cooling of trapped ions using the dynamical Stark shift. In: *New J. Phys.*, 2007, vol.9, pp. 1367-2630.
- [123] BORKJE, K., OJANEN, T. Ground-state cooling of mechanical motion in the unresolved sideband regime by use of optomechanically induced transparency. In: *Phys. Rev. A*, 2014, vol. 90, pp. 013824/1-14.
- [124] LEE, Y. - Sh. *Principles of THz Science and Technology*, Springer, Oregon, USA, 2009, pp.1-7.
- [125] O'HARA, J., EKIN, S., CHOI, W., SONG, I. A perspective on terahertz next-generation wireless communications. In: *Technologies*, 2019, vol. 7, pp. 1-18.
- [126] SAFIAN, R., GHAZI, G., MOHAMMADIAN, N. Review of photomixing continuous-wave terahertz systems and current application trends in terahertz domain. In: *Opt. Eng.*, 2019, vol. 58, pp. 110901/1-28.
- [127] MANGENEY, J., MERIGAULT, A., ZEROUNIAN, N., CROZAT, P. Continuous wave terahertz generation up to 2 THz by photomixing on ion-irradiated $In_{0.53}Ga_{0.47}As$ at 1.55 μm wavelengths. In: *Appl.Phys.Lett.*, vol.91, pp.241102/1-3.
- [128] KUBAREV, V.V., SOZNOV, G.I, SCHEGLOV, M.A et al. The radiation reamline of Novosibirsk free-electron laser facility operating in terahertz, far-infrared, and mid-infrared ranges. In: *IEEE Transactions on Terahertz Science and Technology*, vol. 10, pp. 634-646.
- [129] LAMPIN, J.-F., PAGIES, A., SANTARELLI, G., HESLER, J., HANSEL., W., HOLZWARTH, R., BARBIERI, S. Quantum cascade laser-pumped terahertz molecular lasers: frequency noise and phase-locking using a 1560 nm frequency comb. In: *Opt. Express*, 2020, vol.28, pp.2091-2096.
- [130] KAMPFRATH, T., NOETZOLD, J., WOLF, M. Sampling of broadband terahertz pulses with thick electro-optic crystals. In: *Appl. Phys. Lett.*, 2007, vol. 90, pp.23111/1-3.
- [131] SITNIKOV, D.S., ROMASHEVSKY, S.A., OVCHINNIKOV, A. V., CHEFONOV, O. V., SAVELEV, A.B., AGRANAT, M.B..Estimation of THz field strength by an electro-optic sampling technique using arbitrary long gating pulses. In: *Laser Physics Letters*. 2019, vol.16, pp.115302/1-11.
- [132] PAWAR, A.Y., SONAWANE, D.D., ERANDE, K.B., DERLE, D. V. Terahertz technology and its applications. In: *Drug Invention Today*, 2013, vol.5, pp. 157-163.
- [133] HAFEZ, H.A., CHAI, X., IBRAHIM, A., FERACHOU, D., ROPAGNOL, X., OZAKI, T. Intense terahertz radiation and their applications. In: *J. Opt.*, 2016, vol.18., pp. 093004/1-46.
- [134] LIBERATO DE, S., CIUTI, Cr., PHILIPS, Ch. Terahertz lasing from intersubband polariton-polariton scattering in asymmetric quantum wells. In: *Phys. Rev. B*, 2013, vol. 87, pp. 241304/1-5.
- [135] FULOP, J. A., TZORTZAKIS, St., KAMPFRATH, T. Laser-driven strong-field terahertz sources. In: *Advanced Optical Materials*, 2020, vol. 8, pp. 1900681/1-25.
- [136] SAITO, K., TANABE, T., OYAMA, Y. Cascaded terahertz-wave generation efficiency in excess of the Manley–Rowe limit using a cavity phase-matched optical parametric oscillator. In: *Journal of Optical Society of America B*, 2015, vol. 32, pp. 617-621.
- [137] LI, Z., WANG, S., WANG, M. Highly efficient terahertz generation from periodically poled lithium niobate. In: *J. Opt.*, 2019, vol. 48. pp. 166-171.

- [138] SAZONOV, S.V., USTINOV, N.V. Self-induced transparency of few-cycle terahertz pulses. In: *JETP Letters*, 2020, vol. 112, pp. 24-30.
- [139] GAIZAUSKAS, E., VAICAITIS, V., FEDOTOVA, O., KHASANOV, O. Towards broadband terahertz generation due to coherent phonon-polariton excitations in centrosymmetric media. In: *Optical Materials Express*, 2015, vol. 5, pp. 623-628.
- [140] AVETISSIAN, H. K., AVCHYAN, B. R., MKRTCHIAN, G. F. Tunable high-power terahertz generation in three-level atomic and molecular systems. In: *Phys. Rev. A*, 2010, vol. 82, pp. 063412/1-5.
- [141] ULLAH, Z., WITJAKSONO, G., NAWI, I., TANSU, N., KHATTAK, M. I., JUNAID, M. A review of tunable graphene nanoantennas for terahertz optoelectronic and plasmonic applications. In: *Sensors*, 2020, vol. 20, pp. 1401/1-65.
- [142] TAKANO, K., ASAI, M., KATO, K., KOMIYAMA, H., YAMAGUCHI, A., IYODA, T., TADOKORO, Y., NAKAJIMA, M., BAKUNOV, M.I. Terahertz emission from gold nanorods irradiated by ultrashort laser pulses of different wavelengths. In: *Sc. Rep.*, 2019, vol. 9, pp. 3280/1-7.
- [143] BUTTE, R., GRANDJEAN, N. III-nitride photonic. In: *Nanophotonics*, 2020, vol. 9, pp. 569-598.
- [144] SUN, G., CHEN, R., DING, Y.J., NGUYEN, H. P. T., MI, Z. InGaN/GaN dot-in-a-wire: ultimate terahertz nanostructure. In: *Laser and Photonics Reviews*, 2015, vol. 9, pp. 105-113.
- [145] ZAMANI, F., MIRI, M. Terahertz emission from an array of tunneling-coupled asymmetric two-level systems. In: *Optics Communications*, 2018, vol. 423, pp. 207-214.
- [146] OSTER, F., KEITEL, C. H., MACOVEI, M. Generation of correlated photon pairs in different frequency ranges. In: *Phys. Rev. A*, 2012, vol. 85, pp. 063814/1-5.
- [147] DYKSIK, M., MOTYKA, M., RUDNO-RUDZINSKI, W., SEK, G., MISIEWICZ, J., PUCICKI, D., KOSIEL, K., SANKOWSKA, J., KUBACZKA-TRACZYK, J., BUGASKI, M. Optical properties of active regions in terahertz quantum cascade lasers. In: *Journal of Infrared, Millimeter, and Terahertz Waves*, 2016, vol. 37, pp. 710-719.
- [148] KUNDU, I., BACON, D.R., DEAN, P., LIANHE, L., LINFIELD, E.H., GILES DAVIES, A., FREEMAN, J.R. Programmable, transform-limited pulses from a terahertz quantum cascade laser. In: *ACS Photonics*, 2020, vol. 9, pp. 2423-2428.
- [149] NAKANISHI, A., HAYASHI, S., SATOZONO, H., FUJITA, K. Temperature-insensitive imaging properties of a broadband terahertz nonlinear quantum cascade laser. In: *Appl. Sci.*, 2020, vol. 10, pp. 5926/1-17.
- [150] BAI, Zh., HANG, Ch., HAUNG, G. Subluminal and superluminal terahertz radiation in metamaterials with electromagnetically induced transparency. In: *Optics Express*, 2013, vol. 21, pp. 19675-19680.
- [151] YOSHIDA, K., DU, S., ZHANG, I., HIRAKAWA, K. Terahertz dynamics of electron-vibron coupling in single molecules with tunable electrostatic potential. In: *Nat. Photonics*, 2018, vol. 12, pp. 608-612.
- [152] KIBIS, O.V., SLEPYAN, G. Ya., MAKSIMENKO, S. A., HOFFMAN, A. Matter coupling to strong electromagnetic fields in two-level quantum systems with broken inversion symmetry. In: *Phys. Rev. Lett.*, vol. 110, 2009, pp. 023601/1-4.

- [153] KNILL, E., LAFLAMME, R., MILBURN, G. J. A scheme for efficient quantum computation with linear optics. In: *Nature*, 2001, vol. 409, pp. 56-52.
- [154] MATTLE, K., WEINFURTER, H., KWIAT, P. G. Dense coding in experimental communication. In: *Phys. Rev. Lett.*, vol. 76, 1996, pp. 4656-4659.
- [155] KIRA, M., KOCH, St. W. *Semiconductor Quantum Optics*. Cambridge University Press, 2012. /
- [156] JAYNES, E. T., CUMMINGS, F. W. Comparison of quantum and semiclassical radiation theories with application to the beam maser. In: *Proc. IEEE*, 1963, vol. 51(1), pp. 89-109.
- [157] VILLAS-BOAS, C. J., ROSATTO D. Z. Multiphoton Jaynes-Cummings Model: Arbitrary Rotations in Fock space and quantum filters. In: *Phys. Rev. Lett.*, 2019, vol. 122, pp. 123604/1-7.
- [158] ZHAO, T., YAN, Y., YANG, G.-Q., HUANG, G.-M., ZHU, Y., LI, G.X. Multiphoton non-classical state generated by hyperradiance originating from quasi-subradiant state. In: *Phys. Rev. A.*, 2019, vol. 99, pp. 043814/1-11.
- [159] LIN, J. Z., HOU, K., ZHU, C. J., YANG, Y. P. Multiphoton and improved blockade in a cavity-QED system with two cascade three-level atoms. In: *Phys. Rev. A.*, 2019, vol. 99, pp. 053850/1-8.
- [160] BARANOV, D., PETROV, M., KRASNOK, A. De coupling light and matter: permanent dipole moment induced collapse of Rabi oscillations. In: *arXiv: 1611.06897*, 2016.
- [161] AVETISSIAN, H. K., AVCHYAN, B. R., MKRTCHIAN, G. F. Efficient generation of moderately high harmonics by multiphoton resonant excitation of atoms. In: *Phys. Rev. A*, 2008, vol. 77, pp. 023409/1-7.
- [162] AVETISSIAN, H. K., AVETISSIAN, A. K., MKRTCHIAN, G. F. Multiphoton dynamics of qutrits in the ultrastrong coupling regime with a quantized photonic field. In: *J. Exp. Theor. Phys.*, 2015, vol. 121, pp. 925-933.
- [163] QUAH, H., CHEN, W., SCHREYER, M. Multiphoton harvesting metal-organic frameworks. In: *Nat. Commun.*, 2015, vol. 6, pp.7954/1-7.
- [164] MEATH, W.J., JAGATAP, B.N. On the effects of permanent molecular dipole moments in two-photon molecular excitations: an analytic generalized rotating wave approximation treatment including both the direct permanent dipole and the virtual state excitation mechanisms. In: *J. Phys. B: At. Mol. Opt. Phys.*, 2011, vol. 44, pp.205401/1-13.
- [165] MEATH, W. J. On the optimization, and the intensity dependence, of the excitation rate for the absorption of two-photons due to the direct permanent dipole moment excitation mechanism. In: *AIP Advances*, 2016, vol.7. pp. 075202/1-14.
- [166] KWON, J., JUN, W.S., CHOI, I.S., MAO, X., KIM, J., KOH, E.K., KIM, Y.-H., KIM, S.-K., HWANG, D.Y. FeSe quantum dots for in vivo multiphoton biomedical imaging. In: *Science Advances*, 2019, vol.5, pp.1-7.
- [167] TAGUCHI, A., NAKAYAMA, A., OKETANI, R., KAWATA, S., FUJITA, K. Multiphoton-excited deep-ultraviolet photolithography for 3D nanofabrication. In: *ACS Applied Nano Materials*, 2020, vol.3, pp. 11434-11441.
- [168] JAGATAP, B. N., MEATH, W. J. Contributions of permanent dipole moments to molecular multiphoton excitation cross section. In: *JOSAB*, 2002, vol. 19, pp. 2673-2681.

- [169] KIMBLE, H. J. The quantum internet. In: *Nature*, 2008, vol. 453, pp. 1023-1030.
- [170] NORTHUP, T. E., BLATT, R. Quantum information using photons. In: *Nat. Photonics*, 2014, vol. 8, pp. 356-363.
- [171] HUANG, J., KUMAR, P. Observation of quantum frequency conversion. In: *Phys. Rev. Lett.*, 1992, vol. 68, pp. 2153-2156.
- [172] RAKHER, M. T., MA, L., SLATERRY, O., TANG, X., SRINIVASAN, K. Quantum transduction of telecommunications band single photons from quantum dot by frequency upconversion. In: *Nat. Photonics*, 2010, vol. 4, pp. 786-791.
- [173] GUO, X., ZOU, C.-L., JUNG, H., TANG, H. X. On-Chip strong coupling and efficient frequency conversion between telecom and visible optical modes. In: *Phys. Rev. Lett.*, 2016, vol. 117, pp. 123902/1-5.
- [174] HAN, J., VOGT, Th., GROSS, Ch., JAKSCH, D., KIFFNER, M., LI, W. Coherent microwave-to-optical conversion via six-wave mixing in Rydberg atoms. In: *Phys. Rev. Lett.*, 2018, vol. 120, pp. 093201/1-6.
- [175] KOCKUM, A. F., MACRI, V., GARZIANO, L., SAVASTA, S., NORI, F. Frequency conversion in ultrastrong cavity QED. In: *Scientific Reports*, 2017, vol. 7, pp. 2045-2322.
- [176] D'ANGELO, M., CHEKHOVA, M. V., SHIH, Y. Two-photon diffraction and quantum lithography. In: *Phys. Rev. Lett.*, 2001, vol. 87, pp. 013602/1-4.
- [177] SANCHEZ-MUNOZ, C., VALLE DEL, E., GONZALEZ TUDELA, A., MULLER, K., LICHTMANNECKER, S., KANIIBER, M., TEJEDOR, C., FINLEY, J. J., LAUSSY, F. P. Emitters of N-photon bundles. In: *Nature Photonics*, 2014, vol. 8, pp. 550-555.
- [178] ANDREWS, D. L., BRADSHAW, D. S., FORBES, K. A., SALAM, A. Quantum electrodynamics in modern optics and photonics: tutorial. In: *Jr. Opt. Soc. Am. B*, 2020, vol. 37, pp. 1153-1172.
- [179] VINTSKEVICH, S. V., GRIGORIEV, D. A., MIKLIN, N. I., FEDOROV, M. V. Entanglement of multiphoton two-mode polarization Fock states and their superpositions. In: *Laser Phys. Lett.*, 2020, vol. 17, pp. 035209/1-7.
- [180] LIAO, W.-T., PALFFY, A. Optomechanically induced transparency of X-rays via optical control. In: *Scientific Reports*, 2017, vol. 7, pp. 2045-2322.
- [181] BIN, Q., LU, X.-Y., LAUSSY, F. P., NORI, F., WU, Y. N-Phonon bundle emission via the Stokes process. In: *Phys. Rev. Lett.*, 2020, vol. 124, pp. 053601/1-7.
- [182] ARNESEN, M. C., BOSE, S., VEDREAL, V. Natural thermal and magnetic entanglement in the 1D Heisenberg model. In: *Phys. Rev. Lett.*, 2001, vol. 87, pp. 017901/1-4.
- [183] BRAUN, D. Creation of entanglement by interaction with common heat bath. In: *Phys. Rev. Lett.*, 2002, vol. 89, pp. 277901/1-4.
- [184] BASHAROV, A.M. Entanglement of atomic states upon collective radiative decay. In: *JETP Lett.*, 2002, vol. 75, pp. 123-126.
- [185] FICEK, Z., TANAS, R. Entangled states and collective nonclassical effects in two-atom systems. In: *Phys. Rep.*, 2002, vol.98, pp. 042102/1-4.
- [186] LAWANDE, Q. V., LAWANDE, S. V. Squeezing in Cooperative Resonance Fluorescence. In: *Phys. Rev. A*, 1988, vol.38, pp. 800-807.

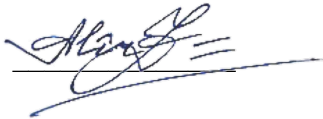
- [187] SCULLY, M.O., ZUBAIRY, M.S. *Quantum Optics*, Cambridge University Press, Cambridge, UK, 1997, p.630.
- [188] MIRZAC, A. Resonance Fluorescence Spectrum in Pumped Molecular Systems with Permanent Dipole. In: *Proceedings VI Scientific Conference of Post-Graduate Students (with international participation): Tendințe Contemporane ale Dezvoltării Științei: Viziuni ale Tinerilor Cercetători*, 2017, vol. I, pp. 79-84.
- [189] MÎRZAC, A. Quantum fluctuations in laser pumped molecular systems with permanent dipole. In: *Tendințe contemporane ale dezvoltării științei: viziuni ale tinerilor cercetători*, 2018, vol. I, pp. 59-64.
- [190] MÎRZAC, A., CIORNEA, V., MACOVEI M. A. Quantum light features scattered by pumped two-level systems with permanent dipoles. In: *Telecommunications, Electronics and Informatics*, 2018, pp. 89-91.
- [191] MÎRZAC, A., CIORNEA, V., MACOVEI M. A. Non-classical light scattered by laser-pumped molecules possessing permanent dipoles. In: *Moldavian Journal of Physical Sciences*, 2018, vol. 17. pp. 95-104.
- [192] ABDI, M., PLENIO, M. B. Quantum effects in a mechanically modulated single - photon emitter. In: *Phys. Rev. Lett.*, 2019, vol. 122, pp. 023602/1-6.
- [193] LEE, J.P., VILLA, B., BENNETT, A. J., STEVENSON, R. M., ELLIS, D. J. P., FARRER, I., RITCHIE, D. A., SHIELDS, A. J. A quantum dot as a source of time-bin entangled multi-photon states. In: *Quantum Sci. Technol*, 2019, vol. 4, pp. 025011/1-9.
- [194] ZAKRZEWSKI, J., LEWENSTEIN, M., MOSSBERG, T. W. Theory of dressed - state lasers. I. Effective Hamiltonians and stability properties. In: *Phys. Rev. A*, 1991, vol. 44, pp. 7717-7731.
- [195] AGARWAL, G.S. *Quantum statistical theories of spontaneous emission and their relation to other approaches*, Springer, 1974.
- [196] FICEK, Z., SWAIN, S. *Quantum Interference and Coherence: Theory and Experiments*, Springer, 2005.
- [197] KIFFNER, M., MACOVEI, M., EVERS, J., KEITEL, C.H. Vacuum induced processes in multilevel atoms. In: *Prog. Opt.*, 2010, vol. 55, pp. 85-197.
- [198] ZHU, J.-P., LI, G.-X.. Ground-state cooling of a nanomechanical resonator with a triple quantum dot via quantum interference. In: *Phys. Rev. A*, 2012, vol. 86, pp. 053828/1-10.
- [199] BOGOLYUBOV, N. N., FRAM LE KLEIN, Jr., SHUMOVSKY, A. S. Dynamics of two-photon processes in a two-level system. In: *Physica*, 1985, vol. 130 A, pp. 273-291.
- [200] GLAUBER, R. J. Quantum theory of optical coherence. In: *Phys. Rev.*, 1963, vol. 130, pp. 2529-2539.
- [201] ALBERT, F., HOPFMANN, C., RETZENTEIN, St., SCHNEIDER, Ch., HOFLING, S., WORSCHER, L., KAMP, M., KINZEL, W., FORCHEL, A., KANTER, I. Observing chaos for quantum-dot microlasers with external feedback. In: *Nature Communications*, vol. 22, pp. 366/1-5.
- [202] GUO, Y., PENG, C., JI, Y., LI, P., GUO, Y., GUO, X. Photon statistics and bunching of a chaotic semiconductor laser. In: *Optical express*, 2018, vol. 26, pp. 5991-6000.

- [203] REGELMAN, D. V., MIZRAHI, U., GERSHONI, D., EHRENFREUND, E. Semiconductor quantum dot: a quantum light source of multicolor photons with tunable statistics. In: *Phys. Rev. Lett.*, 2001, vol. 87, pp. 257401/1-4.
- [204] MIRZAC, A., CÂRLIG, S., MACOVEI, M. Microwave multiphoton conversion via coherently driven permanent dipole systems. In: *Phys. Rev. A.*, 2021, vol. 103, pp. 043719/1-7.
- [205] ZHOU, P., SWAIN, S., FICEK, Z. Resonance fluorescence spectrum of a two - level atom driven by a bichromatic field in a squeezed vacuum. In: *Phys. Rev. A.*, 1997, vol. 55, pp. 2340-2347

Responsibility Declaration

I, hereby, confirm that the scientific results presented in the doctoral thesis refer to my investigations. I understand, that in the contrary case I have to face the consequences.

Alexandra Mirzac

A handwritten signature in blue ink, appearing to read 'Alexandra Mirzac', is written over a horizontal line.

18 March, 2022

ANNEXES

Master equation's variables derived for the resonant case (II):

$$\begin{aligned}\rho^{(0)} &= \rho_{11} + \rho_{22} + \rho_{33}, \\ \rho^{(1)} &= \rho_{22} + \rho_{33}, \\ \rho^{(2)} &= \rho_{22} - \rho_{33}, \\ \rho^{(3)} &= b^\dagger \rho_{21} - \rho_{21} b, \\ \rho^{(4)} &= b^\dagger \rho_{21} + \rho_{21} b, \\ \rho^{(5)} &= \rho_{13} b^\dagger - b \rho_{31}, \\ \rho^{(6)} &= \rho_{13} b^\dagger + b \rho_{31}, \\ \rho^{(7)} &= b^\dagger \rho_{13} - \rho_{31} b, \\ \rho^{(8)} &= b^\dagger \rho_{13} + \rho_{31} b, \\ \rho^{(9)} &= \rho_{21} b^\dagger - b \rho_{12}, \\ \rho^{(10)} &= \rho_{21} b^\dagger + b \rho_{12}, \\ \rho^{(11)} &= b^\dagger \rho_{23} b^\dagger + b \rho_{32} b, \\ \rho^{(12)} &= b^\dagger \rho_{23} b^\dagger - b \rho_{32} b, \\ \rho^{(13)} &= b^{\dagger 2} \rho_{23} + \rho_{32} b^2, \\ \rho^{(14)} &= b^{\dagger 2} \rho_{23} - \rho_{32} b^2, \\ \rho^{(15)} &= \rho_{23} b^{\dagger 2} + b^2 \rho_{32}, \\ \rho^{(16)} &= \rho_{23} b^{\dagger 2} - b^2 \rho_{32}.\end{aligned}\tag{A-1}$$

System of equations of motion describing the resonant case (II):

$$\begin{aligned}
\dot{P}_n^{(0)} &= i\tilde{g}(P_n^{(3)} - P_n^{(5)} - P_n^{(9)} + P_n^{(7)}) - 2\kappa\bar{n}((n+1)P_n^{(0)} - nP_{n-1}^{(0)}) \\
&\quad - 2\kappa(1+\bar{n})(nP_n^{(0)} - (n+1)P_{n+1}^{(0)}), \\
\dot{P}_n^{(1)} &= i\tilde{g}(P_n^{(7)} - P_n^{(9)}) - 2\kappa\bar{n}((n+1)P^{(1)} - nP_{n-1}^{(1)}) \\
&\quad - 2\kappa(1+\bar{n})(nP_n^{(1)} - (n+1)P_{n+1}^{(1)}) + \tilde{\gamma}_0^{(1)}P_n^{(0)} - \tilde{\gamma}_1^{(1)}P_n^{(1)} - \tilde{\gamma}_2^{(1)}P_n^{(2)}, \\
\dot{P}_n^{(2)} &= -i\tilde{g}(P_n^{(9)} + P_n^{(7)}) - 2\kappa\bar{n}((n+1)P_n^{(2)} - nP_{n-1}^{(2)}) \\
&\quad - 2\kappa(1+\bar{n})(nP_n^{(2)} - (n+1)P_{n+1}^{(2)}) + \tilde{\gamma}_0^{(2)}P_n^{(0)} + \tilde{\gamma}_1^{(2)}P_n^{(1)} - \tilde{\gamma}_2^{(2)}P_n^{(2)}, \\
\dot{P}_n^{(3)} &= i\tilde{\delta}P_n^{(4)} - \tilde{\gamma}_3^{(3)}P_n^{(3)} + \tilde{\gamma}_7^{(3)}P_n^{(7)} + i\tilde{g}\left(n(2P_n^{(0)} - P_n^{(1)} - P_n^{(2)}) - (2n+1)P_n^{(1)}\right) \\
&\quad - \kappa(1+\bar{n})\left((2n-1)P_n^{(3)} - 2(n+1)P_{n+1}^{(3)} + 2P_n^{(9)}\right) - \kappa\bar{n}\left((2n+1)P_n^{(3)} - 2nP_{n-1}^{(3)}\right), \\
\dot{P}_n^{(4)} &= i\tilde{\delta}P_n^{(3)} - i\tilde{g}P_n^{(12)} - \kappa(1+\bar{n})\left((2n-1)P_n^{(4)} + 2P_2^{(10)} - 2(n+1)P_{n+1}^{(4)}\right) \\
&\quad - \kappa\bar{n}\left((2n+1)P_n^{(4)} - 2nP_{n-1}^{(4)}\right) - \tilde{\gamma}_4^{(4)}P_n^{(4)} + \tilde{\gamma}_8^{(4)}P_n^{(8)}, \\
\dot{P}_n^{(5)} &= i\tilde{\delta}P_n^{(6)} + i\tilde{g}\left(P_n^{(11)} + (n+1)(P_{n+1}^{(1)} - P_{n+1}^{(2)}) - 2(n+1)(P_n^{(0)} - P_n^{(1)})\right) \\
&\quad - \kappa(1+\bar{n})\left((2n+1)P_n^{(5)} - 2(n+1)P_{n+1}^{(5)}\right) - \kappa\bar{n}\left((2n+3)P_n^{(5)} - 2nP_{n-1}^{(5)} - 2P_n^{(7)}\right) \\
&\quad - \tilde{\gamma}_5^{(5)}P_n^{(5)} + \tilde{\gamma}_9^{(5)}P_n^{(9)}, \\
\dot{P}_n^{(6)} &= i\tilde{\delta}P_n^{(5)} + i\tilde{g}P_n^{(12)} - \kappa\bar{n}\left((2n+3)P_n^{(6)} - 2nP_{n-1}^{(6)} - 2P_n^{(8)}\right) \\
&\quad - \kappa(1+\bar{n})\left((2n+1)P_n^{(6)} - 2(n+1)P_{n+1}^{(6)}\right) - \tilde{\gamma}_6^{(6)}P_n^{(6)} + \tilde{\gamma}_{10}^{(6)}P_n^{(10)}, \\
\dot{P}_n^{(7)} &= i\tilde{\delta}P_n^{(8)} + i\tilde{g}\left(P_n^{(13)} + n(P_n^{(1)} - P_n^{(2)}) - 2n(P_{n-1}^{(0)} - P_{n-1}^{(1)})\right) \\
&\quad - \kappa\bar{n}\left((2n+1)P_n^{(7)} - 2nP_{n-1}^{(7)}\right) - \kappa(1+\bar{n})\left((2n-1)P_n^{(7)} - 2(n+1)P_{n+1}^{(7)} + 2P_n^{(5)}\right) \\
&\quad + \tilde{\gamma}_3^{(7)}P_n^{(3)} - \tilde{\gamma}_7^{(7)}P_n^{(7)}, \\
\dot{P}_n^{(8)} &= i\tilde{\delta}P_n^{(7)} + i\tilde{g}P_n^{(14)} - \kappa\bar{n}\left((2n+1)P_n^{(8)} - 2nP_{n-1}^{(8)}\right) \\
&\quad - \kappa(1+\bar{n})\left((2n-1)P_n^{(8)} - 2(n+1)P_{n+1}^{(8)} + 2P_n^{(6)}\right) + \tilde{\gamma}_4^{(8)}P_n^{(4)} - \tilde{\gamma}_8^{(8)}P_n^{(8)}, \\
\dot{P}_n^{(9)} &= i\tilde{\delta}P_n^{(10)} + i\tilde{g}\left(2(n+1)(P_{n+1}^{(0)} - P_{n+1}^{(1)}) - (n+1)(P_n^{(1)} + P_n^{(2)}) - P_n^{(15)}\right) \\
&\quad - \kappa(1+\bar{n})\left((2n+1)P_n^{(9)} - 2(n+1)P_{n+1}^{(9)}\right) - \kappa\bar{n}\left((2n+3)P_n^{(9)} - 2nP_{n-1}^{(9)} - 2P_n^{(3)}\right) \\
&\quad + \tilde{\gamma}_5^{(9)}P_n^{(5)} - \tilde{\gamma}_9^{(9)}P_n^{(9)}, \\
\dot{P}_n^{(10)} &= i\tilde{\delta}P_n^{(9)} - i\tilde{g}P_n^{(16)} - \kappa\bar{n}\left((2n+3)P_n^{(10)} - 2nP_{n-1}^{(10)} - 2P_n^{(4)}\right) \\
&\quad - \kappa(1+\bar{n})\left((2n+1)P_n^{(10)} - 2(n+1)P_{n+1}^{(10)}\right) + \tilde{\gamma}_6^{(10)}P_n^{(6)} - \tilde{\gamma}_{10}^{(10)}P_n^{(10)},
\end{aligned}$$

$$\begin{aligned}
\dot{P}_n^{(11)} &= 2i\tilde{\delta}P_n^{(12)} + i\tilde{g}\left(nP_n^{(5)} - (n+1)P_n^{(3)}\right) - 2\kappa(1+\bar{n})\left(nP_n^{(11)} - (n+1)P_{n+1}^{(11)} + P_n^{(15)}\right) \\
&\quad - 2\kappa\bar{n}\left((n+1)P_n^{(11)} - nP_{n-1}^{(11)} - P_n^{(13)}\right) - \tilde{\gamma}_{11}^{(11)}P_n^{(11)}, \\
\dot{P}_n^{(12)} &= 2i\tilde{\delta}P_n^{(11)} + i\tilde{g}\left(nP_n^{(6)} - (n+1)P_n^{(4)}\right) - 2\kappa(1+\bar{n})\left(nP_n^{(12)} - (n+1)P_{n+1}^{(12)} + P_n^{(16)}\right) \\
&\quad - 2\kappa\bar{n}\left((n+1)P_n^{(12)} - nP_{n-1}^{(12)} - P_n^{(14)}\right) - \tilde{\gamma}_{12}^{(12)}P_n^{(12)}, \\
\dot{P}_n^{(13)} &= 2i\tilde{\delta}P_n^{(14)} + i\tilde{g}\left((n-1)P_n^{(7)} - nP_{n-1}^{(13)}\right) - 2\kappa(1+\bar{n})\left((n-1)P_n^{(13)} - (n+1)P_{n+1}^{(13)}\right. \\
&\quad \left.+ 2P_n^{(11)}\right) - 2\kappa n\bar{n}\left(P_n^{(13)} - P_{n-1}^{(13)}\right) - \tilde{\gamma}_{13}^{(13)}P_n^{(13)}, \\
\dot{P}_n^{(14)} &= 2i\tilde{\delta}P_n^{(13)} + i\tilde{g}\left((n-1)P_n^{(8)} - nP_{n-1}^{(4)}\right) - 2\kappa(1+\bar{n})\left((n-1)P_n^{(14)} - (n+1)P_{n+1}^{(14)}\right. \\
&\quad \left.+ 2P_n^{(12)}\right) - 2\kappa\bar{n}\left(P_n^{(14)} - P_{n-1}^{(14)}\right) - \tilde{\gamma}_{14}^{(14)}P_n^{(14)}, \\
\dot{P}_n^{(15)} &= 2i\tilde{\delta}P_n^{(16)} + i\tilde{g}\left((n+1)P_n^{(5)} - (n+2)P_n^{(9)}\right) - 2\kappa(1+\bar{n})(1+n)\left(P_n^{(15)} - P_{n+1}^{(15)}\right) \\
&\quad - 2\kappa\bar{n}\left((n+2)P_n^{(15)} - nP_{n-1}^{(15)} - 2P_n^{(11)}\right) - \tilde{\gamma}_{15}^{(15)}P_n^{(15)}, \\
\dot{P}_n^{(16)} &= 2i\tilde{\delta}P_n^{(15)} + i\tilde{g}\left((n+1)P_{n+1}^{(6)} - (n+2)P_n^{(10)}\right) - 2\kappa(1+\bar{n})(1+n)\left(P_n^{(16)} - P_{n+1}^{(16)}\right) \\
&\quad - 2\kappa\bar{n}\left((n+2)P_n^{(16)} - nP_{n-1}^{(16)} - 2P_n^{(12)}\right) - \tilde{\gamma}_{16}^{(16)}P_n^{(16)}. \tag{A-2}
\end{aligned}$$

Spontaneous decay rates for the resonant case (II):

$$\begin{aligned}
\tilde{\gamma}_0^{(1)} &= \gamma_0^{(1)}, \\
\tilde{\gamma}_1^{(1)} &= \gamma_1^{(1)}, \\
\tilde{\gamma}_2^{(1)} &= \gamma \sin \theta \cos^2 \frac{\theta}{2}, \\
\tilde{\gamma}_0^{(2)} &= \gamma_0^{(2)}, \\
\tilde{\gamma}_1^{(2)} &= -\gamma_1^{(2)}, \\
\tilde{\gamma}_2^{(2)} &= \gamma_2^{(2)}, \\
\tilde{\gamma}_3^{(3)} &= \gamma_2 \cos^2 \theta \frac{(1+3\sin\theta)^2}{8} + \gamma_3 \cos^2 \theta \frac{(1-3\sin\theta)^2}{8} + (\gamma^{(+)} + \gamma^{(-)}) \frac{\sin^2 \theta}{4} + \gamma_0^{(0)} \\
&\quad + \Gamma^{(-)} + 9\gamma \frac{\cos^4 \theta}{16} + \frac{\gamma \cos^2 \theta}{4} \left((1+\sin\theta)^2 + \frac{(1-\sin\theta)^2}{2} \right), \\
\tilde{\gamma}_7^{(3)} &= \gamma_0^{(+)} + \gamma \cos^2 \theta \frac{(1-\sin\theta)^2}{4}, \\
\tilde{\gamma}_4^{(4)} &= \tilde{\gamma}_3^{(3)}, \\
\tilde{\gamma}_8^{(4)} &= \tilde{\gamma}_7^{(3)}, \\
\tilde{\gamma}_5^{(5)} &= \gamma_2 \cos^2 \theta \frac{(1-3\sin\theta)^2}{8} + \gamma_3 \cos^2 \theta \frac{(1+3\sin\theta)^2}{8} + (\gamma^{(+)} + \gamma^{(-)}) \frac{\sin^2 \theta}{4} + \gamma_0^{(0)} + \Gamma^{(+)} \\
&\quad + \frac{9\gamma \cos^2 \theta}{16} + \frac{\gamma \cos^2 \theta}{4} \left((1-\sin\theta)^2 + \frac{(1+\sin\theta)^2}{2} \right), \\
\tilde{\gamma}_9^{(5)} &= \gamma_0^{(-)} + \gamma \cos^2 \theta \frac{(1+\sin\theta)^2}{4}, \\
\tilde{\gamma}_5^{(6)} &= \tilde{\gamma}_5^{(5)}, \\
\tilde{\gamma}_{10}^{(6)} &= \tilde{\gamma}_9^{(5)}, \\
\tilde{\gamma}_7^{(7)} &= \tilde{\gamma}_6^{(6)}, \\
\tilde{\gamma}_3^{(7)} &= \tilde{\gamma}_{10}^{(6)}, \\
\tilde{\gamma}_8^{(8)} &= \tilde{\gamma}_7^{(7)}, \\
\tilde{\gamma}_4^{(8)} &= \tilde{\gamma}_3^{(7)}, \\
\tilde{\gamma}_5^{(9)} &= \tilde{\gamma}_0^{(+)} + \gamma \cos^2 \theta \frac{(1-\sin\theta)^2}{4}, \\
\tilde{\gamma}_9^{(9)} &= \tilde{\gamma}_3^{(3)} = \tilde{\gamma}_{10}^{(10)}, \\
\tilde{\gamma}_6^{(10)} &= \tilde{\gamma}_5^{(9)}, \\
\tilde{\gamma}_{11}^{(11)} &= (\gamma_2 + \gamma_3) \frac{\cos^2 \theta}{2} + 2\gamma_0^{(0)} + \Gamma^{(-)} + \Gamma^{(+)} + \gamma \cos^2 \theta \frac{(1+\sin^2 \theta)^2}{4}, \\
\tilde{\gamma}_{11}^{(11)} &= \tilde{\gamma}_{12}^{(12)} = \tilde{\gamma}_{13}^{(13)} = \tilde{\gamma}_{14}^{(14)} = \tilde{\gamma}_{15}^{(15)} = \tilde{\gamma}_{16}^{(16)}.
\end{aligned} \tag{A-3}$$



Alexandra Mirzac

Data nașterii: 17/10/1990 | **Cetățenie:** română , moldoveană | **Gen:** Feminin |

(+49) 15750727675 | (+49) 711335016845 | (+373) 69637125 |

mirzalexandra71@gmail.com | <https://www.researchgate.net/profile/Alexandra-Mirzac> |

Hirschstraße , 7, 71272, Malsheim-Renningen, Germania
Dacia 30/1, 78, MD - 2060, Chișinău, Moldova

EXPERIENȚA PROFESIONALĂ

01/03/2022 – ÎN CURS – Böblingen, Germania

TECHNICAL DOCUMENTATION ENGINEER – NASH TECHNOLOGIES GMBH

Learning Products/ Technical Documentation | Informare și comunicații | info@nashtech.com |

www.nashtech.com | Herrenbergerstraße 130, 71034, Böblingen, Germania

10/05/2021 – 28/02/2022 – Fellbach, Germania

ELECTRONIC SYSTEM ARCHITECTURE – IMI NORGREN PRECISION ENGINEERING GMBH

Activități specializate, științifice și tehnice | <https://www.norgren.com/de/de/uber/kontakt/deutschland> |

Stuttgarter strasse 120, 70736, Fellbach, Germania

01/11/2015 – ÎN CURS – Chișinău, Moldova

CERCETĂTOR ȘTIINȚIFIC STAGIAR – INSTITUTUL DE FIZICĂ APLICATĂ

Activități specializate, științifice și tehnice | director@ifa.md | <https://ifa.md/> |

str. Academiei, 5, MD-2028, Chișinău, Moldova

09/09/2019 – 03/12/2019 – București, România

ASISTENT DOCTORAL DE CERCETARE – INSTITUTUL NAȚIONAL DE CERCETARE-DEZVOLTARE PENTRU FIZICĂ ȘI INGINERIE NUCLEARĂ "HORIA HULUBEI"

Departamentul de Fizică Teoretică | Activități specializate, științifice și tehnice | <https://www.nipne.ro/> |

30 Reactorului, PO Box MG-6 077125, Magurele, Ilfov,, România

21/06/2014 – 31/10/2015 – Chișinău, Moldova

CERCETĂTOR ȘTIINȚIFIC STAGIAR – INSTITUTUL DE CHIMIE

Activități specializate, științifice și tehnice | str. Academiei, 3, MD-2028, Chișinău, Moldova

21/02/2014 – 19/06/2014 – Chișinău, Moldova

CERCETĂTOR ȘTIINȚIFIC STAGIAR – INSTITUTUL DE INGINERIE ELECTRONICĂ ȘI NANOTEHNOLOGII "D. GHIȚU"

Nanotechnology | Activități specializate, științifice și tehnice | directia@nanotech.md | <https://nanotech.md/ro> |

Academiei str., 3/3, MD-2028, Chișinău, Moldova

Activități specializate, științifice și tehnice | ichem@ichem.md | <https://ichem.md/> |

Academiei str. 3, MD-2028, Chișinău, Moldova

● **EDUCAȚIE ȘI FORMARE PROFESIONALĂ**

16/01/2016 – ÎN CURS – str. Alexe Mateevici 60, Chișinău, Moldova
DOCTORAT – Universitatea de Stat din Moldova

Domeniul (domeniile) de studiu

◦ Științe naturale, matematică și statistică : *Fizică*

Lucrarea de diplomă: QUANTUM DYNAMICS IN MOLECULAR DIPOLAR SYSTEMS

Doctor | www.usm.md

01/09/2015 – 09/07/2018 – str. Alexe Mateevici 60, Chișinău, Moldova
LICENȚĂ: MATEMATICĂ – Universitatea de Stat din Moldova

www.usm.md

01/09/2013 – 25/06/2015 – str. Alexe Mateevici 60, Chișinău, Moldova
MASTERAT: FIZICA ȘI INGINERIA SEMICONDUCTORILOR – Universitatea de Stat din Moldova

www.usm.md

01/09/2009 – 28/06/2013 – str. Alexe Mateevici 60, Chișinău, Moldova
LICENȚĂ: FIZICĂ – Universitatea de Stat din Moldova

<http://usm.md/>

● **COMPETENȚE LINGVISTICE**

Limbă(i) maternă(e): **ROMÂNĂ**

Altă limbă (Alte limbi):

	COMPREHENSIUNE		VORBIT		SCRIS
	Comprehensiune orală	Citit	Exprimare scrisă	Conversație	
RUSĂ	C2	C2	C2	C2	C2
GERMANĂ	B2	B2	B1	B1	B1
ENGLEZĂ	C2	C2	C2	C2	C2
FRANCEZĂ	C1	C1	B2	B2	B2

Niveluri: A1 și A2 Utilizator de bază B1 și B2 Utilizator independent C1 și C2 Utilizator experimentat

● **COMPETENȚE DIGITALE**

Java Programming language | MVTEC HALCON | Wolfram Mathematica | MS office/Latex; (Full proficiency, daily use) | C / C++ / C# | Good familiarity with MATLAB, Simulink | SVN Git GitLab | Programming languages: Java, C, Delphi | NXP S32 Family | Arm Cortex M0 | NXP S32k14x

● **PUBLICAȚII**

Quantum Photon Conversion via Coherently Driven Permanent Dipole Systems

5th International Conference on Nanotechnologies and Biomedical Engineering, November 3-5, 2021
https://link.springer.com/chapter/10.1007/978-3-030-92328-0_2 - 2022
S. Cârlig, A. Mîrzac, P. Bardetski, M. Macovei.

Microwave multiphoton conversion via coherently driven permanent dipole systems

Phys. Rev. A. 2021, nr.103, pp.043719/1-8
<https://journals.aps.org/pra/abstract/10.1103/PhysRevA.103.043719> - 2021
A. Mîrzac, S. Carlig, M. Macovei

Interferometric power of gaussian systems in a squeezed thermal bath

Romanian Journal of Physics, nr. 1-2(65), pp. 95-104
2020
A. Mîrzac, T. Mihaescu, M. Macovei, A. Isar.

Steady-state behaviors of a quantum oscillator coupled with a three-level emitter

IFMBE Proceedings, pp.677 - 680
https://link.springer.com/chapter/10.1007/978-3-030-31866-6_119 - 2020
A. Mirzac, M. A. Macovei.

Dinamica răcirii cuantice a unui oscilator cuplat cu un atom artificial

Revista de Știință, Inovare, Cultură și Artă „Akademos”. 2019, nr. 4(55), pp. 16-19
2019
A. Mîrzac.

Dynamics of a quantum oscillator coupled with a three-level Λ -type emitter.

Journal of the Optical Society of America B: Optical Physics. 2019, nr. 9(36), pp. 2473-2480.
<https://www.osapublishing.org/josab/abstract.cfm?uri=josab-36-9-2473> - 2019
A. Mirzac, M. Macovei.

Non-classical light scattered by laser-pumped molecules possessing permanent dipoles.

Moldavian Journal of the Physical Sciences. 2018, nr. 1-2(17), pp. 95-104.
2018
A.Mirzac, V. Ciornea, M. Macovei.

● **CONFERINȚE ȘI SEMINARE**

18/09/2019 – 21/09/2019 – Chișinău, Republica Moldova

The 4th International Conference on Nanotechnologies and Biomedical Engineering

Talk: A. Mirzac and A. Macovei, “Steady-state Behaviors of a Quantum Oscillator Coupled with a Three-level Emitter”.

12/09/2019 – 14/09/2019 – Sinaia, Romania

International Conference on Advanced Scientific Computing

Talk: A. Mirzac, "Lasing and cooling effects of a quantum oscillator coupled with a three-level lambda - type system".

26/03/2019 – 29/03/2019 – Chişinău, Republica Moldova

Conferința tehnico-științifică a studenților, masteranzilor și doctoranzilor

Talk: A. Mirzac, "Steady-state dynamics of a quantum oscillator coupled with a three-level emitter".

25/09/2018 – 28/09/2018 – Chişinău, Republica Moldova

Materials Science and Condensed Matter Physics

Talk: A. Mirzac, M. Macovei, "Non-classical light features scattered by laser pumped molecules with permanent dipoles".

15/06/2018 – 18/06/2018 – Chişinău, Republica Moldova

Tendențe contemporane ale dezvoltării științei : viziuni ale tinerilor cercetători. Ediția VII

Talk: A. Mirzac. "Quantum fluctuations in laser pumped molecular systems with permanent dipole"

2018 – Chişinău, Republica Moldova

Telecommunications, Electronics and Informatics

Talk: A.V. Mirzac, V. Ciornea, M. A. Macovei, "Quantum light features scattered by pumped two-level systems with permanent dipoles".

2017 – Chişinău, Republica Moldova

Tendențe contemporane ale dezvoltării științei: viziuni ale tinerilor cercetători. Ediția a VI-a

Talk: A. Mirzac. "Resonance fluorescence spectrum in pumped molecular systems with permanent dipole".

2017 – Chişinău, Republica Moldova

Humboldt Kolleg, Multidisciplinarity in Modern Science for the Benefit of Society

Poster : A. Mirzac, M. Macovei. "Squeezing in Fluorescence Spectrum of Pumped Molecular System with Permanent Dipole".

12/09/2016 – 16/09/2016 – Chişinău, Republica Moldova

Material Science and Condensed Matter Physics

Talk: A. Mîrzac, M. Macovei. "Resonance fluorescence spectrum for a pumped dipolar molecule"

15/03/2016 – 18/03/2016 – Chişinău, Republica Moldova

Tendențe contemporane ale dezvoltării științei: viziuni ale tinerilor cercetători. Ediția a V-a.

Talk: A. Mirzac. "Kinetics of molecular systems with permanent dipole moment"

● **DISTINCȚII ONORIFICE ȘI PREMII**

2019

Bursă Națională – Federația Mondială a Savanților (Elveția)

21/02/2013

Bursa de Merit – Bursă Soros
